Lipid signalling dynamics of palmitate-induced endoplasmic reticulum stress in skeletal muscle

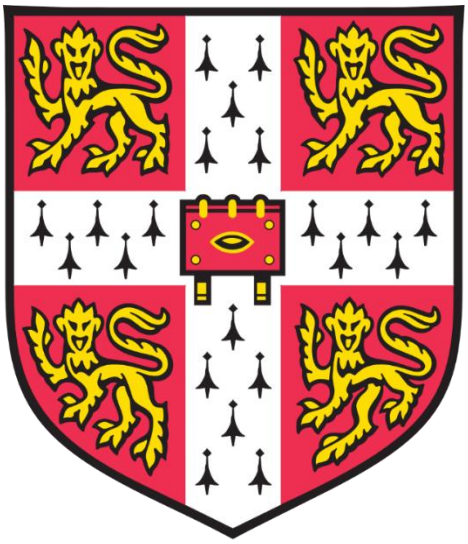

A dissertation submitted for the degree of Doctor of Philosophy at the University of Cambridge.

Submitted September 2018.

Ben Daniel McNally

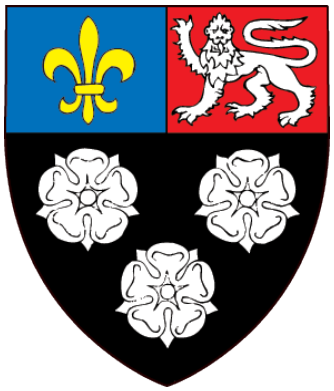

King's College

“Obviously my method of thought and reasoning is influenced by a scientific training – if that were not so my scientific training will have been a waste and a failure.”

Rosalind Franklin – taken from a letter to her father, Ellis Franklin, undated (approximately 1940).

“I was taught that the way of progress is neither swift nor easy.”

Marie Curie - Taken from Pierre Curie (1936).

“Machines will do the heavy work,

Men will supervise the machines,

You owe much to these machines,

Horsepower, not manpower,

Brains, not brawn.”

Progress by Public Service Broadcasting, released in 2017.

Declaration

This dissertation is the result of my own work and includes nothing which is the outcome of work done in collaboration except as declared in the Preface and specified in the text. It is not substantially the same as any that I have submitted, or, is being concurrently submitted for a degree or diploma or other qualification at the University of Cambridge or any other University or similar institution except as declared in the Preface and specified in the text. I further state that no substantial part of my dissertation has already been submitted, or, is being concurrently submitted for any such degree, diploma or other qualification at the University of Cambridge or any other University or similar institution except as declared in the Preface and specified in the text. It does not exceed the prescribed word limit for the relevant Degree Committee. For more information on the word limits for the respective Degree Committee.

Approximately 340 million people worldwide have Type 2 Diabetes Mellitus (T2DM), making identification of the aetiological processes underlying this disease imperative. Endoplasmic reticulum (ER) stress has emerged as a potential mechanism driving the pathogenesis of obesity and T2DM. Palmitate, the predominant saturated fatty acid elevated in the blood plasma of obese individuals, induces ER stress and insulin resistance in skeletal muscle. However, the interaction between ER stress, lipid metabolism and T2DM remains poorly understood. This thesis uses lipidomic tools to investigate skeletal muscle ER stress in cell culture and animal models. Chronic palmitate treatment of both mouse C2C12 and human primary myotubes induced ER stress, concurrent with the cytosolic phospholipase A2-dependent release of polyunsaturated fatty acids (PUFAs) from phosphatidylcholines (PCs). This phenotype was also observed in skeletal muscle from mouse models of diet-induced obesity and T2DM patients. Palmitate-stimulated catabolism of PUFA-containing PCs was concomitant with increases in bioactive eicosanoid secretion, which was shown to be important in the control of ER stress, inflammatory signalling and macrophage activation. This provides a novel link between palmitate and the control of ER stress and inflammation in metabolic disease.

Previous work has suggested that the propagation of ER stress signalling between cells may result from the secretion of a, as yet undefined, cell non-autonomous signal. In this thesis, long-chain ceramides (40:1 and 42:1) were identified as signals transmitting the induction of ER stress between myotubes via exosome-mediated transport. Long-chain ceramide concentrations were increased in skeletal muscle and blood plasma from *in vivo* models of obesity and were elevated in the muscle of T2DM patients. Muscle synthesis of long chain ceramides in response to palmitate was found to occur via the *de novo* pathway and was linked to ER stress by Perk, an important unfolded protein response kinase. This work identifies ceramides as cell non-autonomous signals that propagate ER stress activation following exposure to palmitate, providing a novel mechanism for stress signalling in obesity and insulin resistance.

Roberts, L.D., Ashmore, T., **McNally, B.D**., *et al.* 2017 Inorganic nitrate mimics exercise-stimulated muscular fiber-type switching and myokine and γ-aminobutyric acid release. *Diabetes* 66 (3), 674-688.

Sanders, F., **McNally, B.**, Griffin, J.L., 2016 Blood triacylglycerols: a lipidomic window on diet and disease. *Biochemical Society Transactions* 44 (2), 638-644.

McNally, B., Griffin, J.L., Roberts, L.D. 2016 Dietary inorganic nitrate: From villain to hero in metabolic disease? *Mol Nutr Food Res.* 60(1):67-78.

The past four years have been a challenging and rewarding period, in which I've learnt a lot. I would not have been able to complete this PhD, however, without a number of wonderful people who've helped and supported me throughout my time in Cambridge as a postgraduate student. I'd now like to take the opportunity to acknowledge a few of these.

I owe a lot to not one, but two excellent supervisors. First, thank you to Dr Lee Roberts. You have been the perfect supervisor for me, providing the scientific guidance I've required, and a trust to pursue the questions I've been most interested in. I feared I would struggle when you moved to Leeds, but even from the other end of the country you were still able to keep me on course with our monthly meetings and a speedy reply whenever I've needed you. Your progress in, and enthusiasm for, research has inspired my own interest, and I hope that remains the case as I pursue a career in academia. Secondly, thanks to Professor Jules Griffin for the opportunity to research in your lab and the support and guidance during my PhD, as well as the financial support to keep me going through an unplanned fourth year! Thank you as well for funding experiments beyond my MRC budget and a number of conferences, including two trips the US and one to Swansea! It's been a privilege to work for someone so respected in the field.

I would also like to thank the other people in the group, past and present, for making the past 4 years such a great experience. In particular, to Steve, my third supervisor in all but title. Thank you for putting up with nonsensical and incessant questions for such a long time, allowing my PhD to run as smoothly as possible. Thanks as well for the many pub trips, beer festivals, football games and board game nights. Similarly, it's not going to be the same without our other board game partner in crime, Emma. I'll miss having a Cambridge resident to drag along to gigs as well! I'd also like to thank Tom for his biochemistry guidance and the needless halves, and Zoe, James, Antonio and Christine for teaching me all there is to know about LC-MS. Thanks to Evelina, Dean and Marta, my fellow office residents for keeping the small office the most fun office, and also to Sonia, Mike, Mel and Cecilia, among others, for making tea time a fun and of course important part of the working day, and evening pub trips a necessity.

Outside of the lab, I've been lucky enough to count on the friendship and love of a number of other people. Of course, none have been more supportive and patient than Fiona. Thank you for your understanding with my Saturday morning alarms and the care packages that have seen me through my thesis! Most importantly, thank you for maintaining my life outside of science, even when research feels all encompassing. Thank you as well to Osh and Ellie, the other constants in my life, for the many hours spent listening to me rant about science, the many games of cards and far too many episodes of Rush Hour. Thanks also to Ben, Fliss, Fi and Jo for being fun and supportive housemates.

When Cambridge has got too much, I know I've always been able to count on friends who've moved away to London. Beth, Holly, Ellie, Eva, Becca, Kesia and Aidan – you've always been a message or a train journey away when I've needed you. Thanks for the dinners, the gigs, the parties, the hangouts and more love and support than I deserve. Thanks also to Chris and Harry for the nights out in London and even the odd visit to Cambridge, even if you do insist on going to places PhD students can't afford. Hopefully we'll find an activity that I can actually compete at, because golf and darts certainly haven't gone my way.

My school friends have always been important at keeping me in line. In particular, Daisy, despite everything you've had to go through over the last couple of years, you've still managed to spend more time checking in on me. David, I haven't seen you anywhere near as much as I should have but your messages and the Frank Turner gigs are always important to me, even if you did beat me to the Dr title! To everyone else from school, I always look forward to our Christmas pub trips and wish they were more frequent!

Lastly, and most importantly, I'd like to thank my family. To my parents, Paul and Beverley, and my brother, Joe, thank you for all the support and guidance to get me through this PhD. You've been there whenever I've needed you, be that a message, a trip out or a dinner at home! Family Christmas is always one of the best times of the year as well! I'm blessed to have family such as the three of you, and there's no way I'd be submitting this without you.

4-PBA	Sodium phenylbutyrate
AA	Arachidonic acid
ACC1	Acetyl-CoA carboxylase 1
ACN	Acetonitrile
ADRP	Adipose differentiation-related protein
ALA	α-linolenic acid
ALOX12	Arachidonate 12-lipoxygenase
ALOX15	Arachidonate 15-lipoxygenase
ALOX5	Arachidonate 5-lipoxygenase
AML-12	Alpha mouse liver 12
ARG1	Arginase 1
ATCC	American Type Culture Collection
ATF3	Activating transcription factor 3
ATF4	Activating transcription factor 4
ATF6	Activating transcription factor 6
ATGL	Adipose triacylglyceride lipase
BF_3	Boron trifluoride
BMI	Body mass index
BSA	Bovine serum albumin
Ca^{2+}	Calcium ions
CCL2	C-C motif chemokine ligand 2
cDNA	Complementary DNA
Cer	Ceramide
CERS2	Ceramide synthase 2
CERT	Ceramide transfer protein
CHOP	C/EBP-homologous protein
CID	Collision induced dissociation
COX	Cyclooxygenase
cPLA2	Cytoplasmic phospholipase A2
CRP	C-reactive protein
CT	Cycle threshold
C-trap	Curved ion trap
CYP450	Cytochrome P450
DC	Direct current
DDA	Data-dependent acquisition
DES1	Dihydroceramide desaturase 1
DG	Diacylglyceride
DGAT	Diacylglycerol acyltransferase
DGLA	Dihomo-γ-linolenic acid
DHA	Docosahexaenoic acid
DHCer	Dihydroceramide
DI	Direct infusion
DMEM	Dulbecco's Modified Eagle Medium

DNL	*De novo* lipogenesis
dsDNA	Double stranded DNA
EDEM1	ER degradation enhancing alpha-mannosidase like protein 1
EET	Epoxyeicosatrienoic acid
EGR2	Early growth response 2
EIF2α	Eukaryotic initiation factor 2α
EPA	Eicosapentaenoic acid
EpOME	Epoxyoctadecenoic acid
ER	Endoplasmic reticulum
ERAD	ER-associated degradation
ESI	Electrospray ionisation
FAME	Fatty acid methyl ester
FAS	Fatty acid synthase
FB1	Fumonisin B1
FBS	Foetal bovine serum
FFA	Free fatty acid
FIT	Fat-storage inducing transmembrane protein
FTMS	Fourier transform mass spectrometer
FWHM	Full width at half maximum
GADD34	Growth arrest and DNA damage-inducible 34
GC	Gas chromatography
GLUT4	Glucose transporter type 4
GPCR	G protein-coupled receptor
GRP78	Glucose regulated protein 78
GRP94	Glucose regulated protein 94
GSK3	Glycogen synthase kinase 3
GWAS	Genome-wide association studies
HbA1c	Glycosylated haemoglobin
HDL	High density lipoprotein
HDoHE	Hydroxydocosahexaenoic acid
HEPE	Hydroxyeicosapentaenoic acid
HETE	Hydroxyeicosatetraenoic acid
HFD	High fat diet
HILIC	Hydrophilic-interaction chromatography
HODE	Hydroxyoctadecadienoic acid
HPLC	High-performance liquid chromatography
HS	Horse serum
HSkMC	Human skeletal muscle cells
HSL	Hormone-sensitive lipase
HSPA5	Heat shock protein 70 family protein 5
IDF	International Diabetes Federation
IL	Interleukin
IL-6	Interleukin 6
IM	Ion mobility

IP_3	Inositol 1,4,5-triphosphate
IPA	Propan-2-ol
iPLA2	Calcium-independent phospholipase A2
IRE1	Inositol requiring enzyme 1
IRES	Internal ribosome entry site
IRS	Insulin receptor substrate
KO	Knockout
LC	Liquid chromatography
LDL	Low density lipoprotein
LFC	Low-fat control
LOX	Lipoxygenase
LPC	Lysophosphatidylcholine
LT	Leukotriene
LTB4	Leukotriene B4
m/z	Mass-to-charge ratio
MG	Monoacylglycerol
MGL	Monoacylglycerol lipase
MS	Mass spectrometry
MS/MS	Tandem mass spectrometry
mTORC1	Mammalian target of rapamycin complex 1
MUFA	Monounsaturated fatty acid
NF-κB	Nuclear factor-kappa B
NK	Natural killer
NMR	Nuclear magnetic resonance
NO	Nitric oxide
NOS2	Nitric oxide synthase 2
NPLC	Normal phase liquid chromatography
OGTT	Oral glucose tolerance test
P/S	Penicillin/streptomycin
PC	Phosphatidylcholine
PC/PE	Phosphatidylcholine/phosphatidylethanolamine
PDI	Protein disulphide isomerase
PE	Phosphatidylethanolamine
PERK	Protein kinase R-like endoplasmic reticulum kinase
PG	Prostaglandin
PI	Phosphatidylinositol
PI3K	Phosphoinositide 3-kinase
PKC	Protein kinase C
PLA2	Phospholipase A2
POMC	Pro-opiomelanocortin
PPARγ	Peroxisome proliferator-activated receptor γ
PS	Phosphatidylserine
PUFA	Polyunsaturated fatty acid
QqQ	Triple quadrupole

Q-ToF	Quadrupole-time of flight
R-BEL	R-bromoenollactone
RF	Radio frequency
RIDD	Regulated IRE1-dependent decay
RPLC	Reverse phase liquid chromatography
RT-qPCR	Reverse transcription-quantitative polymerase chain reaction
SCD1	Stearoyl-CoA desaturase 1
SEM	Standard error of the mean
SERCA	Sarco/endoplasmic reticulum calcium ATPase
SFA	Saturated fatty acid
SPT	Serine palmitoyl transferase
SREBP1	Sterol regulatory element-binding protein 1
SREBP2	Sterol regulatory element-binding protein 2
T2DM	Type 2 Diabetes Mellitus
TG	Triacylglyceride
TLR4	Toll-like receptor 4
TNFα	Tumour necrosis factor α
ToF	Time of flight
TUDCA	Tauroursodeoxycholic acid
TXA_2	Thromboxane
UCP	Uncoupling protein
UHPLC	Ultra-high-performance liquid chromatography
UPR	Unfolded protein response
WAT	White adipose tissue
WD	Western diet
XBP1	X-box binding protein 1

Chapter 1

Introduction

1.1 The metabolic syndrome

The metabolic syndrome describes a collection of risk factors for cardiovascular disease and type 2 diabetes mellitus (T2DM) [1]. The World Health Organisation (WHO) definition of the metabolic syndrome states that patients must exhibit insulin resistance, a condition characterised by an inhibited response to insulin, and then two further risk factors, which may include: obesity, defined as the accumulation of white adipose tissue (WAT) and reflected in a body mass index (BMI) above 30; hyperglycaemia, referring to raised fasting blood glucose levels resulting from insulin resistance; dyslipidaemia, indicated by raised plasma triacylglyceride (TG) levels above 150 mg/dL, low high-density lipoprotein (HDL) cholesterol levels (below 35 mg/dL in men and 39 mg/dL in women) and an increase in low density lipoproteins (LDLs); and hypertension – raised blood pressure above 140/90 mm Hg [2,3]. The risk factors are interdependent and underpinned by common mechanisms and features.

The International Diabetes Federation (IDF) estimates that approximately 20-25% of the world's adult population suffer from the metabolic syndrome [4]. The prevalence of the metabolic syndrome is associated with increases in age and BMI, with 42% of individuals aged over 70 suffering from the metabolic syndrome and 60% of obese adults [5,6]. Furthermore, an increase in body weight of 2.25 kg over a period of 16 years increased risk for the development of the metabolic syndrome by 20% in men and 37% in women. Similarly, a 2.25 kg decrease in body weight reduced risk by 48% in men and 40% in women [7].

1.1.1 Type 2 diabetes mellitus

The numbers of individuals suffering from T2DM is increasing at an alarming rate, putting pressure on healthcare systems across the world [8]. In 2011, an estimated 366 million people worldwide suffered from diabetes, with the numbers suffering from T2DM rising to 439 million by 2030 [9]. T2DM arises from an interaction between lifestyle and genetic factors, with the former including physical inactivity, diet, smoking and a high consumption of alcohol [10]. As with the metabolic syndrome, obesity is an important risk factor in the development of T2DM. Studies in the US highlight that 55% of individuals suffering from T2DM are obese, and 85% are overweight [11]. Diagnosis of T2DM relies on raised fasting plasma glucose levels of >7 mmol/L or plasma glucose levels of >11.1 mmol/L 2 hours after an oral dose of glucose, termed an oral glucose tolerance test (OGTT) [12].

T2DM is characterised by insulin resistance, a state defined as an inability for peripheral tissues, such as skeletal muscle, adipose and liver tissues, to respond correctly to insulin [13]. In the healthy state, insulin is secreted in response to raised blood glucose levels, and binds to insulin receptors on peripheral tissues (**Figure 1.1**). This stimulates autophosphorylation of tyrosine residues on the receptor, which, in turn, are recognised by adapter proteins, including insulin receptor substrate (IRS) proteins [14]. Phosphorylation of IRS proteins stimulates the phosphoinositide 3-kinase (PI3K) pathway, leading to the activation of AKT (also known as protein kinase B) [15]. AKT phosphorylates and inactivates glycogen synthase kinase 3 (GSK3), increasing glucose storage in the form of glycogen [16]. Activation of this pathway also stimulates the translocation of glucose transporter type 4 (GLUT4) channels, increasing glucose uptake from the blood into cells of peripheral tissues [17]. GLUT4 translocation is also increased by the insulin-mediated activation of a second pathway. Binding of insulin to its receptor activates the CBL-CAP complex that interacts with a membrane domain enriched in caveolin [18]. The complex then activates the G-protein TC10, which stimulates GLUT4 translocation and glucose uptake [19].

As well as the activation of glucose uptake and storage, insulin also inhibits the production and release of glucose in the liver. Insulin increases transcription of glycolytic genes, such as glucokinase and pyruvate kinase, and decreases expression of phosphoenolpyruvate carboxylase, which mediates the rate-limiting step in gluconeogenesis [20,21]. In this way, liver cells switch from glucose synthesis to utilisation.

Insulin signalling also regulates lipid, as well as carbohydrate, metabolism. AKT activates mammalian target of rapamycin complex 1 (mTORC1), which is important in the regulation of sterol regulatory element-binding protein 1 (SREBP1) [22,23]. SREBP1 is a transcription factor that increases expression of genes associated with lipid synthesis, such as stearoyl-CoA desaturase 1 (SCD1) and fatty acid synthase (FAS) [24].

Furthermore, insulin reduces rates of lipolysis - the hydrolysis of TGs to produce fatty acids - in adipose tissue, decreasing plasma fatty acid levels [25]. The regulation of lipolysis controls the availability of fatty acids to peripheral tissues such as skeletal muscle and the liver depending on their metabolic requirement [26]. The catabolism of TGs is catalysed by 3 enzymes: adipose triacylglyceride lipase (ATGL), which converts TG to diacylglycerides (DG); hormone-sensitive lipase (HSL), which converts DG to monoacylglycerol (MG); and monoacylglycerol lipase (MGL), which hydrolyses MGs [27]. Insulin signalling decreases expression of both ATGL and HSL, reducing the rate of lipolysis [28,29]. Insulin also reduces the activity of both enzymes via the activation of AKT [30].

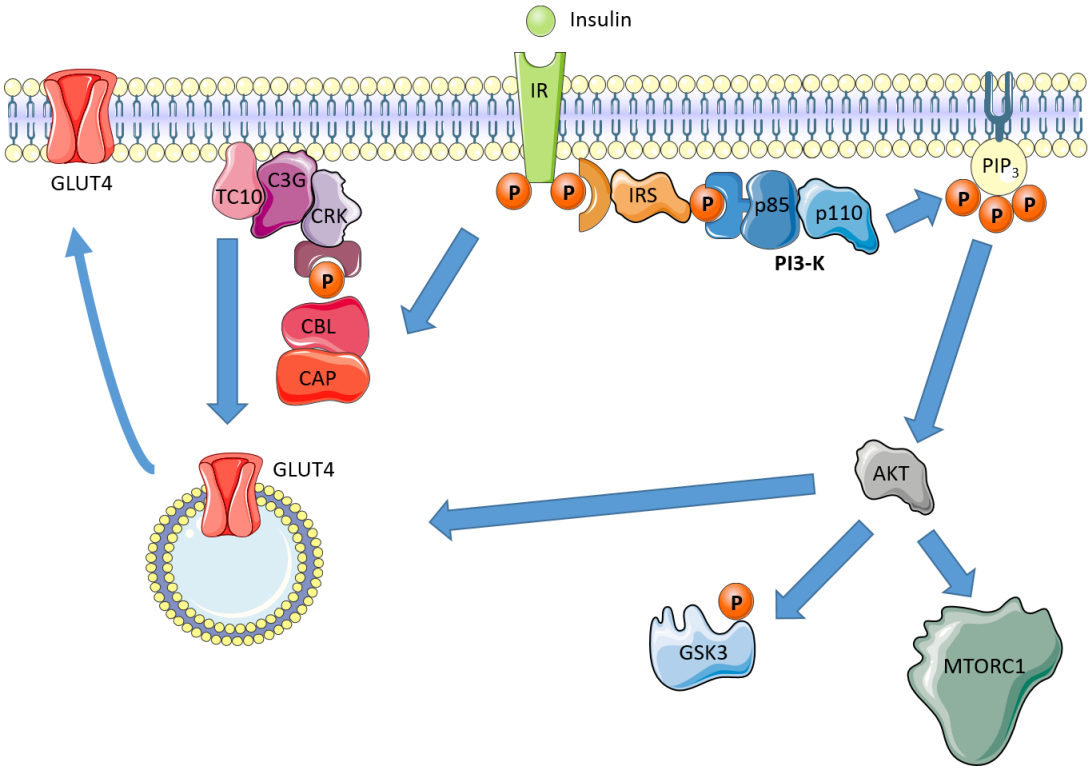

Figure 1.1: The insulin signalling pathway. Insulin binds to the insulin receptor (IR), stimulating its phosphorylation and the recruitment of IRS proteins. Phosphorylated IRS is recognised by the PI3-K heterodimer, leading to the triphosphorylation of phosphatidylinositol (PI) and the formation of the second messenger phosphatidylinositol 3,4,5-phosphate (PIP_3). PIP_3 activates AKT, which is important in stimulating the recruitment of GLUT4-containing vesicles to the plasma membrane to enhance glucose uptake. AKT also phosphorylates GSK3, increasing glycogen synthesis, and mTORC1 to increase fatty acid synthesis. Separately, phosphorylation of the insulin receptor stimulates, via the CBL/CAP heterodimer, the recruitment of a multi-protein complex to microdomains in the plasma membrane. TC10 then also increases the recruitment of GLUT4 to the plasma membrane [405].

1.1.2 Insulin and skeletal muscle

The tissue of focus in this thesis is skeletal muscle, the primary site for glucose uptake from the blood in healthy individuals [31]. In fasting conditions, insulin concentrations in the blood are low, and so plasma free fatty acid (FFA) concentrations are high as a result of uninhibited adipose lipolysis [32]. In these conditions, skeletal muscle is dependent on fatty acid oxidation for ATP generation, but this shifts following feeding. Increases in blood glucose stimulate the release of insulin, inhibiting adipose lipolysis and reducing plasma FFA concentrations. Insulin stimulates skeletal muscle glucose uptake and utilisation, while muscle fatty acid oxidation reduces as a consequence of diminishing plasma FFA concentrations. In this way,

insulin switches the skeletal muscle fuel source from fatty acids to glucose in healthy individuals. In response to insulin, approximately 70% of glucose is converted to glycogen, with the remaining fraction oxidised [33]. Insulin is a crucial hormone in the regulation of skeletal muscle metabolism, and so resistance to insulin signalling has profound metabolic consequences, leading ultimately to T2DM. One study by DeFronzo and colleagues highlighted impairment of skeletal muscle insulin sensitivity in T2DM patients [34]. Total glucose metabolism was reduced by 38% in T2DM patients, while glucose uptake in the leg (primarily by skeletal muscle) was 45% lower in patients compared to healthy controls. The importance of skeletal muscle in glucose disposal places the tissue at the centre of blood glucose homeostasis. Detailed understanding of mechanisms underpinning insulin resistance is, therefore, imperative to improve therapeutics for T2DM patients.

1.1.3 Mechanisms of insulin resistance

Obesity is the leading risk factor for T2DM, thought to be, in part, as a result of adipose dysfunction and the 'overspill' of lipids into other tissues (ectopic lipid deposition). Obesity is associated with an increase in basal lipolysis in adipose tissue, which is reduced following weight loss [35,36]. Dysfunctional lipolysis is enhanced in insulin resistance, preventing the insulin-induced reduction in lipolytic activity in adipocytes [37,38]. Elevated lipolysis results in an increase in release of FFAs from the adipose tissue, with research showing that obese individuals have increased concentrations of FFAs in their plasma [39]. The theory of lipotoxicity links raised plasma FFAs with insulin resistance in peripheral tissues.

1.1.4 Lipotoxicity and metabolic dysfunction

Lipotoxicity is defined as the inappropriate accumulation of lipids in peripheral tissues, leading to cellular dysfunction and insulin resistance [40,41]. This mechanism was initially suggested by Randle and colleagues in a study showing intracellular glucose-6-phosphate increases as a result of incubating rodent heart with fatty acids [42]. They postulated that this was a result of decreased glycolysis, although further studies have indicated that lipid-induced insulin resistance may arise due to impaired insulin signalling and, as a consequence, reduced glucose uptake [43,44]. A number of studies have investigated this phenomenon. Increasing plasma FFA concentrations for 9 healthy volunteers decreased glucose uptake and

glycogen synthesis in skeletal muscle by 46% and 50%, respectively [45]. In a separate study, plasma free fatty acid concentrations were increased by infusion of three different concentrations of Liposyn, a fat emulsion administered intravenously, in healthy individuals. Insulin-stimulated glucose uptake was decreased dose-responsively with increases in plasma FFA concentrations, while skeletal muscle markers of insulin resistance, such as a reduction in phosphorylation of the insulin receptor and Akt, were increased [46]. Similarly, acutely lowering plasma FFA levels with Acipimox, an inhibitor of lipolysis, improved insulin sensitivity and insulin-stimulated glucose uptake in obese individuals [47].

Fatty acids, the building blocks of more complex lipids, comprise a hydrocarbon chain of varying length and saturation, bonded to a carboxylic acid group. Unsaturated fatty acids contain one or more carbon-carbon double bonds (C=C). Differences in fatty acid chain length and saturation can have a profound effect on the shape and structure of the complex lipid they are a part of. For example, increases in the proportion of saturated fatty acids in membrane phospholipids can decrease the fluidity of the membrane [48]. Fatty acids are also substrates for mitochondrial β-oxidation, producing acetyl CoA that feeds in to the tricarboxylic acid cycle, and NADH and $FADH_2$ that transport electrons to the electron transport chain [49]. Metabolism of fatty acids is also important in the generation of signalling molecules, such as eicosanoids – a group of bioactive lipids formed by the oxidation of polyunsaturated fatty acids (PUFAs) [50]. However, research suggests not all fatty acids are equal in metabolic disease, with saturated fatty acids in the plasma, such as palmitate, the predominant drivers of fatty acid-induced lipotoxicity [51]. Exposure of immortalized mouse C2C12 myotubes to palmitate reduced insulin-stimulated glycogen synthesis and inhibited phosphorylation and activation of AKT and GSK3, while the monounsaturated fatty acid oleate had no effect [52]. In a separate study, treatment of rat L6 myotubes with palmitate decreased insulin signalling and glucose uptake, while exposure to the monounsaturated fatty acid palmitoleate showed increases in glucose uptake and glycogen synthesis [53]. Co-treatment of skeletal muscle cells with oleate and palmitate ameliorated palmitate-induced insulin resistance and inflammation [54]. Similarly diets enriched in the polyunsaturated fatty acid linolenic or oleic acid improved high fat diet-induced insulin resistance in mice [55,56].

Mechanisms underpinning lipotoxicity implicate the synthesis of bioactive lipid intermediates including ceramides and DGs [57]. Ceramides and DGs accumulate in adipocytes, myocytes and hepatocytes following acute exposure to palmitate, inducing insulin resistance via protein kinase C (PKC) isoforms [52,58–61]. Evidence supporting a role for DGs in the development of

insulin resistance is convincing in liver tissue, with DG levels and PKCε activity correlating negatively with insulin sensitivity, while knockdown of PKCε in the liver protects against lipid-induced insulin resistance [62]. Mechanisms underpinning the link between DG concentrations, PKC activation and insulin resistance centre on the phosphorylation of IRS-1 (**Figure 1.2A**) [63]. Activation of PKCθ leads to phosphorylation of IRS1 on serine 307, via c-JUN N-terminal kinase (JNK), and serine 1101 [64,65]. This inhibits tyrosine phosphorylation and prevents activation of PI3K, thereby reducing insulin sensitivity. Similarly, PKCε has been shown to phosphorylate serine 636 and 639 to inhibit IRS1 activation [66]. The importance of PKC-mediated IRS1 phosphorylation was highlighted in a study in which serine 302, 307 and 612 were all mutated to alanine, preventing inhibitory phosphorylation [67]. These mice were partially protected from diet-induced insulin resistance.

However, the importance of DG signalling in the control of skeletal muscle insulin sensitivity is questioned since DG content fails to correlate with insulin resistance in a number of different studies [68–70]. Instead, research points to ceramides as the important lipotoxic mediators in skeletal muscle. Ceramides accumulate in the skeletal muscle of mice fed a high fat diet, and plasma concentrations correlate with insulin resistance in T2DM patients [71,72]. Targeting serine palmitoyl transferase (SPT), which catalyses the first step in ceramide biosynthesis, with myriocin, improves insulin sensitivity in mice fed a high fat diet [73]. Mechanisms underpinning ceramide-induced insulin resistance focus on the inhibition of AKT/PKB activity, a key player in the insulin signalling pathway, through activation of PKCζ or the phosphatase PP2A (**Figure 1.2B**) [63]. Ceramides bind PKCζ, and the activated kinase then phosphorylates AKT on threonine 34 [74,75]. This prevents recruitment of AKT to the plasma membrane upon insulin receptor activation. Furthermore, myriocin treatment also alleviated PKB inhibition following palmitate treatment [52,74]. PP2A, on the other hand, is a phosphatase that dephosphorylates AKT, preventing its activation. Ceramides can bind allosterically and activate PP2A, while inhibition of PP2A with okadaic acid ameliorated palmitate-induced insulin resistance in C2C12 myotubes [76]. Ceramides can also negatively impact on the insulin signalling pathway through the kinases JNK and inhibitor of nuclear factor kappa-B kinase subunit β (IKKβ), which phosphorylate IRS1 on serine 312 [77].

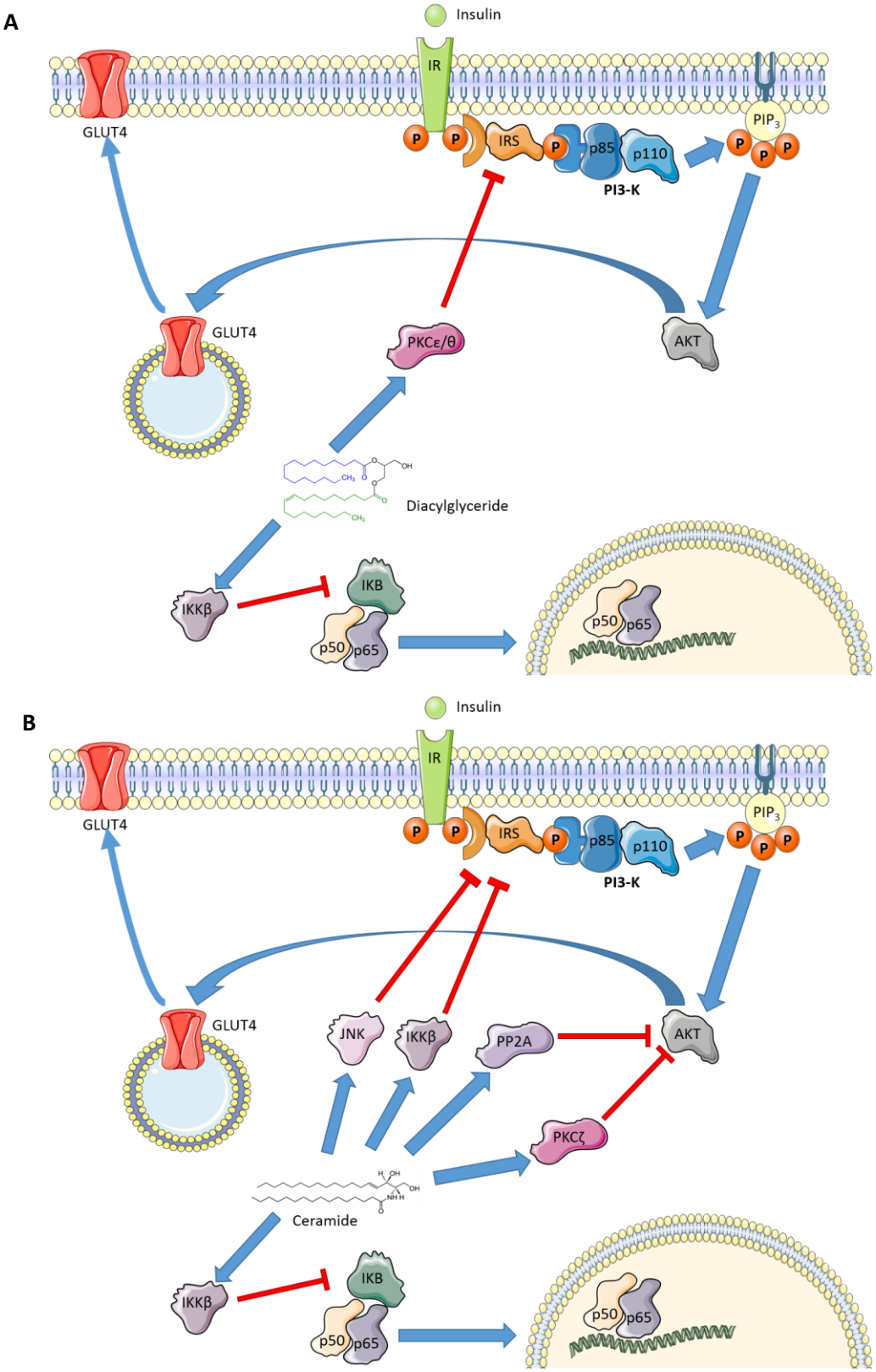

Figure 1.2: (A) Diacylglyceride (DG)-mediated lipotoxicity. DGs can activate PKCθ and PKCε, which phosphorylate and inhibit activation of IRS1 proteins. This disrupts downstream signalling from the insulin receptor. (B) Ceramide-induced lipotoxicity. Ceramide-mediated inhibition of the insulin signalling pathway occurs through multiple mechanisms. Ceramides activate both PP2A and PKCζ, which inhibit AKT activity. Activation of JNK and IKKβ, on the other hand, leads to the inhibition of IRS1. Both DGs and ceramides can also increase IKKβ activity, which leads to the degradation of IKB and activation of the NF-κB complex, comprising p50 and p65. NF-κB can then translocate to the nucleus and increase the transcription of pro-inflammatory genes [405].

1.1.5 Lipotoxicity and Chronic Inflammation

Lipotoxicity is closely integrated with chronic inflammation, now considered a hallmark of metabolic disease [78]. Obese individuals have increased plasma concentrations of pro-inflammatory cytokines such as tumour necrosis factor α (TNFα), interleukins (ILs) 1 and 6, and C-C motif chemokine ligand 2 (CCL2, also known as monocyte chemoattractant protein 1) [79]. Furthermore, lipid/heparin infusion, which raised plasma FFA concentrations, increased the activity of pro-inflammatory nuclear factor-kappa B (NF-κB) in skeletal muscle and liver [80,81]. Palmitate increases the levels of pro-inflammatory cytokines such as TNFα and IL-6 in cultured adipocytes, myocytes and hepatocytes, while knockdown of TNFα ameliorates palmitate-induced insulin resistance in C2C12 cells [82–84]. Plasma ceramides contained in LDL increase skeletal muscle inflammation, and palmitate-induced synthesis of ceramides is dependent on the inflammatory Toll-like receptor 4 (TLR4) [85,86]. Furthermore, ceramides and DGs can activate IKKβ, which triggers the degradation of IKB and the translocation of the NF-κB complex to the nucleus (**Figure 1.2**) [77,80]. Activated NF-κB increases the expression of pro-inflammatory cytokines that include TNFα, IL-1β and IL-6 [87].

Immune cells, particularly macrophages, respond to these cytokine signalling cues, infiltrating peripheral tissues [88–91]. This environment can then alter the phenotype of accumulating macrophages, with consequences for insulin resistance [92]. The concept of macrophage activation (also termed polarisation) and its associated nomenclature is controversial [93]. Traditionally, the activation of macrophages is considered as classical (M1) or alternative (M2) [94]. Classical activation is defined as a pro-inflammatory phenotype, characterised by increases in inflammatory cytokines such as TNFα and IL6, as well as an increase in nitric oxide (NO). Alternatively activated macrophages are considered anti-inflammatory with decreased cytokine secretion and increased activity of arginase 1, reducing nitric oxide availability. However, the concept of only two distinct macrophage activation states is now considered an oversimplification [95]. Instead, macrophages are now considered across a spectrum of phenotypes, and the M1 and M2 definitions better describe properties of pathways that interact to give the macrophage phenotype.

The importance of macrophage phenotype in the development of insulin resistance has been highlighted in a number of studies. CD11c+ proinflammatory macrophages accumulated in the skeletal muscle of mice fed a high fat diet, correlating with insulin resistance, while CCL2-KO mice did not have increased macrophage numbers and maintained insulin

sensitivity [91]. Overexpression of CCL2 in murine adipose tissue increased macrophage infiltration and induced insulin resistance, while expression of a mutant CCL2 ameliorated diet-induced insulin resistance [96]. The secretion of pro-inflammatory cytokines from activated macrophages can induce insulin resistance in adipocytes, highlighting the role these cytokines play in bi-directional cross-talk between peripheral tissues and the immune system (**Figure 1.3**). For example, IL-1β, secreted from pro-inflammatory macrophages, induces insulin resistance in human primary adipocytes, concurrent with an increase in synthesis and secretion of IL-6 and CCL2 [97]. Conversely, macrophages that exhibit a predominantly M2 phenotype confer protection against the development of insulin resistance [98]. Furthermore, palmitate can directly activate immune cells, further enhancing lipid-induced inflammation [99,100]. Macrophages treated with palmitate have increased CD11b expression, as well as higher reactive oxygen species and disrupted oxidative phosphorylation [101]. In a separate study, palmitate treatment increased secretion of pro-inflammatory cytokines from macrophages, including TNFα and IL-6 [102]. Conditioned media from these palmitate-treated macrophages was also capable of inducing insulin resistance in myotubes, highlighting that the deleterious effects of palmitate on insulin sensitivity in peripheral tissues result from the direct lipotoxic insult, as well as a changing inflammatory environment.

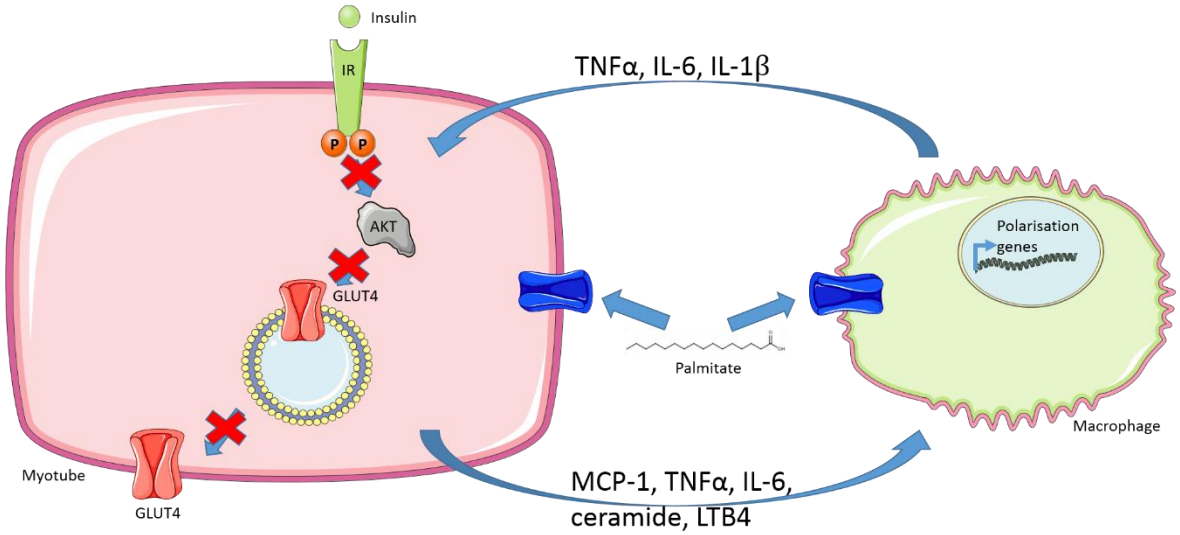

Figure 1.3: Macrophage cross-talk in metabolic disease. Palmitate treatment increase the secretion of pro-inflammatory cytokines from insulin-sensitive cells such as myotubes, adipocytes and hepatocytes. Macrophages respond to these signalling cues, infiltrating peripheral tissues. The increase in cytokine secretion, coupled with exposure to palmitate, also induces a switch in macrophage polarisation towards a pro-inflammatory phenotype. Activated macrophages increase expression and secretion of pro-inflammatory cytokines that can act on peripheral tissues, disrupting insulin signalling and further enhancing the activation of inflammatory pathways [405].

The evidence supporting roles for lipotoxicity and inflammation in the development of insulin resistance is strong. Nonetheless, it is one contributing mechanism in a complex multi-factorial disease. With the prevalence of obesity and T2DM on the rise, impacting the quality of life of those affected and increasing the burden on health services, there is a growing need to determine the mechanisms underpinning other aspects of these diseases. Endoplasmic reticulum (ER) stress has recently emerged as a potentially important mechanism that drives the pathological changes associated with aspects of the metabolic syndrome [103,104].

1.2 The endoplasmic reticulum

The ER is the largest organelle in the cell and responsible for numerous cellular functions including protein folding, oligomer assembly, protein modifications, lipid metabolism, and calcium storage, as well as directing proteins into the secretory pathway [105]. It is composed of membrane-bound branching tubules and flattened sacs, with a membrane that is continuous with the nuclear envelope and encloses the ER lumen [106]. The structure of the ER is dynamic, with this diverse set of roles performed in distinct microdomains specialised for each function [107].

One of the primary functions of the ER is the control of protein homeostasis, including the regulation of protein synthesis and folding. ER-bound ribosomes synthesise integral membrane and secretory proteins, with nascent protein chains co-translationally translocated across the ER membrane [108]. Integral membrane proteins contain a stretch of hydrophobic residues that delay translation during translocation and anchor it in the ER membrane, before the completion of synthesis [109]. Following translocation, secretory proteins are folded into their native structure and modified, such as with N-linked glycosylation or the formation of disulphide bonds [110]. Chaperones, co-chaperones and protein disulphide isomerases aid in this process, providing an environment favourable to protein folding [110]. Recent studies have also shown the accumulation of mRNAs encoding cytosolic proteins on ribosomes attached to the ER, implicating the ER in the translation of a portion of cytosolic proteins [111,112].

In addition to protein synthesis, the ER is crucial to the biogenesis of lipids, particularly membrane lipids. The synthesis of glycerolipids, including phosphatidylcholines (PCs), phosphatidylethanolamines (PEs), phosphatidylinositols (PIs) and phosphatidylserines (PSs)

all take place in the ER, as well as the synthesis of sphingolipids such as ceramides [113]. Furthermore, the mevalonate pathway, leading to the synthesis of cholesterol and other sterols, also takes place in the ER [114,115]. ER-synthesised lipids are then distributed throughout the cell via vesicles or lipid-protein transporters [116]. Lipids can be modified in other cellular compartments, such as the conversion of ceramides to glucosyl- and lactosyl-ceramides, or sphingomyelin, in the Golgi following the transport of ceramides by the ceramide transfer protein (CERT) [117].

Beyond protein and lipid synthesis, the ER is also an essential store of calcium ions (Ca^{2+}), with concentrations much higher in the lumen of the ER compared to the cytosol (100-800 µM vs. 100 nM) [118–120]. Ca^{2+} is an important mediator of inositol 1,4,5-triphosphate (IP_3) secondary messenger signalling pathways and crucial in the regulation of protein function and localisation [121]. Chaperones bind Ca^{2+} as a cofactor and the ion is required for the correct functioning of the proteins [122]. It is therefore crucial that ion levels are tightly regulated by the ER, ensuring fidelity of signalling pathways and protein folding. Calcium concentrations are regulated by ER calcium channels, ryanodine receptors, which are activated in response to elevated Ca^{2+}, and IP_3 receptors, which are stimulated by IP_3 following phospholipase C activation [123].

1.2.1 The unfolded protein response

With such a crucial role in cellular function and protein homeostasis, it's important that the ER can adapt to changing environments that place stress upon the organelle. In particular ER stress arises from the accumulation of unfolded proteins and triggers the unfolded protein response (UPR), a protective signalling cascade [124]. Multiple stimuli have been documented to induce ER stress, impinging on the protein folding capabilities of the ER. These include glucose deprivation, exposure to high concentrations of plasma lipid, disruption of Ca^{2+} ion homeostasis, hypoxia, and changes in the redox state of the ER [125].

Activation of the UPR improves protein folding conditions and reduces protein load on the ER, alleviating stress. The UPR signalling pathway consists of three distinct arms, mediated by protein kinase R-like endoplasmic reticulum kinase (PERK), inositol requiring enzyme 1 (IRE1), and activating transcription factor 6 (ATF6) [126] (**Figure 1.4**). These three proteins are maintained in an inactive state by the chaperone glucose regulated protein 78 kDa (GRP78) (also known as BiP). GRP78 dissociates from the UPR signalling molecules to bind to

accumulating misfolded proteins. This triggers their activation, combining the detection of ER stress with the instigation of the UPR.

Upon activation, PERK oligomerises and phosphorylates both itself and eukaryotic initiation factor 2α (eIF2α), inhibiting protein translation [127]. By reducing protein translation the protein load on the stressed ER is lowered. However, some transcripts, such as the activating transcription factor 4 (ATF4) mRNA, contain an internal ribosome entry site (IRES) and so are exempt from translational repression imparted by PERK activation [128]. ATF4 is a transcription factor whose targets include C/EBP-homologous protein (CHOP) and growth arrest and DNA damage-inducible 34 (GADD34) [129,130]. CHOP is a pro-apoptotic transcription factor, implicating the PERK arm of the UPR in the regulation of programmed cell death following unresolved ER stress [131]. Other targets of ATF4 include protein folding and antioxidant genes to improve the protein folding environment of the ER [132,133].

IRE1 has both kinase and endoribonuclease functions. Following activation and oligomerisation, IRE1 splices x-box binding protein 1 (XBP1) mRNA, producing a basic leucine zipper transcription factor that increases expression of numerous UPR genes responsible for heightening protein folding, secretion and degradation capabilities [134,135]. ER-associated degradation (ERAD) removes misfolded proteins from the ER lumen via ubiquitination and proteasomal degradation [136]. IRE1 also cleaves the ER-localised mRNA of many secretory proteins in a pathway termed regulated IRE1-dependent decay (RIDD), thus reducing the protein load on the ER [137].

The activation of the IRE1 arm of the UPR is also closely integrated with nutrient availability, and metabolic regulation. Forced expression of spliced XBP1 increases levels of phosphatidylcholines, an important phospholipid of the ER membrane, and membrane surface area [138]. XBP1 splicing is also dependent on mTORC1 pathway, which is crucial in nutrient sensing and energy availability [139]. Inhibition of mTORC1 with rapamycin reduced diet-induced activation of IRE1 and XBP1 in rats [140].

Activated ATF6 is transported to the Golgi where it is processed by two site specific serine proteases to release its cytosolic domain [141]. The cytosolic domain then translocates to the nucleus, activating the transcription of UPR target genes. These genes include chaperones such as BiP and glucose regulated protein 94 (GRP94) that aid in protein folding by providing a stable environment in which to fold [142,143]. ATF6 also increases the expression of protein disulphide isomerase (PDI), which aids in the formation of disulphide bonds in

secreted proteins – one of the rate-limiting steps in protein folding [144]. ATF6-null mice have also shown the transcription factor to be important in protecting cells from chronic stresses [145].

Recent work has demonstrated the induction of ER stress can be controlled in an endocrine manner, with the activation of ER stress in one tissue leading to the induction of the UPR in a distal tissue [146]. Studies have highlighted the ability of prostate cancer cells and mammary carcinoma cells to transmit ER stress to neighbouring macrophages, concomitant with a switch to a pro-inflammatory and pro-angiogenic macrophage phenotype [147,148] . This remodelling of macrophage phenotype implicates the cell non-autonomous transmission of ER stress in tumour progression. In a separate study, constitutive expression of spliced XBP1 in the neuronal tissue of *C. elegans* induced ER stress in intestinal cells and increased longevity of the animals by 32% [149]. This work also translates to mouse models, in which constitutive expression of spliced XBP1 in neurons induced ER stress in hepatocytes, whilst also ameliorating diet-induced adiposity and insulin resistance [150]. This final study highlights that cell nonautonomous control of ER stress has implication for metabolic disease, but remains understudied at this point.

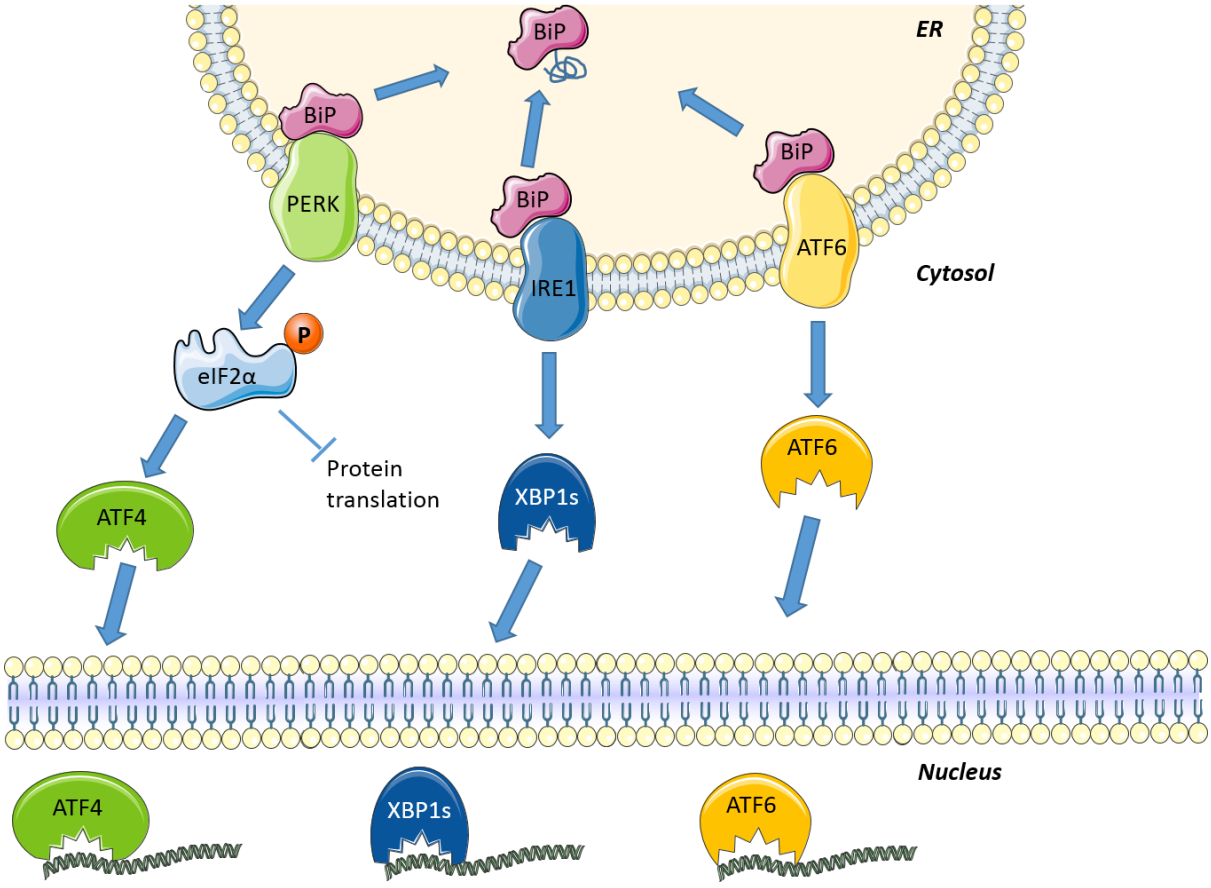

Figure 1.4: The unfolded protein response (UPR) consists of three signalling pathways, mediated by PERK, IRE1 and ATF6. Upon the accumulation of unfolded proteins, BiP dissociates from the luminal domains of PERK, IRE1, and ATF6, activating the UPR. PERK phosphorylates eIF2α, inhibiting translation and concomitantly activating the IRES-containing transcription factor, ATF4. IRE1 splices XBP1, with the spliced transcript producing a transcription factor that activates expression of UPR target genes. ATF6, upon activation, is processed in the Golgi before translocating to the nucleus and increasing expression of genes including XBP1, CHOP and ER chaperones [405].

1.2.2 Endoplasmic reticulum stress and the metabolic syndrome

Beyond its role in proteostasis, the ER is also an important site for lipid metabolism [151]. In particular, the smooth ER is responsible for the synthesis of phospholipids, cholesterol and ceramides [152]. The accumulation of lipids and dysregulation of lipid homeostasis underpins several cardiometabolic risk factors of the metabolic syndrome, and is a well-documented cause of insulin resistance [153]. Thus, it's suggested that disruption of ER homeostasis, and the subsequent activation of the UPR, may impact upon lipid metabolism and contribute to the dyslipidaemia associated with obesity and T2DM [151,154]. Recent work, establishing that elements of the UPR can affect energy homeostasis, insulin sensitivity and lipid metabolism

supports this hypothesis. Mice defective for eIF2α phosphorylation exhibited hypoglycaemia, increased insulin sensitivity and decreased liver glycogen stores [155]. When fed a high-fat diet, these eIF2α-null mice had reduced hepatosteatosis and greater insulin sensitivity when compared to the wild-type mice. Furthermore, these mice exhibited reduced liver expression of peroxisome proliferator-activated receptor γ (PPARγ), a ligand activated nuclear receptor and master regulator of lipid metabolism [156].

ATF4 has also been shown to have an important role in metabolism. ATF4-knockout (KO) mice have reduced WAT, decreased lipogenic gene expression and increased β-oxidation in the WAT [157]. These mice also had increased expression of uncoupling protein 2 (UCP2) in WAT and UCP1, 2 and 3 in brown adipose tissue, implying an increase in fatty acid utilisation and thermogenesis. Expression of ATF4 decreases insulin sensitivity in skeletal muscle, adipose tissue and the liver [158].

IRE1 has been observed to participate in hepatic lipid metabolism and may have a protective effect against ER-stress induced hepatic steatosis [159]. Hepactocyte-specific-IRE1α-KO mice exhibited altered lipid metabolism when treated with the canonical inducer of ER stress, tunicamycin. IRE1α hepatic-null mice had enhanced steatosis and reduced concentration of plasma lipids, accompanied by a reduction in apoB-containing lipoprotein secretion, and an increased expression of the lipogenic genes. These transcriptional changes fell into three categories, with increases in: 1) C/EBP transcription factors and PPARγ; 2) adipose differentiation-related protein (ADRP) and fat-storage inducing transmembrane proteins (FIT) 1 and 2; 3) triglyceride biosynthesis enzymes (DGAT 1 and 2, SCD1, and ACC1). However, it is unclear whether the lack of IRE1 *per se*, or prolonged ER stress as a result of the IRE1-KO, triggered the induction of lipogenic genes and the accumulation of lipid within hepatocytes.

Furthermore, ATF6 has been proposed to antagonise sterol regulatory-element binding protein 2 (SREBP2)-mediated lipogenesis. Tunicamycin-induced ER stress in ATF6-KO mice stimulated the accumulation of neutral lipids, including TGs and cholesterol [160]. These changes were ascribed to increased lipid droplet formation as a result of reduced fatty acid β-oxidation, inhibited VLDL formation and an increase in expression of ADRP. In an analogous situation to the IRE-1 null mouse model, it is unclear whether ATF6 is directly protective, or the loss of the transcription factor leads to prolonged ER stress that underpins the metabolic dysregulation observed.

The interaction between ER stress and metabolic perturbation is bidirectional. While ER stress disrupts lipid metabolism, dysregulation of lipid metabolism can also trigger ER stress, thus forming a self-reinforcing circuit. Mouse models of obesity, including the leptin null Ob/Ob mouse, and mice fed a high-fat diet, exhibit increases in PERK and IRE-1 phosphorylation in adipose tissue and the liver [103]. Similar associations are observed in humans, with Boden and Merali demonstrating an upregulation of ER stress proteins in the adipose tissue of obese individuals compared to lean [161]. There is a positive correlation between body mass index (BMI) and ER stress markers in human subcutaneous adipose tissue [162]. There is also a reduction in ER stress markers in the liver and adipose tissue of obese patients following gastric-band surgery and weight loss [163]. Treatment of humans with sodium phenylbutyrate (4-PBA), a chemical chaperone that improves protein folding, partially alleviated lipid-induced insulin resistance and beta-cell dysfunction [164].

1.2.3 Free fatty acids as inducers of endoplasmic reticulum stress

High-fat diets elevate plasma FFA concentrations [165,166], and these FFAs and dyslipidaemia contribute to whole-body insulin resistance [167]. The treatment of cells and tissues with the fatty acid, palmitate, has been employed as a model to understand the underlying mechanisms of lipid-induced insulin resistance [168,169]. ER stress has been identified as an underlying mechanism behind palmitate-induced insulin resistance in skeletal muscle, adipocytes and hepatocytes [170–172]. Both overexpressing the chaperone protein, BiP, and knocking down expression of PERK attenuated palmitate-induced cell death in liver cells [173,174]. Recent work has highlighted phospholipid bilayer composition as a potential mechanism linking palmitate loading with ER stress in liver. Overexpressing Lpcat3 increased the incorporation of polyunsaturated fatty acids (PUFAs) into phospholipids and ameliorated palmitate-induced ER stress [175]. Elegant work by Fu *et al.* focused on the lipid content of the ER itself, analysing fractionated ER from lean and obese liver tissue from mice. The ER was subjected to comparative proteomic and lipidomic analysis, with the results highlighting a switch from protein to lipid synthesis in the ER. The study highlighted remodelling of ER phospholipids, which incorporated increased amounts of *de novo* synthesised saturated fatty acids in obese livers at the cost of polyunsaturated fatty acids from the diet. Furthermore, they demonstrated that an increase in the phosphatidylcholine/phosphatidylethanolamine (PC/PE) ratio disrupted the functioning of the sarco/endoplasmic reticulum calcium ATPase (SERCA) pump.

Correcting the PC/PE ratio by knocking down *Pemt*, which codes for phosphatidylethanolamine N-methyltransferase, the enzyme that converts PE to PC, in obese mice reduced ER stress and improved glucose homeostasis [176]. This work highlights the potential importance of the lipidome in mediating palmitate-induced ER stress.

Palmitate also induces ER stress in adipocytes, while treatment of adipocytes with TUDCA reduces palmitate-induced inflammation and improves insulin signalling [171,177]. Similarly, inhibition of mTORC1 with rapamycin alleviated palmitate-induced ER stress in adipocytes, via an autophagy-dependent mechanism [178]. In the same study rapamycin also decreased palmitate-induced inflammation, with reduced nuclear translocation of NF-κB and decreased secretion of CCL2 and IL6, suggesting an important role for mTOR signalling in palmitate-induced ER stress and inflammation.

While evidence supporting a role for palmitate-induced ER stress in the liver and adipose tissue is strong, the argument is unclear in skeletal muscle. Treatment of human myotubes with palmitate is associated with increases in UPR markers and this induction is prevented with overexpression of SCD1 [179], which also highlights the potential benefits of fatty acid desaturation in palmitate-induced ER stress and lipotoxicity. Alleviating ER stress using oleate or AMPK/PPARδ activation also ameliorated insulin resistance and inflammation, further implicating ER stress as a connecting mechanism between palmitate and insulin resistance [54,180]. However, this work is contradicted by research demonstrating that chemical chaperones do not improve palmitate-induced insulin resistance [181].

With ER stress markers correlating with obesity, and cell culture and rodent experiments highlighting the mechanistic importance of saturated fatty acid-induced ER stress in the development of lipid-induced insulin resistance, it is important to dissect the effects of ER stress on lipid metabolism in detail. In this way, the contribution of ER stress to the pathologies of obesity and T2DM can be assessed, leading to the identification of potential novel therapeutic targets and strategies. The use of metabolomics and lipidomics can provide a detailed metabolic snapshot, highlighting pathway alterations following the induction of ER stress. This may provide novel insights into the mechanisms underpinning ER stress, dyslipidaemia and insulin resistance.

1.3 Metabolomics and lipidomics

1.3.1 The omics revolution

The term ‘omics’ refers to technologies that allow for the untargeted profiling of molecules in biological samples, which has led to a vast number of applications [182]. This term now encompasses the study of genes (genomics), genetic modifications (epigenomics), mRNA (transcriptomics), proteins (proteomics), and metabolites (metabolomics), including the fast-growing field of lipidomics – the study of lipid metabolism (**Figure 1.5**) [183]. The use and integration of these techniques can provide insight in to disrupted biochemical pathways that underpin disease progression, as well as markers that delineate between healthy and diseased populations [184]. Progress in the field has been driven by rapid advances in technology, highlighted by the improvements in DNA sequencing over the last 50 years and the subsequent impact on the field of genomics [185]. First generation sequencers that used a modified “Sanger sequencing” technique were capable of read lengths less than one kilobase long. Utilised as part of a shotgun sequencing method, these machines were crucial in the Human Genome Project, and the sequencing of the first human genome. Now with the advent of third generation sequencers, read lengths are in excess of 10 kb, aiding in genome assembly, at a much lower cost [186]. Now similar technological advances in mass spectrometry allow for a more cost-effective and sensitive analysis of thousands of small molecule metabolites and proteins [187,188].

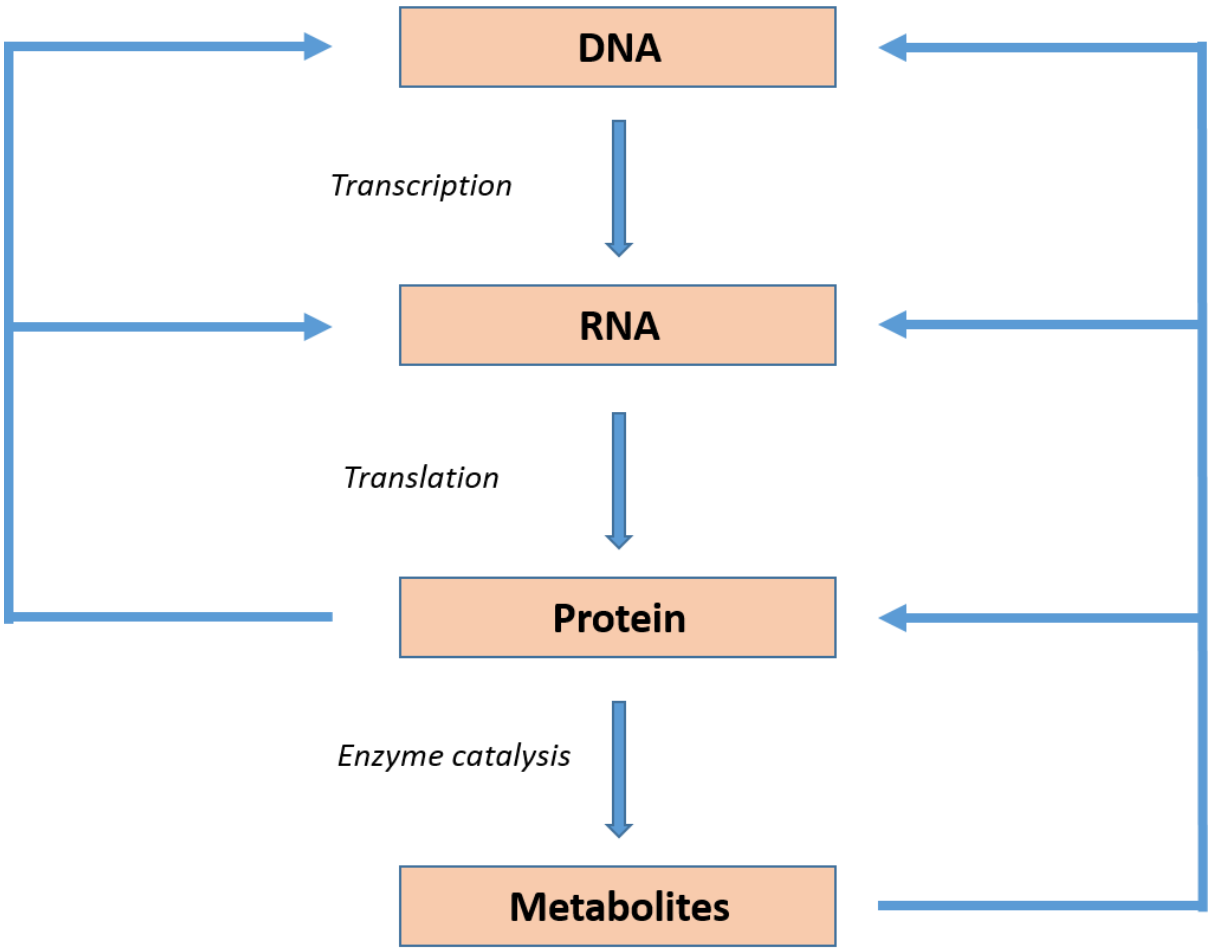

Figure 1.5: Omic techniques profile each layer of the central dogma and have aided our understanding of the interaction between each stage. This is no longer considered a simple linear pathway that begins at the genome and ends in the products of enzyme catalysis. Instead metabolites and proteins feedback into each preceding level, playing critical regulatory roles.

Understanding of biological systems is aided by the integration of multiple omic fields, each adding a complimentary layer of information to help sift through compensatory changes to the key pathway alterations that underpin disease states [183,189,190]. There are a number of different approaches in the design of multi-omic studies [183]. The "genome-first approach" uses genomics for the identification of loci arising from genome-wide association studies (GWAS) of particular diseases. Transcriptomics, proteomics and metabolomics can then be used to understand the causality of these variants and particular pathways that are altered to drive disease. However, the "phenotype-first" approach correlates omic data with observable or measurable aspects of disease to provide insight into disrupted pathways. The integration

of omic techniques is best utilised in the study of complex diseases, which have combined polygenic and environmental influences in their aetiology. The multi-faceted nature of metabolic disease makes it a prime candidate for omic analysis [1]. This thesis employs mass spectrometry-based lipidomics combined with RT-qPCR to understand mechanisms underpinning metabolic disease.

1.3.2 Metabolomics and lipidomics

Metabolomics refers to the study of metabolism at a system-wide level, measuring the small molecule complement of a range of different samples, including cells, tissues and biofluids [191–193]. It provides a global steady-state snapshot of the metabolic profile of a biological system and how this changes upon a shift in conditions, improving on the canonical biochemistry techniques of single metabolite or enzyme analysis, and thus making it ideal for the study of diseases in which metabolism is disrupted.

The analytical techniques commonly used in metabolomic studies include nuclear magnetic resonance (NMR) spectroscopy, and chromatography coupled mass spectrometric (MS) analysis, typically liquid chromatography (LC)- or gas chromatography (GC)-MS. Each technique provides both unique and overlapping information, with no one technique able to provide complete coverage of the metabolome [191]. NMR spectroscopy, although highly quantitative, suffers from comparatively poor sensitivity, covering a smaller range of metabolites compared to MS [194]. Thus this project makes use of MS-based platforms, allowing for the detection of a large number of metabolites across a broad range of concentrations [191].

The term lipidomics was first coined in 2003, and describes a set of techniques for the profiling of lipid metabolism [195]. Our understanding of lipids has evolved from the view of lipids as structural molecules important to the integrity of the cell to one that also places huge importance on the role they play in signalling and coordination of fundamental biochemical and cellular processes. The number of lipid species is predicted to be in the range of tens of thousands to hundreds of thousands [196]. With this, technological advancements have increased our ability to profile a vast range of lipid species using a variety of MS techniques. Below, the uses of GC-MS and LC-MS in lipidomics are discussed. It is important to note that direct infusion mass spectrometry (DI-MS), ion mobility mass spectrometry (IM-MS)

and mass spectrometry imaging are alternative lipidomic techniques, but are not utilised in this thesis and are not expanded upon here.

1.3.3 Gas chromatography-mass spectrometry

Developed over 60 years ago, GC-MS is an analytical technique employed commonly in the metabolomic field that aids in the separation and quantitation of analytes within a mixture [197]. Samples are vaporised and carried by an inert gas through a column during which compounds are separated through their interaction with a stationary phase. Analytes are then detected by a coupled mass spectrometer. Since samples are vaporised, it is important that analytes are volatile and thermally stable. In some cases, these properties can be enhanced by derivatisation – the chemical modification of analytes. GC-MS has been an important metabolomic platform for a number of decades, crucial to the analysis of low molecular weight compounds such as sugars, amino acids and fatty acids [198–202]. Below, the fundamentals of GC-MS will be discussed and its applications to lipidomic analysis in this thesis.

Typically, metabolites are extracted from samples of interest and dissolved in an organic solution. The sample is injected on to the GC instrument where it is vaporised immediately. An inert carrier gas, such as helium, then carries the sample to a capillary column, coated with a siloxane-based stationary phase [203]. Analytes interact with the stationary phase to varying degrees, based on chain length and desaturation, leading to their separation. The column is held in an oven with tight temperature control. The temperature is gradually increased, so analytes with lower boiling points elute first, providing an extra degree of separation.

The end of the GC column is interfaced with a mass spectrometer, connected by a heated transfer line, for identification and quantitation of analytes. The metabolites must be ionised to be detected, with electron ionisation the most commonly used method (**Figure 1.6**). This is a hard ionisation technique, which takes place in a high-vacuum ion source and leads to extensive fragmentation of the parent ion. Analytes are ionised using a fixed electron beam with a voltage of 70 eV. The electron beam is generated by a filament and collected by an electron trap. Analytes and electrons travel at right angles to one another, and the interaction between the two results in the loss of an electron and the generation of a positive ion under

the more commonly used positive ionisation mode. A magnet, with poles at opposite ends of the chamber, induces a spiral in the electron beam to increase interactions between electrons and analytes. Electron ionisation greatly increases the energy of the molecule and so leads to comprehensive fragmentation of the species of interest. This is useful for identification, with the fragmentation pattern of each compound providing important information on the structure of the molecule. Numerous databases, such as the NIST/EPA/NIH standard reference database, contain reference fragmentation spectra to aid in identification of compounds across different types and designs of GC-MS.

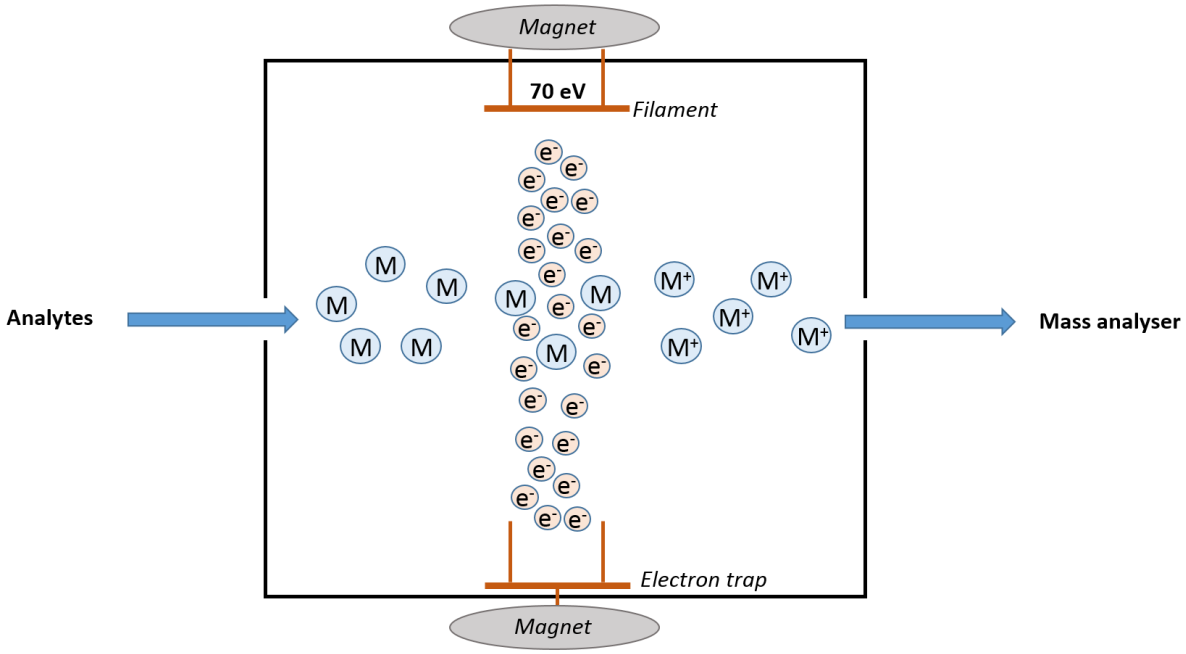

Figure 1.6: In electron ionisation, a beam of electrons is generated from a filament perpendicular to the direction of travel of analyte molecules. Interaction between electrons and analytes leads to the loss of an electron from the analyte, and the formation of a positive ion.

Following ionisation and fragmentation, ions are separated and detected in a mass analyser. In the case of this thesis, GC is coupled to a quadrupole mass analyser. Quadrupoles consist of four parallel rods, typically made of an inert alloy (**Figure 1.7**). Both a direct current (DC) and an alternating radio frequency (RF) potential are applied across the rods. These electric fields focus ions from the source to the detector. Only ions of a particular mass-to-charge (m/z) ratio can pass through the detector, based on the magnitude of the electric field – all other ions are deflected away. The detector generates an electrical signal that is proportional

to the abundance of the ions. By varying the RF, ions of different m/z ratios can be focused to the detector, resulting in a mass spectrum.

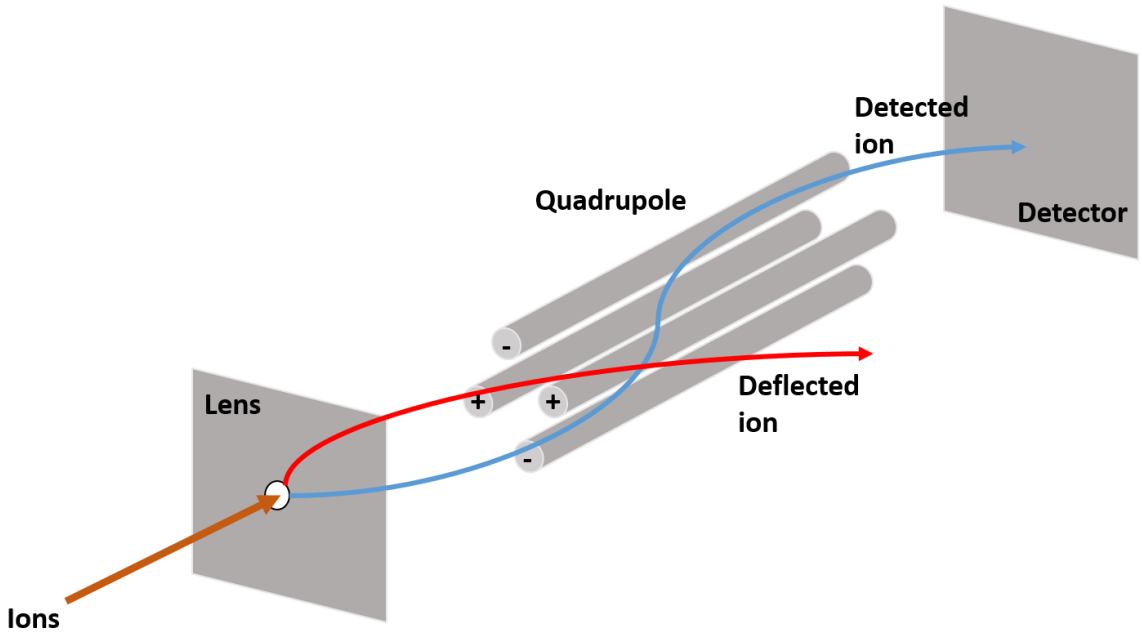

Figure 1.7: A quadrupole mass analyser, consisting of four parallel rods. DC and alternating radio frequency (RF) potentials are applied across the rods, focusing ions from the source to the detector. By varying the RF frequency, ions of a particular m/z ratio are focused to the detector.

In this thesis, GC-MS is employed for the analysis of fatty acids. Fatty acids are the key building blocks for lipids and, therefore, their measurement is important to understanding alterations in lipid metabolism. Fatty acids are commonly measured by GC-MS following their derivatisation to fatty acid methyl esters (FAMEs), a method first employed in 1956 [202]. The derivatisation improves the poor volatility of fatty acids that results from the polar carboxylic acid group [204]. A number of methods have been described for this process, but this thesis uses boron trifluoride (BF_3) in methanol as the catalyst (**Figure 1.8**) [205,206]. This derivatisation is an acid-catalysed transesterification, resulting in the hydrolysis of fatty acids from complex lipids. Therefore, GC-MS analysis is of the total fatty acid profile, providing a good overview of metabolism regardless of the complex lipid the fatty acid originated from.

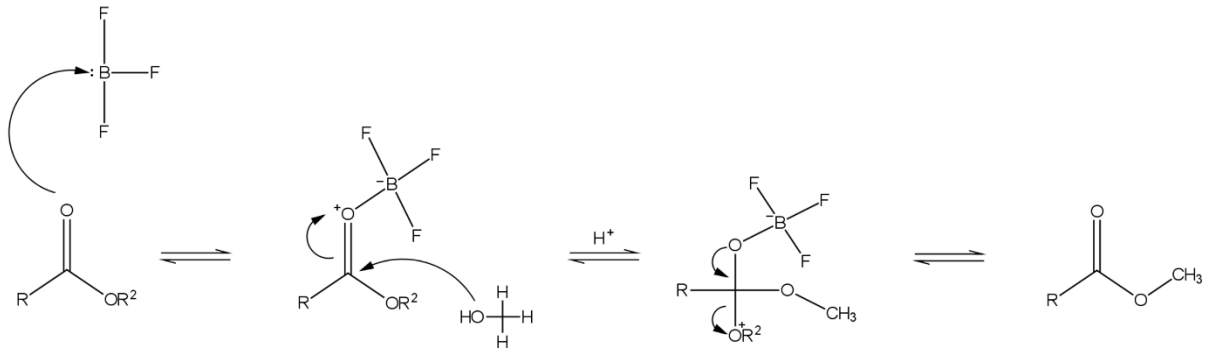

Figure 1.8: Fatty acids are hydrolysed from complex lipid and derivatised using a boron trifluoride (BF_3)-catalysed transesterification in methanol.

GC-MS is a highly robust and reproducible technique for metabolomics. Fragmentation of ions provides a characteristic fingerprint that is important in identifying metabolites and providing structural information on unknown compounds. However, the requirement for derivatisation is a drawback, increasing the workload required for sample analysis. While GC-MS is an excellent technique for analysis of the total fatty acid profile in biological samples, the derivatisation ensures that no information on the complex lipids that the detected fatty acids are a part of can be inferred. Furthermore, the quadrupole mass analyser has a limited mass range of 50-650.

1.3.4 Liquid chromatography-mass spectrometry

To increase coverage of the lipidome, LC-MS techniques can provide complementary information on intact lipids. Liquid chromatography is the most commonly used separation technique in metabolomics, largely due to the variety in columns that facilitates the analysis of a large number of physicochemically diverse metabolites [207]. The technique was pioneered in the early 1900s by a botanist, Mikhail Tswett, who used a column and different eluents to separate out pigments from a leaf, including the separation of chlorophylls a and b [208]. The technique has now evolved from LC through high-performance LC (HPLC) to ultra-high-performance LC (UHPLC) [209].

In LC systems, solvent (the mobile phase) is pumped by a solvent delivery system at a specific flow rate. An autosampler then injects the sample into this flowing solvent, which carries the sample to the column. The column is packed with a stationary phase that mediates separation of species based on a variety of factors including the pressure and temperature of

the column, the chemical properties of the column surface and eluent solvents utilised. Analytes then elute from the column and are detected by a mass spectrometer.

There are two types of solvent system that operate in LC [210]. With isocratic elution, the solvent remains the same throughout the run. In gradient elution, however, the solvent composition varies during the run. The solvent is varied to increase the elution of analytes that interact strongly with the stationary phase. The system used in this thesis makes use of a binary solvent system. In this two solvent system, solvent A is a weak solvent, eluting compounds that weakly interact with the stationary phase, and solvent B is a stronger solvent. The percentage of B is then gradually increased over time. Gradient elution is extremely useful for separating compounds across a wide-range of polarities, such as in the profiling of lipid species.

Column choice is critical in the separation of compounds. Increased column length and reduced particle size increase separation of compounds, but at a cost of increased pressure and longer run times. The choice of stationary and mobile phases are most important to efficient separation of analytes, with separation possible based on polarity, charge or size [211].

The two predominant classes of chromatography used in LC – normal phase liquid chromatography (NPLC) and reverse phase liquid chromatography (RPLC) – rely on separation of analytes based on polarity. In these systems, mobile and stationary phases have different polarities. A compound will therefore have a differing affinity with either the mobile or stationary phase depending on its polarity. If a compound has a greater affinity with the mobile phase, it will elute faster, but elution time is slower for those compounds with greater affinity for the stationary phase. In NPLC, the stationary phase is polar and the mobile phase is non-polar, while this is reversed in RPLC. A stationary phase comprising silica is extremely polar and used for NPLC, while modifications of this silica group, such as the addition of C18 carbon chain, greatly reduce the polarity for the use in RPLC. The latter is a common column used for the LC-MS analysis of lipids. A third separation based on polarity is hydrophilic-interaction chromatography (HILIC), a variant on NPLC that uses a slightly more polar mobile phase to increase elution of highly polar compounds.

Following separation by LC, analytes are detected by the coupled mass spectrometer. While GC-MS traditionally makes use of simple quadrupole analyser, LC-MS can incorporate a number of different spectrometers, each with their own advantages and disadvantages. For example, while robust and relatively low cost, the quadrupole has a small mass range and

poor resolution [212]. Hybrid mass spectrometers and orbitraps may be employed instead and are discussed below. Other mass analysers include time of flight (ToF) and quadrupole ion trap, which are not expanded upon here as they are not employed in this thesis, but are well reviewed elsewhere [212–215].

Most LC-MS systems rely on electrospray ionisation (ESI) to generate ions. The sample, dissolved in the mobile phase of the LC system, is sprayed from a thin needle into the ion source (**Figure 1.9**). A high electrical potential is applied across the needle to form charged droplets with the same charge as the spray needle. The mechanism underpinning the generation of analyte ions differs depending on the type of analyte [216]. Here, the focus is on ion formation of low molecular weight analytes. The charged droplets are repelled from the spray needle, directing them towards the counter electrode. The addition of an inert gas, such as nitrogen, and an increase in temperature leads to the evaporation of the solvent from the charged droplets. With this evaporation, the droplets reduce in size until they are small enough that they cannot hold their charge, which is termed the Rayleigh limit [217]. The charged droplet then undergoes Coulomb fission, which is also known as a Coulombic explosion, as the charge intensity results in the droplets exploding to form a number of smaller, more stable droplets, which can then undergo the same process, producing charged analytes devoid of solvent [218]. These ions are then detected by the analyser.

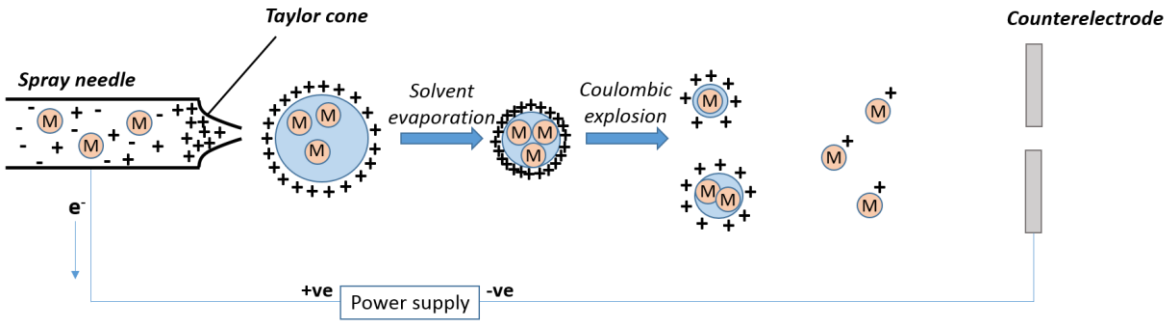

Figure 1.9: In electrospray ionisation, the sample is sprayed from a needle with a high potential difference applied to it. This results in the spray of charged droplets, containing the analytes (in this case in positive ion mode). Solvent evaporates until the Rayleigh limit is reached, and the droplet undergoes Coulomb fission, forming smaller charged droplets and charged analytes.

ESI is a soft ionisation technique, resulting in minimal fragmentation of the analyte, except through in-source fragmentation [219]. Fragmentation results from the collision of multiple charged ions during their acceleration from the source to the high vacuum region of the mass spectrometer [220]. While in some cases this can provide useful structural information, often the data is difficult to interpret as all ions at any given moment are subjected to fragmentation [221]. This, therefore, makes it very difficult to assign fragments to a parent ion and elucidate structural information. Instead, tandem mass spectrometry (MS/MS) is used to fragment a specific parent ion. Analysis of the subsequent fragment ions can then give valuable insight into the structure of the analyte.

MS/MS relies on the sequential connection of multiple mass analysers. One of the most common MS/MS systems is the triple quadrupole (QqQ), which uses three separate quadrupoles (**Figure 1.10**). The first isolates a parent (or precursor) ion of interest, which is then fragmented in the second analyser, termed the collision cell. The final analyser then detects the fragment ions. The collision cell (the second quadrupole, q) fragments precursor ions using collision-induced dissociation (CID). Ions are fragmented following collision with an inert gas, such as nitrogen or helium, which increases the internal energy of precursor ions, leading to fragmentation [222]. However, other types of mass spectrometers have MS/MS capabilities. Hybrid instruments have been developed to combine benefits offered by different mass analysers, such as the hybrid quadrupole-time-of-flight (Q-ToF) mass spectrometer. This takes advantage of the selecting power and MS/MS efficiency of a quadrupole and the enhanced resolution and sensitivity of a ToF [223].

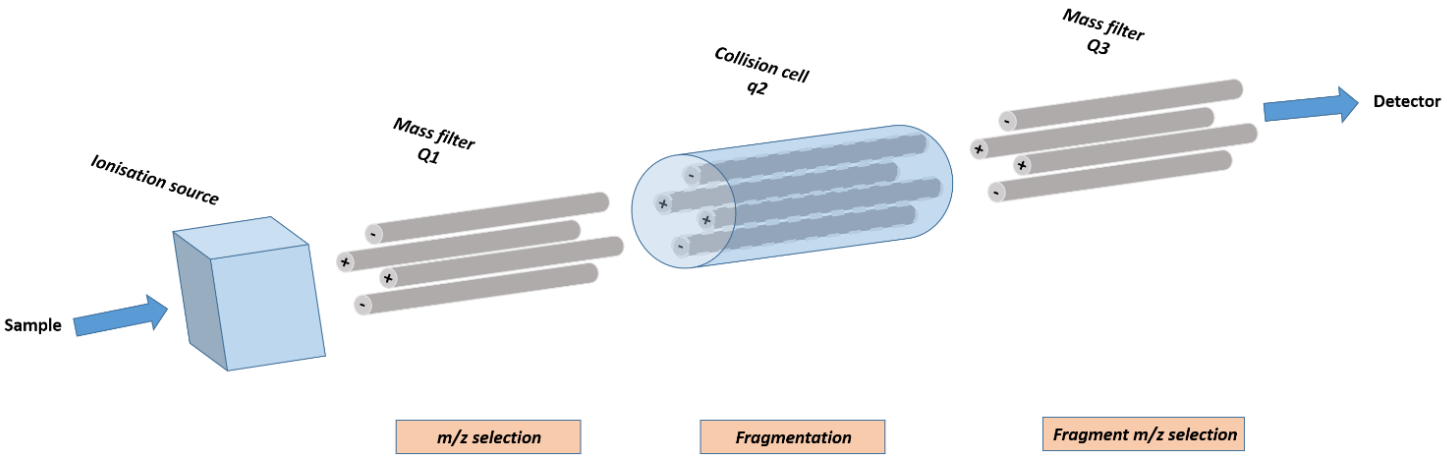

Figure 1.10: A schematic of a triple quadrupole (QqQ), with three quadrupoles joined in series. The first is used to select an m/z ratio of a precursor ion. This is then fragmented in the second quadrupole, termed the collision cell, and the m/z ratios of subsequent daughter ions are selected for in the third quadrupole.

LC-MS/MS is crucial in targeted metabolomics. Targeted metabolomics is defined as the measurement of specified groups of chemically characterised and biochemically annotated metabolites [224]. Conversely, untargeted metabolomics refers to the more comprehensive analysis of analytes in a sample, including those that are chemically unknown. Targeted approaches offer accurate and sensitive measurements of groups of metabolites, with confident annotation. Furthermore, the use of appropriate labelled internal standards – compounds of known concentrations added to each sample – allows for quantitative measurements of species of interest. The applications of targeted LC-MS/MS methods to lipidomics are numerous [225]. Typically, methods can take advantage of structural similarities between members of the same lipid class. For example, a targeted method for the detection of ceramides can focus on the production of a fragment ion with m/z 264 [225]. Due to the increased sensitivity of a targeted approach, LC-MS/MS is often used for the measurement of lipid signalling molecules that are low in abundance, such as eicosanoid lipid species [226].

However, lipidomics also relies heavily on untargeted approaches. In an untargeted approach, a fuller metabolic complement of a biological sample is analysed, requiring no prior hypothesis, unlike targeted approaches. Chromatography is not essential, with direct infusion-mass spectrometry (DI-MS) underpinning the field of "shotgun metabolomics" [227]. However, this thesis makes use of an untargeted LC-MS approach using chromatography to separate isomeric and isobaric species [225]. Crucial to untargeted methods is the use of a mass analyser with excellent mass accuracy, such as the orbitrap mass analyser, which is used in this thesis.

An orbitrap comprises two electrodes (**Figure 1.11**). A central spindle electrode is surrounded by an outer electrode. Ions are injected into the orbitrap by a curved ion trap (c-trap) and are trapped by an electrostatic field. They rotate around the central electrode and oscillate along its axis. The outer electrode detects the image current induced by the moving ions. The frequency of the oscillations is specific to the m/z ratio of the ion, while the size of the image current reflects the abundance of ions with that particular m/z ratio. The image current is then processed by a Fourier transformation, providing information on the frequency and amplitude of each ion. These can then be converted into the m/z ratio and intensity of each ion in the mass spectrum [228,229]. Advantages of the orbitrap over other mass analysers include high mass accuracy and resolution, imperative for untargeted lipidomics.

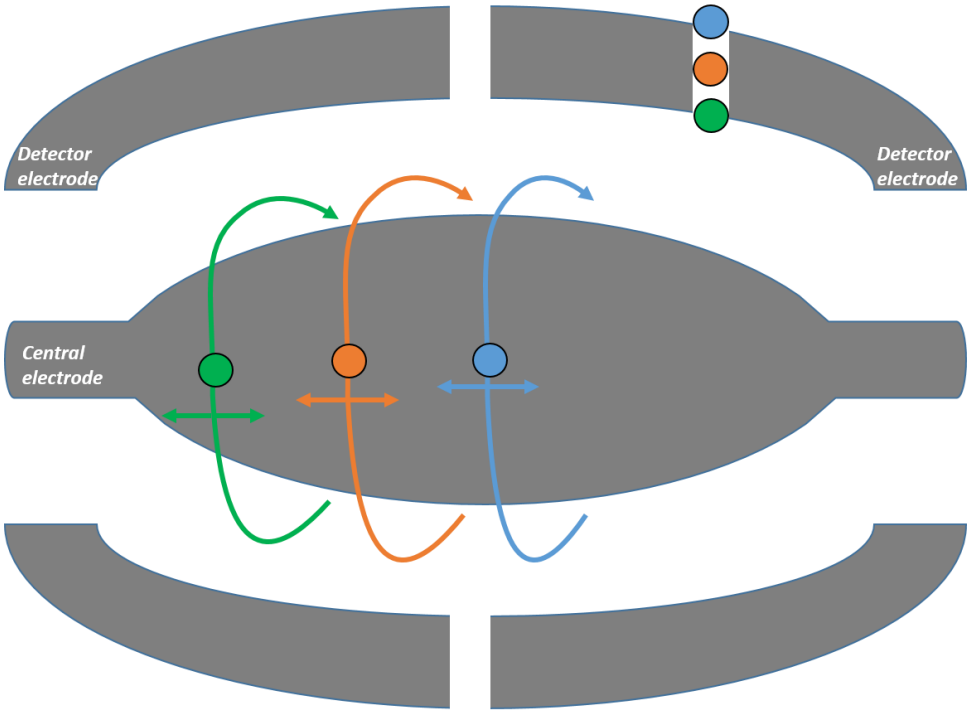

Figure 1.11: An orbitrap is composed of two electrodes. Ions spin around and oscillate along the central electrode. The image current is then detected by the outer detector electrode, which is then processed by a Fourier transformation.

To complement the untargeted approach, data-dependent acquisition (DDA) can be used to fragment species of interest via CID. Targeted approaches using triple quadrupole instruments require the input of *apriori* defined precursor ions of interest. DDA, however, fragments the most intense ion in a particular scan, therefore requiring no prior hypothesis. Interpretation of the fragmentation spectrum then provides structural information for a

precursor ion. This method can be enhanced by the use of a parent ion list, so that only particular species of interest are fragmented – a method more similar to a targeted analysis.

One of the drawbacks of untargeted metabolomics is the intensity of data processing required to identify and annotate lipid features from a vast dataset. This thesis makes use of XCMS, within R, for data processing [230,231]. First, the algorithm extracts features from background noise. This is done using a peak width threshold, based on the full width at half maximum (FWHM), in seconds. Peak quality can be ensured using a signal to noise ratio threshold. Following identification, peaks representing the same species are matched across all samples. Setting a minimum fraction of samples that a peak must be found in can be used to improve the quality of a peak group. The peak matching process is then used to correct retention time drift between samples. This is an iterative process, with peak matching repeated and improved following retention time alignment. Peaks won't be present in all samples if either the peak matching has not worked correctly or if the analyte is not present in the sample. Therefore, the algorithm then fills in these blanks by returning to the raw data and integrating the correct region of the chromatogram for the particular m/z value. Peaks can then be annotated with comparison to databases, such as the LipidMaps database [232]. In untargeted metabolomics, annotations are based on similar accurate mass, with retention time providing complementary information.

1.4 Gene expression analysis

To integrate lipidomic data with functional readouts of gene expression, reverse transcription-quantitative polymerase chain reaction (RT-qPCR) was used. RT-qPCR is a sensitive and quick method for the quantification of specific mRNAs of interest [233]. Complementary DNA (cDNA) is synthesised from purified RNA using a reverse transcriptase enzyme and a set of primers (**Figure 1.12**). Primers can either be an oligo of deoxythymine, which binds to the polyadenosine tail of mRNA species, or random short primers (typically 6-9 bases) that anneal to multiple points along the RNA transcript. Reverse transcriptase enzymes are thermostable, allowing cDNA synthesis to take place at high temperatures, increasing cDNA yield and transcription of RNAs with extensive secondary structure.

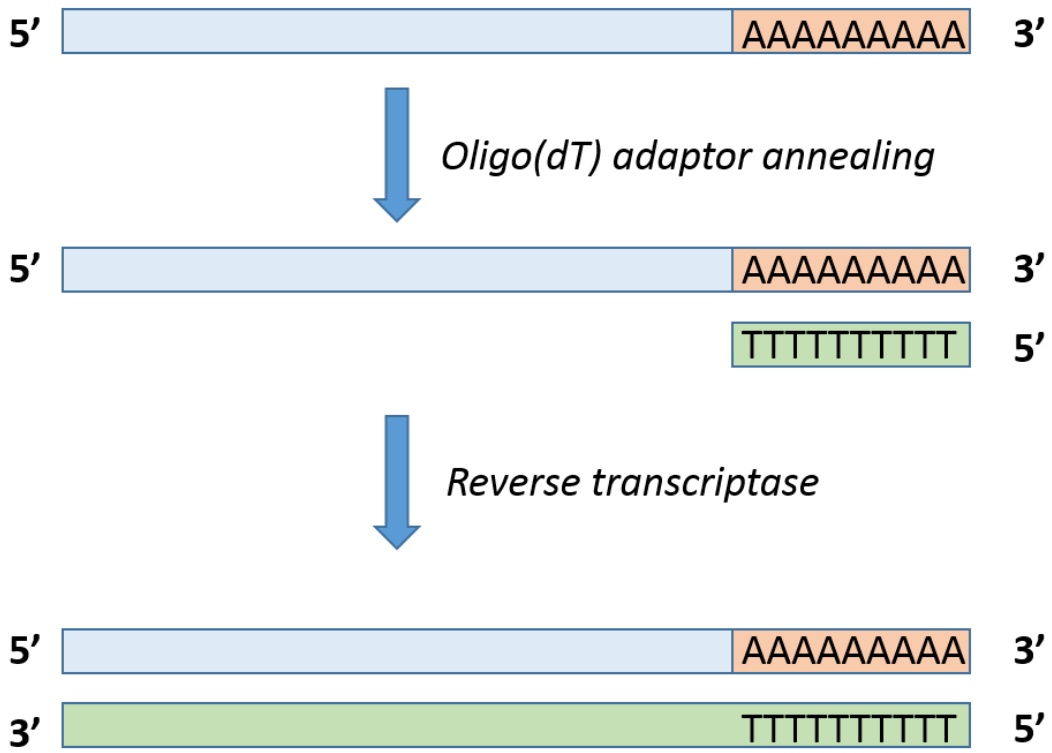

Figure 1.12: The synthesis of cDNA can use oligo(dT) primers that anneal to the poly(A) tail of mRNA molecules or random short primers. Once the primers have annealed, reverse transcriptase synthesises a DNA strand complementary to the mRNA.

Following synthesis of cDNA, the product is amplified by PCR using gene-specific primers (**Figure 1.13**). Use of both forward and reverse primers ensures the synthesis of double stranded DNA (dsDNA) products, which are detected by the binding of a fluorescent dye, such as SYBR-Green [234]. Upon binding to dsDNA, fluorescence increases and is detected by a fluorescence detector. The cycle threshold (CT) value gives the cycle number for the fluorescence to increase above the background threshold. For relative quantification of gene transcription, the transcription of a gene of interest is normalised to the expression of a housekeeping gene, such as the ribosomal 18s gene, to correct for any sample to sample variation in RNA purification or cDNA synthesis [235]. Commonly, the ΔΔCT-method is used to look at differences in transcription between control and treated samples. In this method, the CT-value for the housekeeping gene is subtracted from the CT-value of the gene of interest in each sample, giving a ΔCT-value. The ΔCT-value from a treated sample is then subtracted

from the ΔCT-value of a control sample to give the ΔΔCT-value for that sample. The fold change in gene expression can then be calculated by $2^{(-\Delta\Delta Ct)}$.

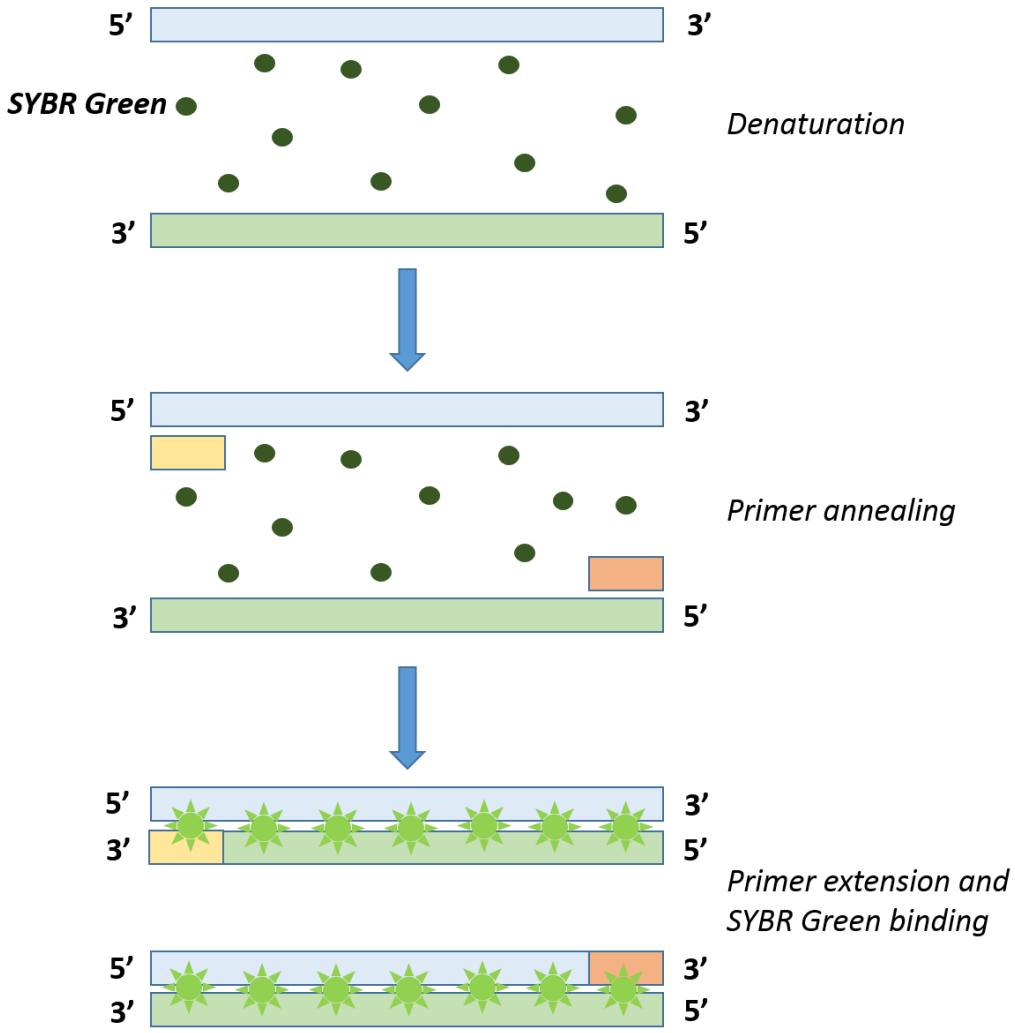

Figure 1.13: In RT-qPCR, cDNA is denatured to separate the two strands. Primers can then anneal to each strand and are extended by DNA polymerase, forming double stranded molecules. SYBR Green is a fluorescent dye that binds only to dsDNA, detecting the amplification of DNA in each cycle.

RT-qPCR is used throughout this thesis as a method of measuring the induction of ER stress. Activation of the UPR results in the upregulation of a number of transcripts encoding transcription factors, such as ATF3 and ATF4, chaperones, including HSPA5 (also known as BiP) and proteins involved in protein degradation, such as EDEM1 [236]. RT-qPCR of these transcripts provides a rapid and sensitive readout for activation of the UPR and the induction of ER stress [236–239].

1.5 Project aims

ER stress has been implicated as a potential mechanism unifying lipotoxicity and inflammation in the development of insulin resistance. However, the role of lipotoxicity-induced ER stress in skeletal muscle, in the setting of the metabolic syndrome, remains poorly defined. This thesis aims to understand the interaction between chronic ER stress and lipid metabolism in the context of obesity and T2DM using a multi-platform lipidomic approach combined with RT-qPCR and applied to skeletal muscle cell biology, murine and clinical studies. Mouse skeletal myotubes will be exposed to palmitate to model raised plasma FFAs observed in the plasma of obese individuals. GC-MS analysis of FAMEs and LC-MS open profiling of intact lipids will be used to understand the effects of palmitate on both the total fatty acid profile and individual complex lipid species within palmitate exposed myotubes. RT-qPCR will be used to confirm the induction of ER stress.

Key metabolic alteration will then be investigated in primary human skeletal myocytes and *in vivo* models of obesity. These models include dietary mouse models of obesity and human skeletal muscle biopsies from diabetic and non-diabetic patients undergoing routine pacemaker surgery. Pharmacological inhibition in skeletal myocytes *in vitro* will then be used to probe the mechanisms and functional consequences of observed lipid changes, with particular focus on the induction of ER stress.

Finally, following the demonstration of cell non-autonomous signalling in the propagation of ER stress, this thesis also seeks to integrate lipid-induced ER stress with intercellular signalling, combining *in vitro* techniques with the lipidomic profiling of culture media.

Aim	Chapter number
To establish a model of chronic palmitate-induced ER stress in mouse C2C12 myotubes, and profile the lipidomic effects of palmitate using GC-MS and LC-MS.	Chapter 3
To translate lipidomic findings from palmitate-induced ER stress in C2C12 myotubes to human primary human skeletal muscle cells and *in vivo* models of obesity.	Chapter 3
To assess the dependence of lipid alterations on ER stress using chemical inducers and pharmacological inhibition of the UPR.	Chapter 3
To use pharmacological inhibition to identify the mechanisms underpinning the metabolic perturbations identified in Chapter 3.	Chapter 4
To use pharmacological inhibition and co-culture assays to understand the functional consequences of palmitate-induced metabolic alterations.	Chapter 4
To identify the presence of cell non-autonomous signals that propagate the induction of ER stress between C2C12 myotubes and human primary skeletal myocytes.	Chapter 5
To use pharmacological inhibition to interrogate the mechanisms underpinning the generation of non-cell autonomous ER stress propagating signals.	Chapter 6

Chapter 2

Materials and Methods

2.1 Cell and tissue culture techniques

2.1.1 C2C12 myoblast culture and differentiation

C2C12 myoblasts were purchased from Sigma Aldrich. The vial was thawed for approximately 1 minute in a water bath set to 37 ºC. Cells were suspended in 10 mL of Dulbecco's Modified Eagle Medium (DMEM; D6429, Sigma Aldrich) supplemented with 10% fetal bovine serum (FBS, Sigma Aldrich, F7524) and 1% penicillin-streptomycin (P/S, Sigma Aldrich, P4333), termed "growth media". Cells were centrifuged (220g, 5 minutes) and the supernatant discarded. The cell pellet was then resuspended in 15 mL growth media and transferred to a T75 flask (Corning, 658175).

At 70% cell confluence, the culture media was aspirated and 5 mL of a trypsin-EDTA solution (Thermo Fisher Scientific, 25300054), warmed to 37 ºC, was added to detach the cells from the flask. Once cells were in suspension, 10 mL of growth media was added to inactivate the trypsin. Cells were centrifuged (220g, 5 minutes) and the supernatant discarded. The cell pellet was resuspended in growth media, and approximately 2 x 10^6 cells were plated in T75 flasks for further subculture, or 1 x 10^5 cells were plated per well of a 12-well plate. Experiments were conducted in 12-well collagen I-coated plates (Corning Biocoat, 734-0295), with 1 mL of the cell suspension added per well, except for eicosanoid analysis in chapter 4, which was conducted in collage I-coated T75 flasks (Corning Biocoat, 734-0290).

Once confluent within plates, differentiation was induced by changing the culture media to DMEM containing 10% horse serum (HS, Sigma-Aldrich, H1270), 1% P/S and 850 nM insulin (Sigma Aldrich, I9278), termed "differentiation media". Cells were differentiated for 6 days. During differentiation cells were treated with either 200 µM palmitate, or the BSA vehicle control, to set up a chronic model of ER stress. Media was changed every day during

differentiation. Furthermore, cells were co-treated with pharmacological inhibitors, as detailed in the relevant chapter specific method section (AMG PERK 44 (Tocris Bioscience, 5517) Chapters 3 and 6; 4μ8c (Tocris Bioscience, 4479) Chapters 3 and 6; tunicamycin from *Streptomyces* (Sigma Aldrich, T7765) Chapter 3; PD146176 (Sigma Aldrich, P4620) Chapter 4; NCTT-956 (Sigma Aldrich, SML0499) Chapter 4; AACOCF3 (Abcam, ab120350) Chapter 4; Fumonisin B1 (Tocris Bioscience, 3103) Chapter 6; Fenretinide (Tocris Bioscience, 1396) Chapter 6; Myriocin (Sigma Aldrich, M1177) Chapter 6).

To develop a stock of C2C12 myoblasts, cells that had undergone 4 passages were lifted from the bottom of flasks using 5 mL of trypsin, diluted in 10 mL of growth media and centrifuged (220g, 5 minutes). The supernatant was discarded and the pellet resuspended in growth media containing 10% DMSO (Sigma Aldrich, D8418) for freezing. Each flask provided two vials of cells for freezing. Cells were stored at -80 ºC overnight, and then in liquid nitrogen for long-term storage.

2.1.2 Primary human skeletal muscle cell culture and differentiation

Primary human skeletal muscle cells (HSKMCs) were purchased from Cell Applications (S150a-05a). The vial was thawed for approximately 1 minute in a water bath set to 37 ºC. HSKMCs were then suspended in 15 mL of Skeletal Muscle Cell Growth Medium (Cell Applications, 151-500) and transferred to a T75 flask.

Cells were subcultured once they reached 90% confluence. They were detached from the flask using 5 mL of trypsin. Trypsin was then inactivated using a trypsin inhibitor solution (Sigma Aldrich). The cell suspension was transferred to a 50 mL falcon tube and centrifuged (220g, 5 minutes). Flasks were subcultured in a 1:3 ratio. The cell pellet was resuspended in 45 mL of Skeletal Muscle Cell Growth Medium and 15 mL of the cell suspension was transferred to each flask (approximately 2.5×10^6 cells).

Experiments were conducted in collagen I-coated 12-well plates. Cells were detached from a T75 flask with trypsin as previously described, and the pellet was resuspended in 75 mL of Skeletal Muscle Cell Growth Media. One mL (approximately 1×10^5 cells) of the cell suspension was added to each well. Once confluent, HSKMCs were differentiated for 6 days using Skeletal Muscle Differentiation Media (Cell Applications, 151D-250). During differentiation cells were treated with either 100 μM palmitate, or the BSA vehicle control, to

set up a chronic model of ER stress. Media was changed every 2 days during differentiation. Furthermore, cells were co-treated with pharmacological inhibitors, as detailed in the relevant chapter specific method section (tunicamycin from *Streptomyces* chapter 3; PD146176 chapter 4; NCTT-956 chapter 4; AACOCF3 chapter 4).

To create a stock of primary HSKMCs, cells that had undergone 3 passages were detached from the flasks and centrifuged (220g, 5 minutes). Cell pellets (approximately 4 x 10^6 cells) were resuspended in Cell Freezing Medium (Cell Applications, 040-50). Each flask provided sufficient cells for two vials. Cells were stored at -80 ºC overnight, and then in liquid nitrogen for long-term freezing.

2.1.3 Conjugation of palmitate to BSA

The conjugation of palmitate to bovine serum albumin (BSA) was based on previous literature and optimized for palmitate-induced ER stress in skeletal myocytes [240]. Fatty-acid free BSA (12 g; Sigma Aldrich, A3803) was dissolved in 120 mL of Milli-Q water at 37ºC, forming a 10% solution. Separately, 0.125g of sodium palmitate (Sigma Aldrich, P9767) was dissolved in 3 mL of 50% ethanol at 70 ºC, forming a 150 mM solution. The 120 mL BSA solution was then split in two. The 3 mL palmitate solution was added to one aliquot in 1 mL intervals, with the palmitate:BSA solution continually stirred at 37 ºC throughout. 3 mL of 50% ethanol was added to the second aliquot of BSA solution, forming the vehicle control. The final palmitate concentration of the stock palmitate:BSA solution was 7.143 mM.

2.1.4 Cell harvesting

C2C12 cells were detached from wells using 0.5 mL of a trypsin-EDTA solution, and then resuspended in 1 mL of serum-free media (DMEM; D6429, Sigma Aldrich) and transferred to Eppendorf tubes. Primary HSkMCs were detached from wells using 0.4 mL of a trypsin-EDTA solution, and then resuspended in 1 mL of Skeletal Muscle Cell Basal Medium (Cell Applications, 150-500). A small aliquot (100 µL) was diluted in 500 µL of phosphate buffered saline (PBS, Sigma Aldrich, D8662) for cell count, which was performed using an automated cell counter (Scepter: Merck). Cells were pelleted with a microcentrifuge (4,600g, 7 minutes), and the supernatant removed, prior to storage at -80°C.

2.2 Animal studies

Below are brief outlines of three mouse studies that provided skeletal muscle (gastrocnemius) and, in some cases, plasma for this PhD. The studies were carried out as part of other projects, but full permission was provided for the use of the tissue in this context. Nutrient information for each diet is summarised in **Table 2.1**. All procedures were carried out in accordance with U.K. Home Office protocols by a personal license holder.

2.2.1 Western diet mouse model

Five-week-old mice (wild-type, strain C57Bl/6J) were purchased from Harlan Laboratory Ltd. Four animals were housed per cage and had an acclimitisation period of 7 days. The temperature was maintained at 20 ± 4 ºC with a 12 hour light/dark cycle. Mice were fed either a western diet (WD, TD88137) or a low-fat control (LFC, TD08485) diet, for 12 weeks (n=8 per group), with diets supplied by Teklad Custom Research Diets (Envigo). Following the conclusion of the study, mice were sacrificed by cervical dislocation, and subsequently dissected. Tissue was flash frozen in liquid nitrogen and stored at -80 ºC. The study was carried out under a project license held by Professor Toni Vidal-Puig (PPL number: 80/2584) and personal license of Dr Michele Vacca (PIL number: I8C7616E4).

2.2.2 High-fat diet mouse model

C57Bl/6J mice were purchased from the Jackson laboratory and housed at 24ºC. Mice were fed either RM3 breeders chow (n=10; Special Diet Services, 801066) or 60% calories-from-fat high-fat diet (n=13; Research Diets, D12492). Mice were culled at 14 weeks of age. They were fasted overnight (4 pm till 10 am) prior to cervical dislocation. Tissues were collected, weighed, immediately frozen on dry ice and stored at -80ºC until further processing. This study was carried out under a project license held by Professor Toni Vidal-Puig (PPL number: 80/2584) and personal license of Dr Sam Virtue (PIL number: 80/9004).

2.2.3 Long-term high-fat diet mouse model

Male C57Bl/6J mice (6 weeks old; n = 10) (Charles River Laboratories) were weight matched and received either standard chow (n = 5; F4031, Bio Serv) or a 60% fat diet (n = 5; F3282, Bio Serv) ad libitum for 17 weeks, with food and water intake monitored. Animals were housed in conventional cages at room temperature with a 12 hour light/dark cycle. On completion of the study mice were culled by cervical dislocation, plasma was collected by left ventricular puncture, and tissues were removed and snap frozen in liquid nitrogen, prior to storage at -80 ºC. This study was carried out under a project license held by Dr Lee Roberts (PPL number: P606320FB) and a personal license held by Dr Lee Roberts (PIL number: I2CD54CD0).

%kcal from	TD08485	TD88137	RM3	D12492	F4031	F3282
Protein	19.1	15.2	27.28	20.0	20.9	14.9
Carbohydrate	67.9	42.7	61.24	20.0	62.6	26.0
Fat	13.0	42.0	11.48	60.0	16.3	59.0

Table 2.1: Nutrient information for the diets used in the animal studies.

2.3 Human skeletal muscle biopsies

75 eligible and consecutive patients (**Table 2.2**) undergoing routine pacemaker therapy in Dr Klaus Witte's clinic at Leeds General Infirmary volunteered to participate in the study. Eligible patients were grouped into two cohorts based on the presence or absence of T2DM. The T2DM cohort had a previous diagnosis of T2DM (>3 months) and/or was receiving treatment for diabetes. In such cases, T2DM was defined as a documented history of diabetes, fasting plasma glucose ≥ 7.0 mmol/L, plasma glucose ≥ 11.1 mmol/L two hours after the OGTT or a glycated haemoglobin (HbA1c) ≥ 6.5% (≥ 48 mmol/L).

Human skeletal muscle (*pectoralis major*) biopsies were obtained from eligible participants during their pacemaker operation. Pacemaker procedures were otherwise entirely routinely carried out: lidocaine was initially injected to anaesthetize the area and a small incision was made under the left clavicle. During creation of the pre-pectoral pocket for the generator

above the *pectoralis major* a portion of the muscle (approximately 100mg) was sampled. This sample was immediately placed into a 1.5 mL Eppendorf tube and snap frozen in liquid nitrogen. The study is approved by the Leeds West Research Ethics Committee (11/YH/0291) and Leeds Teaching Hospitals R&D committee (CD11/10015) and conforms to the Declaration of Helsinki.

	Number of patients	**Number of males**	**Number of females**	**Age (years)**	**BMI (kg/m^2)**	**Weight (kg)**
Control patients	53	43	10	72.05 ± 11.54	27.43 ± 4.829	80.6 ± 13.83
T2DM patients	22	19	3	73.04 ± 10.01	30.94 ± 7.129	93.64 ± 22.50
P				0.7305	0.0157	0.0025

Table 2.2: Data from patients who provided skeletal muscle biopsies during routine pacemaker therapy.

2.4 RNA handling and reverse transcription quantitative polymerase chain reaction

2.4.1 RNA isolation and purification

RNA was extracted and purified *in situ*, using the RNeasy mini kit (Qiagen, 74104), following the manufacturer's instructions. Briefly, 350 µL of lysis buffer was added to the cells *in* situ. Following lysis, 350 µL of 70% ethanol was added, and the sample was well mixed by pipetting up and down, before transfer to a spin column. Ethanol aids RNA binding to the silica membrane in the spin column. Samples were centrifuged (9391g, 30s), and the eluent was discarded. A series of washes with the provided buffers removes contaminants. First, 700 µL of buffer RW1 was added to the column to remove biomolecules such as carbohydrates and fatty acids that non-specifically bind to the membrane. The samples were centrifuged at 9391g for 30s and the eluent discarded. Two 500 µL washes with buffer RPE

followed to remove traces of salts from previous buffers. After the first addition, samples were centrifuged at 9391g for 30s and the eluent discarded. After the second addition samples were centrifuged at 9391g for 2 minutes and the eluent discarded. Spin columns were transferred to a fresh collection tube and centrifuged at full speed for 1 minute to dry the membrane. RNase free water (40 µL) was then added to the spin column and samples centrifuged at 9391g for 1 minute to elute the RNA. Samples were stored at -80 ºC.

2.4.2 cDNA synthesis

The concentration (determined by A_{260}, requirement of > 50 ng/mL RNA) and quality (a requirement of absorbance ratios to be: A_{260}:A_{230} > 1.7; 1.8 < A_{260}:A_{280} < 2) of RNA was determined using the NanoDrop-1000 spectrophotometer (NanoDrop Technologies) and then standardized to 50 ng/mL in a volume of 8 µL for all samples. cDNA was synthesized by a two-step process with the RT^2 First Strand Kit (Qiagen, 330404). Genomic DNA was removed by the addition of 2 µL of genomic elimination buffer followed by incubation at 42 ºC for 5 minutes in a PrimeG thermal cycler (Techne). Ten µL of a reverse transcriptase mix (containing the reverse transcription buffer BC3, RNase free water, the reverse transcriptase enzyme mix RE3, and the primer and external control mix P2 in a ratio of 4:3:2:1) was then added to each sample, mixed well and incubated at 42 ºC for 15 minutes in the thermal cycler. The reaction was ended by increasing the temperature to 95 ºC for 5 minutes. Samples were cooled to 4 ºC. Subsequently samples were diluted with RNase free water to a total volume of 100 µL.

2.4.3 Reverse transcription quantitative polymerase chain reaction

cDNA (5 µL) was mixed with 10 µL of a SYBR Green PCR mastermix containing ROX (Qiagen, 330523), 4.4 µL of RNase-free water and 0.6 µL of a primer mix (Qiagen) for one of the genes in question in each well of a 96-well plate (Applied Biosystems, 4346906). Samples were then analysed using a Step One Plus Real Time Cycler (Applied Biosystems), quantified using the ΔΔ-CT method with expression normalized to the housekeeping gene. This method begins with a 10 minute incubation at 95 ºC, which activates the HotStart DNA *Taq* polymerase. There are then 40 cycles consisting of a 15 second period at 95 ºC to denature the cDNA, followed by 1 minute at 60 ºC, in which primers anneal to the template

and are elongated by the polymerase. Fluorescence is measured as a consequence of the SYBR Green dye binding to the double stranded DNA (excitation and emission maxima are at 494 and 521 nm, respectively), and is collected at the end of each of these 40 cycles. Δ-CT values are calculated by first subtracting the CT-value for the housekeeping gene from the CT-value of the gene of interest for each sample. The ΔCT-value from a treated sample is then subtracted from the ΔCT-value from a control sample giving the ΔΔ-CT value for that sample. The fold-change for each gene is calculated using the equation: fold change = $2^{(-\Delta\Delta Ct)}$.

For murine samples, *Rn18s* (PPM72041A) was used as the housekeeping gene, while *ACTB* (PPH00073G) was used for analysis of primary HSKMCs. The induction of ER stress was assessed throughout this thesis using primers for *Atf3* (PPM04669C), *Atf4* (PPM04670E), *Hspa5* (PPM03586B) and *Edem1* (PPM26189B) for murine samples, and *ATF3* (PPH00408C), *ATF4* (PPH02016A), *HSPA5* (PPH00158E) and *EDEM1* (PPH12935B) for human samples.

2.5 Metabolite extractions

2.5.1 Cell metabolite and lipid extraction for mass spectrometry

Metabolites were extracted using a modified Bligh and Dyer method [241]. The cells were treated with 600 µl methanol/chloroform (2:1) and sonicated until the cell pellet broke up. Then, 200 µl chloroform and 200 µl water were added, and the samples vortexed and sonicated for 15 minutes. Subsequently, the samples were centrifuged (16,100g, 20 minutes), giving an aqueous layer and an organic layer containing the lipid fraction. The two layers were separated and the relevant internal standard mixture was added to the organic fraction. The fractions were dried under nitrogen gas flow and then stored at -80°C.

2.5.2 Human and mouse skeletal muscle tissue extraction

Approximately 30 mg of tissue was weighed for extraction. 600 µL of methanol/chloroform (2:1) was added to each sample, and they were lysed in a TissueLyser (Qiagen) in 5 minute intervals for a total of 20 minutes, at 20 Hz. Once the samples were homogenous, 200 µL of water and 200 µL of chloroform were added, and samples were then well vortexed and

centrifuged (16,100g, 20 minutes). Aqueous and organic layers were separated and dried as before, prior to storage at -80 ºC.

2.5.3 Plasma extraction

For plasma, 600 µL of methanol/chloroform (2:1) was added to 20 µL of plasma, and vortexed thoroughly. Samples were then centrifuged (16,100g, 20 minutes), and the two phases were separated, dried and stored as described previously.

2.5.4 Cell media extraction

One mL of cell media was mixed with 800 µL of methanol/chloroform (1:1) and vortexed well. Samples were then centrifuged (16,100g, 20 minutes), and the two phases separated, dried and stored as outlined above.

2.5.5 Internal standard mixture for lipidomics

The internal standard mix was composed of deuterated standards sourced from Avanti Polar Lipids (C16-d31 Ceramide, 16:0-d31-18:1 phosphatidic acid, 16:0-d31-18:1 phosphatidylcholine, 16:0-d31-18:1 phosphatidylethanolamine, 16:0-d31-18:1 phosphatidylglycerol, 16:0-d31-18:1 phosphatidylinositol, 14:0 phosphatidylserine-d54, and 16:0-d31 sphingomyelin) and CDN Isotopes/QMX Laboratories (18:0-d6 cholesteryl ester, 15:0-d29 fatty acid, 17:0-d33 fatty acid, 20:0-d39 fatty acid, 14:0-d29 lysophosphatidylcholine-d13, 45:0-d87 triacylglyceride, 48:0-d83 triacylglyceride, and 54:0-d105 triacylglyceride). The internal standards were dissolved in methanol/chloroform (1:1) to form stock solutions at a concentration of 0.5 mg/mL. One mL of each stock solution was then mixed together with a further 184 mL of methanol/chloroform (1:1), with each internal standard at a final concentration of 2.5 µg/mL.

This internal standard mixture was used for peak normalisation in LC-MS open profiling of lipids and GC-MS analysis of fatty acid methyl esters (FAMEs) to adjust for non-biological sample-to-sample variation. For each sample, 250 µL was added to the organic phase prior to evaporation under nitrogen. For LC-MS profiling, internal standards were annotated based on accurate mass. For GC-MS analysis, the internal standard mixture underwent FAME

derivatisation along with the sample. Identification of internal standard peaks was achieved by comparison of fragmentation patterns to a derivatised blank sample containing only the internal standard mixture.

2.6 Liquid chromatography-mass spectrometry open profiling of lipids

2.6.1 Sample preparation

Metabolites from the organic phase were reconstituted in 50 µL of methanol/chloroform (1:1) and vortexed thoroughly. Ten µL of the sample was then diluted into 190 µL of propan-2-ol/acetonitrile/water (IPA:ACN:H_2O; 2:1:1). Samples were briefly vortexed to ensure they were well mixed.

2.6.2 Chromatography parameters

For both positive and negative ionisation modes, 5 µL of sample was injected onto a C18 CSH column, 2.1 x 100 mm (1.7 µm pore size; Waters, 186005297), which was held at 55ºC using an Ultimate 3000 UHPLC system (Thermo Fisher Scientific). The mobile phase comprised solvents A (ACN/H_2O; 60:40) and B (ACN/IPA; 10:90), run through the column in a gradient (40% B, increased to 43% B after 2 minutes, 50% B at 2.1 minutes, 54% B at 12 minutes, 70% B at 12.1 minutes, raised to 99% B at 18 minutes before returning to 40% for 2 minutes). Total run time was 20 minutes, with a flow rate of 0.400 µL/min. In positive mode, 10 mM ammonium formate (Fisher Scientific, A/3440/53) was added to solvents A and B. In negative mode, 10 mM ammonium acetate (Sigma Aldrich, 516961) was the solvent additive. Solvent additives were chosen based on current literature [242].

2.6.3 Mass spectrometry parameters

Mass spectrometry was then carried out using the LTQ Orbitrap Elite Mass Spectrometer (Thermo Fisher Scientific) in positive and negative mode. Metabolites were ionised by heated electrospray before entering the spectrometer. The source temperature was set to 420 ºC, and

the capillary temperature to 380 ºC. In positive mode, the spray voltage was set to 3.5 kV, while in negative it was 2.5 kV. Data was collected using the Fourier transform mass spectrometer (FTMS) analyser. The resolution was set to 60,000 and the data was obtained in profile mode. The full scan was performed across an m/z range of 110-2000.

2.6.4 Fragmentation analysis

To overcome limitations in LC-MS annotation of lipid species arising from the isobaric nature of many lipid species, and to facilitate the identification of the fatty acyl chains esterified to complex lipids, a tandem mass spectrometry (LC-MS/MS) fragmentation method was used. The subsequent fragmentation spectra were then used to conclusively identify the fatty acid composition of each PC that contained 4 or more double bonds.

The method described in **Section 2.6.3** *Mass spectrometry parameters* was adapted to include a second scan event. Ions were fragmented using collision induced dissociation (CID) at a normalised collision energy of 35. Precursor ions were selected from a mass list, with the most intense ion on the list fragmented in each scan. The minimum signal required was set to 5000 counts and the isolation width was set to 1. The activation time was 10 ms and the activation Q was set to 0.25. Fragmentation spectra were acquired in centroid mode at a resolution of 15,000 using the FTMS analyser. The interpretation of fragmentation spectra was aided by online resources, with common fragmentation patterns summarised in **Table 2.3** [243].

Phosphatidylcholine (PC) species	Precursor ion (m/z)	Fragment ion 1 (m/z)	Fragment ion 2 (m/z)	Fragment ion 3 (m/z)	Fragment ion 4 (m/z)
PC 16:0/18:3	756.55	478.35	500.33	496.36	518.34
PC 16:0/20:4	782.57	478.35	526.35	496.36	544.36
PC 16:0/20:5	780.55	478.35	524.33	496.36	542.34
PC 16:0/22:6	806.57	478.35	550.35	496.36	568.36
PC 16:1/18:3	754.54	476.33	500.33	494.34	518.34
PC 16:1/20:4	780.55	476.33	526.35	494.34	544.36
PC 16:1/20:5	778.54	476.33	524.33	494.34	542.34
PC 16:1/22:6	804.55	476.33	550.35	494.34	568.36
PC 18:0/18:3	784.59	506.38	500.33	524.39	518.34
PC 18:0/20:4	810.60	506.38	526.35	524.39	544.36
PC 18:0/20:5	808.59	506.38	524.33	524.39	542.34
PC 18:0/22:6	834.60	506.38	550.35	524.39	568.36
PC 18:1/18:3	782.57	504.36	500.33	522.37	518.34
PC 18:1/20:4	808.59	504.36	526.35	522.37	544.36
PC 18:1/20:5	806.57	504.36	524.33	522.37	542.34
PC 18:1/22:6	832.59	504.36	550.35	522.37	568.36

Table 2.3: Fragment *m/z* values for common polyunsaturated fatty acid-containing phosphatidylcholines

2.6.5 Data processing using R

For data processing, spectra were converted from Xcalibur .raw files into .mzML files using MS Convert (Proteowizard) for analysis by XCMS within R studio. XCMS software was used to process data and identify peaks. Peaks were identified based on an approximate FWHM of 5 seconds and a signal to noise threshold of 5. To improve peak identification, peaks had to be present in a minimum of 25% of the samples. Peaks were annotated by accurate mass, using an automated R script and comparison to the LipidMaps database [232]. Intensity was normalised to internal standards, and cell number (or dry protein pellet weight for animal tissue).

2.7 Statistics

Univariate statistics was used to assess the significance of changes in individual metabolites. Statistical significance was assessed using either a one-way ANOVA with a Tukey's multiple comparisons test, two-way ANOVA with Sidak's multiple comparisons test or Student's t-test, as detailed in each figure. Linear regression was used to analyse human skeletal muscle biopsies for correlations between lipid species and BMI. In each case, $n \geq 3$ and the significance level was set to $p \leq 0.05$. All univariate analysis was conducted using GraphPad Prism (version 6) software.

Chapter 3

Chronic palmitate treatment induces ER Stress and stimulates phospholipid remodelling in skeletal muscle

3.1 Introduction

T2DM is estimated to affect over 370 million people worldwide aged between 20 and 79 years old, with obesity as the leading risk factor [244–246]. Obese individuals have increased concentrations of plasma free fatty acids resulting from, in part, increased lipolysis in dysfunctional white adipose tissue [247]. The association between these fatty acids in plasma and impaired insulin action is well established in the context of obesity and T2DM [42,248]. However, research has since suggested that it is not solely total fatty acid concentration, but also the specific fatty acid species, which contributes to metabolic perturbation in T2DM [249]. Current thought emphasises the importance of saturated fatty acids, in particular palmitate, in the development of insulin resistance. Putative mechanisms suggested to underpin the relationship between saturated fatty acids and insulin resistance include lipotoxicity and inflammation [78,248,250].

Lipotoxicity stems from the perturbation of lipid storage resulting in elevated concentrations of lipid species within plasma and ectopic lipid storage in non-adipose tissues, such as skeletal muscle and liver [251]. As the concentration of these ectopic lipids increase they disrupt cellular processes, including insulin signalling. Ceramides and DGs have been suggested as the primary mediators of saturated fatty acid-induced insulin resistance in skeletal muscle, adipose and the liver [52,57,58,252].

Lipotoxicity is closely integrated with inflammatory signalling in metabolic disease [78]. Palmitate increases the levels of pro-inflammatory cytokines such as Tnfα, Ccl2 and Il6 [82–84,253]. Circulating macrophages respond to these inflammatory signalling cues, infiltrating peripheral tissues and switching from an M2 alternative activation state to a more classical, pro-inflammatory M1 polarisation [88–91]. This phenotypic switch has been causally linked to

increases in insulin resistance [254]. Palmitate can also directly activate immune cells, further enhancing lipid-induced inflammation [99,100].

ER stress, and the subsequent activation of the UPR, may represent a unifying mechanism underpinning palmitate-induced insulin resistance. ER stress was initially linked to metabolic disease following analysis of UPR markers in the tissues of dietary and genetic mouse models of obesity, with ER stress identified in liver and adipose tissue of obese mice [103]. Markers of UPR activation and inflammation were attenuated in obese individuals following gastric bypass-induced weight loss, concomitant with improvements in insulin sensitivity in adipose tissue and the liver [163]. Similarly, treatment of obese individuals with tauroursodeoxycholic acid (TUDCA), a chemical chaperone that improves protein folding and reduces ER stress, increased insulin sensitivity in the liver and skeletal muscle [255].

Saturated fatty acids may provide a mechanistic link between lipotoxicity, inflammation and ER stress as part of metabolic diseases. Palmitate has been shown to induce ER stress in key insulin-sensitive tissues, including adipose, liver and skeletal muscle [171,172,179,256]. Mechanisms linking palmitate with ER stress are under-investigated, but alterations of phospholipid bilayer composition may represent one potential mechanism. Forced expression of Lpcat3, the gene encoding lysophosphatidylserine acyltransferase 3, increased the incorporation of PUFAs into phospholipids and ameliorated palmitate-induced ER stress in hepatocytes [175]. Furthermore, an increase in the PC/PE ratio, found in the livers of obese mice, increases ER stress, while correcting this ratio reduced ER stress and improved glucose homeostasis [176].

While there has been significant study of ER stress and lipotoxicity in the liver and adipose tissue, the link between lipotoxicity and ER stress in skeletal muscle remains poorly defined. Treatment of human myotubes with palmitate increased expression of UPR markers, which was prevented with forced expression of SCD1 [179], also highlighting the potential benefits of fatty acid desaturation in palmitate-induced ER stress and lipotoxicity. Oleate treatment and AMPK/PPARδ activation attenuated palmitate-induced ER stress, and ameliorated insulin signalling and inflammation, further implying ER stress as a connecting mechanism between palmitate and insulin resistance [54,180]. However, this work is contradicted by research demonstrating that chemical chaperones do not improve palmitate-induced insulin resistance in myotubes [181]. Further work is required to delineate the importance of ER stress as a mechanism mediating the effects of lipotoxicity in skeletal muscle during metabolic disease.

3.2 Aims and objectives

This chapter aims to better understand the link between chronic lipotoxicity, the induction of ER stress and lipid metabolism in skeletal myocytes using a multi-modal mass spectrometry approach. This work focuses on the analysis of skeletal muscle, a tissue critical to whole-body glucose homeostasis in which the importance of ER stress in the development of insulin resistance is poorly understood. Previous research in this area has investigated the effects of saturated fatty acids at high doses, in an acute setting, typically no longer than 24 hours [54,103,257–260]. However, obesity and T2DM are chronic disorders, with chronically increased levels of plasma fatty acids. Therefore, this study aims to develop a more physiological approach and utilises an *in vitro* model of chronic lipotoxicity to understand the effects of prolonged palmitate exposure on lipid metabolism in skeletal myocytes.

This investigation is supported with the following objectives:

1) The establishment of a model of chronic, lipid-induced ER stress in C2C12 myotubes, an immortalised skeletal muscle cell line.
2) GC-MS analysis of total fatty acids in C2C12 myotubes following chronic palmitate exposure.
3) Investigation of the effects of chronic palmitate treatment on the intact lipid profile of C2C12 myotubes using LC-MS.
4) Analysis of primary human skeletal muscle cells and *in vivo* models of metabolic disease to increase the relevance of results to the clinical setting.
5) Assessment of ER stress as an underpinning mechanism of palmitate-induced lipid changes, using both pharmacological inhibition of the Perk and Ire1 signalling arms, and tunicamycin as a chemical inducer of ER stress.

3.3 Materials and Methods

3.3.1 C2C12 culture

C2C12 cells were grown and differentiated as described in **Chapter 2 Materials and Methods** (section 2.1.1 *C2C12 myoblast culture and differentiation*)**.** Cells were differentiated and treated in 12-well plates. Cells were treated with inhibitors (detailed in section 3.3.4 *Pharmacological inhibitors*) for the final 24 hours of experiments.

3.3.2 Primary human skeletal muscle cell culture

Primary human skeletal muscle cells (HSkMCs) were cultured as described in **Chapter 2 Materials and Methods** (section 2.1.2 *Primary human skeletal muscle cell culture and differentiation*)**.** Cells were treated with inhibitors (detailed in section 3.3.4 *Pharmacological inhibitors*) for the final 24 hours of experiments. All cells were treated in 12-well plates.

3.3.3 Conjugation of palmitate to BSA

Palmitate was conjugated to BSA as described in **Chapter 2 Materials and Methods** (section 2.1.3 *Conjugation of palmitate to BSA*).

3.3.4 Pharmacological inhibitors

AMG PERK 44 and 4μ8c were purchased from Tocris Bioscience, and dissolved in DMSO to a concentration of 20 mM. The inhibitors were diluted into culture media to a final concentration of 10 μM. Tunicamycin from *Streptomyces* (Sigma Aldrich, T7765) was dissolved in DMSO to a concentration of 100 μg/mL. The inhibitor was then diluted into culture media to a final concentration of either 10 ng/mL or 50 ng/mL.

3.3.5 Cell harvesting

Cells were harvested and pelleted as described in **Chapter 2 Materials and Methods** (section 2.1.4 *Cell harvesting*). Cell counts were performed using a Scepter automated cell counter (Millipore).

3.3.6 Animal studies

The detail of three mouse studies analysed in this chapter are summarised in **Chapter 2 Materials and Methods** (section 2.2 *Animal studies*)**.**

3.3.7 Human skeletal muscle biopsies

Biopsies of *pectoralis major* were taken from volunteers undergoing pacemaker therapy, as described in **Chapter 2 Materials and Methods** (section 2.3 *Human skeletal muscle biopsies*)**.**

3.3.8 RNA isolation and purification

RNA was harvested and purified from cells *in situ* using the Qiagen RNeasy Mini kit, following manufacturer's instructions, as described in **Chapter 2 Materials and Methods** (section 2.4.1 *RNA isolation and purification*)**.**

3.3.9 cDNA synthesis

cDNA was synthesised using the Qiagen RT^2 First Strand kit, following the manufacturer's instructions, as summarised in **Chapter 2 Materials and Methods** (section 2.4.2 *cDNA synthesis*)**.**

3.3.10 Reverse transcription quantitative polymerase chain reaction

Samples were than analysed using the Applied Biosystems StepOnePlus Real-Time PCR system, as described in **Chapter 2 Materials and Methods** (Section 2.4.3 *Reverse transcription quantitative polymerase chain reaction*)**.** Expression of *Atf3, Atf4, Hspa5* and *Edem1*, normalised to *Rn18s*, was used to assess ER stress activation in C2C12 myotubes. Expression of *ATF3, ATF4, HSPA5* and *EDEM1*, normalised to *Actb*, was used to assess ER stress induction in primary human skeletal muscle cells.

3.3.11 Metabolite extraction from cells

Metabolites were extracted from cells using a modified Bligh and Dyer method, as described in **Chapter 2 Materials and Methods** (section 2.5.2 *Cell metabolite and lipid extraction for mass spectrometry*)**.**

3.3.12 Metabolite extraction from skeletal muscle tissue

Approximately 30 mg of tissue was first homogenised using a TissueLyser (Qiagen), and metabolites were then extracted using a Bligh and Dyer extraction, outlined in **Chapter 2 Materials and Methods** (section 2.5.2 *Human and mouse skeletal muscle tissue extraction*).

3.3.13 FAME derivatisation

Dried organic samples were made up in 750 µl methanol/chloroform (1:1). Samples were then derivatised using 125 µl 10% BF_3 in methanol, and incubated at 80°C for 90 minutes. 500 µl MilliQ water and 1 ml hexane were added, and the samples vortexed, forming two layers. The organic phase was extracted and dried down, before reconstitution in 100 µl hexane.

3.3.14 Gas chromatography-mass spectrometry analysis of FAMEs

All samples were run on a Trace GC Ultra paired to a DSQ II single-quadrupole mass spectrometer [261]. For organic samples, a 30 m x 0.25 mm 70% cyanopropyl polysilphenylene-siloxane column (0.25 µm TR-FAME stationary phase; Thermo Scientific) was used. 4 µl of the sample was injected, with a split ratio of 8. The injector temperature was set to 230 °C, the transfer line to 240 °C, the ion source to 250 °C and the helium carrier gas was used at a constant flow rate of 1.2 ml/min. The initial column temperature of 60 °C was held for 2 minutes and then increased by 15 °C/min to 150 °C and then by 4 °C/min to 230 °C. The run time for each sample was 28 minutes.

The subsequent chromatograms were analysed using Xcalibur software (version 2.2; Thermo Scientific). Each peak was integrated and normalized to an internal standard peak. Peak assignment was based on mass fragmentation patterns matched to the NIST/ EPA/NIH mass

spectral library. Identification was supported by comparison with a FAME standard mix (Supelco 37 Component FAME Mix; Sigma Aldrich).

3.3.15 Liquid chromatography-mass spectrometry analysis of lipids

Samples were dissolved in 50 µl methanol/chloroform (1:1) and 10 µl of this was added to 190 µl IPA/ACN/H_2O (2:1:1). They were then analysed using an Orbitrap Elite mass spectrometer (Thermo Fisher), as described in **Chapter 2 Materials and Methods** (section 2.6 *Liquid chromatography-mass spectrometry open profiling of lipids*)**.** Chromatogram files were converted using MSConvert (Proteowizard), and processed using XCMS within an R script. Peaks were normalised to a relevant internal standard and then either cell number, for *in vitro* experiments, or dry protein pellet weight, for the analysis of skeletal muscle tissue.

3.3.16 Statistics

Statistical significance was assessed using either one-way ANOVA, with Tukey's multiple comparison test, or Student's t-tests, as detailed in each figure. In each case, $n \geq 3$ and the significance level was set to $P \leq 0.05$. The GraphPad Prism (version 6) software was used for all univariate analysis.

3.4 Results

3.4.1 The induction of ER stress in C2C12 myotubes under differing culture media serum conditions

C2C12 cells, isolated from mice recessive for the dystrophic *dy* gene, are capable of undergoing differentiation from myoblasts to myotubes [262–264]. They have been reported as cultured to confluence as myoblasts in media containing 10% foetal bovine serum (FBS) and 1% penicillin-streptomycin [83,265]. The myoblasts are then differentiated into myotubes with the addition of differentiation media. The composition of this differentiation media varies, with media containing 2% horse serum (HS) reported [83,265], while American Type Culture Collection (ATCC) instruct use of a media containing 10% horse serum [266].

To determine the optimal serum conditions for palmitate-induced ER stress, C2C12 myoblasts were cultured to confluence and then differentiated in media containing either 2% or 10% HS, as well as 1% penicillin-streptomycin and 750 nM insulin. Insulin is widely-accepted to not only enhance differentiation but also increase fatty acid, and therefore palmitate, uptake [267–269]. Cells were then differentiated for 6 days, during which they were treated with either 100 µM or 200 µM palmitate conjugated BSA, or the BSA vehicle. Concentrations of palmitate were based on measured plasma concentrations in the literature (122 µM free palmitate, measured by GC-MS) [270].

RT-qPCR of a panel of four UPR-related genes – *Atf3*, *Atf4*, *Hspa5* and *Edem1* - was used to determine the induction of ER stress. *Atf4* is downstream of Perk signalling [271], while Atf6 and Atf4 increase the expression of *Hspa5* and *Atf3* [272,273]. Ire1 activation triggers elevated transcription of *Edem1*, via spliced Xbp1 [274]. Transcriptional analysis of these four genes provides an assessment of induction of the three arms of the UPR.

In 10% HS conditions, 100 µM palmitate did not induce expression of the ER stress gene panel, but 200 µM palmitate significantly increased the expression of all four genes (1.8-fold increase in *Atf3*, 2.3-fold increase in *Atf4*, 1.7-fold increases in *Hspa5* and *Edem1)* (**Figure 3.1B).** Conversely, 200 µM palmitate had no effect on the expression of the gene-panel when myotubes were grown in 2% HS (**Figure 3.1A**). The lower concentration of palmitate was able to increase transcription of *Atf3* (1.5-fold) and *Hspa5* (1.3-fold), but this was not to the same extent as with 200 µM palmitate in 10% HS conditions. Therefore, 10% HS differentiation media was utilised to assess palmitate-induced ER stress in C2C12 cells.

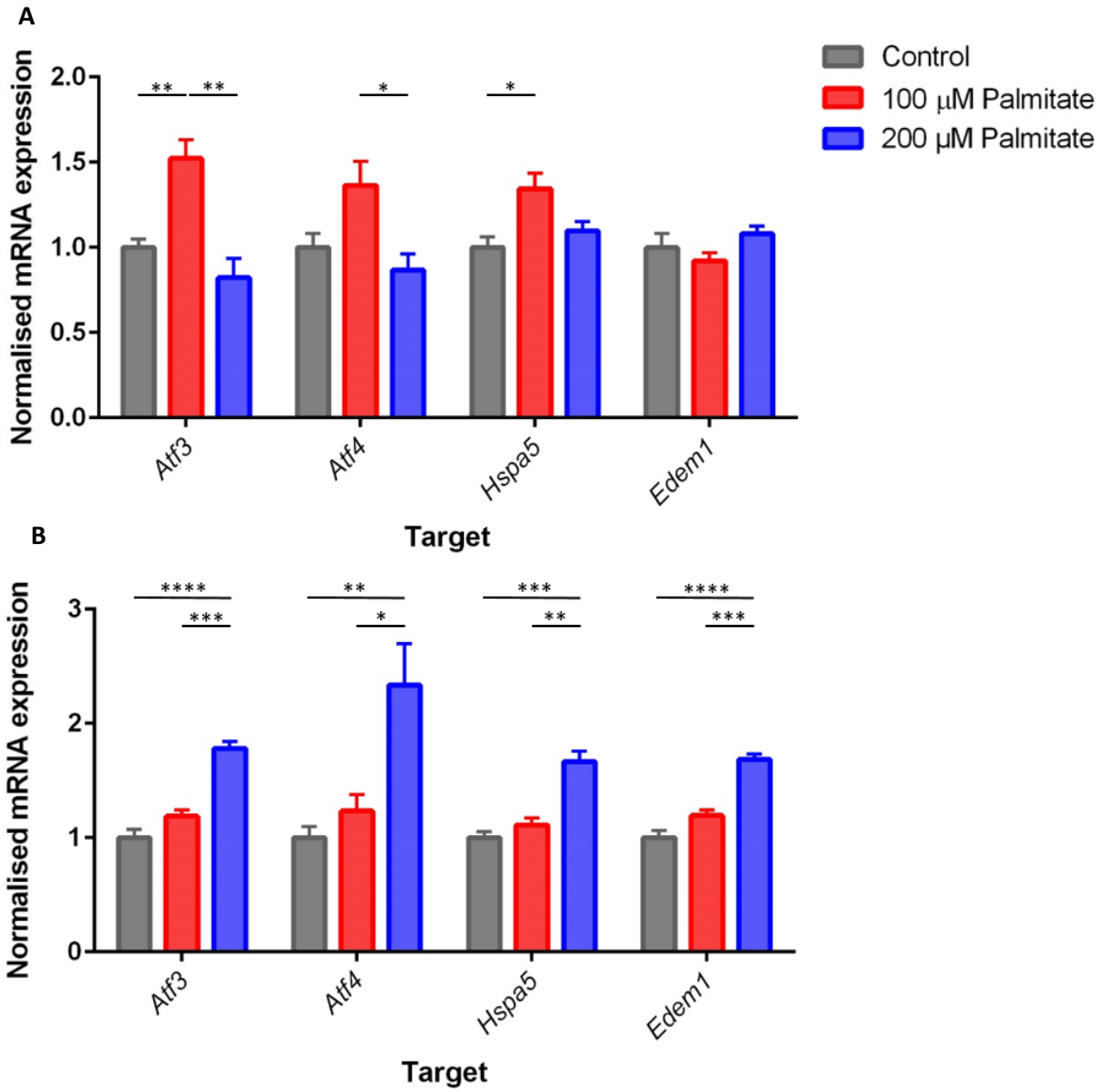

Figure 3.1: Chronic palmitate treatment increases expression of unfolded protein response genes in C2C12 cells differentiated in 10% serum-containing media

C2C12 cells were differentiated for 6 days in media containing either 2% **(A)** or 10% **(B)** horse serum. During this period, myotubes were exposed to either 100 or 200 µM palmitate, or the vehicle control. RT-qPCR was used to analyse the expression of key unfolded protein response genes (*Atf3*, *Atf4*, *Hspa5* and *Edem1*). Each gene was analysed using a one-way ANOVA test with Tukey's multiple comparison test. * $P \leq 0.05$, ** $P < 0.01$, *** $P < 0.001$, **** $P < 0.0001$. Data are expressed as mean ± SEM (n=4).

3.4.2 Acute exposure to palmitate induces ER stress in C2C12 myotubes

Canonically, palmitate-induced ER stress has been investigated using acute treatment with the fatty acid, typically for 18-24 hours [54,103,257–260]. To compare the C2C12 model used in this thesis with the acute investigations of the effects of high-concentration palmitate in other *in vitro* cell culture systems reported in the literature, cells were grown to confluence, and then differentiated for 5 days in 10% HS. Following this, myotubes were treated with 750 µM palmitate for 24 hours, or the vehicle control. RNA was extracted from the cells and the expression of UPR gene-panel was analysed using RT-qPCR. Palmitate significantly increased the expression of *Atf3* (13.5-fold), *Atf4* (4-fold), *Hspa5* (2-fold) *and Edem1* (12-fold), indicating activation of ER stress (**Figure 3.2**). The increase in expression of UPR markers is much greater following an acute treatment, but the gene expression changes observed in the chronic model are much more in keeping with alterations seen *in vivo* in murine skeletal muscle, following high-fat feeding [275]. This suggests that a chronic model of palmitate-induced ER stress is more physiologically relevant to understanding the link between lipotoxicity and ER-stress in metabolic disease. The acute treatment regime does not reflect the physiological scenario in obesity, where saturated plasma fatty acid concentrations are chronically elevated [166,276]. To replicate the pathophysiological environment, experiments within this thesis will use C2C12 cells treated with a lower, more physiological dose of palmitate (200 µM), for a prolonged period of time (6 days).

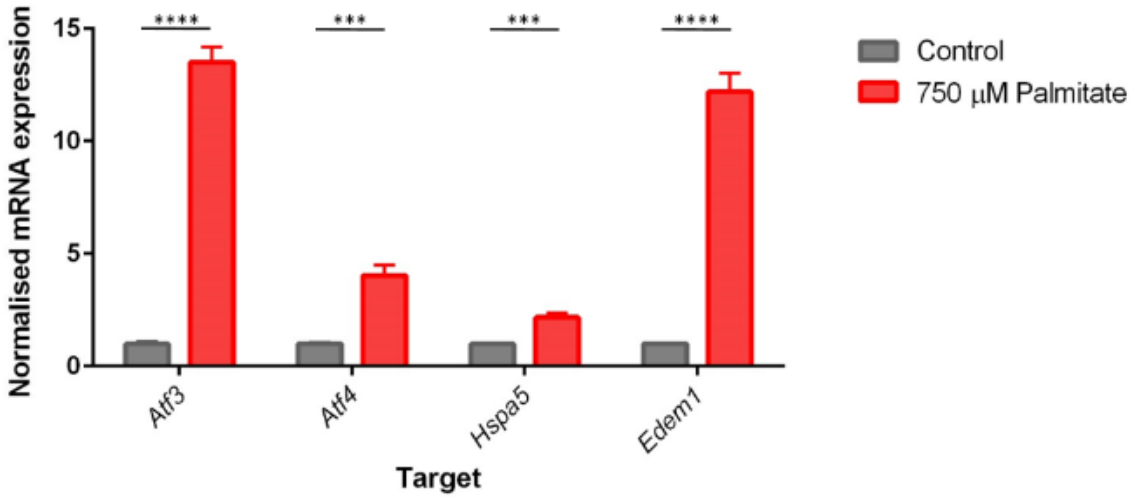

Figure 3.2: Acute palmitate treatment induces endoplasmic reticulum stress

Differentiated C2C12 myotubes were treated with 750 μM palmitate, or the BSA vehicle control, for 24 hours. The transcription of unfolded protein response genes (*Atf3*, *Atf4*, *Hspa5* and *Edem1*) was analysed using RT-qPCR. Each gene was analysed using a Student's t-test. * $P \leq 0.05$, ** $P < 0.01$, *** $P < 0.001$, **** $P < 0.0001$. Data are expressed as mean ± SEM (n=4).

3.4.3 Chronic palmitate treatment alters fatty acid metabolism in C2C12 myotubes

To investigate potential metabolic alterations that may derive from palmitate-driven lipotoxicity and ER stress in skeletal myocytes, GC-MS was used to interrogate the fatty acid profile of C2C12 cells treated for 6 days with either 100 or 200 μM palmitate, or a BSA vehicle control. Lipids were extracted from the cells and derivatised to yield FAMEs prior to analysis with GC-MS. The use of this derivatisation hydrolyses fatty acids from complex lipid species, and so this GC-MS analysis is of the total intracellular fatty acid profile.

Exposing C2C12 myotubes to palmitate greatly increased the intracellular concentration of palmitate in a dose responsive manner, which may reflect uptake from the media (**Figure 3.3A**). Concentrations of palmitoleate, the desaturation product of palmitate, were also increased analogously (**Figure 3.3B**).

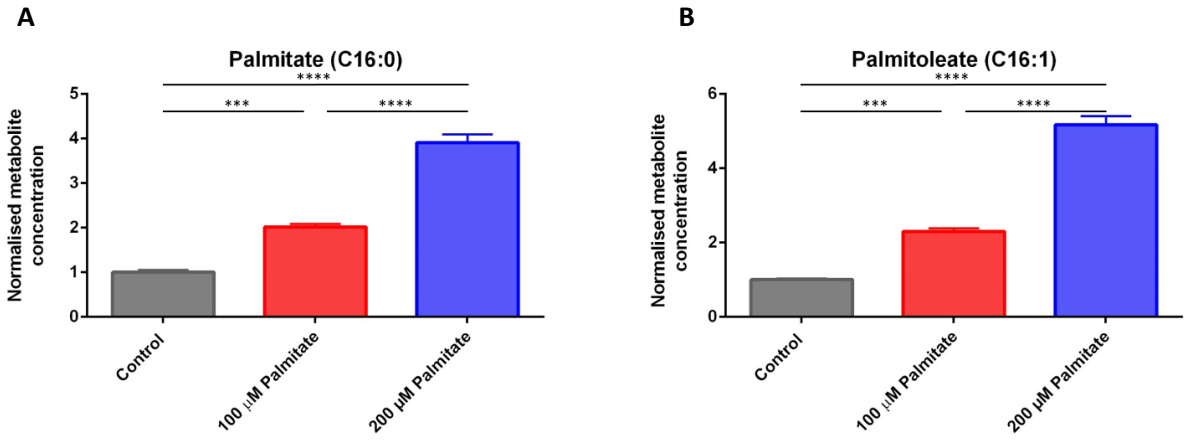

Figure 3.3: Chronic palmitate treatment increases total intracellular palmitate and palmitoleate concentrations

C2C12 myotubes were treated with either 100 or 200 µM palmitate for 6 days. Fatty acid methyl ester (FAME) analysis by gas chromatography-mass spectrometry demonstrates increases in palmitate (A) and palmitoleate (B). FAMEs were analysed using a one-way ANOVA test with Tukey's multiple comparison test. * $P \leq 0.05$, ** $P < 0.01$, *** $P < 0.001$, **** $P < 0.0001$. Data are expressed as mean ± SEM (n=4).

Chronic palmitate treatment also induced changes in both n-6 and n-3 PUFAs. In the n-6 pathway, γ-linolenic acid (GLA, 18:3) concentration is dose-responsively increased, while the concentration of downstream metabolites - dihomo-γ-linolenic acid (DGLA, 20:3), arachidonic acid (AA, 20:4) and docosatetraenoic acid (22:4) – are all decreased (**Figure 3.4A**).In the n-3 pathway palmitate treatment results in a dose-dependent increase in α-linolenic acid (ALA, 18:3) and eicosatetraenoic acid (20:4) concentration, and a decrease in docosapentaenoic acid (22:5). Eicosapentaenoic acid (EPA, 20:5), however, was unchanged (**Figure 3.4B**).

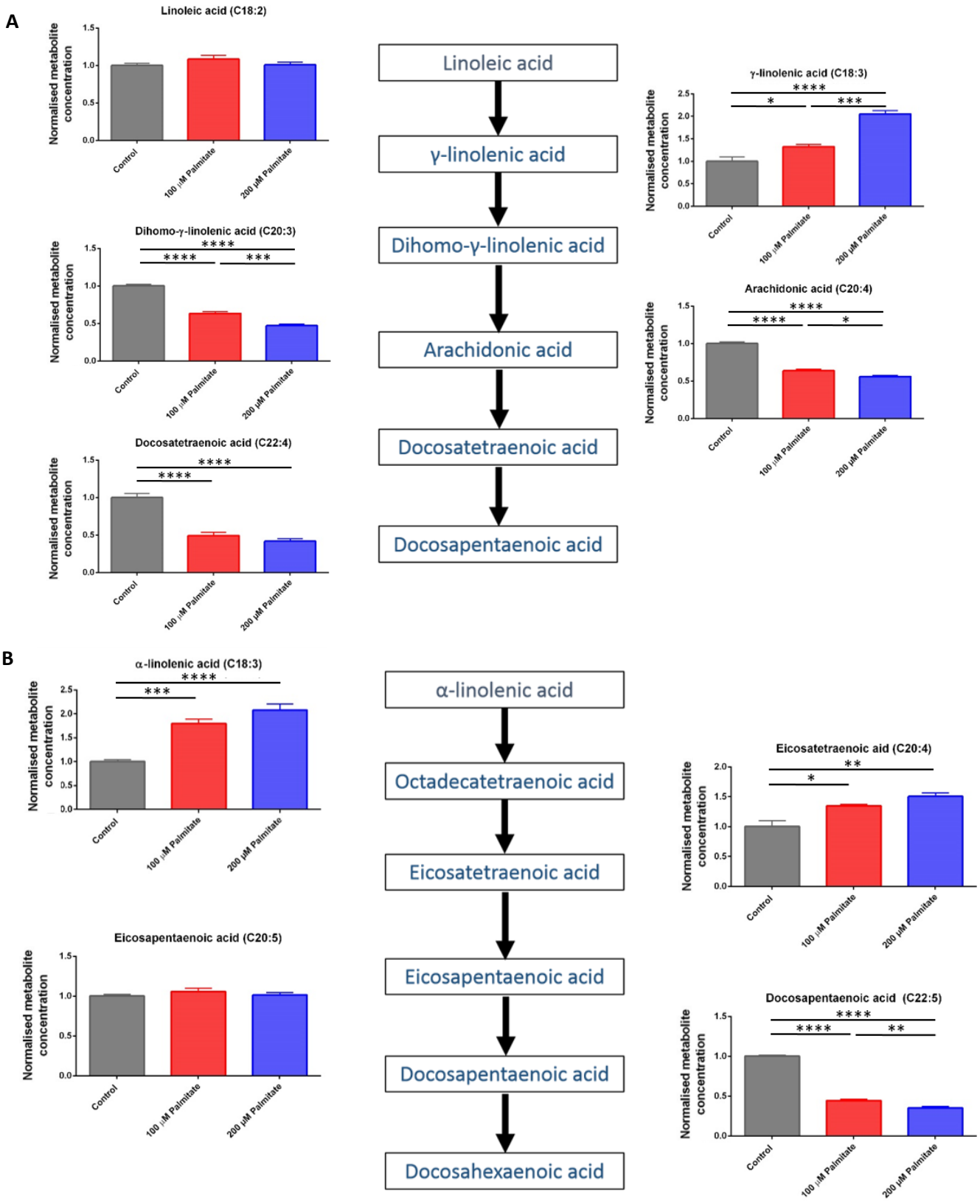

Figure 3.4: Chronic palmitate alters the levels of polyunsaturated fatty acid methyl esters

C2C12 myotubes were treated with either 100 or 200 μM palmitate for 6 days. Fatty acid methyl ester (FAME) analysis by gas chromatography-mass spectrometry highlights alterations in both the n-6 (A) and the n-3 (B) polyunsaturated fatty acid pathways. FAMEs were analysed using a one-way ANOVA test with Tukey's multiple comparison test. * $P \leq 0.05$, ** $P < 0.01$, *** $P < 0.001$, **** $P < 0.0001$. Data are expressed as mean ± SEM (n=4).

3.4.4 Acute palmitate treatment of C2C12 myotubes induces less pronounced perturbation of fatty acid metabolism

To investigate the effect of acute palmitate-induced ER stress on fatty acid metabolism, differentiated C2C12 myotubes were treated with 750 µM palmitate for 24 hours. Lipids were isolated and derivatised to yield FAMEs and analysed using GC-MS. Acute palmitate treatment increased intracellular palmitate concentrations to a much greater extent than chronic palmitate treatment, reflecting the higher concentration in the media. Palmitoleate was also increased, but to a lesser extent than in the chronic scenario (**Figure 3.5**).

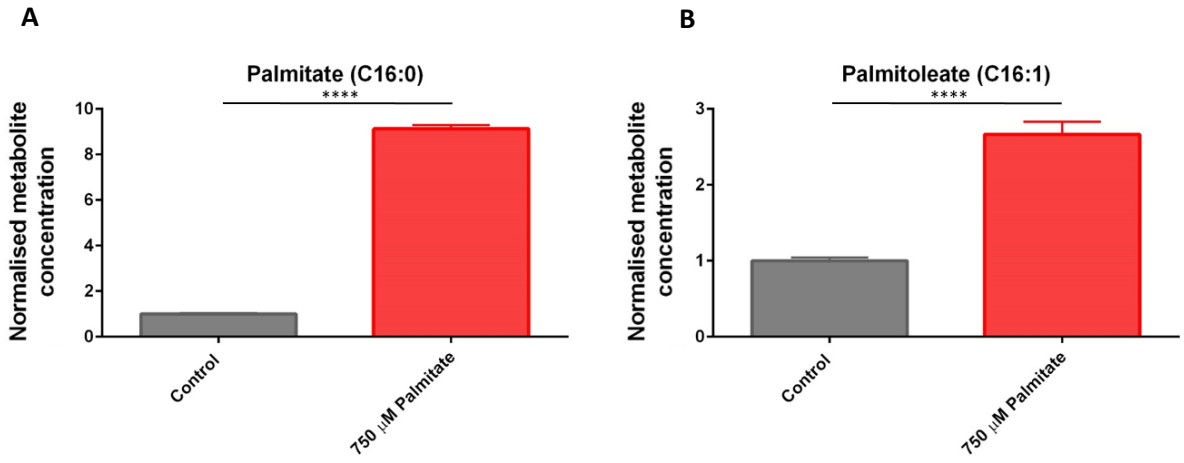

Figure 3.5: Acute palmitate treatment increases total palmitate and palmitoleate concentrations

Differentiated C2C12 myotubes were treated with 750 µM palmitate, or the vehicle control, for 24 hours. Gas chromatography-mass spectrometry analysis of fatty acid methyl esters (FAMEs) shows increases in palmitate (A) and palmitoleate (B) following acute exposure to palmitate. FAMEs were analysed using a Student's t-test. * $P \leq 0.05$, ** $P < 0.01$, *** $P < 0.001$, **** $P < 0.0001$. Data are expressed as mean ± SEM (n=4).

In comparison to the chronic model, however, acute palmitate treatment had a reduced effect on PUFA metabolism. Within the n-6 pathway, there was an increase in linoleic acid (18:2), while concentrations of DGLA and AA decreased. The direction of changes were in keeping with the chronic model, but differences between control and treatment groups were much smaller (**Figure 3.6A**). Similarly, in the n-3 pathway acute palmitate treatment increases ALA concentrations, with concomitant decreases in EPA and docosapentaenoic acid (**Figure 3.6B**).

The analysis of total fatty acid metabolism highlights that, while acute palmitate induces greater expression of UPR genes, a lower, chronic dose of palmitate has far greater effects on intracellular fatty acid concentrations, against a background of ER stress, more in keeping with the *in vivo* situation in obese murine skeletal muscle. In particular, chronic palmitate treatment increases the concentration of early members of the n-6 and n-3 PUFA pathways, including GLA, ALA and eicosatetraenoic acid, while downstream fatty acids – DGLA, AA, docosatetraenoic acid, and docosapentaenoic acid – were all decreased.

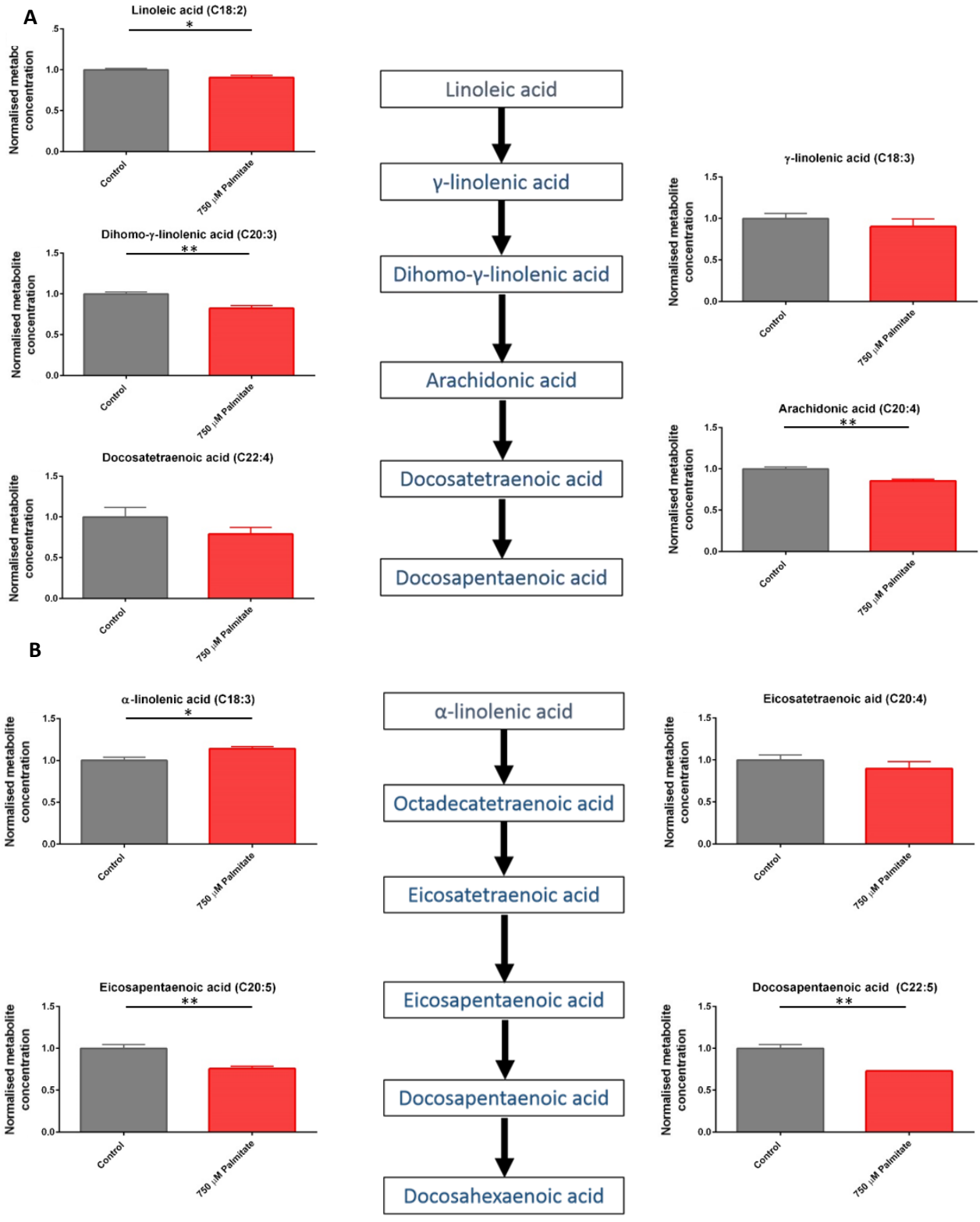

Figure 3.6: Acute palmitate treatment alters the concentrations of intracellular polyunsaturated fatty acids in C2C12 myotubes

C2C12 myotubes were treated with 750 μM palmitate, or the vehicle control, for 24 hours. Fatty acid methyl ester (FAME) analysis by gas chromatography-mass spectrometry highlights alterations in both the n-6 (A) and the n-3 (B) polyunsaturated fatty acid pathways. FAMEs were analysed using a Student's t-test. * $P \leq 0.05$, ** $P < 0.01$, *** $P < 0.001$, **** $P < 0.0001$. Data are expressed as mean ± SEM (n=4).

3.4.5 Chronic palmitate treatment induces breakdown of PUFA-containing phosphatidylcholines in C2C12 myotubes

GC-MS analysis of FAMEs provides information on the total fatty acid profile, but does not give information on the intact lipid the fatty acid may be derived from. An untargeted LC-MS method was employed to investigate the effects of chronic palmitate treatment on intact complex lipids. Cells were treated with either 100 or 200 µM palmitate, or the BSA vehicle for 6 days during differentiation. Metabolites were extracted from the cells as before and the organic phase was analysed using LC-MS. In positive mode, diacyl- and triacylglycerols, as well as phosphatidylcholines, lysophosphatidylcholines and sphingomyelins were all detected. In negative mode, free fatty acids, ceramides and other phospholipid species such as phosphatidylethanolamines, phosphatidylglycerols and phosphatidylinositols were analysed.

Approximately 500 annotated lipid species were detected in positive ionisation mode and a further 150 in negative ionisation mode. As well as increases in saturated glycerolipids, chronic palmitate treatment decreased levels of PUFA-containing PCs, in keeping with alterations observed in FAME profiles. Fragmentation spectra were then used to conclusively identify fatty acid composition of each PC that contained 4 or more double bonds. In particular, intracellular PC 16:0/20:4 and 18:0/20:4 were significantly decreased in C2C12 cells with palmitate treatment (**Figure 3.7A**). Similar changes were also seen in PCs containing EPA, with PC 16:0/20:5, 16:1/20:5 and 18:1/20:5 all decreased following exposure to palmitate (**Figure 3.7B**). This suggests that the decreases in total PUFAs within the cells detected via GC-MS analysis correspond to a reduction in PUFA- containing PCs.

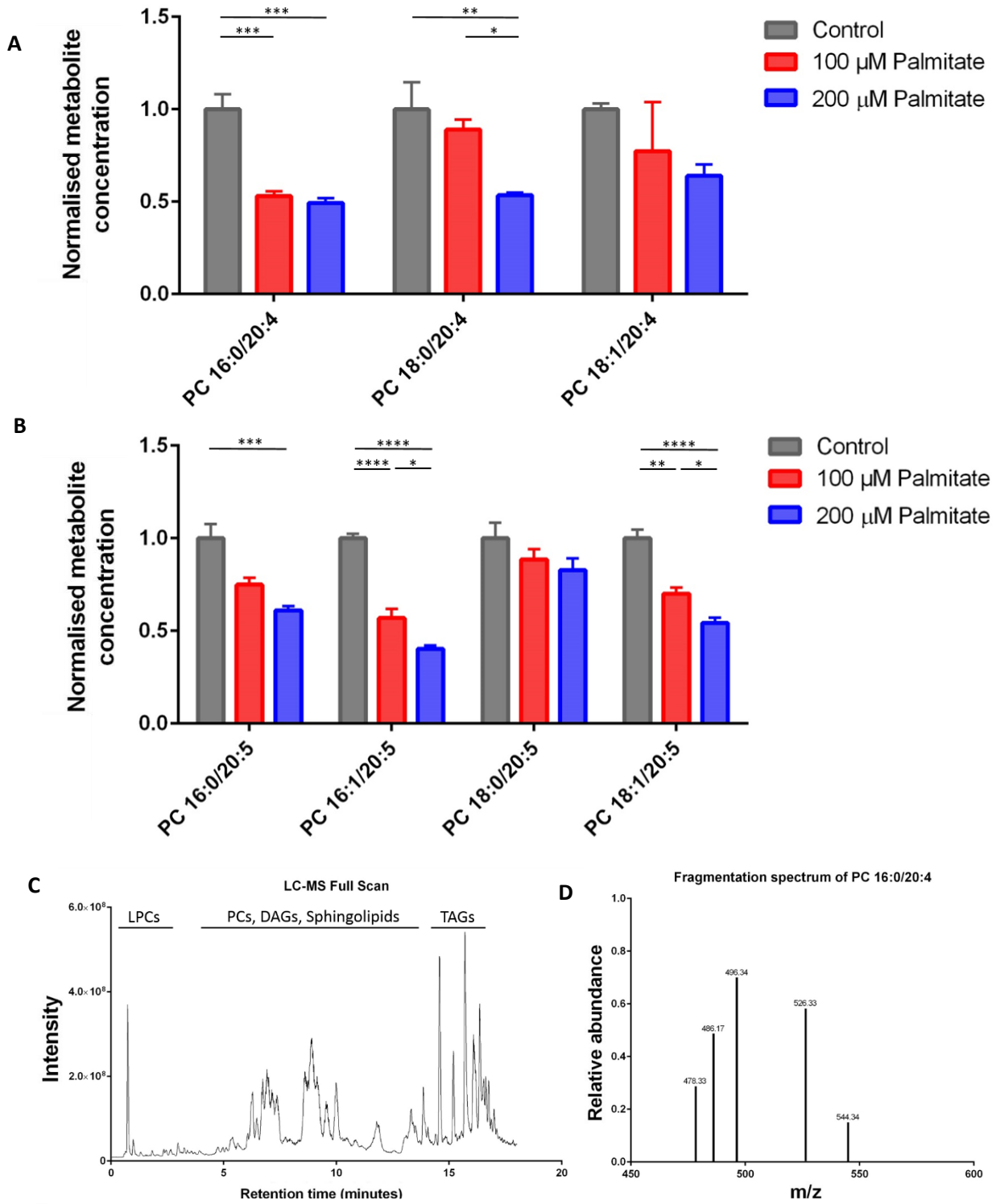

Figure 3.7: Chronic palmitate treatment induces breakdown of polyunsaturated fatty acid-containing phosphatidylcholines

C2C12 myotubes were treated with either 100 or 200 µM palmitate for 6 days, or the vehicle control. Liquid chromatography-mass spectrometry analysis shows palmitate-induced breakdown of phosphatidylcholine (PC) species containing arachidonic acid (A) and eicosapentaenoic acid (B). (C) shows a typical LC-MS chromatogram, while (D) is a typical fragmentation spectrum of m/z 782.57. Peaks at m/z of 478 and 496 are typical of a PC containing palmitate, while peaks at 526 and 544 indicate the presence of arachidonic acid. PCs were analysed using a one-way ANOVA test with Tukey's multiple comparison test. * $P \leq 0.05$, ** $P < 0.01$, *** $P < 0.001$, **** $P < 0.0001$. Data are expressed as mean ± SEM (n=4).

3.4.6 Chronic palmitate treatment increases expression of ER stress genes and induces breakdown of PUFA-containing phosphatidylcholines in primary human skeletal muscle cells

To determine whether palmitate increases ER stress and phospholipid remodelling in human skeletal muscle, experiments were also conducted using primary human skeletal muscle cells (HSkMCs). HSkMCs represent a model more applicable to investigations of lipotoxicity-induced ER stress in human disease when compared with the C2C12 myoblast immortalised mouse cell line. HSkMCs were grown to confluence in growth media and then differentiated for 6 days in differentiation media. During differentiation, cells were treated with either 50 or 100 µM palmitate, or the BSA vehicle. Reduced palmitate concentrations were used compared to C2C12 myotube culture due to high levels of cell death at 200 µM. RNA was extracted and analysed using RT-qPCR to assess induction of the UPR. Metabolites were extracted using a modified Bligh and Dyer method, and the lipid-containing organic phase was analysed using an open-profiling LC-MS/MS lipidomics method.

Palmitate increased the expression of the UPR gene panel in a dose-responsive manner (control vs. 100 µM palmitate: *ATF3* 2.6-fold, *ATF4* 1.3-fold, *HSPA5* 1.6-fold, *EDEM1* 1.2-fold), indicating the induction of ER stress (**Figure 3.8A**). Five phosphatidylcholine species were conclusively annotated. Palmitate dose-responsively decreased the levels of the AA-containing PCs (PC 16:0/20:4, PC 18:0/20:4, and PC 18:1/20:4) (**Figure 3.8B**), consistent with observations made in C2C12 myotubes. However, PC 16:0/20:5 was increased with palmitate exposure, in contrast to results seen in the C2C12 model. It's important to note, however, that this data is reported as fold-change. The concentration of PC 18:0/20:4 is much higher than PC 16:0/20:5, and so the impact of this palmitate-stimulated increase may be reduced in this model. These data indicate that chronic palmitate treatment stimulates phospholipid remodelling in HSkMCs, particularly in relation to the concentrations of AA-containing species.

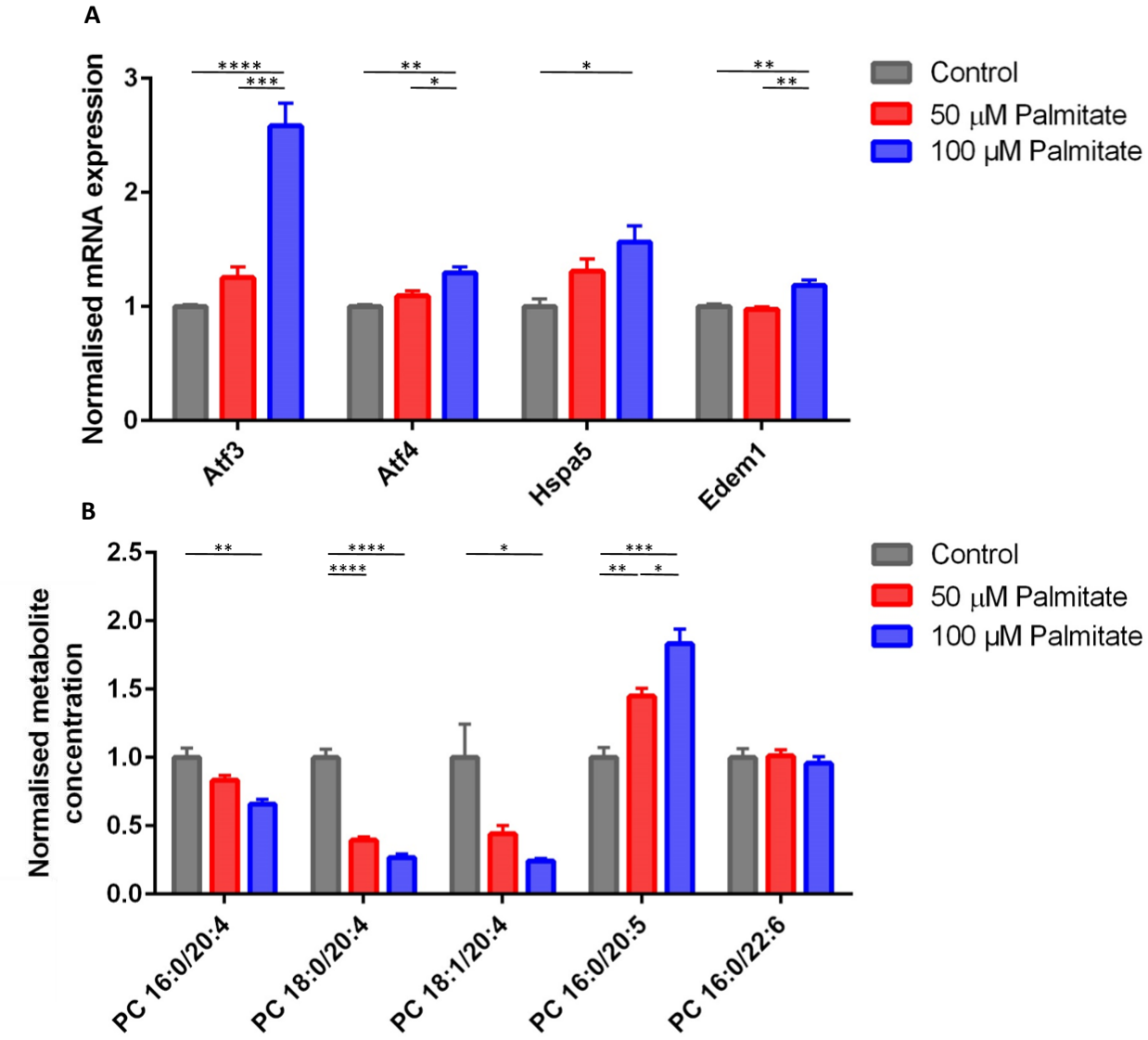

Figure 3.8: Chronic palmitate treatment stimulates phospholipid remodelling in primary human skeletal muscle cells, concomitant with an increase in ER stress

Primary human skeletal muscle cells were treated with 50 or 100 µM palmitate, or the vehicle for 6 days. (A) RT-qPCR was used to analyse transcription of unfolded protein response markers. (B) Phospholipid species were measured using liquid chromatography-mass spectrometry. Each species was analysed using a one-way ANOVA test with Tukey's multiple comparison test. * $P \leq 0.05$, ** $P < 0.01$, *** $P < 0.001$, **** $P < 0.0001$. Data are expressed as mean ± SEM (n = 4).

3.4.7 Phospholipid remodelling in high-fat diet mouse models

Sustained feeding of mice with a high fat diet (HFD) increases body weight and reduces insulin sensitivity, providing a model for obesity and T2DM [277]. This project makes use of two separate studies in which mice were fed either a regular chow diet or a high-fat diet to investigate phospholipid remodelling in the skeletal muscle of an *in vivo* model of obesity.

In the first study, 10 male C57Bl6 mice were fed a regular chow diet and 13 were fed a high-fat diet for 14 weeks. Metabolites from the gastrocnemius muscle of these mice were extracted from the tissue, and the lipid fraction was analysed by LC-MS. Ten PUFA-containing PC species were definitively annotated in positive mode, using fragmentation analysis. Intensities were normalised to an internal standard, and dried protein pellet weight. Lipidomic analysis identified a phospholipid profile inconsistent with *in vitro* studies. PC 14:0/20:4, 16:0/20:4 and 18:0/20:4 were all increased in the muscle of mice fed a high-fat diet. PC 16:1/20:4 was the only AA-containing PC concentration decreased in the muscle of HFD fed mice (**Figure 3.9A**). However, the behaviour of EPA and DHA-containing PCs was consistent with the results observed in palmitate-treated myotubes, with PC 16:0/20:5, 16:1/20:5, 16:0/22:6 and 18:1/22:6 decreased in the muscle of mice fed a high-fat diet (**Figure 3.9B**).

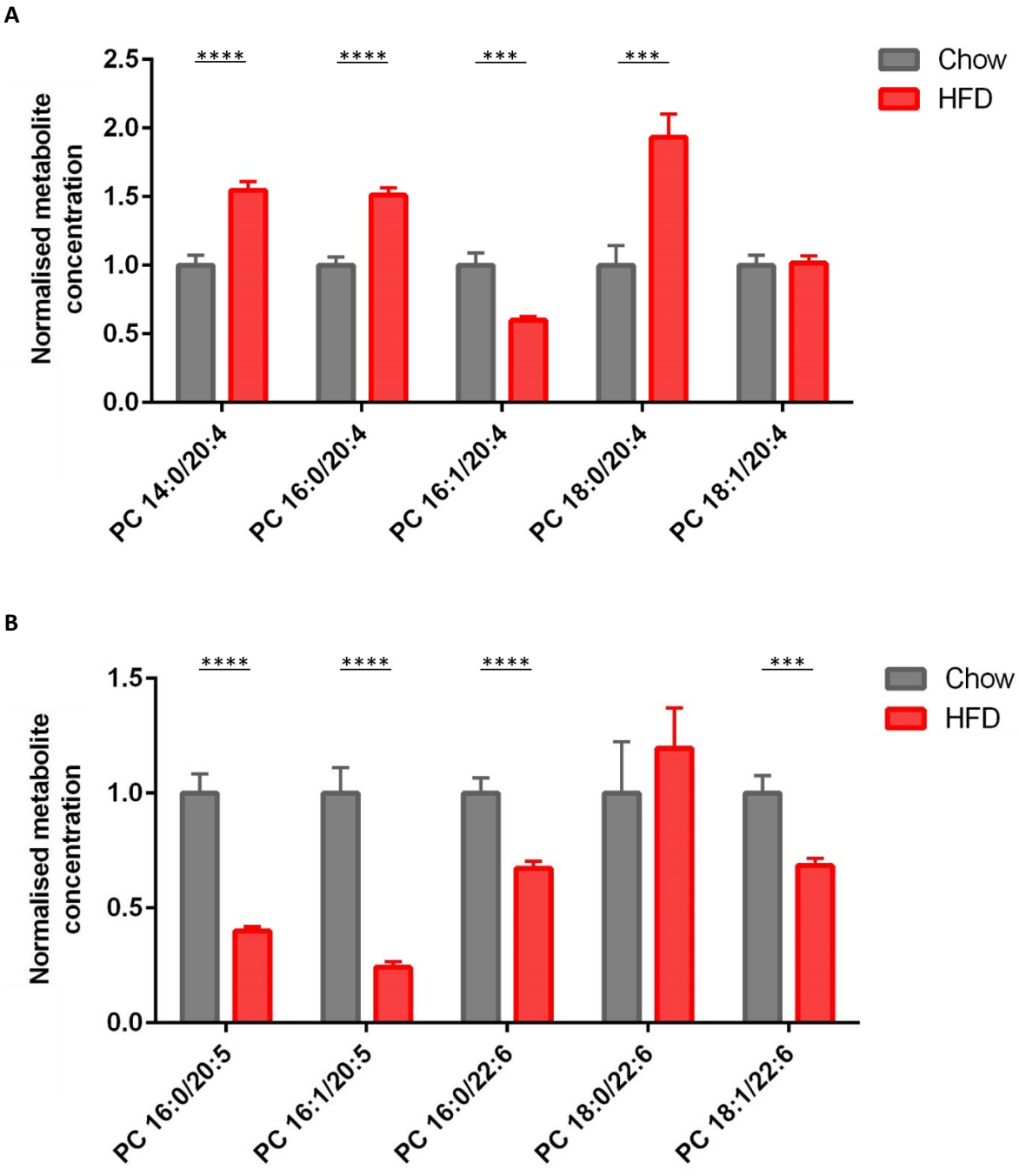

Figure 3.9: High fat diet-fed mice have alterations in polyunsaturated fatty acid-containing phosphatidylcholines in skeletal muscle

Mice were fed either a chow or high-fat diet (HFD) for 14 weeks. Liquid chromatography-mass spectrometry analysis of phospholipids extracted from gastrocnemius tissue show alteration in (A) arachidonic acid-, (B) eicosapentaenoic acid- and docosahexaenoic acid-containing phosphatidylcholines. Each species was analysed using a Student's t-test. * $P \leq 0.05$, ** $P < 0.01$, *** $P < 0.001$, **** $P < 0.0001$. Data are expressed as mean ± SEM (chow: n = 10, HFD: n = 13).

In the second study, male C57Bl6 mice were fed either a regular chow (n = 5) or a high fat diet (n = 5) for 17 weeks. The gastrocnemius muscle lipid profile was then analysed using LC-MS, with CID fragmentation to confirm lipid annotations. Intensities were normalised to an internal standard, and dried protein pellet weight. Unlike the first study, and the *in vitro* studies, the majority of detected PUFA-containing PCs were unaffected by high fat diet feeding. However, PC 16:1/20:4, 18:2/20:5 and 16:0/22:6 concentrations were decreased by a high fat diet (**Figure 3.10**). These murine studies suggest that while increased lipid exposure does increase breakdown of some PUFA-containing PCs, the effect is blunted when compared to the remodelling observed when exposing myotubes to palmitate *in vitro*.

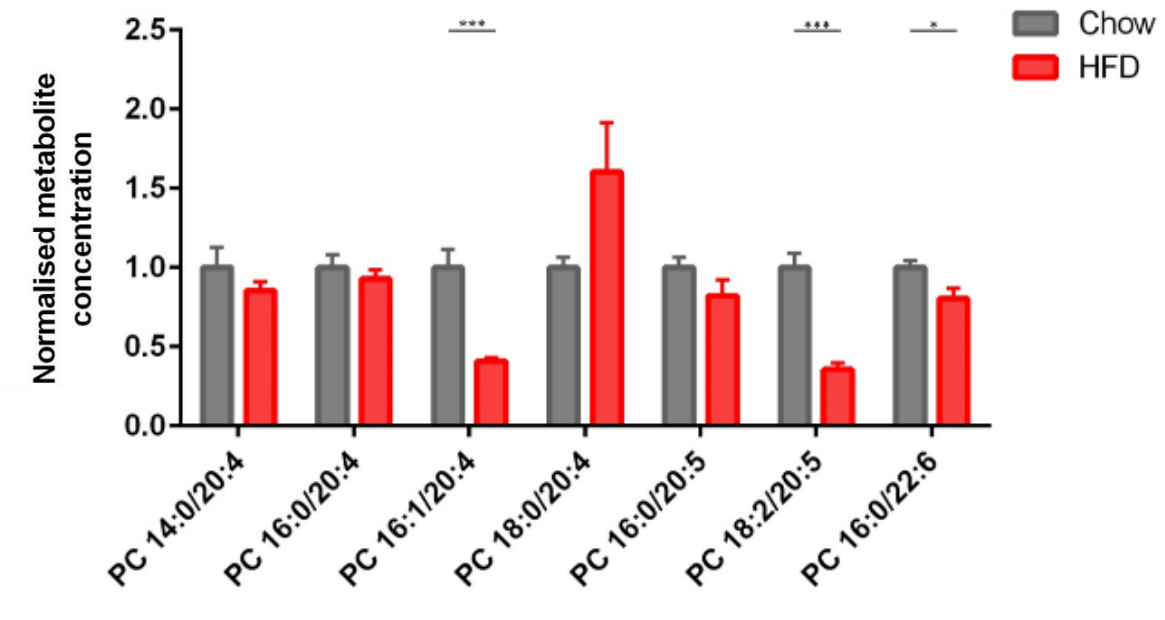

Figure 3.10: Changes in polyunsaturated fatty acid-containing phosphatidylcholines are less pronounced in a second mouse study

Mice were fed either a chow or high-fat diet for 17 weeks. Liquid chromatography-mass spectrometry analysis of phospholipids extracted from gastrocnemius tissue show polyunsaturated fatty acid-containing phosphatidylcholines are partially affected by high-fat diet. Each species was analysed using a Student's t-test. * $P \leq 0.05$, ** $P < 0.01$, *** $P < 0.001$, **** $P < 0.0001$. Data are expressed as mean ± SEM (n = 5).

3.4.8 Mice fed a "western-style" diet have reduced concentrations of skeletal muscle PUFA-containing phosphatidylcholines compared with mice fed a low-fat control diet

A recent study highlighted the importance of diet composition in the induction of obesity and insulin resistance [278]. The authors demonstrated that a diet closely related to the human Western diet (WD), enriched in fat and carbohydrate, provided a robust obesogenic model. Therefore, phospholipid remodelling was analysed in a WD-fed mouse model. Eight male C57Bl6 mice were fed either a low-fat control diet or a western diet for 12 weeks.

Metabolites were extracted from the gastrocnemius skeletal muscle using a Bligh and Dyer extraction, and the organic fraction was dried and analysed by LC-MS/MS. Eleven PUFA-containing PCs were annotated using fragmentation analysis. The intensity of each lipid species was normalised to the relevant internal standard and dried protein pellet weight. Mice fed a western diet had decreased levels of PUFA-containing phosphatidylcholines suggesting an induction of phospholipid breakdown similar to that detected *in vitro* (**Figure 3.11**). Unlike mice fed a high fat diet, decreases in phospholipids were not fatty acid-specific, with decreases observed in AA-, EPA-, and DHA-containing PCs.

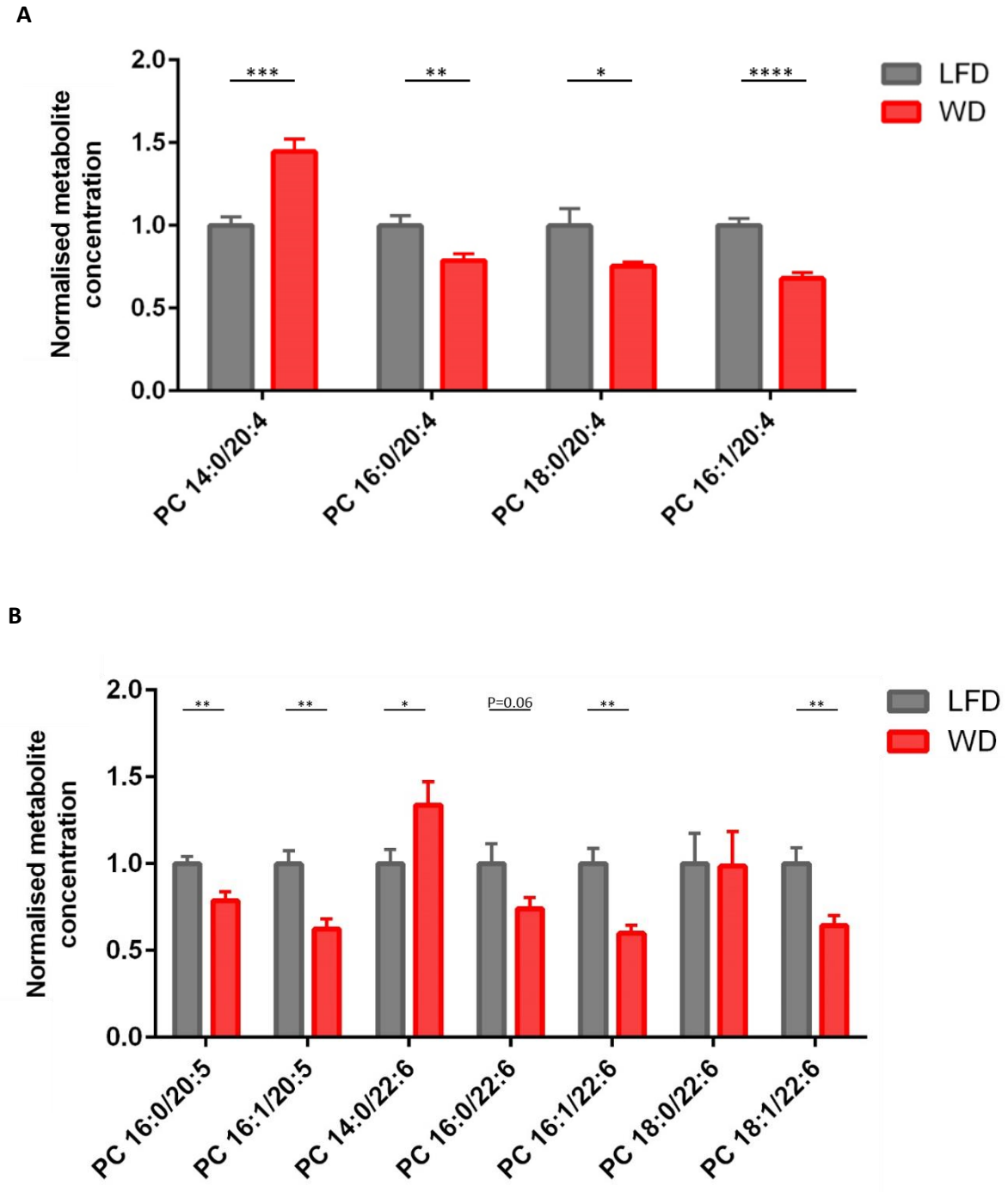

Figure 3.11: Mice fed a western diet have reduced concentrations of polyunsaturated fatty acid-containing phosphatidylcholines

Mice were fed either a "western-style" diet or a low fat control diet for 12 weeks. Liquid chromatography-mass spectrometry analysis of gastrocnemius muscle shows mice fed a western diet had reduced levels of phosphatidylcholines containing (A) arachidonic acid (B) eicosapentaenoic acid and docosahexaenoic acid. Each species was analysed using a Student's t-test. * $P \leq 0.05$, ** $P < 0.01$, *** $P < 0.001$, **** $P < 0.0001$. Data are expressed as mean ± SEM (n = 8).

3.4.9 Concentrations of PUFA-containing phosphatidylcholines are reduced in skeletal muscle biopsies of type 2 diabetic patients

With free fatty acid-induced phospholipid remodelling observed in murine and human skeletal muscle cells, as well as dietary mouse models of obesity, it was hypothesised that phosphatidylcholine catabolism may be perturbed in the skeletal muscle of clinical patients with T2DM. To test this, biopsies were taken from the *pectoralis major* muscle of 75 patients during fitting of a pacemaker, and lipids were extracted using a modified Bligh and Dyer extraction. Phospholipid species were analysed using LC-MS/MS, with peaks normalised to an internal standard and dry protein pellet weight. Five PUFA-containing PCs – PC 16:0/20:4, 18:0/20:4, 18:1/20:4, 16:0/20:5 and 16:0/22:6 - were definitively identified using LC-MS/MS, and correlation of each species with BMI was assessed using linear regression (**Figure 3.12**). While the slope of each regression line was negative, correlations between intensity and BMI were not significant. Furthermore, low R^2 values indicate that the regression models failed to explain the majority of the variation in the dataset. It's important to note that adiposity data was not available, which may be a better measure of obesity than BMI. The concentrations of each phospholipid, when compared between patients suffering from T2DM (n = 22) and non-diabetics (n = 53) demonstrated phospholipid remodelling in T2DM, with concentrations of PC 16:0/20:4, 16:0/20:5 and 16:0/22:6 significantly decreased in the skeletal muscle of T2DM patients (**Figure 3.12F**).

This data highlights that phospholipid remodelling in skeletal muscle is not simply an artefact of *in vitro* cell culture, but translates to both *in vivo* models of metabolic disease and patients with T2DM. Analysis of patients here also serves to highlight that phospholipid remodelling is not only associated with lipid accumulation, but also defects in insulin sensitivity.

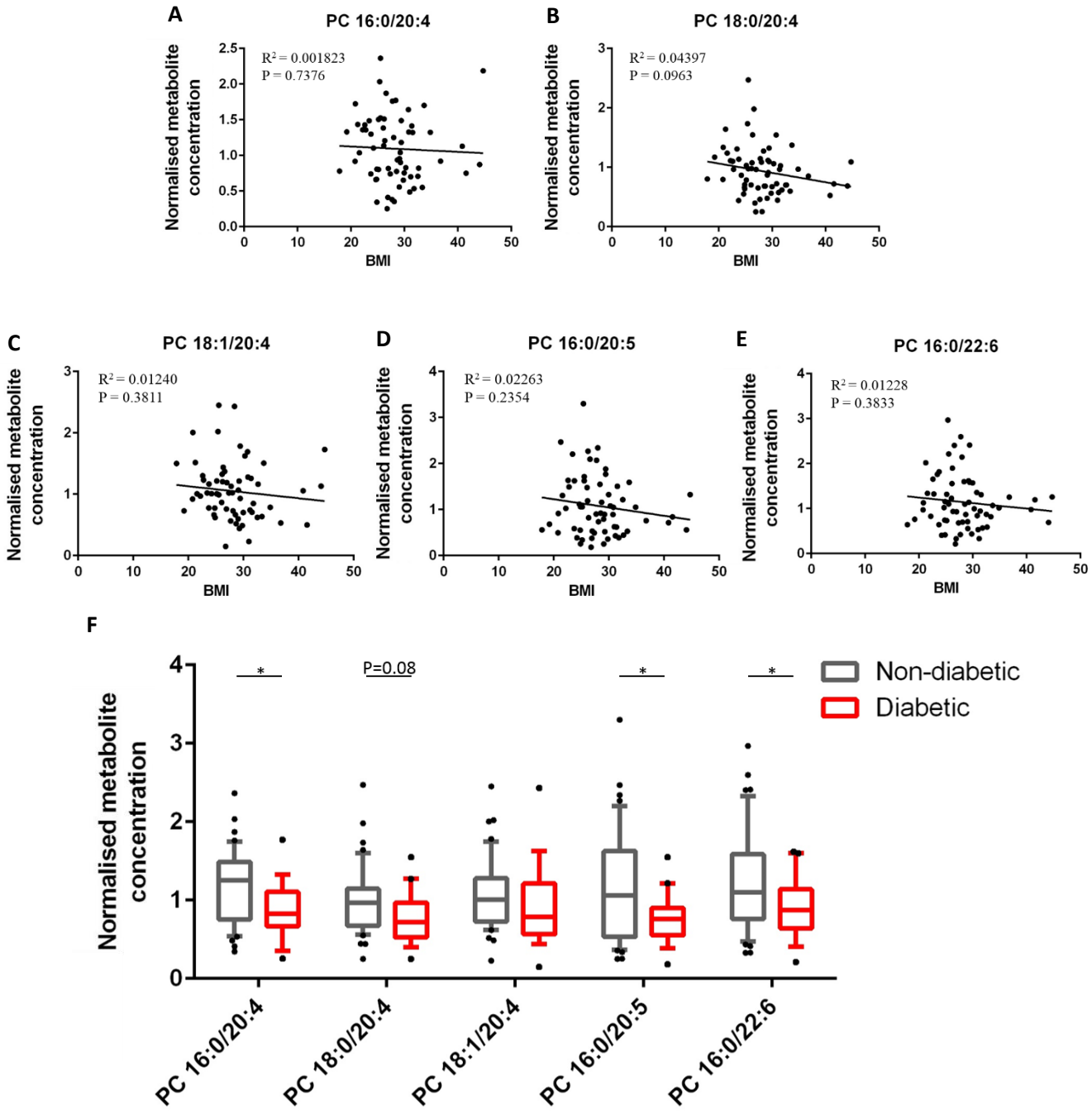

Figure 3.12: Concentrations of polyunsaturated fatty acid-containing phosphatidylcholines are reduced in skeletal muscle biopsies from patients with type 2 diabetes

Liquid chromatography-mass spectrometry analysis of skeletal muscle biopsies collected from patients during pacemaker fitting. Normalised concentration of phosphatidylcholines (PCs) (A) 16:0/20:4, (B) 18:0/20:4, (C) 18:1/20:4, (D) 16:0/20:5, and (E) 16:0/22:6 from skeletal muscle biopsies plotted against patient BMI, with correlations analysed by linear regression. (F) Concentration of polyunsaturated fatty acid-containing phosphatidylcholines in non-diabetic controls and patients with type 2 diabetes. Each species was analysed using a Student's t-test. * $P \leq 0.05$, ** $P < 0.01$, *** $P < 0.001$, **** $P < 0.0001$. Data are expressed as mean (10-90th percentile) (non-diabetic: n = 43, diabetic: n = 19).

3.4.10 Chronic tunicamycin treatment increases ER stress but not phospholipid remodelling in skeletal myocytes

The reduction in PUFA-containing phospholipids correlates with the induction of ER stress, but to understand if the lipid changes are due to activation of the UPR, the ER stress effects of palmitate need to be separated from the lipotoxic effects. Therefore, C2C12 cells were treated with tunicamycin, which inhibits n-linked glycosylation, leading to a build-up of unfolded proteins and ER stress. Cells were treated with 10 or 50 ng/ml tunicamycin, or the appropriate volume of DMSO as a vehicle control, for the 6 days of differentiation, with concentrations chosen based on the literature [279,280]. RNA was extracted and analysed by RT-qPCR. Metabolites were extracted from cells and the organic fraction was analysed by LC-MS as described previously.

The 50 ng/ml dose of tunicamycin increased the expression of *Atf3* (1.5-fold), *Atf4* (1.9-fold), *Hspa5* (1.4-fold) and *Edem1* (1.7-fold), indicating the induction of ER stress (**Figure 3.13**). The lower 10 ng/ml dose of tunicamycin also significantly increased the expression of *Atf4*.

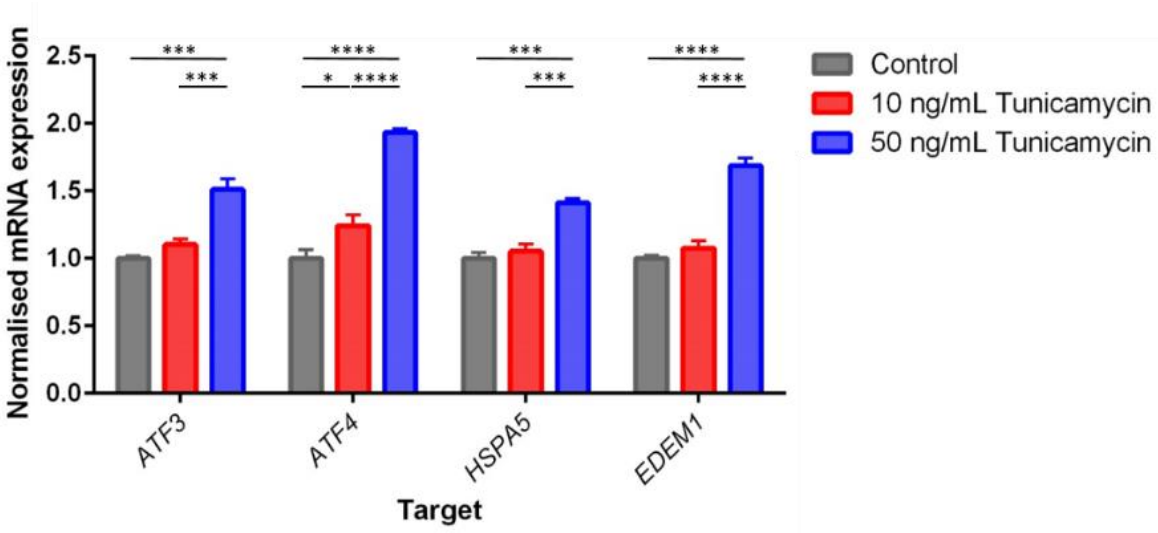

Figure 3.13: Chronic tunicamycin treatment increases expression of unfolded protein response genes

C2C12 cells were treated for 6 days with either 10 or 50 ng/ml tunicamycin, or the vehicle control. RT-qPCR analysis highlights tunicamycin-induced increases in the transcription of unfolded protein response genes (*Atf3*, *Atf4*, *Hspa5* and *Edem1*). Each gene was analysed using a one-way ANOVA test with Tukey's multiple comparison test. * $P \leq 0.05$, ** $P < 0.01$, *** $P < 0.001$, **** $P < 0.0001$. Data are expressed as mean ± SEM (n=4).

However, despite the induction of ER stress, LC-MS analysis showed that tunicamycin treatment did not affect concentrations of PCs containing arachidonic acid (**Figure 3.14A**). Furthermore, EPA-containing PCs were predominantly unchanged following tunicamycin exposure, with the exception of PC-18:1/20:5, which was increased (**Figure 3.14B**). These data do not follow the pattern of palmitate treatment, suggesting that the palmitate-induced alterations in PC and PUFA metabolism are not due to ER stress, but rather an independent effect of the lipotoxic insult.

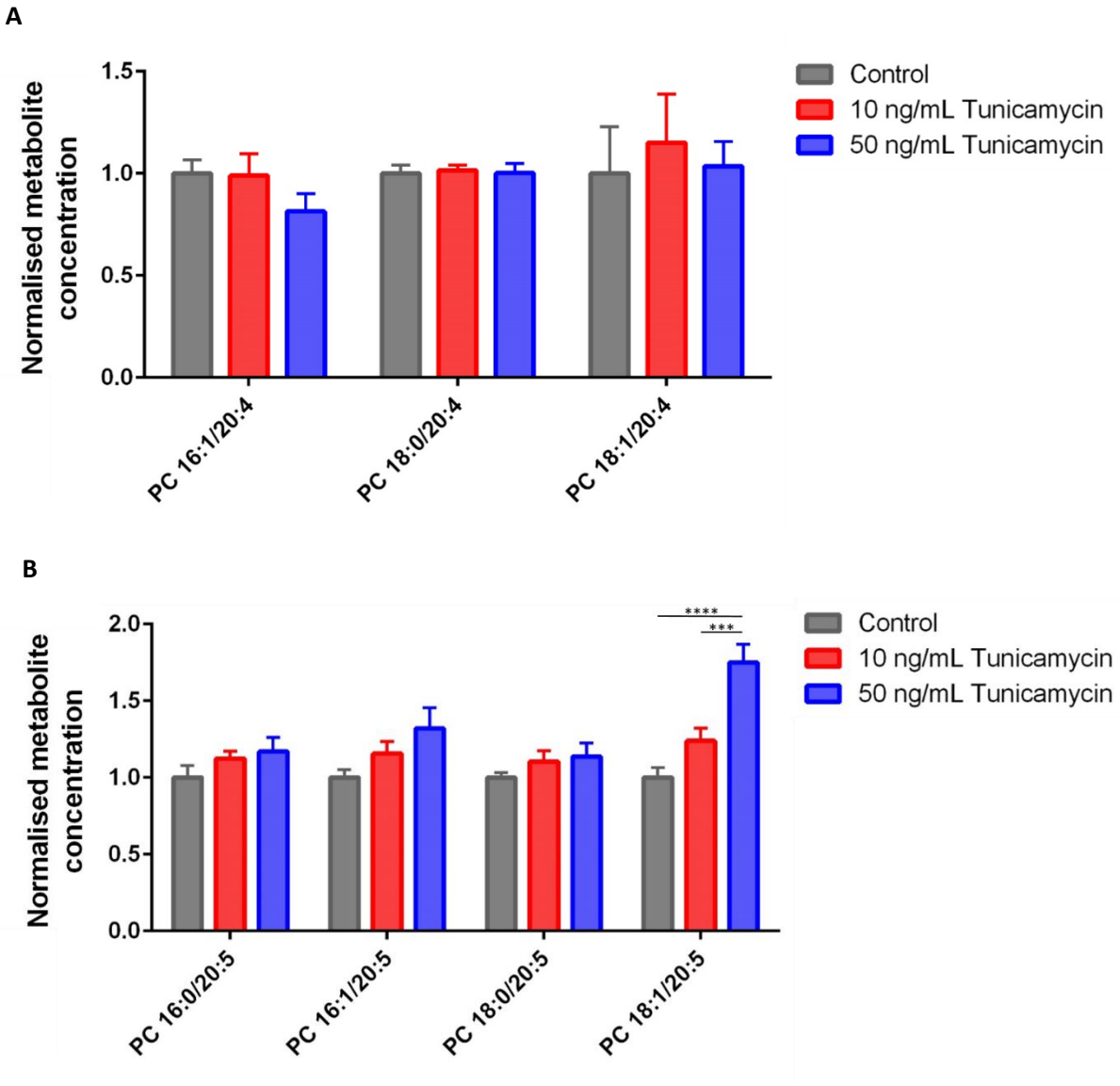

Figure 3.14: Chronic tunicamycin treatment does not affect the concentration of polyunsaturated fatty acid-containing phosphatidylcholines

C2C12 cells were treated for 6 days with either 10 or 50 ng/ml tunicamycin, or the vehicle control. Liquid chromatography-mass spectrometry analysis demonstrates the negligible effects of tunicamycin on (A) arachidonic acid- and (B) eicosapentaenoic acid-containing phosphatidylcholines (PCs). PCs were individually analysed using a one-way ANOVA test with Tukey's multiple comparison test. * $P \leq 0.05$, ** $P < 0.01$, *** $P < 0.001$, **** $P < 0.0001$. Data are expressed as mean ± SEM (n=4).

To confirm these results, HSkMCs were also treated with 10 or 50 ng/ml of tunicamycin, or the DMSO vehicle. RNA was extracted, and activation of ER stress was analysed using RT-qPCR analysis of the expression of a panel of UPR genes. A modified Bligh and Dyer extraction was used to purify lipids for LC/MS analysis. Phospholipid intensities were normalised to an internal standard and cell number.

Increases in the expression of *Atf3* (2.3-fold), *Atf4* (1.6-fold), *Hspa5* (1.7-fold) and *Edem1* (1.9-fold) demonstrate that tunicamycin induced ER stress in a dose-responsive manner (**Figure 3.15A**). However, LC-MS analysis showed that tunicamycin had no effect on the concentration of PC-containing PUFAs (**Figure 3.15B**). These results, in conjunction with analogous experiments in C2C12 cells, suggest that palmitate-induced phospholipid remodelling is independent of the activation of UPR signalling.

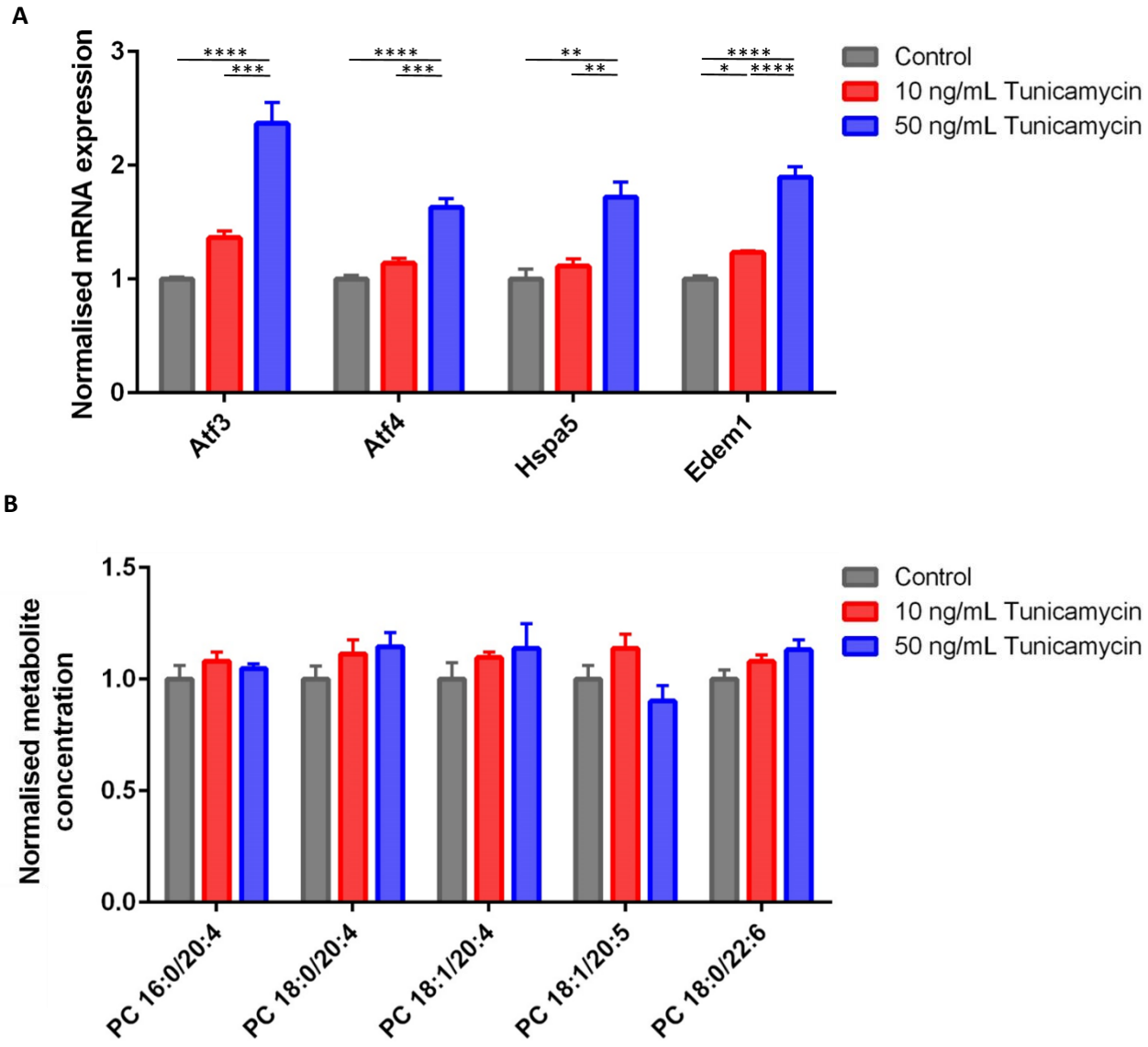

Figure 3.15: Tunicamycin induces endoplasmic reticulum stress in primary human skeletal muscle cells but has no effect on the concentration of polyunsaturated fatty acid-containing PCs

Primary human skeletal muscle cells were treated with 50 or 100 ng/mL tunicamycin, or the DMSO vehicle control for 6 days. (A) Induction of expression of endoplasmic reticulum stress-associated genes (*Atf3*, *Atf4*, *Hspa5* and *Edem1*) were assessed using RT-qPCR. (B) Polyunsaturated fatty acid-containing phosphatidylcholines were measured using liquid chromatography-mass spectrometry. Each species was analysed using a one-way ANOVA test with Tukey's multiple comparison test.* $P \leq 0.05$, ** $P < 0.01$, *** $P < 0.001$, **** $P < 0.0001$. Data are expressed as mean ± SEM (n = 4).

3.4.11 Inhibition of Perk and Ire1 suggests phosphatidylcholine remodelling is independent of the UPR

Although models of chemical-induced ER stress did not induce PC catabolism, a role for UPR induction in PC remodelling cannot be ruled out. Therefore, a pharmacological inhibitor approach was used to probe the relationship between phospholipid remodelling and ER stress. C2C12 myoblasts were grown to confluence and then treated with either 200 µM palmitate or the BSA vehicle for 6 days during differentiation. During these 6 days, cells were also co-cultured with either 10 µM AMG PERK 44, which selectively binds to the kinase domain of Perk to inhibit its activity [281], or 10 µM 4µ8C, an inhibitor of Ire1 ribonuclease activity [282]. Inhibitor concentrations were chosen based on the literature [283,284]. Metabolites were then extracted using a modified Bligh and Dyer extraction, and the organic fraction was analysed by LC-MS. Phospholipid species were annotated using fragmentation analysis, and normalised to an internal standard and cell number.

Treatment with the inhibitor of Perk signalling showed no significant effect on the six PUFA-containing PCs definitively annotated, irrespective of the fatty acid composition (**Figure 3.16A).** Similarly, inhibition of Ire1, did not reverse palmitate-induced breakdown of PUFA-containing PCs, although treatment with 4µ8C did reduce levels of PC 16:0/20:5, while increasing PC 16:1/22:6 (**Figure 3.16B**). As previously observed palmitate significantly decreases the concentrations of PC 16:0/20:4 and 18:0/20:4, while the other lipid species, although not significantly decreased, trend towards lower concentrations. This is a likely product of a lower replicate number (3), and an increase in variation within the drug-treatment groups. These results suggest neither Perk nor the Ire1 UPR signalling arms mediate palmitate-induced phospholipid remodelling, consistent with the inference from the tunicamycin treatment studies which suggested that phospholipid catabolism is independent of the induction of ER stress.

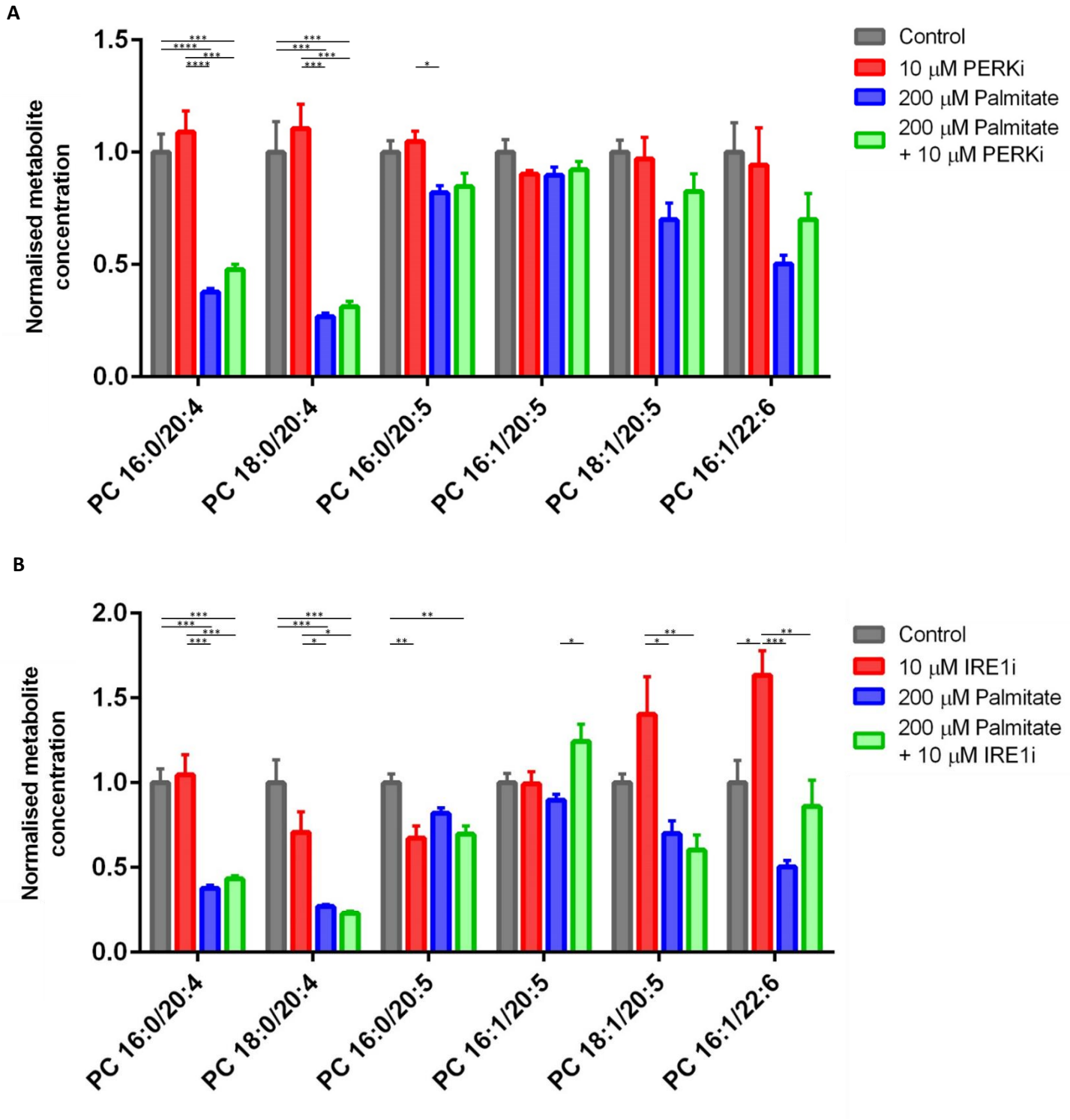

Figure 3.16: Phospholipid remodelling is not dependent on the Perk and Ire1 arms of the unfolded protein response

C2C12 myotubes were treated with 200 μM palmitate, or the vehicle for 6 days. For the final 24 hours, cells were also co-incubated with either (A) 10 μM AMG PERK 44 (B) 10 μM 4μ8c, or the relevant vehicle. Polyunsaturated fatty acid-containing phosphatidylcholines were profiled using liquid chromatography-mass spectrometry. Each species was analysed using a one-way ANOVA test with Tukey's multiple comparison test.* P<0.05, ** P<0.01, *** P<0.001, **** P<0.0001. Data are expressed as mean ± SEM (n = 3).

3.5 Discussion

Palmitate-induced lipotoxicity and ER stress are proposed mechanisms behind the aetiology of T2DM and obesity [103,104,248,285]. This chapter aimed to define the effects of palmitate-induced lipotoxicity on lipid metabolism, in the context of ER stress.

Previous studies performed to address the contribution of ER stress to insulin resistance and metabolic pathology have focussed on the effects of acute stresses [54,103,181,257–260,286]. However, in a clinical setting in humans with obesity or T2DM, the phenotype is of chronic stress resulting from raised blood FFA concentrations [166,276]. Therefore, the analyses carried out in this chapter aimed to define the metabolic differences between acute and chronic FFA-induced lipotoxicity and ER stress within skeletal muscle cells.

While acute palmitate treatment increased transcript levels of ER stress-mediated UPR genes to a greater extent than chronic exposure, UPR gene expression was still activated by the lower, chronic dose of palmitate and the transcriptional changes were more consistent with *in vivo* data in murine skeletal muscle [275]. Therefore, chronic treatment of cells with palmitate may represent a more accurate representation of the physiological obese state *in vivo*. Chronic palmitate exposure induced UPR gene expression in cells cultured in differentiation medium containing 10% horse serum, an effect not observed with 2% horse serum. The reasons for this, however, are unclear, but are likely a result of increased lipid load on myotubes.

Fatty acid analysis by GC-MS demonstrated that while the effect of chronic palmitate on UPR induction was less than that of acute palmitate, the impact on fatty acid metabolism was far greater. Increases in cellular palmitate and palmitoleate suggest that exogenous palmitate is entering the cell. The increase in palmitoleate is a well described mechanism to detoxify palmitate through the generation of monounsaturated fatty acids, including palmitoleate, in the context of lipotoxicity [53,287–289]. Perhaps most interesting was the effect of chronic palmitate exposure on PUFA metabolism. PUFAs can be separated into the n-6 and n-3 pathways. While GLA was elevated following chronic palmitate treatment, the subsequent PUFAs in the n-6 pathway were all decreased. A similar pattern was observed in the n-3 pathway, with ALA and eicosatetraenoic acid increased, but docosapentaenoic acid decreased. One possible explanation is an enzymatic block or inhibition in the pathway, increasing the concentration of metabolites prior to the block and subsequently decreasing proceeding species. However, the block is situated in different reactions of the n-3 and n-6 pathway despite a shared enzymatic set. The block for the n-6 pathway would occur between

GLA and DGLA, catalysed by Elovl5 [290]. However, this elongase also catalyses the conversion of octadecatetraenoic acid to eicosatetraenoic acid, the latter of which is increased with palmitate treatment.

Instead, LC-MS profiling of intact lipids from C2C12 myotubes and primary HSkMCs showed chronic palmitate treatment stimulated catabolism of PUFA-containing PCs, suggesting that reductions in total PUFAs are a result of phospholipid remodelling. These results also translated to both murine and human *in vivo* models of metabolic disease. It is important to note that results from mice fed a western diet, comprising 42.7% carbohydrate and 42.0% fat (%kcal), were more consistent with *in vitro* models than mice fed a high-fat diet, which contained approximately 20% carbohydrate and 60% fat. Previous work has demonstrated that mice fed a western diet have increased *de novo* lipogenesis, a product of which is palmitate, and so may explain the differences between the *in vivo* models [291].

The phospholipid changes are consistent with previous work showing concentrations of PUFA-containing PCs correlate with insulin sensitivity [292]. Similarly, skeletal muscle from individuals treated with nicotinic acid, which induces insulin resistance, had reduced concentrations of PUFA-containing PCs [293]. While there is evidence for phospholipid remodelling in the literature, the results of this chapter highlight the importance of palmitate in driving phospholipid remodelling. Further work will seek to understand the functional consequences of these changes.

Hydrolysis of phospholipids by cytoplasmic phospholipase A2 (cPLA2) releases free PUFAs for the synthesis of eicosanoids, a class of bioactive lipids with an important role in inflammatory signalling [294]. Decreases in PUFA-containing PCs following chronic exposure to palmitate may be a result of increased cPLA2 activity and eicosanoid synthesis. Eicosanoids have been implicated in metabolic disease previously, with mice lacking both 5- and 12/15-lipoxygenase, enzymes important in the generation of a subset of eicosanoid species, protecting against diet-induced insulin resistance [295,296]. Furthermore, work has shown that eicosanoids may function in the control of ER stress, with inhibition of 5-lipoxygenase ameliorating palmitate-induced ER stress in C2C12 myotubes [297]. This suggests that while phospholipid remodelling is not dependent on ER stress, the consequences of PC catabolism could influence the induction of UPR signalling.

Conclusion

Chronic palmitate induces ER stress in C2C12 myotubes and primary human skeletal myocytes, concomitant with decreases in PUFA-containing PCs. This phospholipid remodelling in skeletal muscle translates to mouse and human models of metabolic disease and will be investigated further in subsequent chapters.

Chapter 4

Phospholipid remodelling and eicosanoid generation regulates ER stress and inflammatory signalling

4.1 Introduction

The processes linking obesity to the aetiology of T2DM remain to be fully described. A role for inflammation in the development of insulin resistance in a number of insulin-sensitive tissues, including skeletal muscle, has long been postulated [104]. The inflammatory response in these tissues observed during obesity is distinct from that of infection or autoimmunity. Instead, it has been referred to as "low-grade" inflammation [298], or "metaflammation" [299]. Circulating inflammatory markers, such as C-reactive protein (CRP), and the chemokines chemokine (C-C motif) ligand 2 (CCL2) and interleukin-6 (IL-6), predict T2DM onset in large population studies [300–302]. Increases in inflammatory cytokines, such as TNFα (Tumour Necrosis Factor α), IL-6 and CCL2, in peripheral tissues, including skeletal muscle, adipose and the liver, of obese individuals, reinforce the observed associations seen in plasma from patients [303–307]. An increased inflammatory environment in peripheral tissues is then infiltrated by immune cells, with increased immune cell infiltration in the skeletal muscle of both mice fed a high-fat diet and obese humans having been reported [91].

The *in vivo* associations between obesity, insulin resistance and inflammation are mimicked by exposing cultured myocytes to saturated fatty acids. Treating C2C12 cells with palmitate increases *Tnf* expression, concomitant with decreases in *Glut4* transcription and glucose uptake [83]. Similarly, palmitate has been shown to increase concentrations of other proinflammatory cytokines, including IL-6 and CCL2, in human primary and C2C12 myotubes, respectively [89,308].

However, inflammatory signalling can also be controlled by lipid signalling, as well as by protein cytokines. Eicosanoids are bioactive lipids produced by the oxidation of free PUFAs, following their hydrolysis from phospholipids by cPLA2 (**Figure 4.1**) [50]. They represent a

group of autocrine and paracrine signalling molecules, diffusing from their site of synthesis to bring about receptor-mediated effects on inflammation in nearby cells [309,310]. As shown in Chapter 3, chronic palmitate treatment increases breakdown of PUFA-containing PCs. GC-MS analysis of total fatty acids also showed decreases in a number of PUFAs, such as arachidonic acid. One explanation for these results is an increase in substrate usage. Experiments in this chapter, therefore, investigate the hypothesis that the palmitate-induced breakdown of PUFA-containing PCs was to provide increased substrate for eicosanoid synthesis.

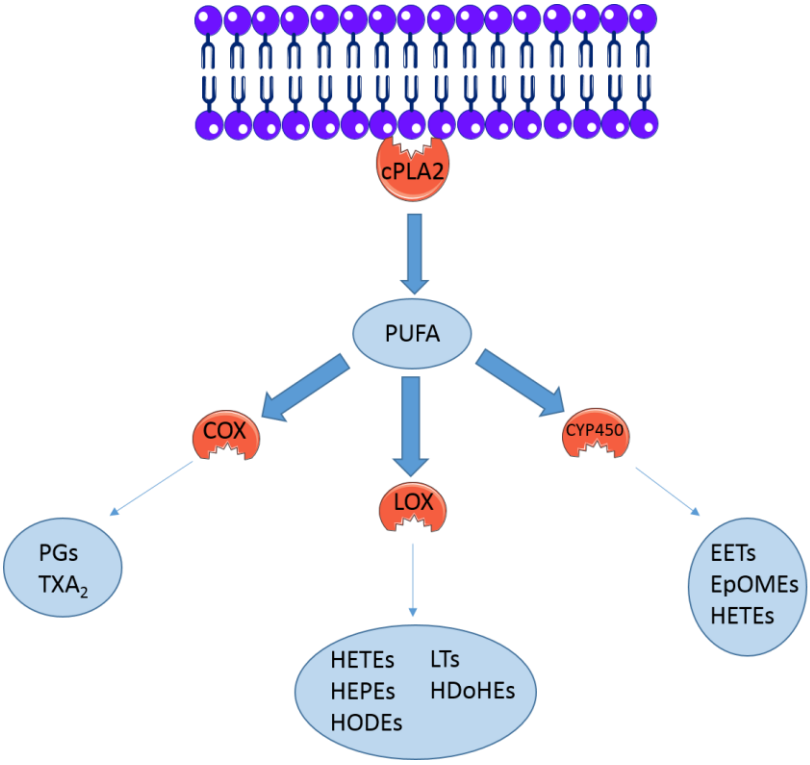

Figure 1: Eicosanoid synthesis pathway

Diagram depicting the key enzymatic pathways in the synthesis of eicosanoids. Free polyunsaturated fatty acids (PUFAs) are released from the phospholipid bilayer by cytoplasmic phospholipase A2 (cPLA2). Cyclooxygenase (COX), lipoxygenase (LOX) and cytochrome P450 (CYP450) enzymes convert PUFAs to varying eicosanoid species. Prostaglandins (PGs) and thromboxane (TXA_2) are produced by COX. Hydroxyeicosatetraenoic acids (HETEs), hydroxyeicosapentaenoic acids (HEPEs), hydroxyoctadecaenoic acids (HODEs), leukotrienes (LTs) and hydroxydocosahexaenoic acids (HDoHEs) are produced by LOX enzymes. Epoxyeicosatrienoic acids (EETs), epoxyoctadecenoic acids (EpOMEs) and HETEs are produced by CYP450 enzymes [405].

Previous work has shown the potential importance of eicosanoids in metabolic disease. Mice lacking 5-LOX show reduced immune cell infiltration in adipose tissue and partial protection from HFD-induced insulin resistance [295]. Leukotriene B4 (LTB4), a 5-LOX product, is increased in the adipose, skeletal muscle and liver tissue of obese mice [311]. In the same study, LTB4 was then also shown to increase inflammation and insulin resistance in cultured myotubes, macrophages and hepatocytes, while inhibition of the LTB4 receptor improved insulin sensitivity and protected against hepatic steatosis. Similarly, 12/15-LOX-KO mice are also protected against diet-induced insulin resistance and adipose tissue inflammation, highlighting roles for a number of different lipoxygenase enzymes in the development of the chronic inflammation observed during obesity and T2DM [296].

The palmitate-induced breakdown of PUFA-containing PCs in C2C12 myotubes was accompanied by increases in the activation of ER stress. While tunicamycin treatment suggested that phospholipid remodelling was not ER stress-dependent, it remains unclear whether eicosanoid generation impacts on UPR activation. There is evidence supporting a role for eicosanoids in the regulation of ER stress. Inhibition of 5-lipoxygenase with zileuton in C2C12 myotubes reduced markers of ER stress, confirming a potential link between eicosanoids and ER stress [297]. Furthermore, 15-HETE has been shown to increase ER stress markers in in human retinal endothelial cells, while Alox15-KO mice had reduced diabetes-induced ER stress in the retina [312].

4.2 Aims and Objectives

The aim of this chapter was to define the functional consequences of the palmitate-induced phospholipid remodelling identified in Chapter 3. A key set of objectives were designed to investigate this process:

1) Pharmacological inhibition of phospholipase enzymes to determine the important isoform in membrane remodelling.

2) LC-MS/MS profiling of eicosanoids in response to palmitate treatment.

3) Pharmacological inhibition of key eicosanoid synthesis enzymes to probe the roles of distinct classes of eicosanoids lipids and their signalling pathways in the induction of ER stress and inflammatory signalling in myotubes.

4) Co-culturing of myotubes and macrophages to investigate the role of eicosanoids in immune cell activation.

4.3 Materials and Methods

4.3.1 C2C12 culture

C2C12 cells were cultured as described in **Chapter 2 Materials and Methods** (Section 2.1.1 *C2C12 myoblast culture and differentiation*)**.** Pharmacological inhibitors (detailed in section 4.3.5 *Pharmacological inhibitors*) were used for the final 24 hours of experiments. Cells for analysis by RT-qPCR, ELISA or LC-MS analysis of phospholipids were treated in collagen I-coated 12-well plates. Cells for eicosanoid analysis were treated in collage I-coated T75 flasks.

4.3.2 Primary human skeletal muscle cell culture

Primary human skeletal muscle cells (HSkMCs) were cultured as described in **Chapter 2 Materials and Methods** (section 2.1.2 *Primary human skeletal muscle cell culture and differentiation*). Cells were treated with inhibitors (detailed in section 4.3.5 *Pharmacological inhibitors*) for the final 24 hours of experiments. All cells were treated in 12-well plates.

4.3.3 Raw 264.7 macrophage culture and co-culturing assays

Raw 264.7 cells (ATCC) were grown to confluence in DMEM supplemented with 10% FBS (Sigma Aldrich) and 1% P/S (Sigma Aldrich). For co-culture assays, C2C12 cells were grown to confluence in 12-well plates, and then differentiated for 6 days. During this 6 day period, C2C12 cells were cultured with their respective agonists. Separately, Raw 264.7 macrophages were grown to confluence in a T75 flask. Transwell inserts (Corning) were initially submerged in 1.5 mL of serum-free media for 24 hours to improve cell adherence. Macrophages were lifted from the flask using trypsin, and pelleted in a centrifuge. Subsequently, they were resuspended in growth media (10% FBS, 1% P/S) and transferred to the inserts for 24 hours to adhere to the membrane, corresponding to the final 24 hours of C2C12 treatment. Culture media was then switched to serum-free, agonist-free media on both sets of cells. Finally, the inserts were combined with the plate of C2C12 cells and co-culture assays lasted for 24 hours.

4.3.4 Conjugation of palmitate to BSA

Palmitate was bound to BSA following the protocol summarised in **Chapter 2 Materials and Methods** (section 2.1.3 *Conjugation of palmitate to BSA*)**.**

4.3.5 Pharmacological inhibitors

PD146176 and NCTT-956 were purchased from Sigma Aldrich (Gillingham, UK), and dissolved in DMSO to a concentration of 20 mM. The inhibitors were diluted into culture media to achieve a final concentration of 10 µM. AACOCF3 was purchased from Abcam (Cambridge, UK) and dissolved in DMSO to a concentration of 100 mM. The inhibitor was diluted in culture media to a final concentration of 100 µM.

4.3.6 Cell harvesting

Cells were harvested and pelleted as described in **Chapter 2 Materials and Methods** (section 2.1.4 *Cell harvesting*). Cell counts were performed using a Scepter automated cell counter (Millipore).

4.3.7 RNA isolation and purification

RNA was extracted and purified from cells using an RNeasy mini kit (Qiagen), according to the manufacturer's instructions and as outlined in **Chapter 2 Materials and Methods** (section 2.4.1 *RNA isolation and purification*).

4.3.8 cDNA synthesis

RNA concentrations were standardised and cDNA then synthesised using an RT^2 First Strand kit (Qiagen), following manufacturer's instructions as set out in **Chapter 2 Materials and Methods** (section 2.4.2 *cDNA synthesis*).

4.3.9 Reverse transcription quantitative polymerase chain reaction

Transcript levels were analysed using the StepOnePlus Real-Time PCR system (Applied Biosystems), as described in **Chapter 2 Materials and Methods** (section 2.4.3 *Reverse transcription quantitative polymerase chain reaction*). Transcription of *Atf3, Atf4, Hspa5* and *Edem1*, normalised to *Rn18s*, was used to assess the induction of ER stress in C2C12 myotubes. Expression of *ATF3, ATF4, HSPA5* and *EDEM1*, normalised to *ACTB*, was used to assess the induction of ER stress in primary HSkMCs. Other murine primers used in this chapter are *Ccl2* (PPM03151G), *Il6* (PPM03015A), *Alox5* (PPM28755C), *Alox12* (PPM25685A), *Tnf* (PPM03113G), *Arg1* (PPM31770C), *Nos2* (PPM02928B) and *Egr2* (PPM04478F), with all expression normalised to *Rn18s*. Other human primers used in this chapter are *CCL2* (PPH00192F) and *IL6* (PPH00560C), with all expression normalised to *ACTB*. All primers are purchased from Qiagen.

4.3.10 Metabolite extraction from cells

Metabolites were extracted from cells using a modified Bligh and Dyer method, described in **Chapter 2 Materials and Methods** (section 2.5.1 *Cell metabolite and lipid extraction for mass spectrometry*).

4.3.11 Liquid chromatography-mass spectrometry of lipids

The dried-down organic fraction was dissolved in 50 µl methanol/chloroform (1:1), and diluted into 190 µl IPA/ACN/H_2O (2:1:1). Samples were then analysed using an Orbitrap Elite mass spectrometer, using a method with two scan events as described in **Chapter 2 Materials and Methods** (section 2.6 *Liquid chromatography-mass spectrometry open profiling of lipids*). Chromatogram files were converted using MSConvert (Proteowizard), and processed using XCMS within an R script. Peaks were normalised to a relevant internal standard and then either cell number, for *in vitro* experiments, or dry protein pellet weight, for the analysis of skeletal muscle tissue.

4.3.12 Eicosanoid extraction from cells and media

Cell pellets were resuspended in 1mL water and mixed with 2.5 mL IPA/hexane/1M acetic acid (20:30:2). 5 mL of conditioned cell culture media was dried down under nitrogen to a total volume of 1 mL, and mixed with 2.5 mL IPA/hexane/1M acetic acid (20:30:2). 10 µL of a 1 ng/µL internal standard mix (12-HETE-d8, PGE2-d4, and 8-iso-PGF2a-d4) was added and each sample was vortexed for 30 seconds. 2.5 mL hexane was then added and samples vortexed for another 30 seconds before centrifugation (5 minutes, 1500rpm, 4ºC). The upper layer was transferred to a glass vial and dried down under nitrogen gas for storage at -80ºC.

4.3.13 Liquid chromatography-mass spectrometry/mass spectrometry of eicosanoids

Dried samples were reconstituted in 50 µL of methanol and analysed using a TSQ Quantiva Triple Quadrupole mass spectrometer (Thermo Fisher), coupled to a Vanquish UHPLC system (Thermo Fisher). Five µL of sample was injected and separated using a C18 CSH column (1.7 µM, 2.1x100 mm, Waters). The flow rate was set at 0.5 mL/min. Solvent A was composed of H_2O/solvent B (95/5, 0.1% glacial acetic acid) and solvent B was acetonitrile/methanol (80:20, 0.1% glacial acetic acid). Solvent B begins at 30% until the first minute, when it is increased to 35% by 4 minutes, 67.5% by 8 minutes, and 100% at 13 minutes. It is held in this condition for 3 minutes, before returning to initial conditions for 2 minutes. Eicosanoids were detected in negative ionisation mode, with an electrospray voltage of 2.5 kV. The source temperature was set to 420 ºC, and nitrogen was used as the drying gas for solvent evaporation. Eicosanoid species were detected using a targeted MS/MS analysis, with precursor and fragment ions detailed in **Table 4.1**.

Compound	Precursor ion (m/z)	Fragment ions (m/z)	Retention time (minutes)
5-HEPE	317.2	255,299,115	11.62
12-HEPE	317.2	179,255,299	11.35
15-HEPE	317.21	219,255,299	11.12
5-HETE	319	301,257,115	12.78
12-HETE	319	179	12.71
15-HETE	319	301,257,219	13.57
9-HODE	295.25	277,171,123	11.76
13-HODE	295.2	277,195,179	11.8
8,9-EET	319	301,257,275	13.76
11,12-EET	319	167,301,179	13.64
7-HDOHE	343	325,281,201	12.59
13-HDOHE	343.2	193,281,325	12.35
17-HDOHE	343.2	193,281,326	12.26
9,10-EPOME	295.2	277,170,183	13.41

Table 4.1: Fragment *m/z* values for eicosanoids

4.3.14 Statistics

Statistical significance was assessed using either a one-way ANOVA, with Tukey's multiple comparison test, or Student's t-test, as detailed in each figure. In each case, $n \geq 3$ and the significance level was set to $p \leq 0.05$. All univariate analysis was conducted using GraphPad software (version 6, Prism).

4.4 Results

4.4.1 Cytosolic phospholipase A2 inhibition reverses palmitate-induced catabolism of PUFA-containing phosphatidylcholines

Phospholipid breakdown is catalysed by hydrolytic phospholipase enzymes [313]. This enzyme class comprises a number of sub-families and isoforms with differing preferences of substrate and hydrolytic site. PLA2 enzymes hydrolyse the phospholipid *sn*-2 fatty acyl chain and have a preference for PUFAs [314]. There are a number of PLA2 classes, but it is cPLA2 that is best documented for its roles in intracellular arachidonic acid metabolism, as well as inflammatory signalling [315].

To determine if cPLA2 has a role in palmitate-driven phospholipid remodelling, C2C12 myotubes were grown to confluence and treated with 200 µM palmitate, or the BSA vehicle, for 6 days. For the final 24 hours, cells were also co-treated with 100 µM AACOCF3, a cPLA2 inhibitor, or the DMSO vehicle. The concentration of AACOCF3 used was based on treatment of C2C12 myotubes in previous papers [316,317]. Metabolites were extracted and the lipid phase was analysed by LC-MS/MS. AACOCF3 greatly increased the concentrations of PUFA-containing PCs with and without palmitate treatment, highlighting a pronounced role for cPLA2 in palmitate-driven PC remodelling (**Figure 4.2A and 4.2B**).

AACOCF3 does have off-target effects, including a potency for calcium-independent phospholipase A2 (iPLA2). Therefore, separately cells were also co-treated with 10 µM R-bromoenollactone (R-BEL), an iPLA2 inhibitor, for the final 24 hours of a 6-day palmitate treatment (**Figure 4.2C**). The concentration of R-BEL was based on the literature [318]. PUFA-containing phospholipid levels were unaffected by R-BEL treatment, demonstrating that palmitate-driven phospholipid remodelling is cPLA2-specific.

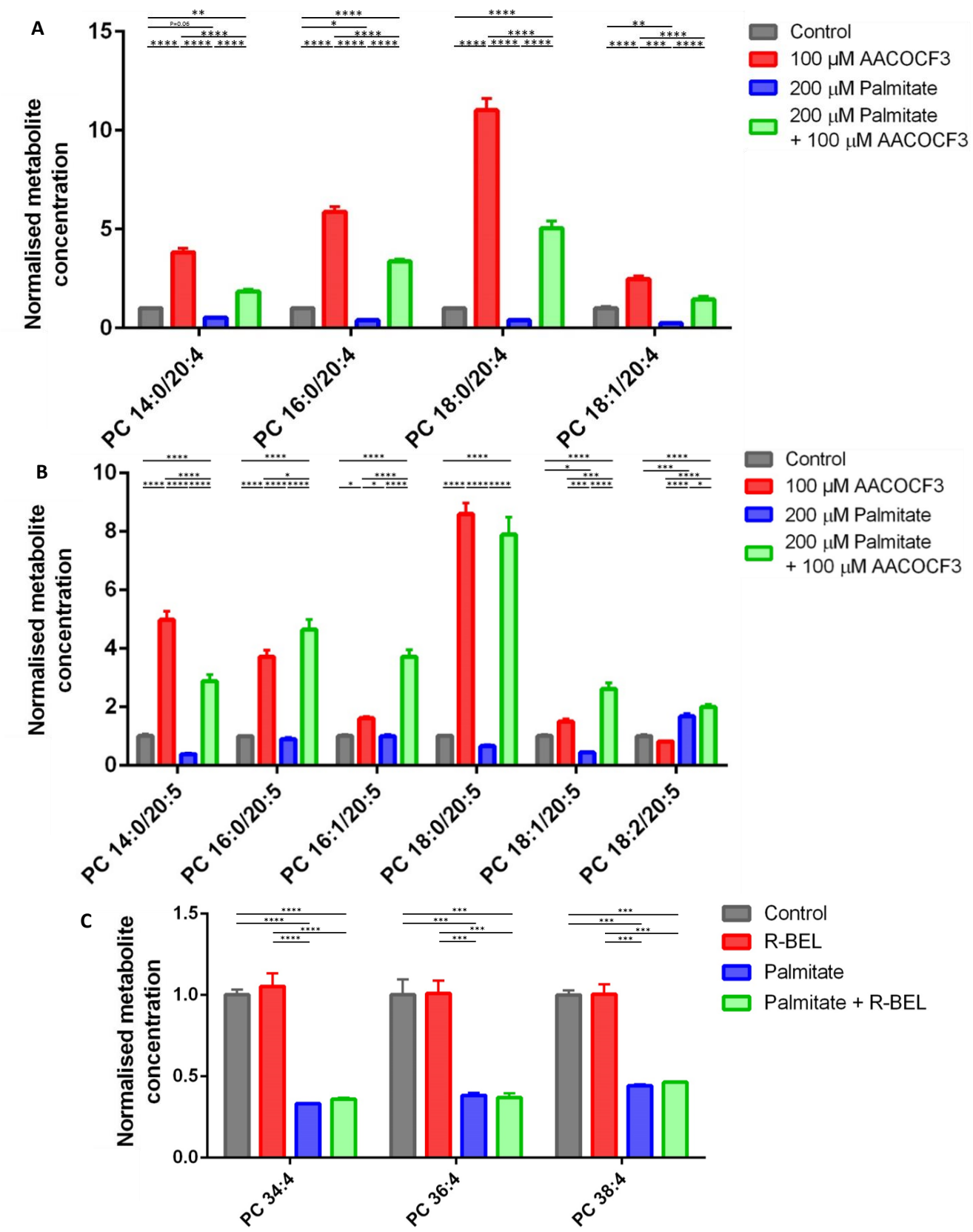

Figure 4.2: Palmitate-induced phosphatidylcholine breakdown is dependent on cytosolic phospholipase A2

C2C12 myotubes were treated with 200 μM palmitate for 6 days, or the vehicle control. Liquid chromatography-mass spectrometry (LC-MS) analysis of (A) arachidonic acid- and (B) eicosapentaenoic acid-containing phosphatidylcholines (PCs) from cells following co-treatment with 100 μM AACOCF3, or the vehicle control. (C) LC-MS analysis after co-treatment with 10 μM R-BEL, or the vehicle control. PCs were analysed using a one-way ANOVA test with Tukey's multiple comparison test. * $P \leq 0.05$, ** $P < 0.01$, *** $P < 0.001$, **** $P < 0.0001$. Data are expressed as mean ± SEM (n=3).

4.4.2 Chronic palmitate treatment induces changes in eicosanoid synthesis and secretion

Phospholipid remodelling catalysed by cPLA2 provides a source of free cytosolic PUFAs, in particular AA and EPA, which are precursors for the synthesis of eicosanoids. This class of bioactive lipids have key roles in inflammatory signalling. Palmitate-driven breakdown of PUFA-containing PCs may be a result of increased eicosanoid synthesis, and so a targeted LC-MS/MS method was used to investigate the eicosanoid concentrations.

C2C12 cells were grown to confluence, and differentiated for 5 days. During this period cells were treated with 200 μM palmitate, or the BSA-vehicle. Eicosanoids are typically unstable, transient mediators, and so a time-course was carried out to understand the dynamics of eicosanoid synthesis during chronic palmitate treatment. Cells were harvested every 24 hours for the 5 days, and eicosanoids were analysed using LC-MS/MS. Analysis identified palmitate-induced changes in the concentrations of eicosanoid species generated by lipoxygenase (LOX) enzymes, including hydroxyeicosatetraenoic (HETE), hydroxyeicosapentaenoic (HEPE) and hydroxyoctadecadienoic (HODE) acids. After 24 hours of treatment, palmitate increased the concentrations of arachidonic acid-derived 5-, 12- and 15-HETE (**Figure 4.3A**). 5- and 12-HEPE, produced from EPA by the same LOX isoforms, were also increased at the 24 hour time point (**Figure 4.3B**). Levels of these eicosanoids fell during the subsequent 4 days, with 15-HETE significantly decreased for the final 3 days of palmitate treatment. Similarly, 13-HODE and 9-HODE, produced from linoleic acid, were increased in response to palmitate treatment after 24 hours, before falling back to control levels for the subsequent 4 days (**Figure 4.3C**). On the other hand, epoxyeicosatrienoic (EET) acids are produced by cytochrome P450 epoxygenase enzymes. 8,9-, 11,12-, and 14,15-EET were found to decrease in palmitate-treated cells from 3 days onwards (**Figure 4.3D**).

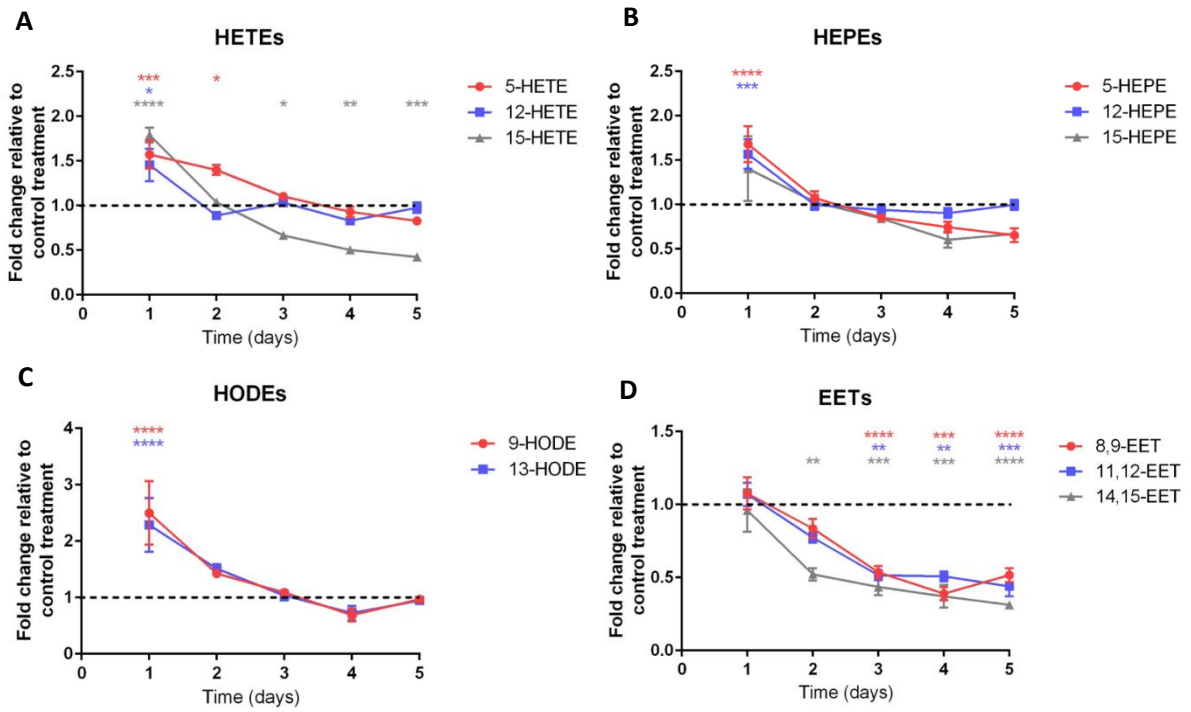

Figure 4.3: Intracellular eicosanoid concentrations in response to palmitate treatment over a 5-day timecourse

C2C12 myotubes were treated with 200 µM palmitate for 6 days, or the vehicle control. Samples were harvested every 24 hours, and eicosanoid levels were analysed by liquid chromatography-mass spectrometry, identifying changes in (A) hydroxyeicosatetraenoic acids, (B) hydroxyeicosapentaenoic acids, (C) hydroxyoctadecadienoic acids, and (D) epoxyeicosatrienoic acids. Eicosanoids were analysed using a Student's t-test * $P \leq 0.05$, ** $P < 0.01$, *** $P < 0.001$, **** $P < 0.0001$. Data are expressed as mean ± SEM (n=4).

Eicosanoids function as local signalling molecules. They are released from the cell and bind to receptors on nearby cells. Therefore, to better understand the potential effect of palmitate exposure on eicosanoid-driven signalling, the concentrations of eicosanoids within conditioned cell culture media were analysed. C2C12 cells were grown and treated as before, across a 5-day timecourse. For the final 24 hours, media was changed to serum-free media. Therefore, eicosanoids were only present in the media as a result of secretion from the cells, rather than as a constituent part of the media serum. Media was extracted and analysed in an analogous manner to the cells.

Similar to the intracellular eicosanoid species detected, the predominant eicosanoids observed in the media were LOX-derived. However, the secretory time-course profile differed from the intracellular pattern. As before, the HETE and HEPE species detected were increased after the first 24 hours of palmitate treatment, but this increase prolonged to 48 hours before falling

over days three and four (**Figure 4.4A and B**). Following 5 days of palmitate-treatment, the release of 5- and 12-HETE and 5-, 12-, and 15-HEPE into the media was significantly increased. Similarly, 9- and 13-HODE were increased at the 24 hour mark, but, while 9-HODE levels continued to follow the profile seen intracellularly, 13-HODE concentration in the media was increased across the time course by palmitate treatment (**Figure 4.4C**).

EET species were not detected in the media, but two other classes of eicosanoids were found to change in response to palmitate exposure. Hydroxydocosahexaenoic (HDoHE) acids are produced from DHA. The secretion of 5-LOX-generated 7-HDoHE and 15-LOX-generated 17-HDoHE were increased on days 1, 2 (only 17-HDoHE), and 5 of palmitate treatment (**Figure 4.4D**). A similar pattern was also observed for the COX2-derived 13-HDoHE. Finally, two cytochrome P450 products of linoleic acid were also increased in the media in response to palmitate. 9(10)-EpOME (leukotoxin) was increased after 1, 2 and 5 days of palmitate treatment, while 12(13)-EpOME (isoleukotoxin) was elevated at day 1 and 5 (**Figure 4.4E**). These data highlight that palmitate-induced PC remodelling leads to alterations in eicosanoid synthesis and secretion.

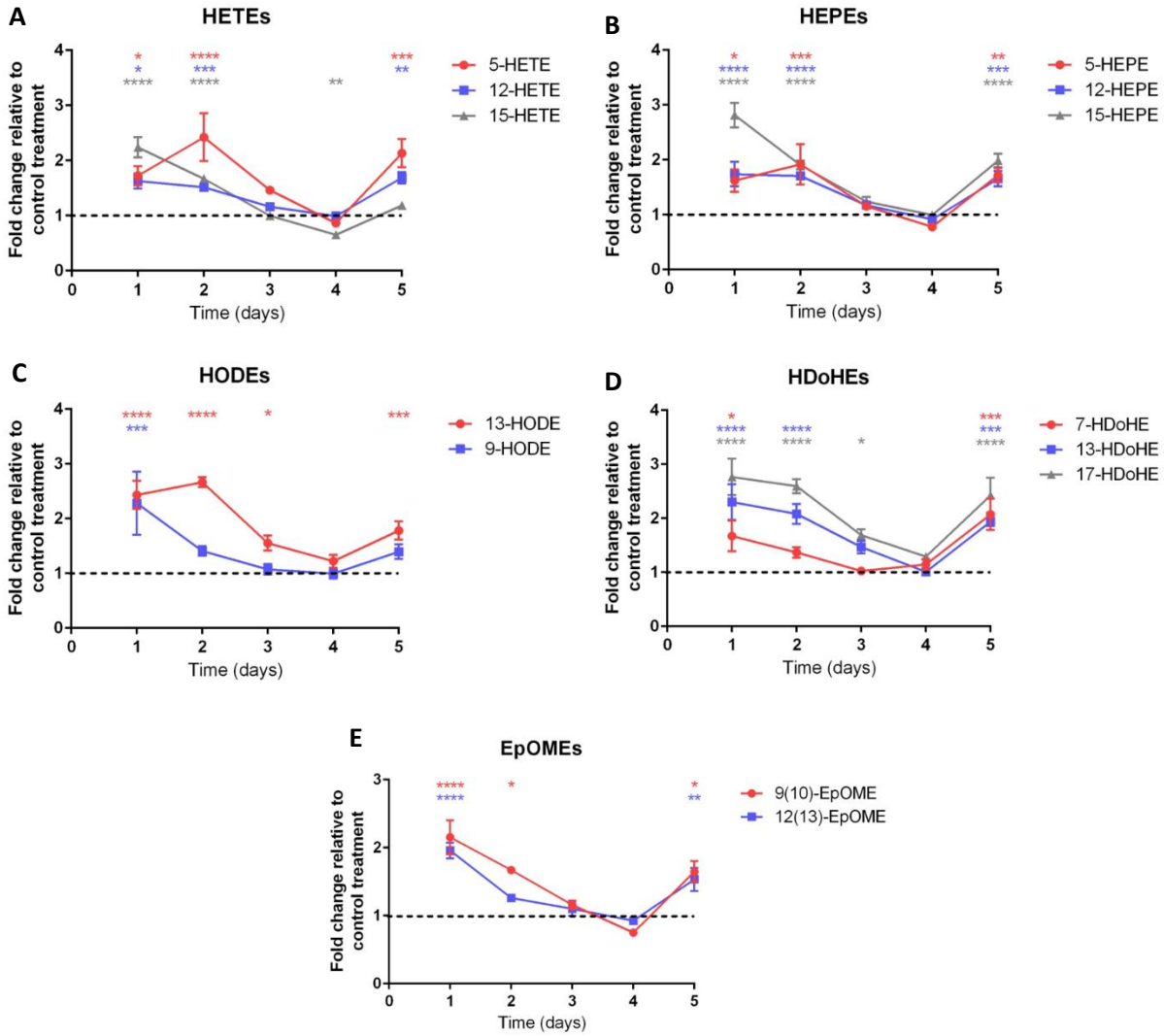

Figure 4.4: Secretion of eicosanoids in response to palmitate treatment over a 5-day timecourse

C2C12 myotubes were treated with 200 µM palmitate for 6 days, or the vehicle control. Media samples were taken every 24 hours, and eicosanoid levels were analysed by liquid chromatography-mass spectrometry, identifying changes in (A) hydroxyeicosatetraenoic acids, (B) hydroxyeicosapentaenoic acids, (C) hydroxyoctadecadienoic acids, (D) hydroxydocosahexaenoic and (E) epoxyoctadecenoic acids. Eicosanoids were analysed using a Student's t-test * $P \leq 0.05$, ** $P < 0.01$, *** $P < 0.001$, **** $P < 0.0001$. Data are expressed as mean ± SEM (n=4).

4.4.3 Chronic palmitate treatment alters expression of key inflammatory cytokines

Increases in eicosanoid secretion may influence the control of inflammatory signalling. Previous literature has shown palmitate treatment increases the expression of inflammatory cytokines, including *Tnf*, *Il6*, and *Ccl2* in skeletal muscle [83,89,253]. However, in keeping with investigations into ER stress, the majority of experiments have focused on acute palmitate exposures. Therefore, the effect of chronic palmitate on the expression of key inflammatory cytokines in myotubes was assessed by RT-qPCR. C2C12 cells were grown to confluence, and differentiated for 6 days, during which myotubes were treated with either 200 µM palmitate or the BSA vehicle. RNA was extracted and purified at the end of 6 days, and cDNA was synthesised. RT-qPCR analysis shows chronic palmitate exposure increases expression of *Ccl2*, while expression of *Il6* decreased (**Figure 4.5**). These results confirm that chronic palmitate treatment impacts not only UPR induction but also the expression of inflammatory cytokines. A decrease in *Il6* expression contradicts previous work in which acute palmitate increases expression of *Il6*, suggesting differences between acute and chronic models of FFA-induced lipotoxicity.

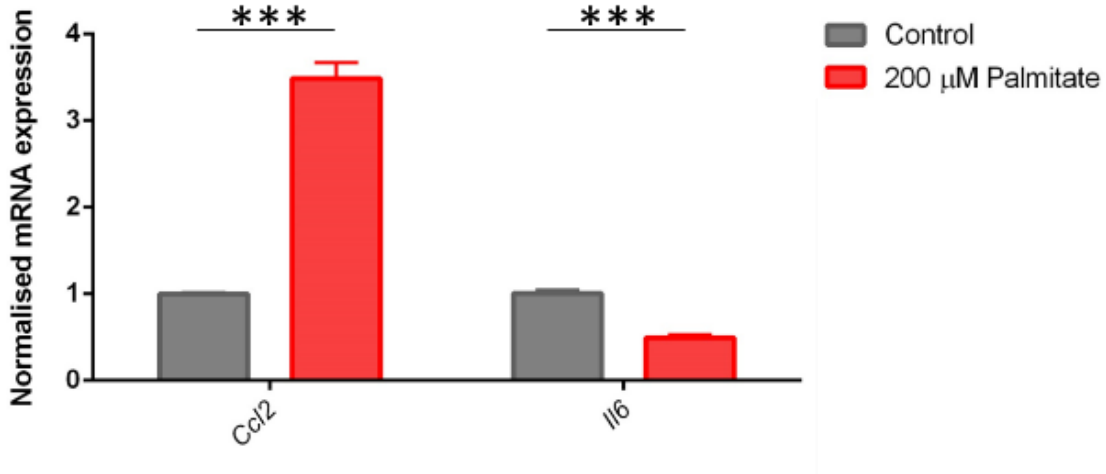

Figure 4.5: Chronic palmitate treatment increases expression of *Ccl2* but decreases transcription of *Il6* in C2C12 myotubes

C2C12 myotubes were treated with 200 µM palmitate, or the vehicle for 6 days. Transcription of inflammatory markers (*Ccl2* and *Il6*) were assessed using RT-qPCR. Each species was analysed using a Student's t-test. * $P \leq 0.05$, ** $P < 0.01$, *** $P < 0.001$, **** $P < 0.0001$. Data are expressed as mean ± SEM (n = 4).

To confirm the effects of chronic palmitate treatment on inflammatory cytokine expression translate in human-derived cells, experiments were repeated in primary HSkMCs. HSkMCs were grown to confluence and then treated with 100 µM palmitate or the BSA vehicle

throughout 6 days of differentiation. RNA was subsequently extracted, and RT-qPCR was used to analyse mRNA expression. Chronic palmitate significantly elevated expression of *Ccl2*, similar to results seen in C2C12 cells (**Figure 4.6**). *Il6* expression, however, was not consistent with that in C2C12 myotubes, with palmitate exposure here increasing expression of *Il6.* While expression patterns are slightly inconsistent between the two cell types, the results still highlight a role for palmitate in the alteration of inflammatory cytokine expression.

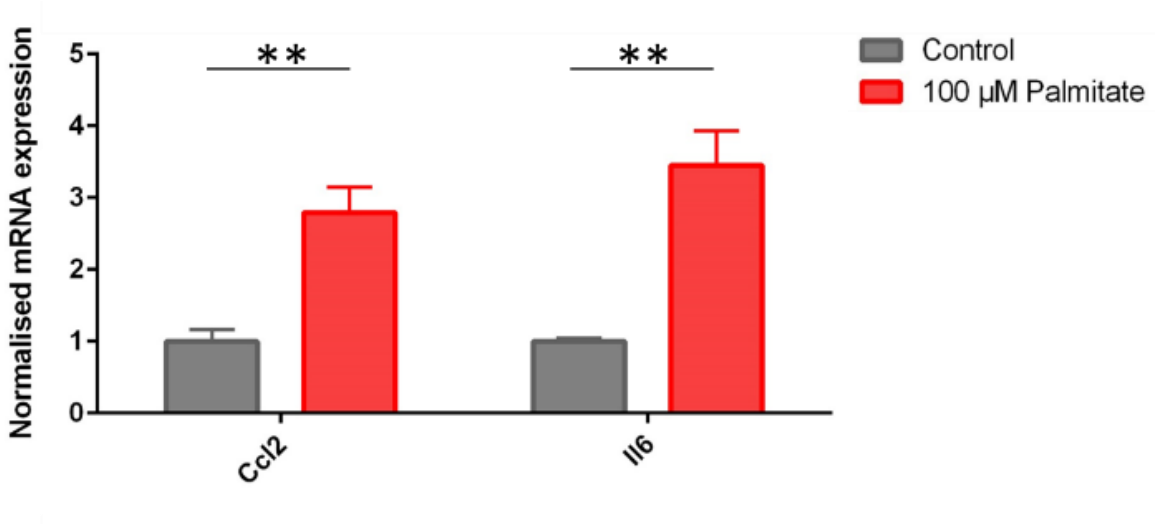

Figure 4.6: Chronic palmitate treatment increases expression of *CCL2* and *IL6* in primary human skeletal muscle cells

Primary human skeletal myocytes were treated with 100 µM palmitate, or the vehicle for 6 days. Transcription of inflammatory cytokines (*CCL2* and *IL6*) were assessed using RT-qPCR. Each species was analysed using a Student's t-test. * $P \leq 0.05$, ** $P < 0.01$, *** $P < 0.001$, **** $P < 0.0001$. Data are expressed as mean ± SEM (n = 4).

4.4.4 Expression of lipoxygenase isoforms are increased with palmitate exposure in myocytes

Induction of ER stress and alterations in expression of inflammatory cytokines were concomitant with changes in lipoxygenase-derived eicosanoid secretion and synthesis. To further understand the mechanism behind these changes, C2C12 cells were grown to confluence and treated with either 200 µM palmitate, or the BSA vehicle, during a 6-day differentiation period. RNA was extracted and purified, prior to analysis of the expression of the lipoxygenase isoforms arachidonate 5-lipoxygenase (Alox5), arachidonate 12-lipoxygenase (Alox12) and arachidonate 15-lipoxygenase (Alox15) by RT-qPCR. Chronic palmitate exposure increased the expression of *Alox5* and *Alox12* compared to BSA vehicle

control-treated myotubes (**Figure 4.7**). Expression of *Alox15*, however, was below the limit of detection in the myocytes. These results highlight that increases in eicosanoid secretion are concomitant with increased gene expression of key synthetic enzymes.

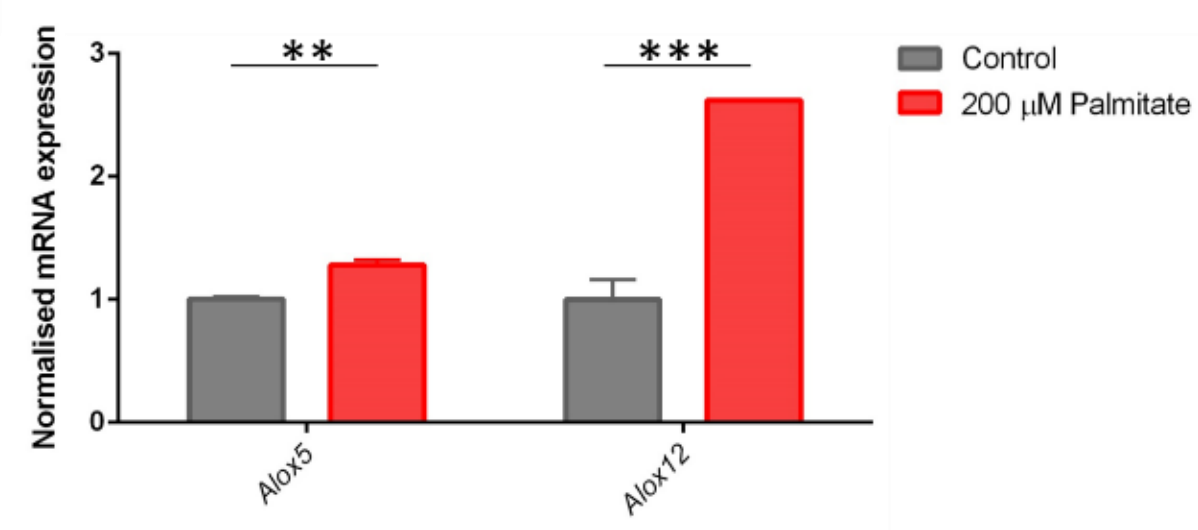

Figure 4.7: Chronic palmitate treatment increases expression of 5-lipoxygenase and 12-lipoxygenase isoforms.

C2C12 myotubes were treated with 200 μM palmitate, or the BSA vehicle for 6 days. Transcription of lipoxygenase enzymes, 5-lipoxygenase (Alox5) and 12-lipoxygenase (Alox12) was measured using RT-qPCR. Each species was analysed using a Student's t-test. * P<0.05, ** P<0.01, *** P<0.001, **** P<0.0001. Data are expressed as mean ± SEM.

4.4.5 Inhibition of eicosanoid synthesis exacerbates palmitate-induced ER stress and inflammation in C2C12 myotubes

With chemical inhibition highlighting little role for ER stress in phospholipid remodelling, and therefore eicosanoid generation, the question remained of whether eicosanoid synthesis may lie upstream in signalling leading to the activation of the UPR following palmitate treatment. Previous research has highlighted a potential role for 5-LOX, via LTB4, in palmitate-induced ER stress [297], but little other work has addressed this question. Here, pharmacological inhibitors of cPLA2 (AACOCF3), 12-LOX (NCTT-956), and 15-LOX (PD146176) have been used to assess the role that other lipoxygenase isoforms may have in the activation of inflammatory and stress signalling pathways.

RT-qPCR was used to profile the effects of phospholipase and lipoxygenase inhibition on ER stress signalling and inflammatory cytokines. C2C12 cells were grown to confluence and

treated for 6 days through differentiation with 200 µM palmitate or the BSA vehicle. For the final 24 hours, cells were co-treated with either 100 µM of the PLA2 inhibitor AACOCF3, 10 µM of the 15-LOX inhibitor PD146176 or 10 µM of the 12-LOX inhibitor NCTT-956, or the relevant volume of the DMSO vehicle control [319,320]. RNA was then extracted and the expression of UPR and inflammatory markers were analysed using RT-qPCR.

Inhibition of cPLA2 had a profound effect on the activation of ER stress. Treatment with AACOCF3 increased the expression of all four UPR markers (*Atf3* increased 12.7-fold, *Atf4* increased 7.5-fold, *Hspa5* increased 5.7-fold, *Edem1* 1.8-fold), and exacerbated palmitate-induced ER stress relative to control-treated cells (*Atf3* increased 6.6-fold, *Atf4* increased 6.7-fold, *Hspa5* increased 3-fold, *Edem1* increased 2-fold) (**Figure 4.8A**). However, a combination of palmitate and the cPLA2 inhibitor reduced expression of *Atf3* and *Hspa5* when compared to cells treated with the inhibitor alone, suggesting the two treatments are not additive. While cPLA2 inhibition had a profound effect on UPR gene expression, the consequences of inhibition on inflammatory cytokines were less clear (**Figure 4.8B**). There were no significant effects on *Ccl2* expression with AACOCF3 treatment, although inhibition did increase levels of *Il6* (4-fold). These results suggest that palmitate-induced eicosanoid secretion may have an important role in controlling the induction of ER stress. Since cPLA2 inhibition increased expression of UPR markers, eicosanoid signalling may function to oppose the induction of ER stress following palmitate treatment.

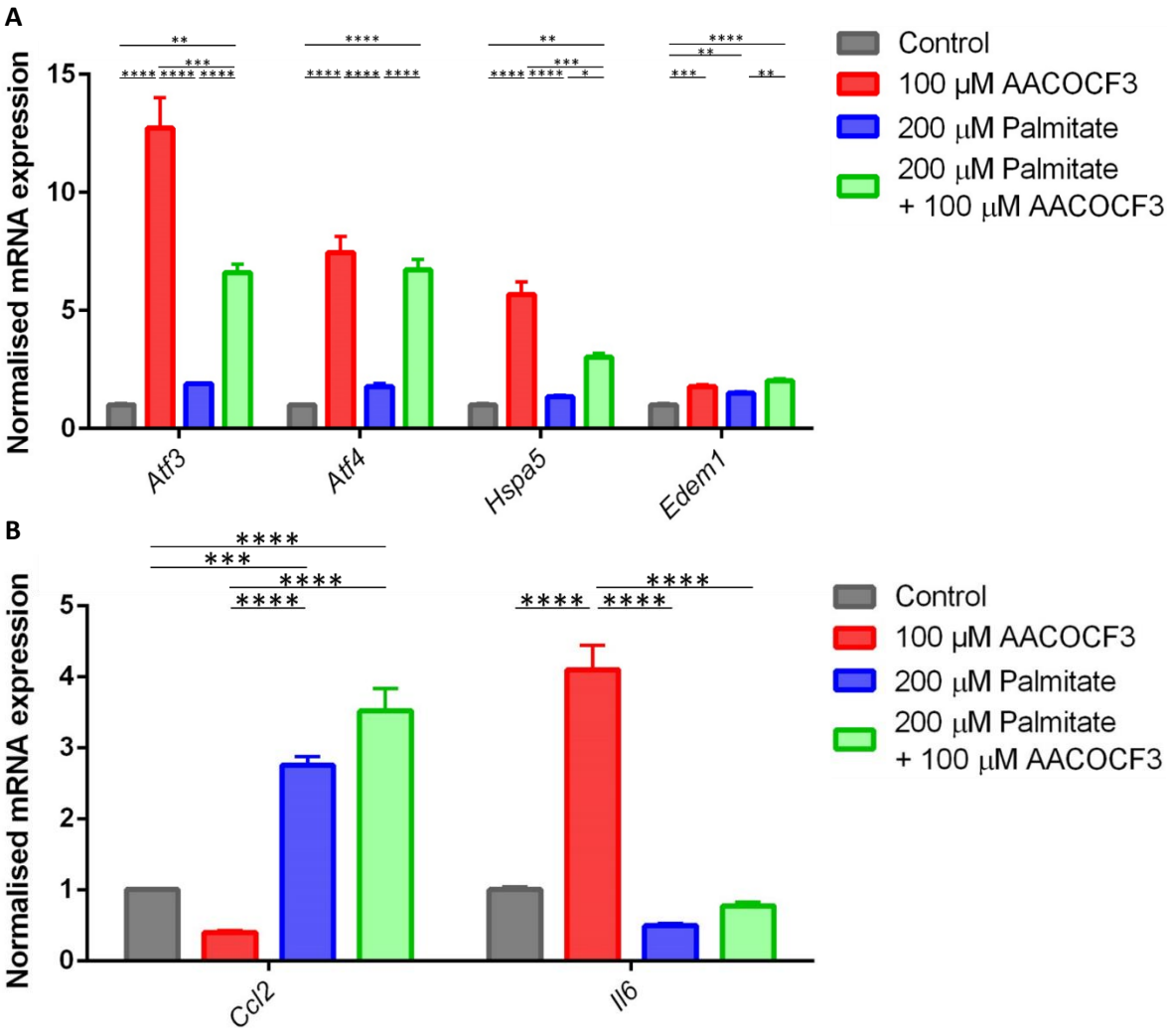

Figure 4.8: Inhibition of cytosolic phospholipase A2 exacerbates palmitate-induced endoplasmic reticulum stress

C2C12 myotubes were treated with 200 μM palmitate, or the vehicle for 6 days during differentiation. For the final 24 hours, myotubes were also co-incubated with either 100 μM AACOCF3, or the vehicle. Transcription of (A) unfolded protein response markers (*Atf3*, *Atf4*, *Hspa5* and *Edem1*) and (B) inflammatory cytokines (*Ccl2* and *Il6*) were measured using RT-qPCR. Each species was analysed using a one-way ANOVA with Tukey's multiple comparison test. * $P \leq 0.05$, ** $P < 0.01$, *** $P < 0.001$, **** $P < 0.0001$. Data are expressed as mean ± SEM (n = 3).

However, cPLA2 inhibition also greatly increased concentrations of PUFA-containing PCs, potentially through inhibition of PUFA release from PCs within the plasma membrane, which is likely to affect membrane shape and fluidity. Previous work has highlighted the importance of membrane composition in the induction of ER stress, and so the exacerbation of palmitate-induced ER stress by cPLA2 inhibition may not be a result of disrupted eicosanoid synthesis

[175,176]. Chemical inhibition of LOX isoforms circumvents the issues related to membrane structure by inhibiting eicosanoid synthesis further down the pathway. Furthermore, it provides a more detailed analysis of eicosanoid function, focusing on specific branch points of the pathway and a subset of the eicosanoid species (**Figure 4.1**).

Inhibition of 15-LOX with PD146176 had little effect on the induction of UPR genes in the Ire1 mediated pathways, but the palmitate-induced increase in *Atf3* expression was exacerbated 1.5-fold when combined with the inhibition (**Figure 4.9A**). 15-LOX abrogation did, however, have a more pronounced effect on inflammatory markers. PD146176 treatment of cells exposed to palmitate significantly increased the expression of *Ccl2* 1.6-fold compared to those cells treated with only palmitate, while 15-LOX inhibition also increased the mRNA levels of *Il6* (1.8-fold) (**Figure 4.9B**).

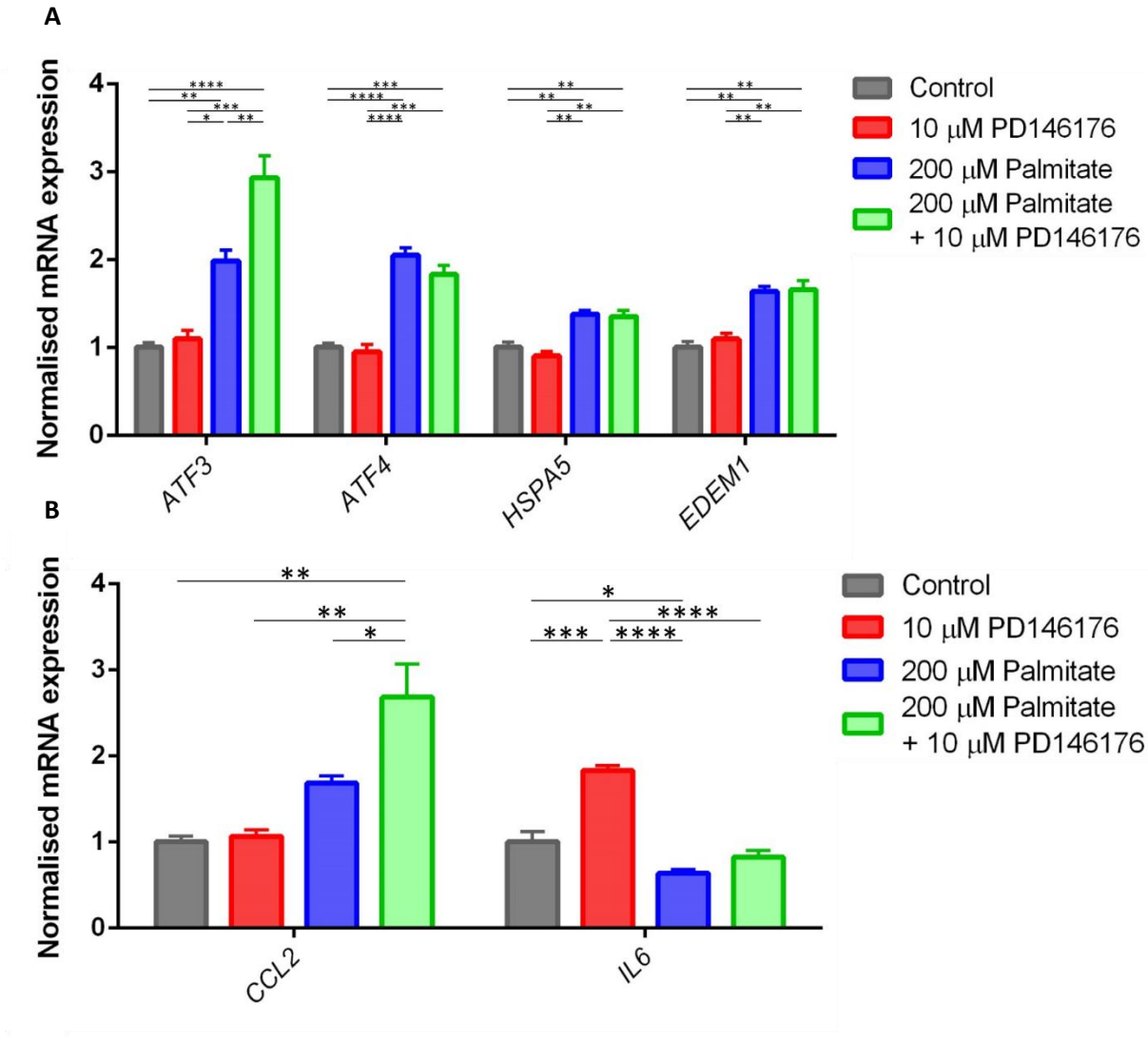

Figure 4.9: Inhibition of 15-lipoxygenase increases expression of inflammatory cytokines in C2C12 myotubes.

C2C12 myotubes were treated with 200 μM palmitate, or the vehicle for 6 days during differentiation. For the final 24 hours, myotubes were also co-incubated with either 10 μM PD146176, or the vehicle. Transcription of (A) unfolded protein response markers (*Atf3, Atf4, Hspa5* and *Edem1*) and (B) inflammatory cytokines (*Ccl2* and *Il6*) were measured using RT-qPCR. Each species was analysed using a one-way ANOVA with Tukey's multiple comparison test. * $P \leq 0.05$, ** $P < 0.01$, *** $P < 0.001$, **** $P < 0.0001$. Data are expressed as mean ± SEM (n = 3).

In contrast, 12-LOX inhibition, using NCTT-956, was associated with increases in the expression of *Atf3* (1.9-fold), *Atf4* (2.5-fold), and *Edem1* (1.3-fold) (**Figure 4.10A**). Furthermore, cells co-treated with palmitate and the inhibitor exhibited additive expression of *Atf3* (1.9-fold), *Atf4* (1.4-fold), and *Edem1* (1.3-fold) when compared to those exposed only to palmitate. The effect of 12-LOX inhibition on *Ccl2* and *Il6* was less pronounced when

compared with 15-LOX inhibition, although co-treatment of palmitate with NCTT-956 significantly increased the expression of *Ccl2* (2.4-fold) and reduced expression of *Il6* (by 60%) compared to cells treated with the vehicle control (**Figure 4.10B**).

These data highlight a role for 12-LOX-derived eicosanoids in the regulation of UPR gene expression, and suggests that eicosanoids generated via 12-LOX oppose palmitate-mediated activation of the UPR.

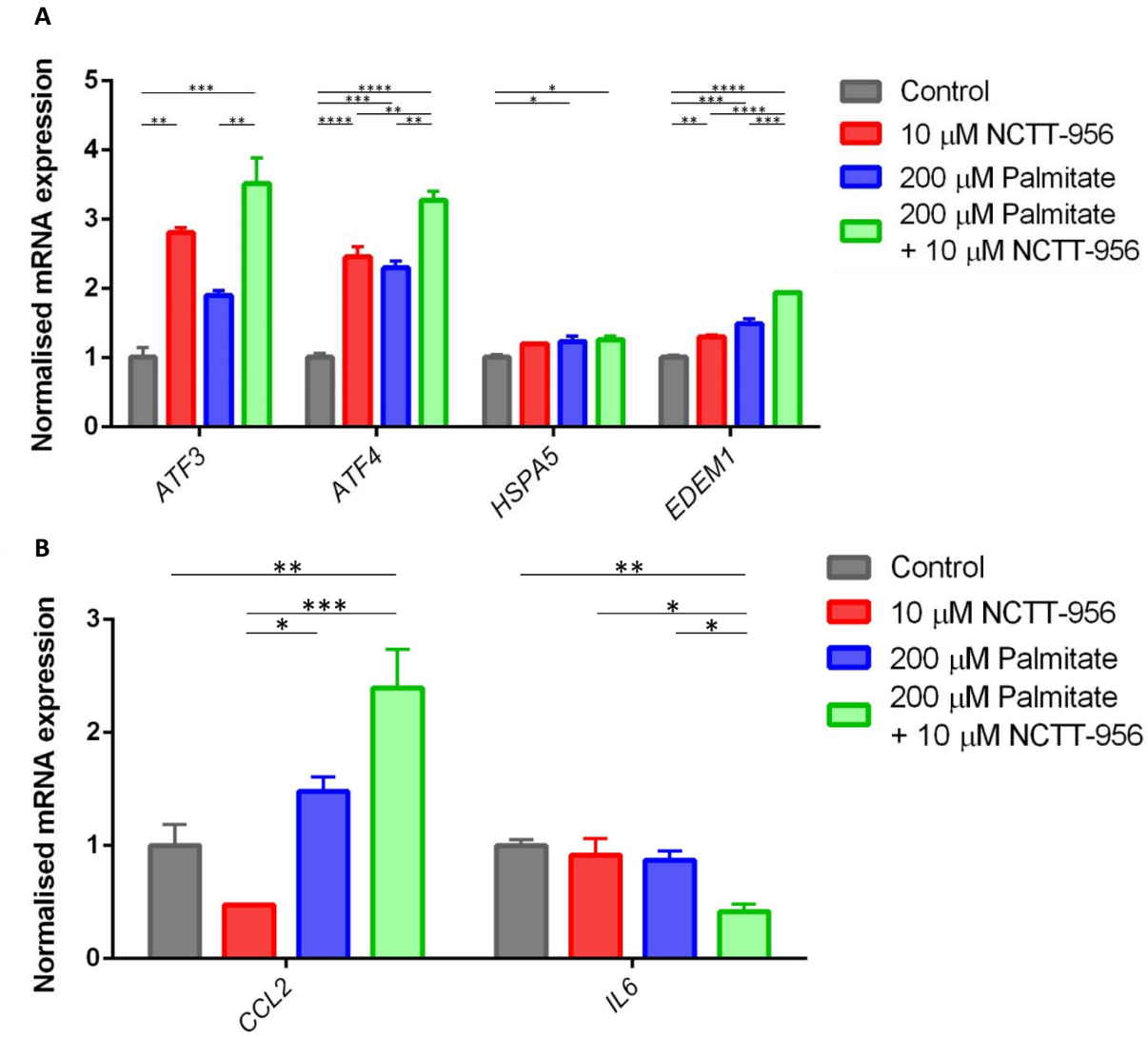

Figure 4.10: Inhibition of 12-lipoxygenase amplifies palmitate-induced unfolded protein response gene expression in C2C12 myotubes

C2C12 myotubes were treated with 200 μM palmitate, or the vehicle for 6 days during differentiation. For the final 24 hours, myotubes were also co-incubated with either 10 μM NCTT-956, or the vehicle. Transcription of (A) unfolded protein response genes (*Atf3*, *Atf4*, *Hspa5* and *Edem1*) and (B) inflammatory cytokines (*Ccl2* and *Il6*) were measured using RT-qPCR. Each species was analysed using a one-way ANOVA with Tukey's multiple comparison test. * $P \leq 0.05$, ** $P < 0.01$, *** $P < 0.001$, **** $P < 0.0001$. Data are expressed as mean ± SEM (n = 3).

4.4.6 Inhibition of 12- and 15-lipoxygenase increases unfolded protein response induction in primary human skeletal muscle cells

To investigate whether the observations made in mouse C2C12 cells translate to a human model of skeletal myocytes, experiments were repeated in primary HSkMCs. Cells were cultured to confluence and treated with 100 µM palmitate, or the BSA vehicle, throughout a 6 day differentiation period. For the final 24 hours, cells were also co-cultured with either 10 µM PD146176 (15-LOX inhibitor), 10 µM NCTT-956 (12-LOX inhibitor), or the DMSO vehicle control. RNA was isolated and the mRNA levels of UPR genes (*ATF3*, *ATF4*, *HSPA5* and *EDEM1*) and inflammatory cytokines (*CCL2* and *IL6*) were measured using RT-qPCR.

Inhibition of 15-LOX with PD146176 exacerbated palmitate-induced ER stress, with expression of *ATF4* (2.1-fold), *HSPA5* (1.3-fold), and *EDEM1* (2-fold) significantly higher in myocytes treated with both palmitate and the inhibitor compared with palmitate alone (**Figure 4.11A**). The expression of *CCL2* (5-fold, compared to the control) and *IL6* (11.1-fold, compared to the control) were also increased following co-treatment of myocytes with both the 15-LOX inhibitor and palmitate (**Figure 4.11B**). These results suggest a more prominent role for 15-LOX derived metabolites in human myocytes than the immortalised C2C12 mouse cell line.

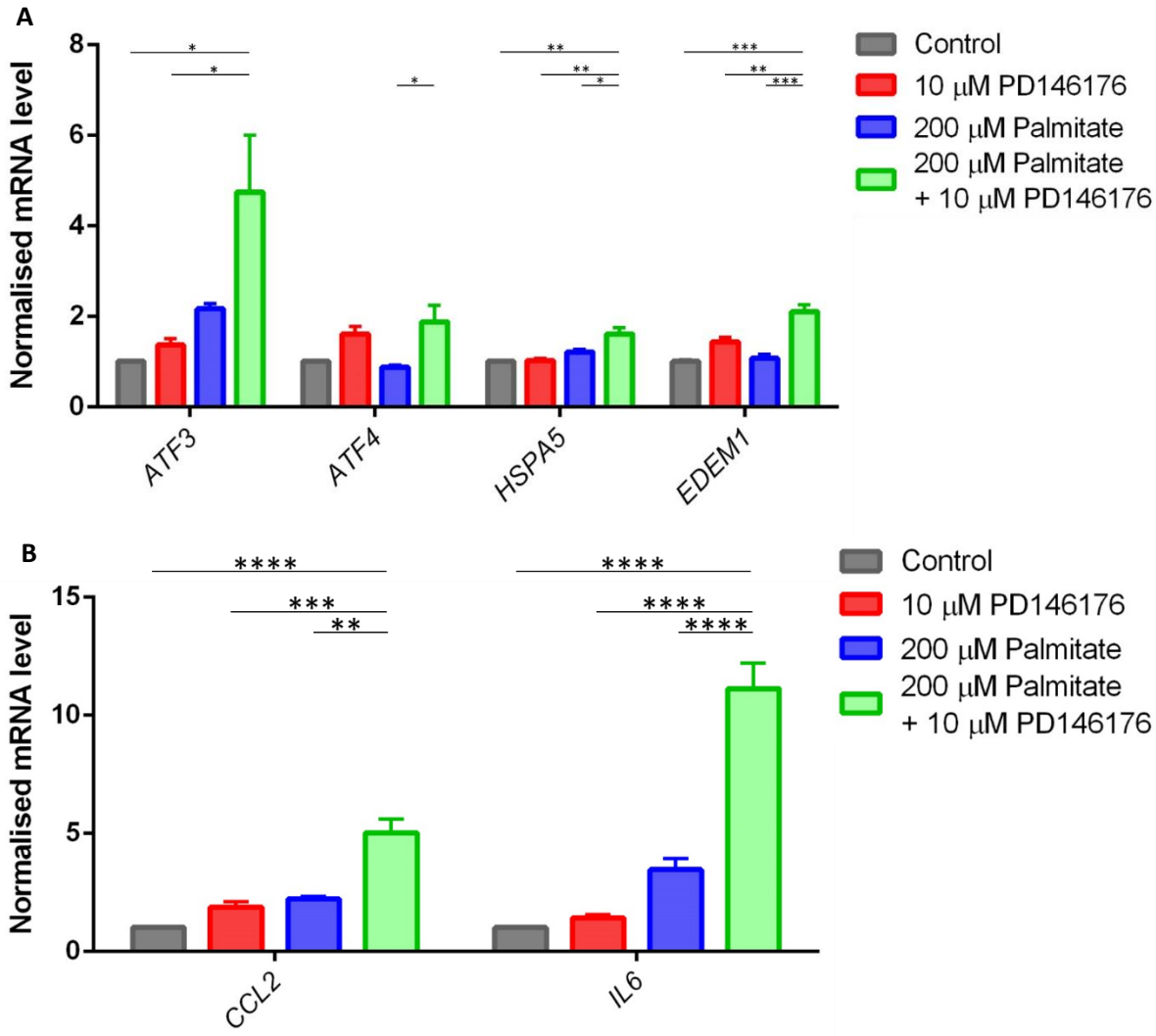

Figure 4.11: Inhibition of 15-lipoxygenase exacerbates palmitate-induced endoplasmic reticulum stress in primary human skeletal muscle cells

Primary human skeletal muscle cells were treated with 100 μM palmitate, or the vehicle for 6 days during differentiation. For the final 24 hours, myotubes were also co-incubated with either 10 μM PD146176, or the vehicle. Transcription of (A) unfolded protein response markers (*Atf3*, *Atf4*, *Hspa5* and *Edem1*) and (B) inflammatory cytokines (*Ccl2* and *Il6*) were measured using RT-qPCR. Each species was analysed using a one-way ANOVA with Tukey's multiple comparison test. * $P \leq 0.05$, ** $P < 0.01$, *** $P < 0.001$, **** $P < 0.0001$. Data are expressed as mean ± SEM (n = 3).

Inhibition of 12-LOX, via NCTT-956 treatment, also increased palmitate-induced transcription of UPR genes including *ATF3* (1.7-fold compared to palmitate treated), *HSPA5* (1.5-fold compared to palmitate treated) and *EDEM1* (1.7-fold compared to control), similar to results detected in C2C12 cells (**Figure 4.12A**). The effect of 12-LOX inhibition on inflammatory cytokine expression was negligible, however (**Figure 4.12B**). These data are, at

least partially, in agreement with experiments conducted in C2C12 cells, and reinforce a potential role for LOX-derived eicosanoids in the control of ER stress and the expression of inflammatory cytokines.

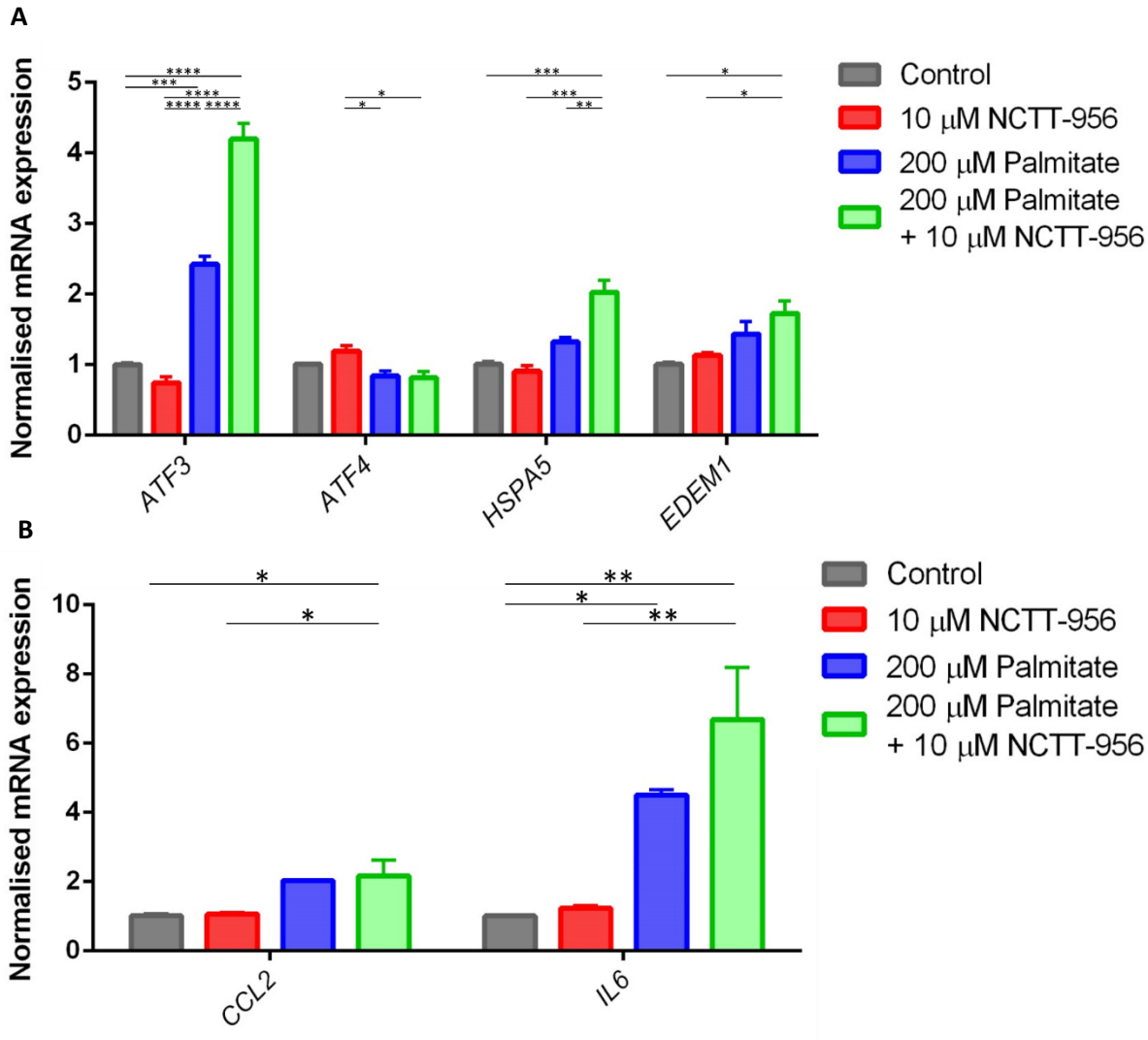

Figure 4.12: Inhibition of 12-lipoxygenase increases palmitate-induced endoplasmic reticulum stress in primary human skeletal muscle cells

Primary HSkMCs were treated with 100 μM palmitate, or the vehicle for 6 days during differentiation. For the final 24 hours, myotubes were also co-incubated with either 10 μM NCTT-956, or the vehicle. Transcription of (A) unfolded protein response markers (*Atf3, Atf4, Hspa5* and *Edem1*) and (B) inflammatory cytokines (*Ccl2* and *Il6*) were measured using RT-qPCR. Each species was analysed using a one-way ANOVA with Tukey's multiple comparison test. * $P \leq 0.05$, ** $P < 0.01$, *** $P < 0.001$, **** $P < 0.0001$. Data are expressed as mean ± SEM (n = 3).

4.4.7 Co-culturing palmitate-conditioned C2C12 myotubes with untreated Raw 264.7 macrophages increases transcription of genes associated with macrophage activation

Palmitate-induced eicosanoid secretion increases local concentrations of the oxidised lipids for cells in close proximity. Thus far, the effects of these eicosanoids have been considered on myocytes, but they may also provide a means of communication between myocytes and cells of the immune system. Immune cell infiltration is associated with obesity in skeletal muscle, while *in vitro* experiments have suggested the potential for cross-talk between myocytes and macrophages [91,100,321]. To investigate a role for myocyte-derived eicosanoids in paracrine and endocrine signalling to immune cells, C2C12 myotubes were co-cultured with Raw 264.7 cells, an immortalised macrophage cell line. C2C12 cells were grown to confluence and differentiated for 6 days, during which they were treated with either 200 µM palmitate or the BSA vehicle. For the final 24 hours, myotubes were also co-treated with 100 µM AACOCF3 to inhibit cPLA2, and therefore eicosanoid production, or the DMSO vehicle. Separately, Raw 264.7 cells were grown to confluence and then plated in Transwell inserts for 24 hours. Following the end of the C2C12 treatment regime, culture media was switched to serum-free media on both myocytes and macrophages, and the inserts were then added to the wells of C2C12 cells. The two cell lines were co-cultured for 24 hours, and RNA was harvested from both cell types at the end of this time period. Expression of both ER stress associated genes and macrophage polarisation markers were measured by RT-qPCR.

Macrophage activation states exist between the pro-inflammatory M1 and the anti-inflammatory M2 phenotypes [322]. Here, expression of two M1 markers – tumour necrosis factor (*Tnf*) and nitric oxide synthase 2 (*Nos2*) – and two M2 markers – early growth response 2 (*Egr2*) and arginase 1 (*Arg1*) – were measured to understand if cross-talk with myocytes influences macrophage activation. Expression of *Arg1* (3-fold), *Tnf* (2.6-fold) and *Nos2* (2-fold) were all significantly elevated in macrophages co-cultured with palmitate-treated myocytes (**Figure 4.13A**). This suggests an increase in macrophage polarisation and activation, but with higher levels of both M1 and M2 markers, it is unclear whether these macrophages display both M1 and M2 phenotypes or if there are a mixed population of cells responding to different pro- and anti-inflammatory cues. Inhibition of cPLA2 had only a limited effect on the activation markers. AACOCF3 treatment increased *Arg1* expression (2.9-fold), suggesting a potential role for eicosanoids in suppressing M2 activation, but combining palmitate treatment with cPLA2 inhibition did not exacerbate the phenotype. Furthermore, inactivation of cPLA2 also impacted on the transcription of *Nos2*, with co-

treatment of myocytes with palmitate and AACOCF3 insignificant compared with vehicle control treated cells.

Macrophages co-cultured with palmitate-treated C2C12 cells also exhibited increased expression of *Atf4* (2.9-fold) and *Hspa5* (1.8-fold), indicating the induction of ER stress (**Figure 4.13B**). Inhibiting cPLA2 in palmitate-treated C2C12 myotubes reduced transcription of these UPR markers, suggesting that myocyte-derived eicosanoids are important in the induction of macrophage ER stress.

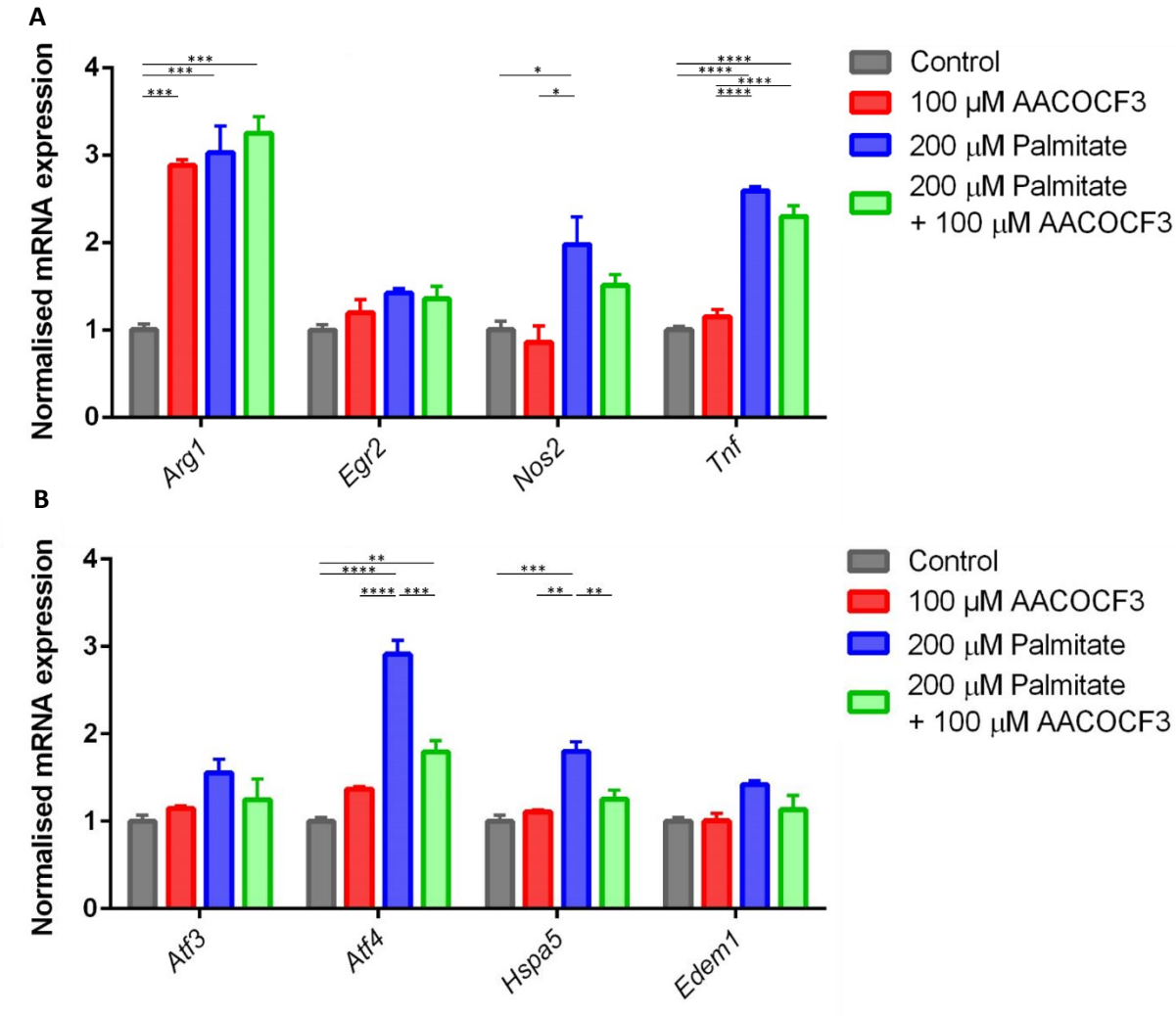

Figure 4.13: Co-culture of Raw 264.7 macrophages with palmitate-treated C2C12 myotubes increases macrophage polarisation and endoplasmic reticulum stress

C2C12 myotubes were treated with 200 μM palmitate, or the vehicle for 6 days during differentiation. For the final 24 hours, myotubes were also co-incubated with either 100 μM AACOCF3, or the vehicle. Subsequently, media was switched to serum-free media and myotubes were co-cultured with Raw 264.7 macrophages grown on Transwell inserts. Transcription of (A) macrophage activation markers (*Arg1*, *Egr2*, *Nos2* and *Tnf*) and (B) UPR genes (*Atf3, Atf4, Hspa5* and *Edem1*) in Raw 264.7 macrophages were measured using RT-qPCR. Each species was analysed using a one-way ANOVA with Tukey's multiple comparison test. * $P \leq 0.05$, ** $P < 0.01$, *** $P < 0.001$, **** $P < 0.0001$. Data are expressed as mean ± SEM (n = 3).

RT-qPCR analysis of C2C12 myotubes co-cultured with the macrophages demonstrated that the effects of cPLA2 inhibition were consistent with previous experiments, as expression of *Atf3, Atf4, Hspa5* and *Edem1* were increased independent of palmitate exposure (**Figure 4.14A**). However, expression of ER stress genes were unchanged between control and palmitate treatment groups, which suggests that macrophages confer a degree of protection against palmitate-induced ER stress in myotubes. The effects of cPLA2 inhibition on inflammatory markers were also consistent with previous experiments not involving co-culture (**Figure 4.14B**).

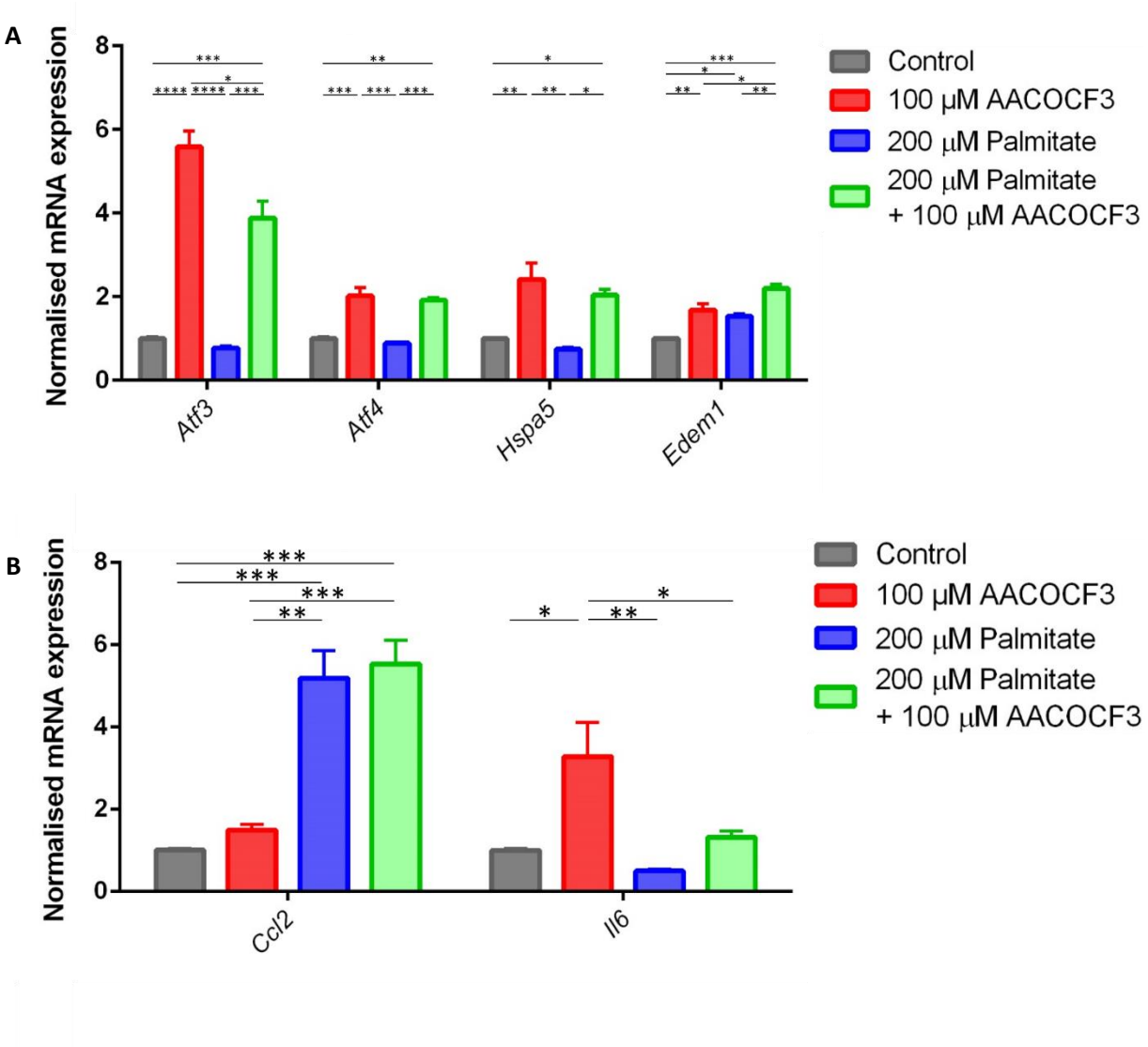

Figure 4.14: Co-culturing C2C12 myotubes with Raw 264.7 macrophages reduces palmitate-induced endoplasmic reticulum stress in myotubes

C2C12 myotubes were treated with 200 µM palmitate, or the vehicle for 6 days during differentiation. For the final 24 hours, myotubes were also co-incubated with either 100 µM AACOCF3, or the vehicle. Subsequently, media was switched to serum-free media and myotubes were co-cultured with Raw 264.7 macrophages grown on Transwell inserts. Transcription of (A) endoplasmic reticulum stress markers (*Atf3*, *Atf4*, *Hspa5* and *Edem1*) and (B) inflammatory cytokines (*Ccl2* and *Il6*) in C2C12 myotubes were measured using RT-qPCR. Each species was analysed using a one-way ANOVA with Tukey's multiple comparison test.* $P \leq 0.05$, ** $P < 0.01$, *** $P < 0.001$, **** $P < 0.0001$. Data are expressed as mean ± SEM (n = 3).

4.4.8 Inhibition of lipoxygenase isoforms in C2C12 myotubes reduces macrophage activation in co-cultured Raw 264.7 macrophages

Inhibition of cPLA2 in myotubes partially impacted upon co-cultured macrophage expression of *Arg1* and *Nos2*, suggesting a potential role for eicosanoids in macrophage polarisation. To investigate the effects of the downstream 12-LOX and 15-LOX branches of eicosanoid metabolism, C2C12 cells were cultured to confluence and treated for 6 days during differentiation with 200 µM palmitate or the BSA vehicle. For the final 24 hours, cells were co-treated with either 10 µM of the 15-LOX inhibitor PD146176, 10 µM of the 12-LOX inhibitor NCTT-946, or the DMSO vehicle. Following the end of the treatment regime, cell culture media was switched to serum-free media, and myotubes were co-cultured with macrophages grown on Transwell inserts. After 24 hours, RNA was extracted from macrophages and transcription of ER stress and macrophage polarisation markers were analysed using RT-qPCR.

Treatment of C2C12 cells with the 15-LOX inhibitor PD146176 and palmitate reduced macrophage expression of *Arg1* and *Tnf* so that it was unchanged relative to the cells treated with the vehicle control, suggesting a role for 15-LOX-derived eicosanoids in the control of macrophage activation (**Figure 4.15A**). Macrophage transcription of ER stress markers, on the other hand, were unaffected by exposure to PD146176 (**Figure 4.15B**).

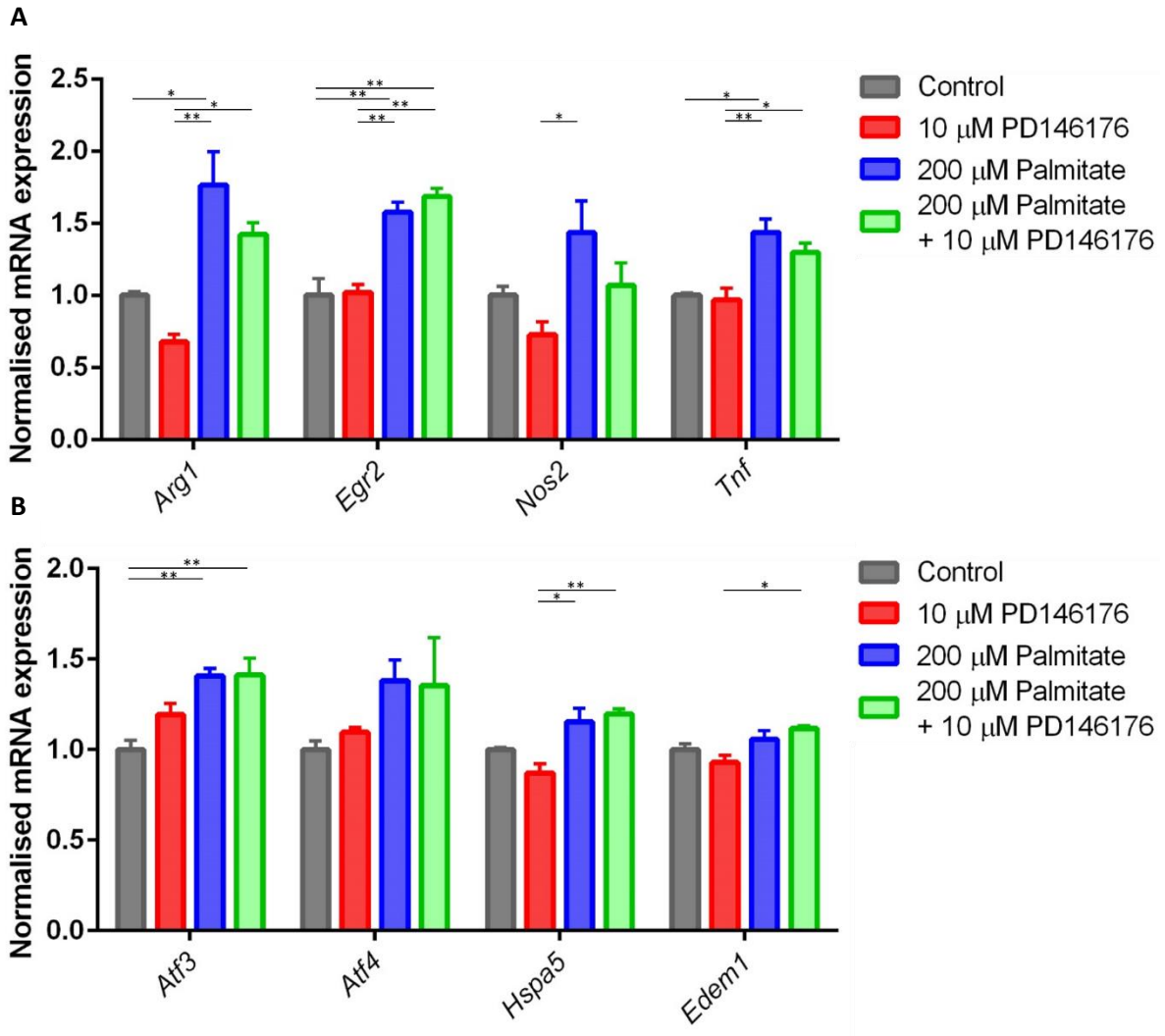

Figure 15: Inhibition of 15-lipoxygenase in C2C12 myotubes partially reduces activation of Raw 264.7 macrophages

C2C12 myotubes were treated with 200 μM palmitate, or the vehicle for 6 days during differentiation. For the final 24 hours, myotubes were also co-incubated with either 10 μM PD146176, or the vehicle. Subsequently, media was switched to serum-free media and myotubes were co-cultured with Raw 264.7 macrophages grown on Transwell inserts. Transcription of (A) macrophage activation markers (*Arg1*, *Egr2*, *Nos2* and *Tnf*) and (B) unfolded protein response genes (*Atf3*, *Atf4*, *Hspa5* and *Edem1*) in Raw 264.7 macrophages were measured using RT-qPCR. Each species was analysed using a one-way ANOVA with Tukey's multiple comparison test. * $P \leq 0.05$, ** $P < 0.01$, *** $P < 0.001$, **** $P < 0.0001$. Data are expressed as mean ± SEM (n = 3).

Inhibition of 12-LOX in myotubes treated with palmitate reduced expression of *Tnf* in co-cultured macrophages to a level that was the same as vehicle-treated control cells. However, NCTT-946 treatment exacerbated palmitate-induced expression of *Egr2* (1.8-fold compared to the control), with the increase reaching significance compared to cells treated with the vehicle controls, suggesting that eicosanoids synthesised by 12-LOX may have opposing

effects on some M1 and M2 markers (**Figure 4.16A**). Similar to 15-LOX inhibition, treatment with NCTT-946 had little effect on macrophage expression of ER stress markers (**Figure 4.16B**).

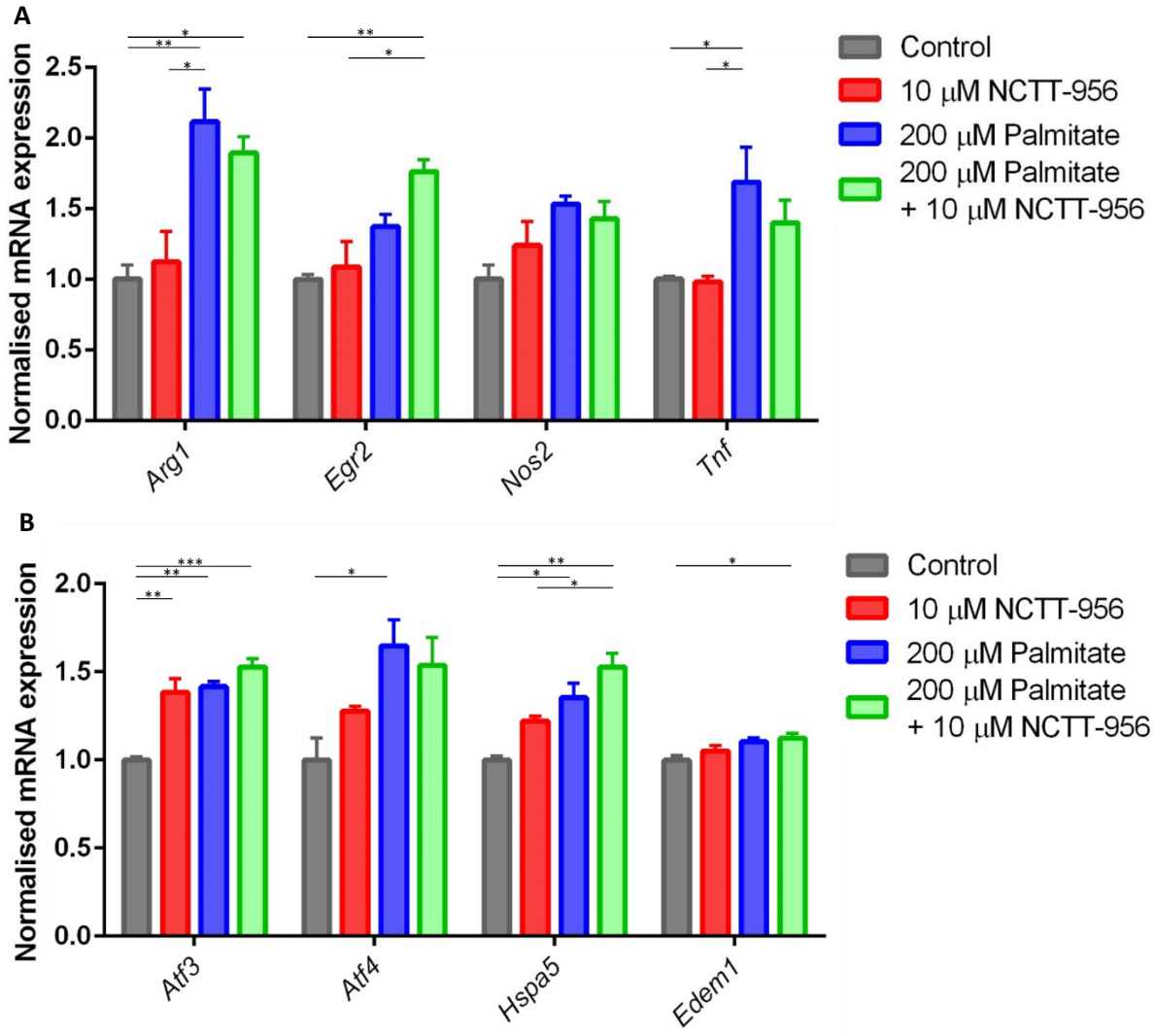

Figure 4.16: 12-lipoxygenase-derived eicosanoids secreted from C2C12 myotubes may push Raw 264.7 macrophages towards an M1 phenotype

C2C12 myotubes were treated with 200 μM palmitate, or the vehicle for 6 days during differentiation. For the final 24 hours, myotubes were also co-incubated with either 10 μM NCTT-956, or the vehicle. Subsequently, media was switched to serum-free media and myotubes were co-cultured with Raw 264.7 macrophages grown on Transwell inserts. Transcription of (A) macrophage activation markers (*Arg1*, *Egr2*, *Nos2* and *Tnf*) and (B) UPR genes (*Atf3*, *Atf4*, *Hspa5* and *Edem1*) in Raw 264.7 macrophages were measured using RT-qPCR. Each species was analysed using a one-way ANOVA with Tukey's multiple comparison test. * $P \leq 0.05$, ** $P < 0.01$, *** $P < 0.001$, **** $P < 0.0001$. Data are expressed as mean ± SEM (n = 3).

The effects of LOX inhibition on C2C12 expression of UPR markers were minimal, although 15-LOX and 12-LOX inhibition reduced palmitate-induced expression of *Atf4* and *Atf3*, respectively, to a level that's insignificant from vehicle-treated cells (**Figure 4.17**). However, it is important to note that ER stress levels do appear to be lower than previously observed in experiments without macrophages, suggesting a potential role for macrophages in suppressing palmitate-induced ER stress.

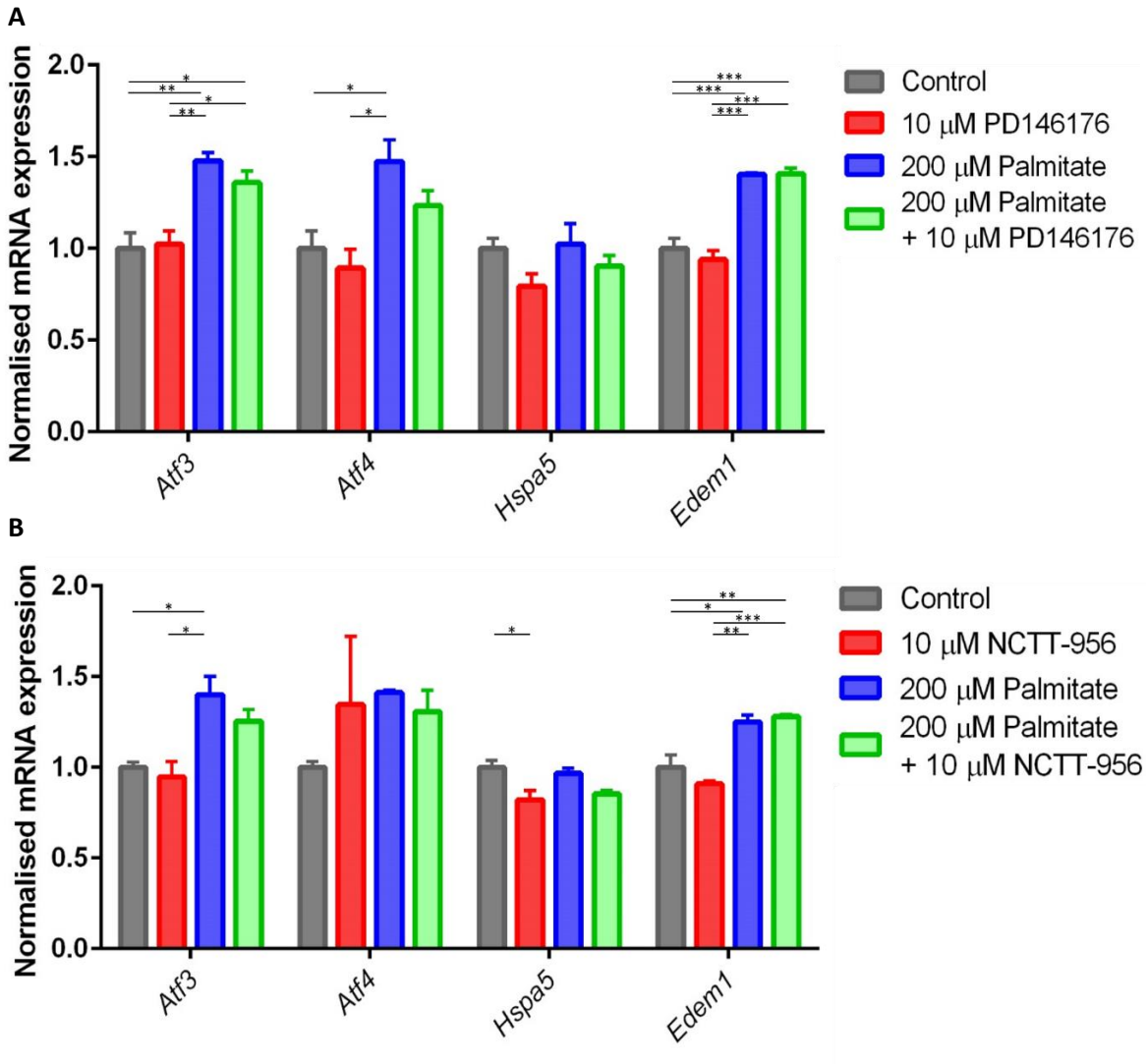

Figure 4.17: Lipoxygenase inhibition has little effect on endoplasmic reticulum stress in C2C12 myotubes following co-culture with Raw 264.7 macrophages

C2C12 myotubes were treated with 200 μM palmitate, or the vehicle for 6 days during differentiation. For the final 24 hours, myotubes were also co-incubated with either 10 μM PD146176, 10 μM NCTT-956, or the vehicle. Subsequently, media was switched to serum-free media and myotubes were co-cultured with Raw 264.7 macrophages grown on Transwell inserts. Transcription of endoplasmic reticulum stress markers (*Atf3*, *Atf4*, *Hspa5* and *Edem1*) in C2C12 myotubes following treatment with (A) PD1467176 and (B) NCTT-956) were measured using RT-qPCR. Each species was analysed using a one-way ANOVA with Tukey's multiple comparison test. * $P \leq 0.05$, ** $P < 0.01$, *** $P < 0.001$, **** $P < 0.0001$. Data are expressed as mean ± SEM (n = 3).

Cell Type	Inhibitor	Phenotype
Raw 264.7	AACOCF3 (cPLA2)	Palmitate stimulated an increase in macrophage activation and ER stress markers. Inhibition of cPLA2 reduced induction of ER stress, suggesting a role for eicosanoid signalling in the propagation of UPR activation, but had limited effect on activation markers.
C2C12	AACOCF3 (cPLA2)	Induction of palmitate-stimulated ER stress was abrogated by co-culture with macrophages. Inhibition of cPLA2 increased ER stress markers and *Il6* expression.
Raw 264.7	PD146176 (15-LOX)	Inhibition of 15-LOX slightly reduced palmitate-induced increases in expression of *Nos2* and *Tnf* to a level insignificant to the vehicle control. ER stress markers were unaffected.
C2C12	PD146176 (15-LOX)	15-LOX inhibition had limited effect on ER stress genes.
Raw 264.7	NCTT-956 (12-LOX)	Inhibition of 12-LOX partially reduced expression of *Tnf* and increased expression of *Egr2*. Furthermore, there were increases in *Atf3* expression and palmitate-induced transcription of *Edem1*.
C2C12	NCTT-956 (12-LOX)	12-LOX inhibition had limited effect on ER stress genes.

Table 4.1: Summary table of results from co-culture experiments

4.5 Discussion

This chapter sought to understand the functional consequences of palmitate-induced phospholipid remodelling. LC-MS/MS analysis of C2C12 myotube culture media showed an increase in eicosanoid secretion in response to both acute and chronic palmitate treatment, with lipoxygenase-derived species particularly affected. Signalling dynamics between skeletal muscle and the immune system have previously been considered at the protein level, centring on a role for cytokines in transmitting inflammation between cells [323,324]. However, the palmitate-induced increases in eicosanoid secretion discussed here represent an alternative route for myocyte-myocyte and myocyte-macrophage cross-talk.

Inhibiting cPLA2 activity greatly increased expression of ER stress markers in myocytes, suggesting a role for eicosanoids in the control of lipotoxic ER stress in muscle. Previous work has implicated LOX-derived eicosanoids in the induction of UPR signalling, with zileuton, a pharmacological inhibitor of 5-LOX, reducing lipid induced ER stress in C2C12 myotubes and mouse models of obesity [297]. Similarly, human retinal endothelial cells treated with 15-HETE exhibited increased ER stress, while diabetes-induced ER stress was reduced in the retina of Alox15-KO mice [312]. Further evidence for an association between ER stress and eicosanoids stems from research on the role of Lpcat3 in liver [175]. Elevated Lpcat3 activity, which increases incorporation of PUFAs into the phospholipid membrane, thereby reducing eicosanoid generation, decreased markers of lipid-induced ER stress, in both *in vitro* and *in vivo* models. It's important to note, however, that the effect of elevated LPCAT3 activity in the previous study, as well as AACOCF3 treatment in this chapter, will also affect membrane composition and fluidity, potentially impacting on UPR induction. This is highlighted by decreases in expression of *Atf3* and *Hspa5* in palmitate and AACOCF3 co-treatment groups compared to myotubes treated with only AACOCF3, suggesting a normalised membrane composition reduces ER stress. It's likely, therefore, that the effects of AACOCF3 on UPR induction may result from both membrane composition and eicosanoid signalling.

The role of 12- and 15-LOX derived eicosanoids in myocyte ER stress and inflammatory signalling has not been investigated. In C2C12 myotubes 12-LOX-derived eicosanoids appear important in suppressing ER stress induction, while 15-LOX inhibition increased expression of inflammatory markers. Differences between murine and human LOX isoforms likely explain the differing results in primary HSkMCs, with chemical inhibition indicating

an important role for 15-LOX in both ER stress induction and inflammation. Notably, mouse isoforms of Alox12 and Alox15 are both capable of producing 12- and 15-HETE, for example, while the human isoforms are much more stringent in their products, with ALOX12 and ALOX15 forming only 12-HETE and 15-HETE, respectively [325].

The results suggest that these bioactive lipids finely regulate protein-induced signalling responses and that the manipulation of specific eicosanoid pathways and species could alleviate ER stress and inflammatory signalling. The experiments presented here have focused on loss-of-function. Future work should look at increasing activity of LOX isoforms and exogenously exposing cells to different eicosanoids species. It will then be possible to isolate specific eicosanoid species important in the control of these signalling cascades. Importantly, very little research, if any, has focused on the eicosanoid species detected here by LC-MS/MS. Investigating the roles species such as HETEs, HEPEs and HODEs may play in metabolic disease represents an interesting and under-investigated field of research.

In contrast with the results of this chapter, inhibition of 12/15-LOX (Alox15) has previously been identified to ameliorate tunicamycin-induced ER stress in cultured adipocytes, while exogenously exposing these cells to 12-HETE increased induction of the UPR [326]. However, this work looked only at ER stress induced by tunicamycin, rather than palmitate, and used only acute treatments, never exceeding longer than 24 hours. Furthermore, Cole and colleagues also showed that 12/15-LOX knockout mice had increased expression of *Hspa5* and *Atf4*. While exposing cultured adipocytes extracted from these mice to tunicamycin for 4 hours highlighted a potential protective role for 12/15-LOX, this effect largely diminished after 24 hours of tunicamycin treatment. The results of experiments in this chapter differ from the work of Cole *et al.* on differences in both substrate and treatment time, as well as cell tissue type.

The role for eicosanoid signalling between C2C12 myotubes and Raw 264.7 macrophages was assessed in this chapter, using Transwell inserts for co-culturing of the two cell lines. Analysis of M1 and M2 marker expression showed increases in macrophage activation following co-culture with C2C12 cells treated with palmitate. Interestingly, however, expression of both M1 and M2 markers were increased. This may be explained by a mixed population of macrophages – exhibiting a distinct preference for either a M1-like or M2-like phenotype. These cells may be responding to variable local concentrations of inflammatory mediators, a theory supported by the eicosanoid profiling results, which demonstrated

increases in species that are both pro- and anti-inflammatory. However, a general increase in the M1 and M2 markers may also simply represent an alternative activation state, separate from the rigid and increasingly debated M1/M2 polarisation states [95]. Single-cell flow cytometry analysis of macrophage activation markers would provide greater insight into this scenario.

In this chapter inhibition of both 15- and 12-LOX in myotubes appeared to weakly impact on both M1 and M2 marker expression in co-cultured macrophages. Increasing replicate number in these experiments (from n = 3) may reduce some of the variation in the data, giving greater statistical power to make inference. Furthermore, using lentiviral-mediated knockdown of LOX isoforms may provide a more specific and targeted ablation of function, and provide greater insight into the roles LOX-derived eicosanoids originating from myocytes play in the regulation of macrophage polarisation.

The assessment of macrophage polarisation in this chapter is preliminary. Analysis of protein levels of important polarisation markers, while also investigating any switch in oxidative metabolism using respirometry techniques would strengthen the phenotyping [327,328]. Using flow cytometry cell sorting to assess populations of M1 and M2 macrophages would also be important. To improve the relevance to human disease, these experiments could also be repeated using primary HSkMCs and human macrophages.

With experiments investigating the roles of eicosanoids in macrophage polarisation inconclusive, it is likely that protein signals and cytokines may also play a major role in this process. Chronic palmitate treatment increased the expression of Ccl2 in C2C12 cells and previous work has highlighted the importance of Ccl2 in macrophage infiltration and polarisation [91]. Il-6 has also been shown to increase macrophage infiltration during muscle regeneration [329]. However, expression of Il-6 was reduced in C2C12 myotubes in response to palmitate treatment and so is unlikely to be important in this model.

The data for Il-6 in metabolic disease is conflicting, with roles in both insulin sensitivity and resistance reported [330]. Previous work has shown an increase in *Il6* expression in response to acute palmitate treatment, but experiments in this chapter demonstrate that chronic palmitate decreased transcription of *Il6* in C2C12 myotubes [253]. Chronic exposure to Il6 increased insulin resistance in cultured myocytes, but acute treatment was associated with increases in glucose uptake, indicating a dual role for Il-6 in glucose homeostasis [331]. Furthermore, exercise increases both insulin sensitivity and circulating levels of Il-6, creating the paradox

of Il-6 in mediating insulin sensitivity and resistance [332–334]. The differences observed here between acute and chronic palmitate treatment in C2C12 cells, as well as between C2C12 and primary human myotubes highlights the complexity of Il-6 signalling in metabolic disease. Much work is required to disentangle the role that Il-6 may play during palmitate-induced lipotoxicity and inflammation.

The interaction between C2C12 myocytes and Raw 264.7 macrophages highlights an interaction between skeletal muscle and the immune system following palmitate exposure. Macrophage polarisation in adipose tissue from obese individuals is also dependent on the activation of a population of natural killer (NK) cells, demonstrating a role for other immune cell classes in insulin resistance [335]. Furthermore, neutrophils are one of the first immune cell types recruited to sites of inflammation, and this infiltration in adipose and liver tissue promotes insulin resistance in mice fed a high fat diet [336]. Future work, could extend studies into the interaction of skeletal muscle with different immune cell populations and the role this interaction may play in the diet-induced inflammation and insulin resistance.

Analysis of ER stress markers in C2C12 myocytes following co-culture with macrophages demonstrated potential bi-directional signalling between the two cell types. Co-culture with macrophages reduced transcription of UPR markers compared to previous experiments, suggesting a role for macrophages in resolving ER stress. This suggests previous experiments focusing on ER stress in myocyte monoculture do not provide a complex enough model for the *in vivo* scenario. These findings also open a therapeutic avenue, with potential treatments harnessing the immune system to relieve stress signalling in peripheral tissues. Further questions may focus on the active macrophage phenotype required to alleviate stress, whether there are any consequences for insulin signalling and glucose uptake, and whether these results translate to other insulin-sensitive tissues such as adipose and the liver.

Conclusion

Here, chronic palmitate increased secretion of lipoxygenase-derived eicosanoid species, a set of bioactive lipids under-investigated in metabolic disease. Pharmacological inhibition suggests a role for lipoxygenase-derived eicosanoids in the control of ER stress and inflammatory signalling in myocytes and co-cultured macrophages.

Chapter 5

Ceramides are cell non-autonomous secreted signals propagating ER stress between myocytes

5.1 Introduction

While a role for palmitate in activating ER stress is well documented, the underlying mechanisms remain poorly understood. A number of putative mechanisms have been suggested, with phospholipid composition thought to play an important role. Knock down of SCD1 in HeLa cells increased the SFA/MUFA ratio in phospholipids, and induced ER stress, while combining palmitate treatment with SCD1-knockdown exacerbated UPR induction [289]. Construction of mutant UPR kinases highlighted that Ire1 and Perk sense alterations in ER membrane composition through their transmembrane domains, which enhance dimerisation and activation of the proteins [337]. Phospholipid composition of the ER in the liver of obese mice was shown to inhibit the sarco/endoplasmic reticulum calcium ATPase (SERCA) pump and induce ER stress [176]. In particular, an increase in the PC/PE ratio in the ER of obese mice impaired calcium homeostasis, and correcting this ratio with shRNA-mediated knockdown of *Pemt*, the enzyme responsible for converting PE to PC, improved calcium handling and ameliorated lipid-induced ER stress.

However, induction of ER stress in the context of metabolic disease is complex, and there is evidence for alternative mechanisms linking saturated fatty acid exposure with the activation of the UPR. Increases in bioactive lipid species, including eicosanoids and ceramides are important for the activation of ER stress. Inhibition of 5-LOX ameliorates palmitate-induced ER stress in C2C12 myotubes, via downregulation of LTB4 levels and AMPK activation [297]. In pancreatic β-cells, palmitate increased synthesis of ceramides, concomitant with the induction of ER stress, while inhibition of ceramide synthesis attenuated palmitate-induced ER stress. [338]. Moreover, siRNA-mediated knockdown of ceramide synthases 5 and 6 suppressed myristate-induced Xbp1 splicing in intestinal epithelial cells [339]. While it is worth noting that an earlier paper demonstrated that increased ceramide production did not mediate

palmitate-induced ER stress in the liver [172], a number of papers have highlighted a causative role for ceramides in insulin resistance, which is integrated strongly with the induction of ER stress [58,74,340–343]. Furthermore, infusing rats with C6-ceramide, a cell-permeable ceramide that is then converted to longer chain ceramides intracellularly, increased ER stress in the hypothalamus [344]. C2-ceramide also increased ER stress in human adenoid cystic carcinoma cells, via the inhibition of the SERCA pump [345].

The mechanisms linking palmitate with the induction of ER stress have focused on the generation of palmitate-derived mediators that function in a cell autonomous manner. However, recent evidence suggests the presence of a non-autonomous secreted signal that can propagate ER stress [146]. Macrophages exposed to conditioned medium from murine prostate tumour cells, chemically-treated with thapsigargin to induce ER stress, increased levels of UPR markers, demonstrating the ability for tumour-derived signals to propagate ER stress signalling to separate cell types [147]. Indeed, a similar response is seen in the Raw 264.7 macrophages co-cultured with C2C12 cells in Chapter 4.

This phenomenon has also been reported *in vivo*, with constitutive activation of spliced Xbp1 in pro-opiomelanocortin (*Pomc*) neurons reducing diet-induced adiposity and insulin resistance, concomitant with induction of ER stress in the liver [150]. This work demonstrated that cell non-autonomous propagation of ER stress can have profound effects on metabolic phenotypes and glucose homeostasis. However, the identity of the cell non-autonomous ER stress propagating signals remain unknown. The discovery of ER stress propagating signals could have a large impact on our understanding of the fundamental biological process of ER stress and further elucidate its role in metabolic disease.

5.2 Aims and Objectives

The aim of this chapter was to assess the role cell non-autonomous signalling may play in ER stress propagation following palmitate exposure. The following set of objectives were designed to achieve this:

1) Identify the presence and nature of a paracrine ER stress signal, aided by LC-MS profiling of culture media to produce a list of candidate signals.
2) Assay candidate signals with RT-qPCR of a UPR gene panel.
3) Recapitulate the results in primary HSkMCs and *in vivo* models of metabolic disease.

5.3 Materials and Methods

5.3.1 C2C12 culture

C2C12 cells were cultured as described in **Chapter 2 Materials and Methods** (Section 2.1.1 *C2C12 myoblast culture and differentiation*)**.** Cells were differentiated and treated in collagen I-coated 12-well plates.

5.3.2 Primary human skeletal muscle cell culture

Primary human skeletal muscle cells (HSkMCs) were cultured as described in **Chapter 2 Materials and Methods** (Section 2.1.2 *Primary human skeletal muscle cell culture and differentiation*). Cells were treated in collagen I-coated 12-well plates.

5.3.3 Production of conditioned media and conditioned media transfer experimentation

Myocytes were treated with 200 μM palmitate or the BSA vehicle during 6 days of differentiation. At the end of this period culture media was switched to serum-free media, free from any agonists, for 24 hours, allowing for the accumulation of secreted factors from the myocytes. This conditioned media was then transferred on to untreated myocytes for 10 hours.

5.3.4 Boiling protocol

Conditioned media was submerged in a water bath set to 100 ºC for 5 minutes. Media was then allowed to cool, before transfer on to untreated myocytes.

5.3.5 Conjugation of palmitate to BSA

Palmitate was bound to BSA following the protocol summarised in **Chapter 2 Materials and Methods** (2.1.3 *Conjugation of palmitate to BSA*)**.**

5.3.6 Cell harvesting

Cells were harvested and pelleted as described in **Chapter 2 Materials and Methods** (section 2.1.4 *Cell harvesting*). Cell counts were performed using a Scepter automated cell counter (Millipore).

5.3.7 Animal studies

The detail of three mouse studies analysed in this chapter are summarised in **Chapter 2 Materials and Methods** (Section 2.2 *Animal studies*)**.**

5.3.8 Human skeletal muscle biopsies

Biopsies of *pectoralis major* were taken from volunteers undergoing pacemaker therapy, as described in **Chapter 2 Materials and Methods** (Section 2.3 *Human skeletal muscle biopsies*)**.**

5.3.9 RNA isolation and purification

RNA was extracted and purified from cells using an RNeasy Mini kit (Qiagen), as outlined in **Chapter 2 Materials and Methods** (Section 2.4.1 *RNA isolation and purification*)**.**

5.3.10 cDNA synthesis

RNA concentrations were standardised and cDNA then synthesised using a RT^2 First Strand kit (Qiagen), following manufacturer's instructions as set out in **Chapter 2 Materials and Methods** (Section 2.4.2 *cDNA synthesis*)**.**

5.3.11 Reverse transcription quantitative polymerase chain reaction

Transcript levels were analysed using the StepOnePlus Real-Time PCR system, as described in **Chapter 2 Materials and Methods** (Section 2.4.3 *Reverse transcription quantitative polymerase chain reaction*)**.**

5.3.12 Metabolite extraction from cells

Metabolites were extracted from cells using a modified Bligh and Dyer method, described in **Chapter 2 Materials and Methods** (Section 2.5.1 *Cell metabolite extraction for mass spectrometry*)**.**

5.3.13 Metabolite extraction from skeletal muscle tissue

Tissue was first homogenised using a TissueLyser (Qiagen), and metabolites were then extracted using a Bligh and Dyer extraction, outlined in **Chapter 2 Materials and Methods** (Section 2.5.2 *Human and mouse skeletal muscle tissue extraction*)**.**

5.3.14 Metabolite extraction from plasma

600 µL of methanol/chloroform (2:1) was added to 20 µL of plasma, followed by 200 µL of water and 200 µL of chloroform. Samples were vortexed and centrifuged (16,100*g*, 20 minutes). The organic layer was separated and dried under nitrogen gas prior to storage at -80 ºC.

5.3.15 Metabolite extraction from media

One mL of serum-free cell culture media was collected. 800 µL of methanol/chloroform (1:1) was added to each sample and mixed well by vortexing. Samples were centrifuged (16,100*g*, 20 minutes), and the organic layer subsequently separated and dried down under nitrogen gas. Dried samples were stored at -80 ºC.

5.3.16 Liquid chromatography-mass spectrometry analysis of lipids

The dried-down organic fraction was dissolved in 50 µl methanol/chloroform (1:1), and diluted into 190 µl IPA/ACN/H_2O (2:1:1). Samples were then analysed using an Orbitrap Elite mass spectrometer, as described in **Chapter 2 Materials and Methods** (Section 2.6 *Liquid chromatography-mass spectrometry open profiling of lipids*)**.** Chromatogram files were converted using MSConvert (Proteowizard), and processed using XCMS within an R

script. Peaks were normalised to a relevant internal standard and then either cell number, for *in vitro* experiments, or dry protein pellet weight, for the analysis of skeletal muscle tissue.

5.3.17 Statistics

Statistical significance was assessed using either a one-way ANOVA with Tukey's multiple comparisons test, a two-way ANOVA with Sidak's multiple comparisons test or Student's t-test, as detailed in each figure. Linear regression was used to analyse human skeletal muscle biopsies for correlations between phospholipids and BMI. In each case, $n \geq 3$ and the significance level was set to $P \leq 0.05$. All univariate analysis was conducted using GraphPad (version 6) software.

5.4 Results

5.4.1 Conditioned media transfer induces ER stress in C2C12 cells

Recent work has highlighted a role for paracrine and endocrine signalling in the propagation of ER stress [146]. Manipulating the paracrine and endocrine intercellular communication of ER stress could represent a novel therapeutic approach. However, the identity of these signals and the mechanisms through which they operate are not known. To investigate the potential of paracrine signalling in palmitate-induced ER stress, C2C12 myotubes were treated with 200 μM palmitate or the BSA vehicle for 6 days during differentiation. The media was then changed to serum-free and palmitate-free media for 24 hours, allowing any secreted signals to accumulate in the media. This conditioned media was then collected and transferred to naïve C2C12 myotubes for 10 hours. RNA was then extracted and analysed by RT-qPCR to assess UPR induction. Conditioned media from palmitate treated cells significantly increased the expression of *Atf4* (3.4-fold), *Edem1* (2-fold) and *Hspa5* (1.3-fold), indicating activation of the UPR, although expression of Atf3 was unaffected (**Figure 5.1**). This data suggests the presence of a paracrine signal released from myocytes capable of transmitting ER stress.

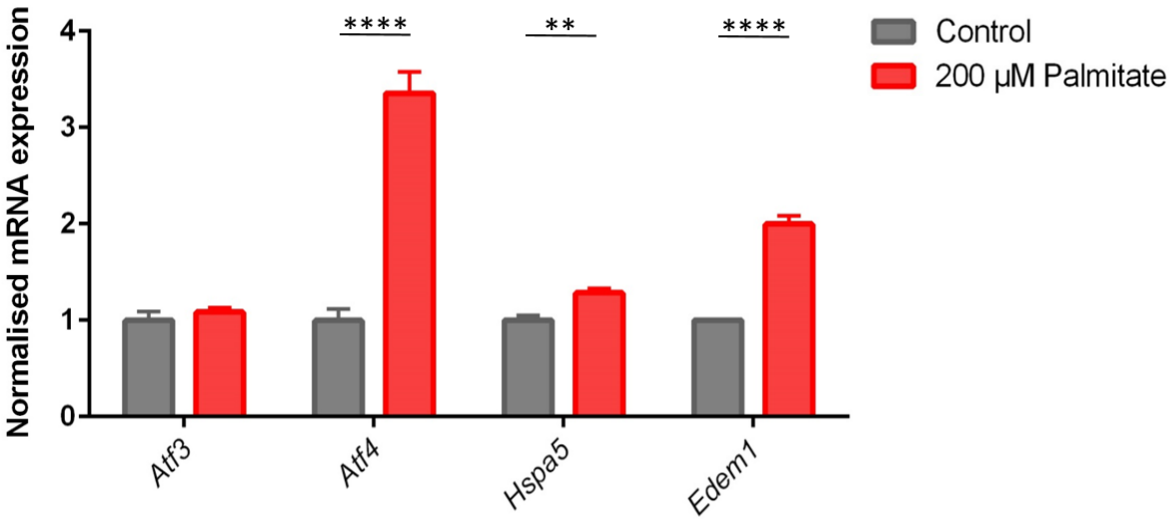

Figure 5.1: Conditioned media from palmitate-treated C2C12 myotubes induces ER stress in untreated myotubes

C2C12 cells were treated with 200 µM palmitate or the BSA vehicle control during a 6-day differentiation period. Subsequently, media was switched to serum-free media for 24 hours, allowing for the accumulation of secreted factors. This conditioned media was then transferred to untreated myotubes for 10 hours and RT-qPCR was used to analyse the expression of key unfolded protein response genes (*Atf3, Atf4, Hspa5* and *Edem1*). Each gene was analysed using a Student's t-test. * $P \leq 0.05$, ** $P < 0.01$, *** $P < 0.001$, **** $P < 0.0001$. Data are expressed as mean ± SEM (n = 4).

To define the nature of this signal, conditioned media from palmitate- or vehicle-treated C2C12 myotubes was boiled for 5 minutes to denature proteins in the media prior to transfer to untreated cells. RT-qPCR analysis of UPR gene expression showed that conditioned media from cells treated with 200 µM palmitate increased expression of *Atf4* (3-fold) and *Edem1* (2.5-fold) as before (**Figure 5.2**). Similarly, conditioned media from palmitate treated cells that was subjected to boiling also increased expression of *Atf4* (2.9-fold) and *Edem1* (2.4-fold) compared to cells treated with boiled conditioned media from control treated cells. As boiling of conditioned media did not ablate the induction of ER stress, the paracrine signal is likely a small molecule and non-protein.

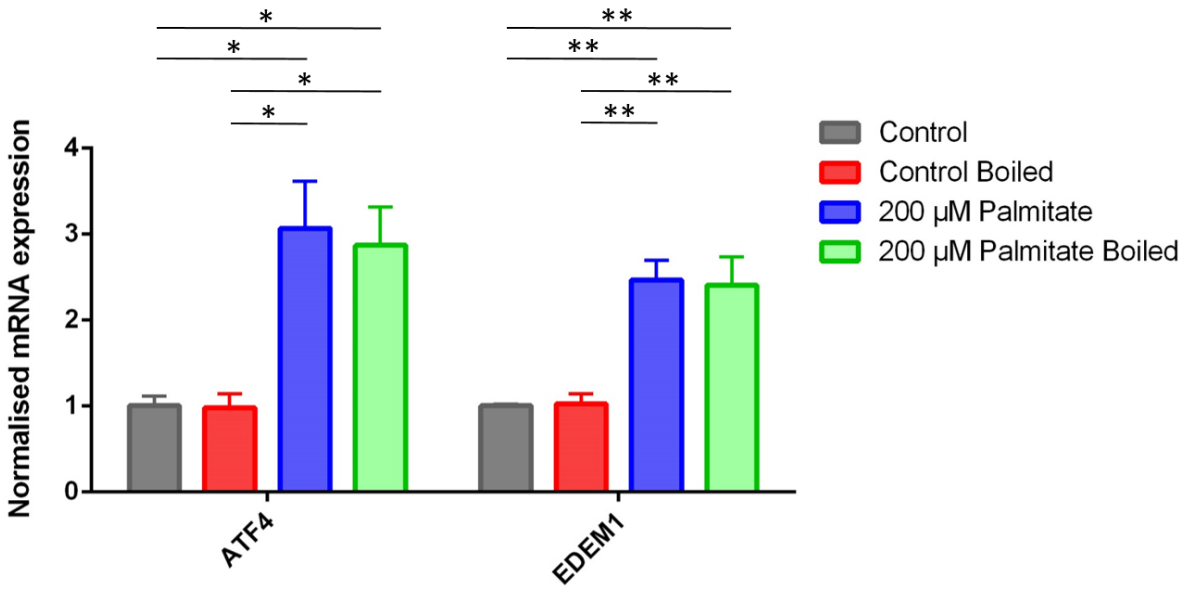

Figure 5.2: Boiling of conditioned media does not ablate the induction of endoplasmic reticulum stress

C2C12 cells were treated with 200 µM palmitate or the BSA vehicle control during a 6-day differentiation period. Subsequently, media was switched to serum-free media for 24 hours, allowing for the accumulation of secreted factors. Conditioned media was harvested and left either at room temperature or boiled for five minutes. This conditioned media was then transferred to untreated myotubes for 10 hours and RT-qPCR was used to analyse the expression of key unfolded protein response genes (*Atf4* and *Edem1*). Each gene was analysed using a one-way ANOVA test with Tukey's multiple comparison test. * $P \leq 0.05$, ** $P < 0.01$, *** $P < 0.001$, **** $P < 0.0001$. Data are expressed as mean ± SEM (n = 3).

5.4.2 Liquid chromatography-mass spectrometry profiling of conditioned media

Previous literature has demonstrated palmitate-induced secretion of a number of lipid species, including triacylglycerols, ceramides and sphingosine-1-phosphate, which may represent potential signals [346–348]. To identify putative signals in the organic fraction, C2C12 myotubes were treated with either 100 or 200 µM palmitate, or the BSA vehicle, for 6 days during differentiation. Culture medium was then switched to serum-free media, free from palmitate and BSA, for 24 hours. Conditioned media was harvested and extracted using a modified Bligh and Dyer method, and the organic fraction was analysed using LC-MS. Approximately 300 lipid species, including lysophosphatidylcholines, ceramides, phosphatidylcholines, diacylglycerides and triacylglycerides, were detected in positive and negative ion mode. Peak intensities were normalised to an internal standard of relevant lipid class.

Analysis of free fatty acids showed concentrations of palmitate in conditioned media were unchanged across the three treatment groups (**Figure 5.3**). This indicates that the increase in transcription of ER stress markers following conditioned media transfer from palmitate-treated cells is independent of the fatty acid.

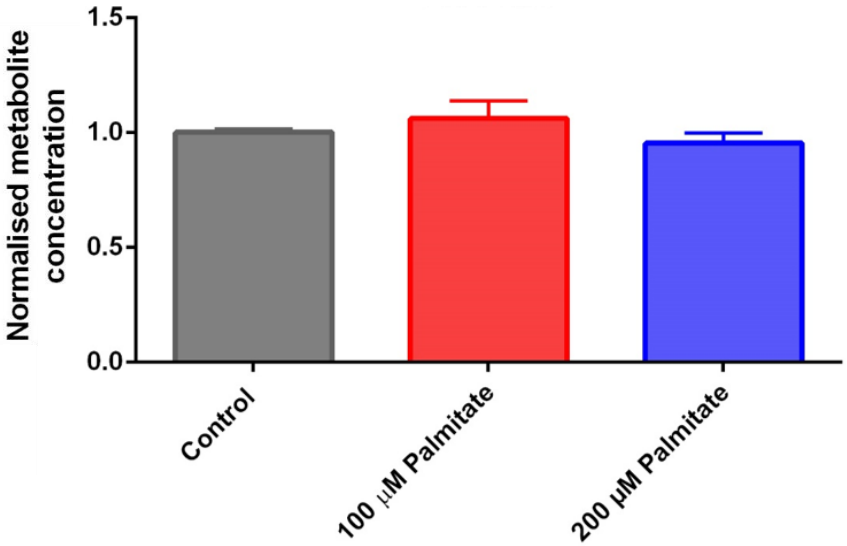

Figure 5.3: Palmitate concentrations are unchanged in conditioned media

Conditioned media was collected from C2C12 myotubes treated with either 100 or 200 µM palmitate, or the BSA vehicle control. Metabolites were extracted from the media and analysis of the organic phase by LC-MS shows free palmitate concentrations were unchanged between the three treatment groups. Palmitate was analysed using a one-way ANOVA test with Tukey's multiple comparison test. * $P \leq 0.05$, ** $P < 0.01$, *** $P < 0.001$, **** $P < 0.0001$. Data are expressed as mean ± SEM (n = 4).

However, concentrations of a number of other lipid species were increased in conditioned media collected from myotubes treated with palmitate, representing potential ER stress propagating signals. The list of potential signals was narrowed based on the literature; lipids with documented bioactivity in cell signalling were investigated further to assess any potential in activating ER stress. Lysophosphatidylcholines (LPCs) are produced from phospholipids following hydrolysis of the *sn2* fatty acid by phospholipase enzymes. Previous literature has suggested a potential bioactive role for these metabolites [349,350]. Here, treatment of C2C12 myotubes with 200 µM of palmitate increased the secretion of LPC 16:0, 16:1 and 18:0 (**Figurer 5.4A**).

Palmitate treatment also increased the secretion of diacylglycerol (DG) and ceramide species. Both classes of lipid are important in mediating saturated fatty acid-induced insulin resistance

in peripheral tissues including skeletal muscle, adipose and the liver [40]. Saturated and monounsaturated DG species were all increased following exposure to 200 µM palmitate, with DG 32:0, 34:1, and 36:1 approximately 5-fold higher in the treatment group (**Figure 5.4B**).

Ceramides have previously been shown to mediate palmitate-induced insulin resistance [40]. Ceramide 34:1, 40:1 and 42:1 all accumulated in the media of palmitate-treated myotubes, with the increase in ceramide 40:1 dose-dependent (**Figure 5.4C**).

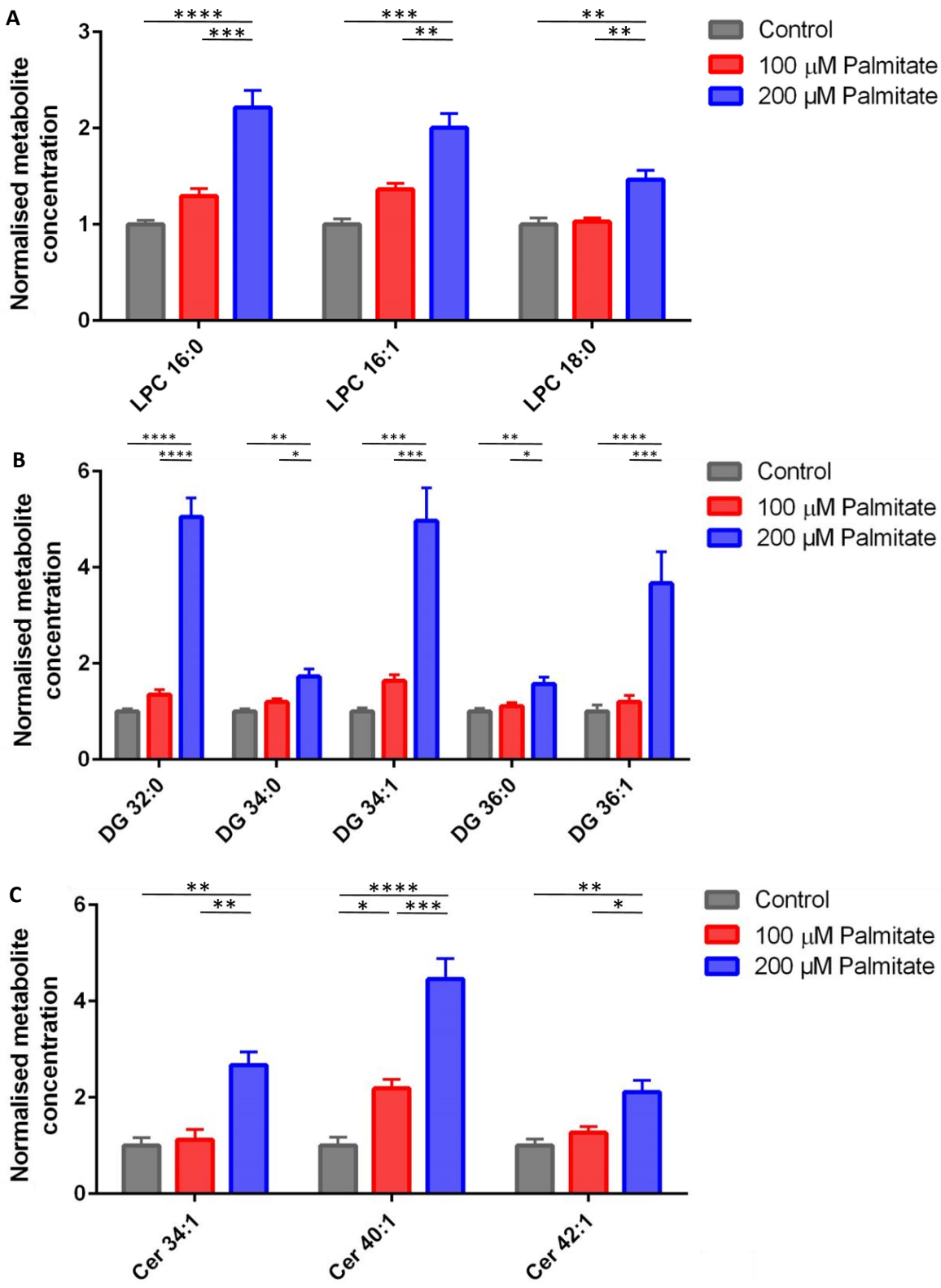

Figure 5.4: Chronic palmitate treatment of myotubes increases concentrations of lysophosphatidylcholines, diacylglycerides and ceramides in conditioned media

Conditioned media was collected from C2C12 myotubes treated with either 100 or 200 µM palmitate, or the BSA vehicle control. Metabolites were extracted from the media and analysis of the organic phase by LC-MS shows increases in (A) lysophosphatidylcholines, (B) diacylglycerides and (C) ceramides following chronic palmitate treatment. Species were analysed using a one-way ANOVA test with Tukey's multiple comparison test. * $P \leq 0.05$, ** $P < 0.01$, *** $P < 0.001$, **** $P < 0.0001$. Data are expressed as mean ± SEM (n = 4).

5.4.3 Exogenous ceramides induce ER stress

To identify potential signals from the candidate lipid species, the ability of ceramides 40:1 (C22) and 42:1 (C24), DG 16:0/16:0, and LPCs 16:0 and 18:0 to induce ER stress in C2C12 myotubes was investigated. Myotubes were grown to confluence and differentiated for 6 days. For the final 10 hours, cells were exposed to two concentrations of each candidate, or the vehicle control. RNA was harvested and the transcription of *Atf4* and *Edem1* were analysed by RT-qPCR. A reduced panel of genes was used to assay the effects of potential signalling candidates to increase throughput for each test. Treatment of cells with DG 32:0 had no effect on the expression of UPR markers compared to myotubes treated with the ethanol vehicle control (**Figure 5.5A**). Similarly, LPC 16:0 did not induce ER stress, compared to cells cultured with the saline vehicle control (**Figure 5.5B**). However, both 5 and 50 µM of LPC 18:0 did increase the expression of *Edem1* (1.4-fold and 1.3-fold, respectively), suggesting that LPC 18:0 may be a potential ER stress propagating signal (**Figure 5.5C**). However, the expression of *Atf4* was unchanged despite conditioned media increasing transcript levels of *Atf4* 3.4-fold. Furthermore, the increase in expression of *Edem1* following treatment with LPC 18:0 was much smaller than that induced by conditioned media transfer. Together, this suggests the presence of other signals.

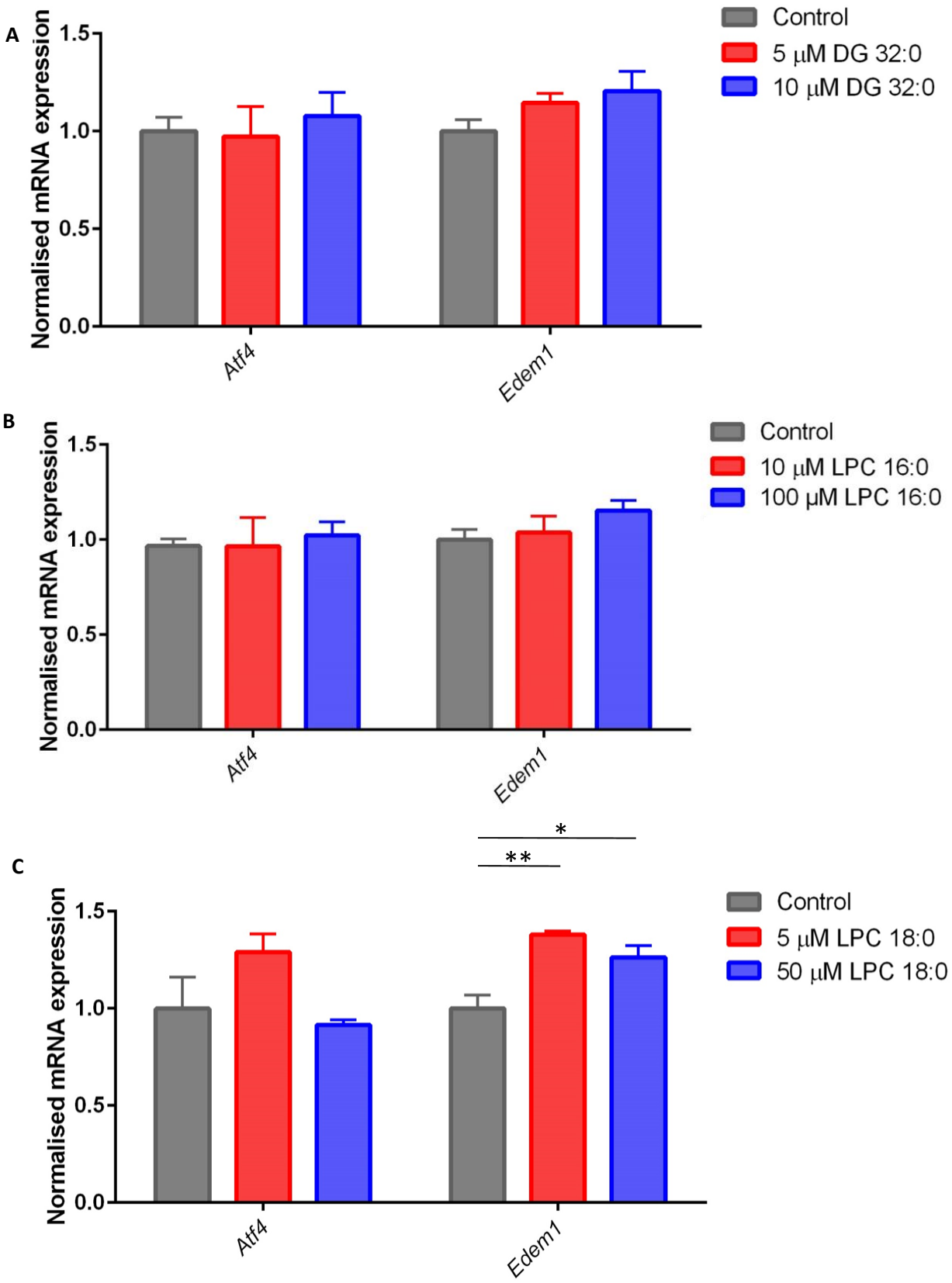

Figure 5.5: Lysophosphatidylcholine 18:0 increases the expression of *Edem1*

C2C12 myotubes were differentiated for six days and then treated for 10 hours with either (A) diacylglyceride (DG) 16:0/16:0, (B) lysophosphatidylcholine (LPC) 16:0, or (C) LPC 18:0. Induction of ER stress was assessed by RT-qPCR of a reduced panel of unfolded protein response genes (*Atf4* and *Edem1*). Species were analysed using a one-way ANOVA test with Tukey's multiple comparison test. * $P \leq 0.05$, ** $P < 0.01$, *** $P < 0.001$, **** $P < 0.0001$. Data are expressed as mean ± SEM (n = 4).

Treatment with C22 ceramide increased transcription of *Atf4* in a dose-dependent manner, compared to myotubes treated with the ethanol vehicle control (**Figure 5.6A**). Both 5 and 10 μM C24 ceramide also increased expression of *Atf4*, although transcription of *Edem1* was unaffected with both ceramide treatments (**Figure 5.6B**). These data suggest exogenous treatment of myotubes with ceramides C22 and C24 may increase the induction of ER stress. However, while some chemical distributors suggest solubility of ceramide in ethanol, some publications have opted for a ethanol/dodecane (98:2) vehicle, which may improve the solubility of ceramides [351].

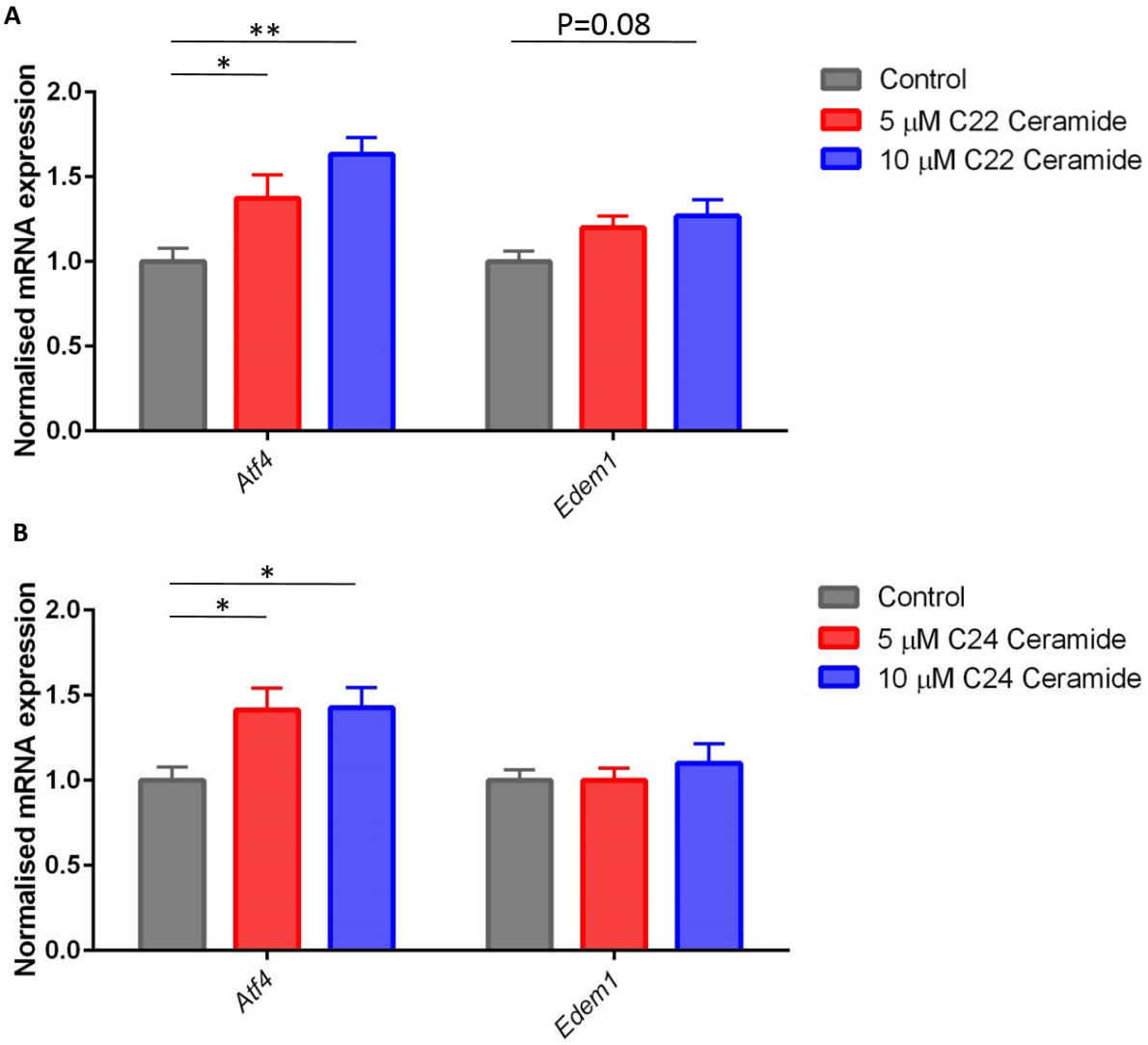

Figure 5.6: Long chain ceramides increase the expression of *Atf4*

C2C12 myotubes were differentiated for six days and then treated for 10 hours with either (A) C22 ceramide (ceramide 40:1) or (B) C24 ceramide (ceramide 42:1). Induction of ER stress was assessed by RT-qPCR of a reduced panel of unfolded protein response genes (*Atf4* and *Edem1*). Species were analysed using a one-way ANOVA test with Tukey's multiple comparison test. * $P \leq 0.05$, ** $P < 0.01$, *** $P < 0.001$, **** $P < 0.0001$. Data are expressed as mean ± SEM (n=4).

To test if an ethanol/dodecane vehicle improved sensitivity to ceramide induced ER stress, C2C12 myoblasts were differentiated for 6 days with either 10 μM C22 ceramide, 10 μM C24 ceramide, or the ethanol/dodecane (98:2) vehicle control treatment for the final 10 hours. RNA was harvested and the induction of UPR target genes was assessed using RT-qPCR. C24 ceramide increased the expression of *Atf4* (2.9-fold) and *Hspa5* (1.5-fold), while C22 ceramide also increased expression of *Hspa5* (1.6-fold) (**Figure 5.7**). Expression of *Atf3* and *Edem1* were unaffected with ceramide treatment. These data suggest that treatment with individual ceramides increase the expression of key markers of ER stress.

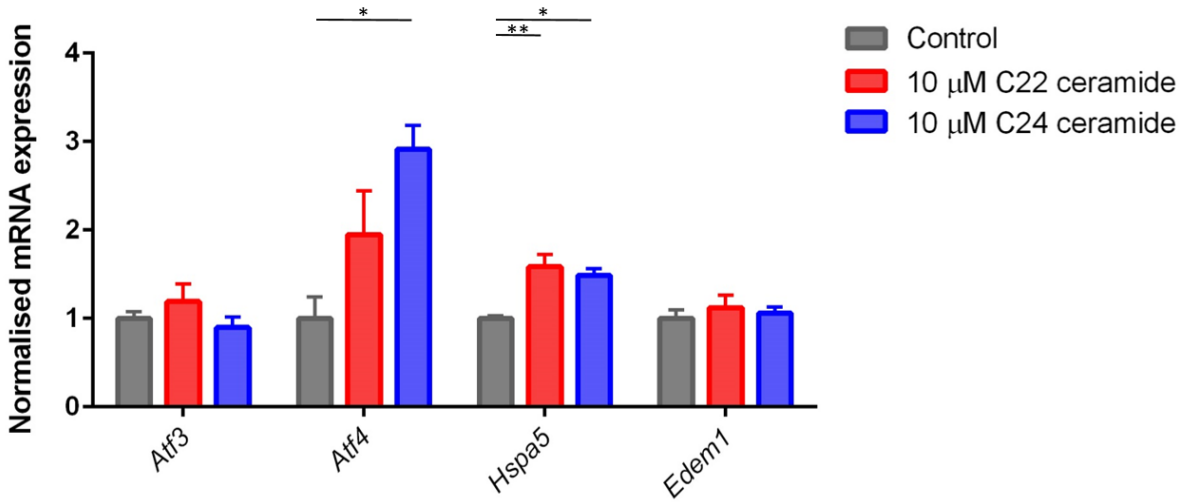

Figure 5.7: An ethanol/dodecane vehicle enhances sensitivity to ceramide-induced increases in *Atf4* expression

C2C12 myotubes were differentiated for six days and then treated for 10 hours with either 10 μM C22 ceramide (ceramide 40:1) or 10 μM C24 ceramide (ceramide 42:1), dissolved in ethanol/dodecane (98:2). Induction of ER stress was assessed by RT-qPCR of a panel of unfolded protein response genes (*Atf3, Atf4, Hspa5* and *Edem1*). Species were analysed using a one-way ANOVA test with Tukey's multiple comparison test. * $P \leq 0.05$, ** $P < 0.01$, *** $P < 0.001$, **** $P < 0.0001$. Data are expressed as mean ± SEM (n = 3).

However, LC-MS analysis of cell culture media demonstrated concomitant increases in a number of ceramides. Thus, multiple ceramide species may act in an additive or synergistic manner to increase the expression of UPR genes. Therefore, the effect of combined ceramide treatment on the induction of ER stress was investigated. C2C12 myotubes were differentiated for 6 days, as before. For the final 10 hours, myotubes were treated with a combination of 10 μM C22 ceramide and 10 μM C24 ceramide, or the ethanol/dodecane (98:2) vehicle control. RNA was harvested and the induction of ER stress was assessed using RT-qPCR. Ceramide treatment increased the expression of *Atf4* (3.2-fold) and *Hspa5* (1.4-

fold) and *Edem1*, while *Atf3* narrowly missed out on significance (p=0.06) (**Figure 5.8**). This suggests that combined treatment with ceramides 22 and 24 can increase the expression of UPR target genes.

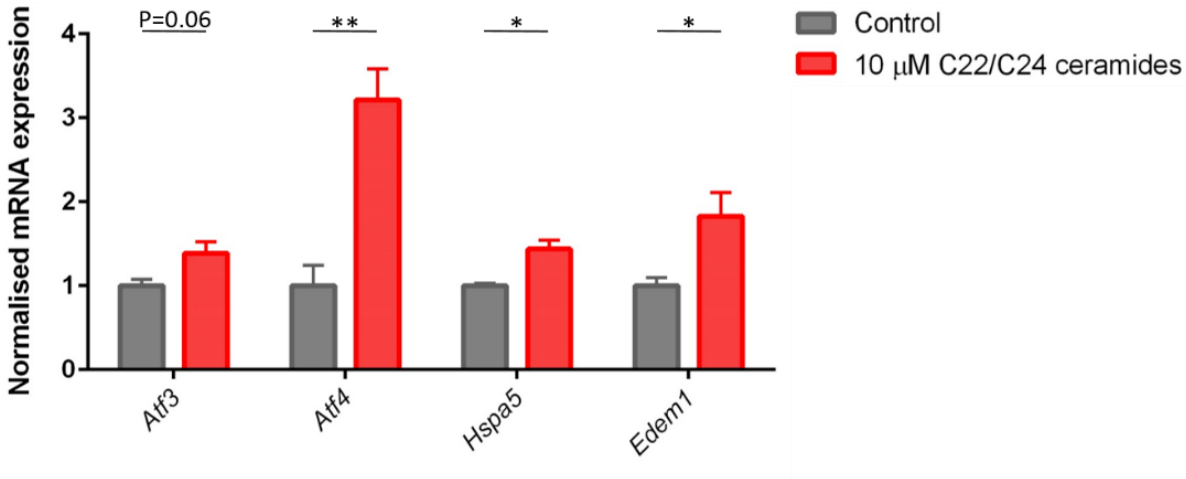

Figure 5.8: Combined long chain ceramide treatment induces endoplasmic reticulum stress

C2C12 myotubes were differentiated for six days and then treated for 10 hours with a combination of 10 μM C22 ceramide (ceramide 40:1) and 10 μM C24 ceramide (ceramide 42:1), dissolved in ethanol/dodecane (98:2). Induction of ER stress was assessed by RT-qPCR of a panel of unfolded protein response genes (*Atf3*, *Atf4*, *Hspa5* and *Edem1*). Species were analysed using a Student's t-test. * $P \leq 0.05$, ** $P < 0.01$, *** $P < 0.001$, **** $P < 0.0001$. Data are expressed as mean ± SEM (n = 3).

Whether the induction of ER stress was dependent on the acyl chain-length of the ceramide species was investigated. Differentiated C2C12 myotubes were treated with medium chain length ceramide species 10 μM C16 (ceramide 34:1) or 10 μM C18 (ceramide 36:1), or the ethanol:dodecane (98:2) vehicle control. RNA was harvested and the expression of UPR target genes was assessed using RT-qPCR. While C16 ceramide only increased the expression of *Atf4* (1.6-fold), C18 ceramide elevated transcription of *Atf4* (2.1-fold), *Hspa5* (1.7-fold) and *Edem1* (1.6-fold) (**Figure 5.9**). Therefore, ceramide-induced ER stress is not restricted to signalling from individual species but is conserved across long and medium chain acyl chain-containing species.

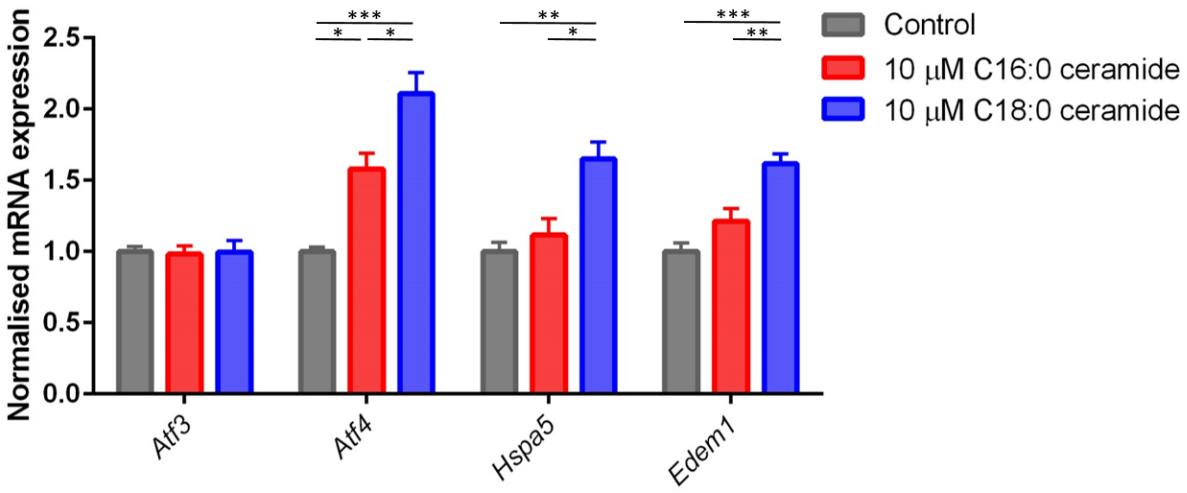

Figure 5.9: Exogenous treatment with medium length acyl chain-containing ceramides induces endoplasmic reticulum stress

C2C12 myotubes were differentiated for six days and then treated for 10 hours with either 10 μM C16 ceramide (ceramide 34:1) or 10 μM C18 ceramide (ceramide 36:1), dissolved in ethanol/dodecane (98:2). Induction of ER stress was assessed by RT-qPCR of a panel of unfolded protein response genes (*Atf3*, *Atf4*, *Hspa5* and *Edem1*). Species were analysed using a one-way ANOVA test with Tukey's multiple comparison test. * $P \leq 0.05$, ** $P < 0.01$, *** $P < 0.001$, **** $P < 0.0001$. Data are expressed as mean ± SEM (n = 4).

5.4.4 Long chain ceramide induced ER stress is conserved in primary human skeletal muscle cells

To understand if the effects of long chain ceramides on ER stress translate to human disease, experiments were repeated in primary HSkMCs. HSkMCs were grown to confluence and treated with 100 μM palmitate, or the BSA vehicle control, during a 6-day differentiation period. Culture media was then switched to basal media for 24 hours to allow for the accumulation of secreted factors. Subsequently, conditioned media was transferred on to untreated primary HSkMCs for 10 hours. RNA was then harvested and the induction of ER stress assessed using RT-qPCR. Conditioned media from palmitate treated-HSkMCs increased expression of *Atf3* (1.8-fold), *Atf4* (1.7-fold) and *Hspa5* (1.7-fold), compared to cells exposed to conditioned media from vehicle-treated control cells, although *Edem1* expression was unchanged (**Figure 5.10**). These results show that primary HSkMCs also secrete an ER stress propagating signal or signals.

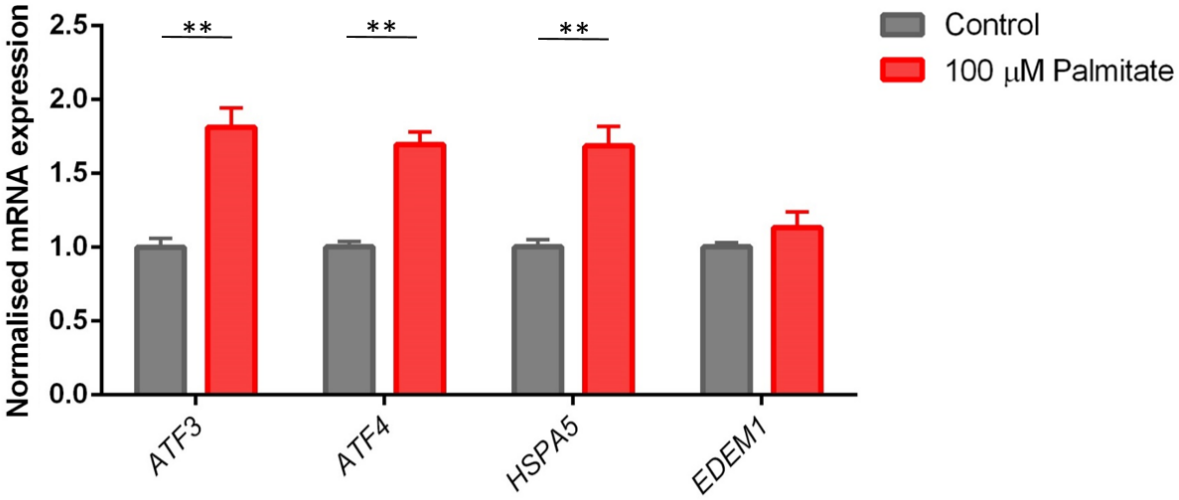

Figure 5.10: Conditioned media from palmitate-treated primary human myocytes increases endoplasmic reticulum stress in untreated myocytes

Primary human skeletal muscle cells (HSkMCs) were treated with 200 µM palmitate or the BSA vehicle during a 6-day differentiation period. Media was switched to basal media for 24 hours and this conditioned media was then transferred on to untreated HSkMCs for 10 hours. Induction of ER stress was assessed by RT-qPCR of a panel of unfolded protein response genes (*ATF3*, *ATF4*, *HSPA5* and *EDEM1*). Species were analysed using a Student's t-test. * $P \leq 0.05$, ** $P < 0.01$, *** $P < 0.001$, **** $P < 0.0001$. Data are expressed as mean ± SEM (n = 4).

To investigate the role long-chain ceramides may play in paracrine stress signalling in primary HSkMCs, conditioned media from HSkMCs treated for 6 days with either 50 or 100 µM palmitate, or the BSA vehicle control, were analysed by LC-MS. The palmitate-induced secretion of ceramides 34:1, 40:1 and 42:1 in a dose-dependent manner, observed in C2C12 myotubes, was conserved in HSkMCs. Therefore, the ceramides may act as paracrine signals in primary HSkMCs (**Figure 5.11A**).

To confirm that exogenous treatment of primary HSkMCs with long-chain ceramides can induce ER stress, HSkMCs were grown to confluence and differentiated for 6 days. Myocytes were then treated with either 10 µM C22 ceramide (40:1), 10 µM C24 ceramide, a combination of the both, or the ethanol/dodecane (98:2) vehicle control, for 10 hours. RNA was harvested and the transcription of UPR markers analysed by RT-qPCR. Combined treatment with C22 and C24 ceramide increased expression of *ATF3* (2.5-fold), *ATF4* (1.7-fold) and *EDEM1* (2-fold), relative to cells exposed to the vehicle control, although *HSPA5* expression was only increased with C22 ceramide treatment (2.6-fold) (**Figure 5.11B**). These results highlight that long chain ceramides are potential cell non-autonomous ER stress propagating signals.

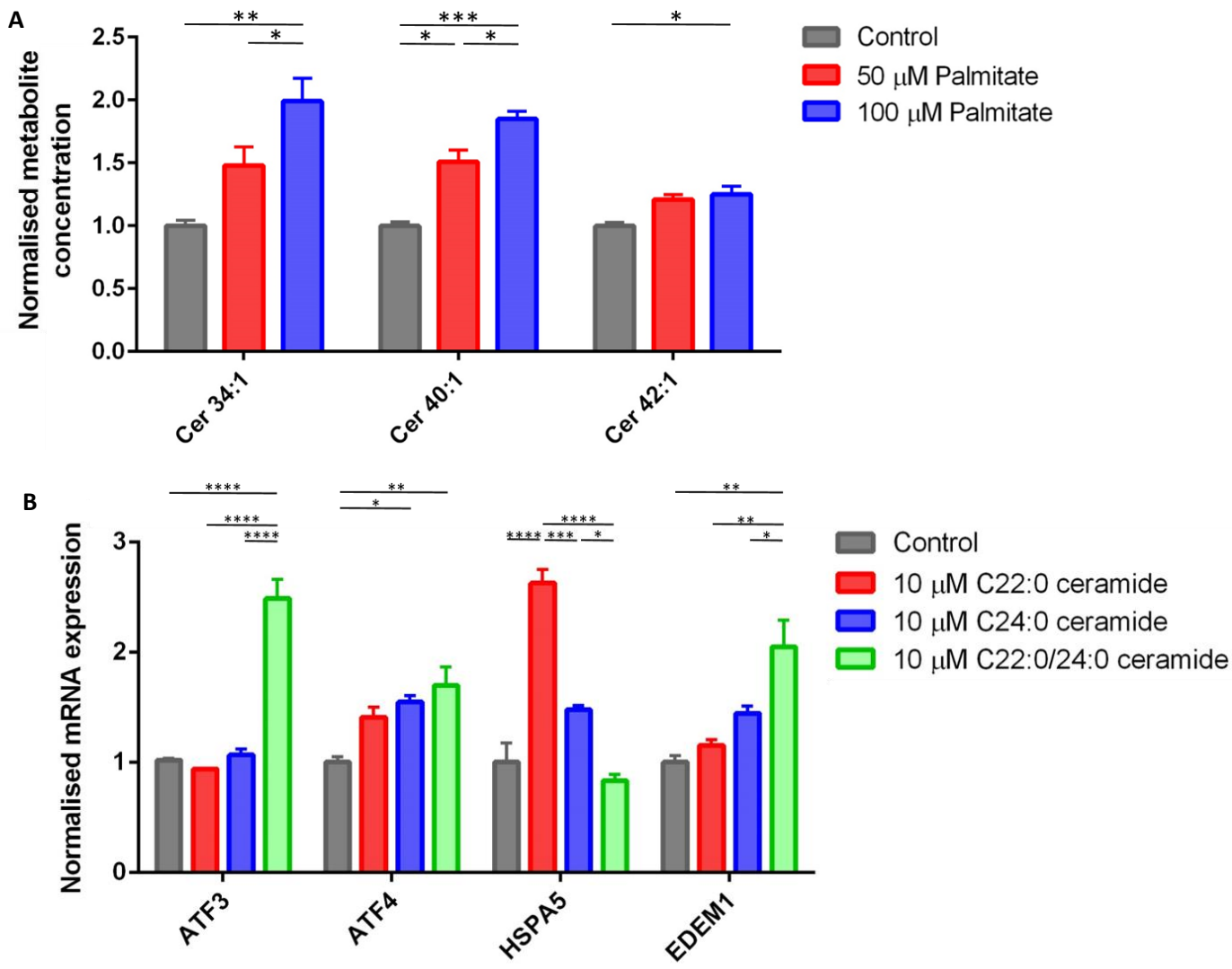

Figure 5.11: Long chain ceramides increase endoplasmic reticulum stress in primary human skeletal muscle cells

(A) Primary human skeletal muscle cells (HSkMCs) were treated with 200 µM palmitate or the BSA vehicle during a 6-day differentiation period. Media was switched to basal media for 24 hours and metabolites were subsequently extracted from conditioned media. Liquid chromatography-mass spectrometry analysis of the organic phase shows chronic palmitate treatment increases media ceramide concentrations. (B) Treatment of differentiated HSkMCs with either 10 µM C22:0 ceramide, 10 µM C24:0 ceramide, a combination of both, or the vehicle control. Induction of ER stress was assessed by RT-qPCR of a panel of unfolded protein response genes (*ATF3, ATF4*, *HSPA5* and *EDEM1*). Species were analysed using a one-way ANOVA test with Tukey's multiple comparison test. * $P \leq 0.05$, ** $P < 0.01$, *** $P < 0.001$, **** $P < 0.0001$. Data are expressed as mean ± SEM ((A) n = 4, (B) n = 3).

5.4.5 Palmitate increases intracellular concentrations of ceramides

With the identification of ceramides as potential paracrine signals, subsequent experiments sought to investigate if the palmitate-stimulated secretion of ceramides was a result of increased intracellular synthesis. C2C12 myotubes were grown to confluence and differentiated for 6 days. During this period, cells were treated with either 100 or 200 µM palmitate, or the BSA vehicle control. Cells were then harvested and metabolites extracted using a modified Bligh and Dyer method. The organic phase was analysed using LC-MS. Peaks were annotated based on accurate mass and intensities were normalised to a relevant internal standard and cell number. Myotubes treated with 200 µM palmitate had increased concentrations of ceramides 34:1, 40:1 and 42:1, while 100 µM palmitate also increased concentrations of ceramide 34:1 relative to control treated cells (**Figure 5.12A**).

These results were also confirmed in primary HSkMCs. Human myocytes were grown to confluence and differentiated for 6 days. During this period, cells were exposed to either 50 or 100 µM palmitate, or the BSA vehicle control. Metabolites were extracted from cell pellets using a modified Bligh and Dyer extraction, and the organic phase was analysed by LC-MS. Annotated peaks were normalised to a relevant internal standard and cell number. Ceramides 34:1 and 42:1 were increased with 100 µM palmitate treatment, while ceramide 40:1 was increased in a dose-dependent manner (**Figure 5.12B**). Together, these results show that treating myocytes chronically with palmitate increases ceramide synthesis as well as secretion.

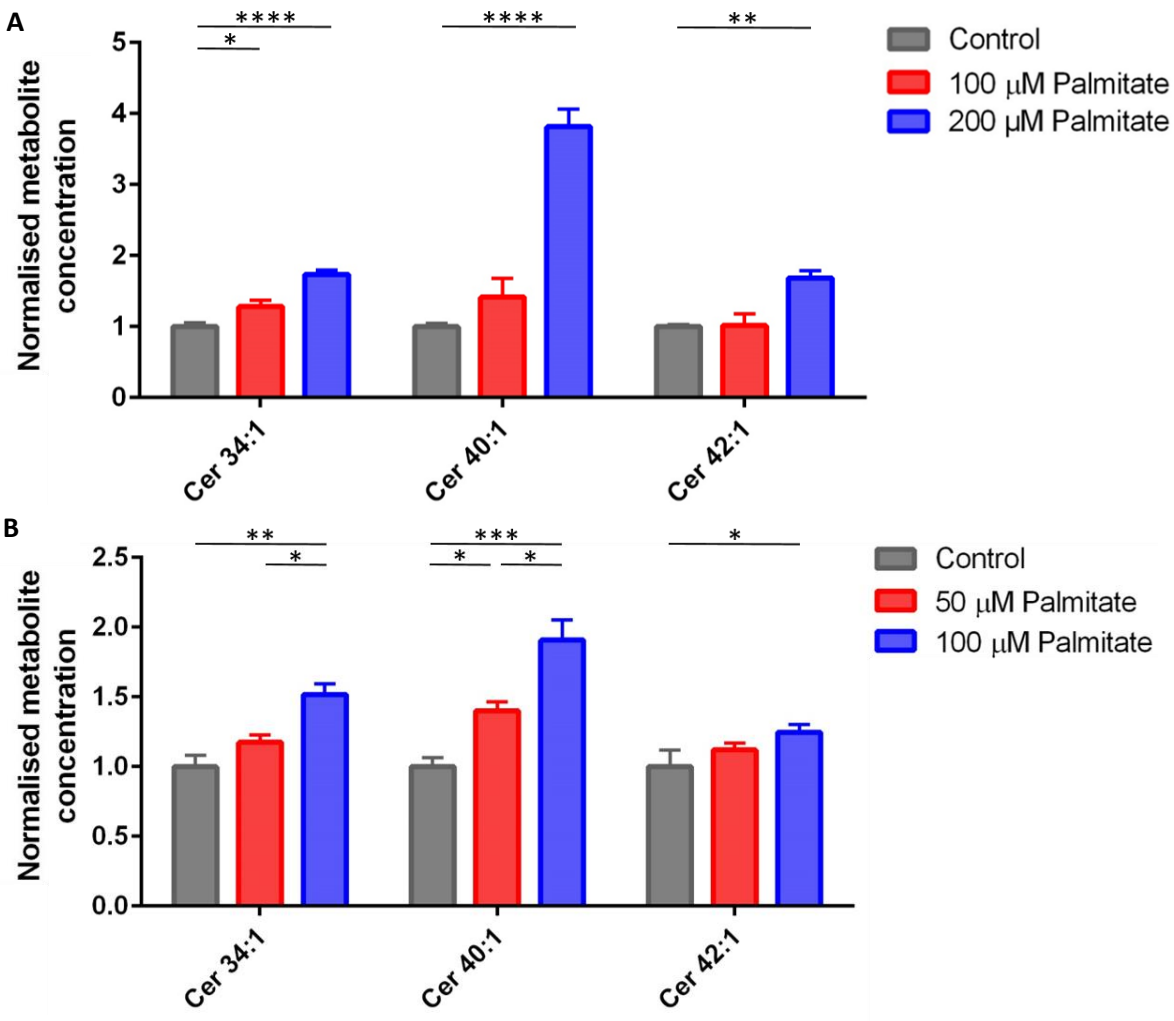

Figure 5.12: Chronic palmitate treatment increases intracellular ceramide concentrations in skeletal myocytes

(A) C2C12 myotubes were treated with either 100 or 200 µM palmitate, or the vehicle control during a 6-day differentiation period. Metabolites were extracted from cells and ceramides were analysed by liquid chromatography-mass spectrometry (LC-MS). (B) LC-MS analysis of primary human skeletal muscle cells following treatment with either 50 or 100 µM palmitate, or the vehicle control, during 6 days of differentiation. Species were analysed using a one-way ANOVA test with Tukey's multiple comparison test. * $P \leq 0.05$, ** $P < 0.01$, *** $P < 0.001$, **** $P < 0.0001$. Data are expressed as mean ± SEM (n=4).

5.4.6 Ceramide concentrations in the plasma and skeletal muscle of mice fed a high fat diet

Following the demonstration that secreted ceramides can propagate intercellular palmitate-induced ER stress signalling *in vitro*, experiments sought to understand the regulation of ceramides in mouse models of dyslipidaemia and obesity. Gastrocnemius skeletal muscle was analysed from mice across three dietary studies. In the first study, 5 C57Bl6 mice were fed a regular chow diet and 5 mice were fed a high-fat diet for 17 weeks. Metabolites were extracted from approximately 25 mg of gastrocnemius skeletal muscle using a modified Bligh and Dyer extraction, and the organic phase was analysed by LC-MS. Peaks were annotated using accurate mass, and intensities normalised to a relevant internal standard and dry protein pellet weight. Analysis of the lipidome highlighted that ceramides 40:1 and 42:1 were unchanged with high fat diet (**Figure 5.13A**). However, other long chain ceramides were altered with a high fat diet, with increases observed in ceramides 36:1, 38:1 and 42:3, demonstrating that high fat diet can increase concentrations of some longer chain ceramides (**Figure 5.13B**).

Since *in vitro* experiments highlighted an important role for secreted ceramides in the propagation of ER stress signalling, the concentrations of ceramides in plasma are also of interest. Metabolites from 20 µL of plasma were extracted using a modified Bligh and Dyer extraction, and the organic phase was analysed using LC-MS. Peaks were annotated using accurate mass, and normalised to a relevant internal standard. High fat diet significantly increased ceramide 40:1 in the plasma of these mice (**Figure 5.13C**).

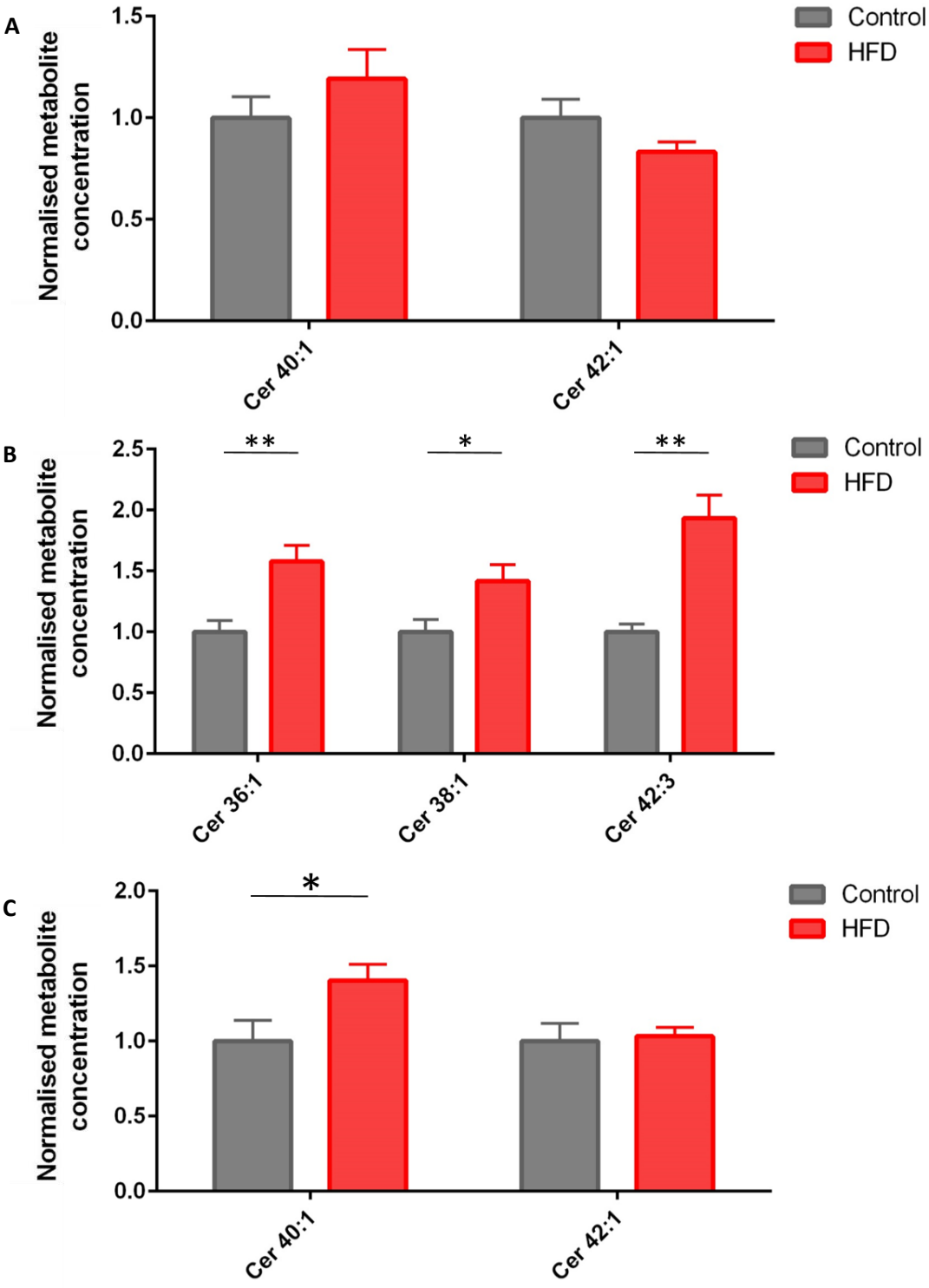

Figure 5.13: Long chain ceramides are increased in skeletal muscle of mice fed a high-fat diet

Mice were fed either a chow or high-fat diet for 17 weeks. (A) and (B) Liquid chromatography-mass spectrometry analysis of ceramides extracted from gastrocnemius tissue. (C) LC-MS analysis of ceramides extracted from plasma. Species were analysed using a Student's t-test. * $P \leq 0.05$, ** $P < 0.01$, *** $P < 0.001$, **** $P < 0.0001$. Data are expressed as mean ± SEM (n=5).

In a second dietary mouse study, 10 mice were given a regular chow diet and 13 mice were fed a high fat diet for 14 weeks. Approximately 25 mg of gastrocnemius skeletal muscle was extracted using a modified Bligh and Dyer extraction, and the organic phase was analysed using LC-MS. Peaks were annotated using accurate mass and peak intensities were normalised to a relevant internal standard and dry protein pellet weight. Ceramide 40:1 was significantly increased in the muscle of high fat diet fed mice (**Figure 5.14A**). Plasma was also available from these mice and 20 µL was extracted and analysed in an analogous manner to the previous study. While plasma concentrations of ceramide 42:1 were unaffected, ceramides 40:1 and 42:2 were both significantly increased with high fat diet (**Figure 5.14B**). This shows that high fat diet stimulates an increase in ceramide 40:1 concentration in the muscle and a concomitant increase in circulation.

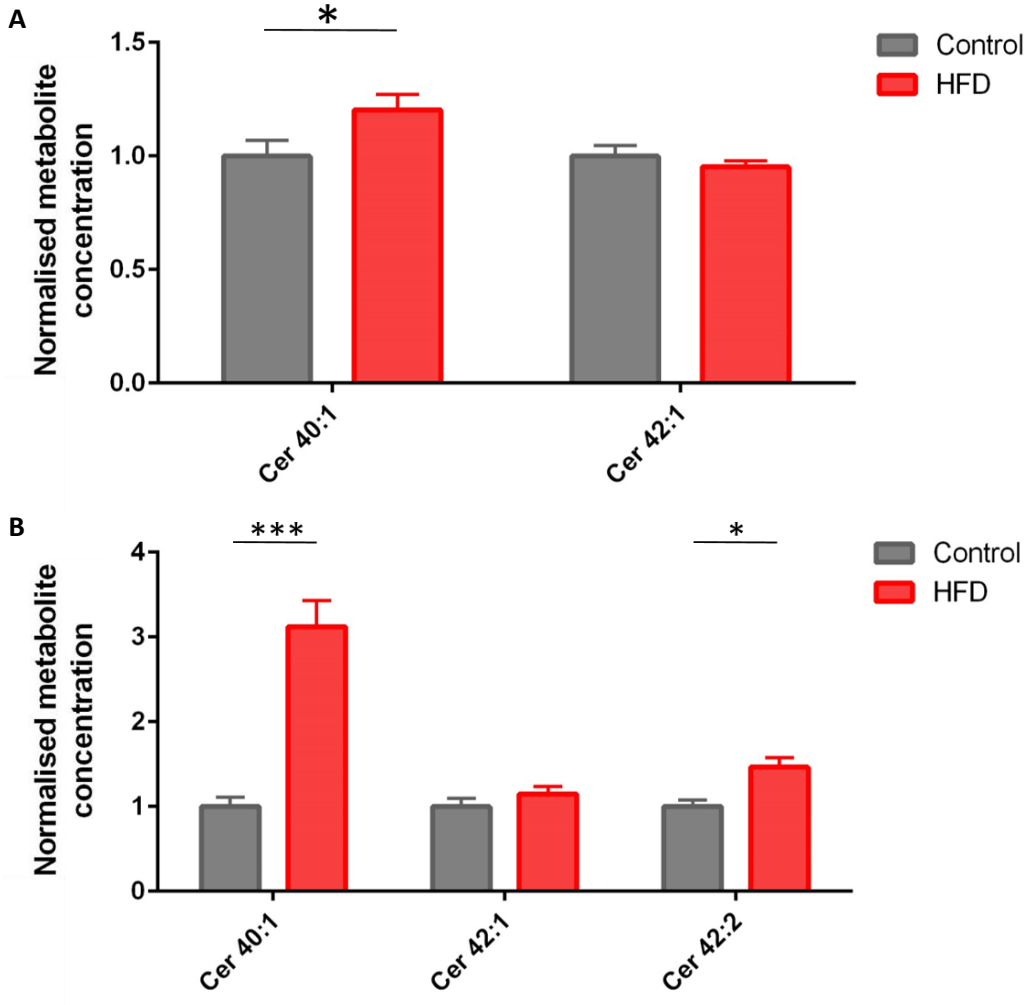

Figure 5.14: Long chain ceramides are increased in plasma of mice fed a high-fat diet in a second *in vivo* study

Mice were fed either a chow or high-fat diet (HFD) for 14 weeks. (A) Liquid chromatography-mass spectrometry analysis of ceramides extracted from gastrocnemius tissue. (B) LC-MS analysis of ceramides extracted from plasma. Species were analysed using a Student's t-test. * $P \leq 0.05$, ** $P < 0.01$, *** $P < 0.001$, **** $P < 0.0001$. Data are expressed as mean ± SEM (Chow: n = 10, HFD: n = 13).

5.4.7 Long chain ceramides are increased in the skeletal muscle of mice fed a western diet

In Chapter 3, phospholipid changes observed in C2C12 myotubes and primary HSkMCs exposed to palmitate more closely resembled changes observed in the skeletal muscle of mice in response to a western-style, compared with a high-fat diet. Previous literature has also suggested that a western diet (WD) is a more representative model for obesity and insulin

resistance in humans [278]. Here, ceramides were analysed from 8 mice fed WD and 8 mice fed a low fat control diet for 12 weeks. Approximately 25 mg of gastrocnemius tissue was extracted using a modified Bligh and Dyer extraction, and the organic phase was analysed by LC-MS. Peaks were annotated using accurate mass and peaks were normalised to a relevant internal standard and dry protein pellet weight.

Mice fed a western diet had increased concentrations of ceramide 40:1 and 42:1 compared to mice fed a low fat, control diet (**Figure 5.15A**). Furthermore, ceramide 36:1 was also increased suggesting a general upregulation in longer chain ceramides, although ceramide 38:1 was unchanged (**Figure 5.15B**). These results highlight that dietary mouse models of obesity and insulin resistance do have increased skeletal muscle ceramides. Furthermore, these results reinforce the evidence in Chapter 3 supporting a WD mouse model as a better model for saturated fatty acid exposure *in vitro*. Unfortunately, plasma from this study was not available for analysis, so the effect of WD on circulating concentrations of ceramides could not be investigated.

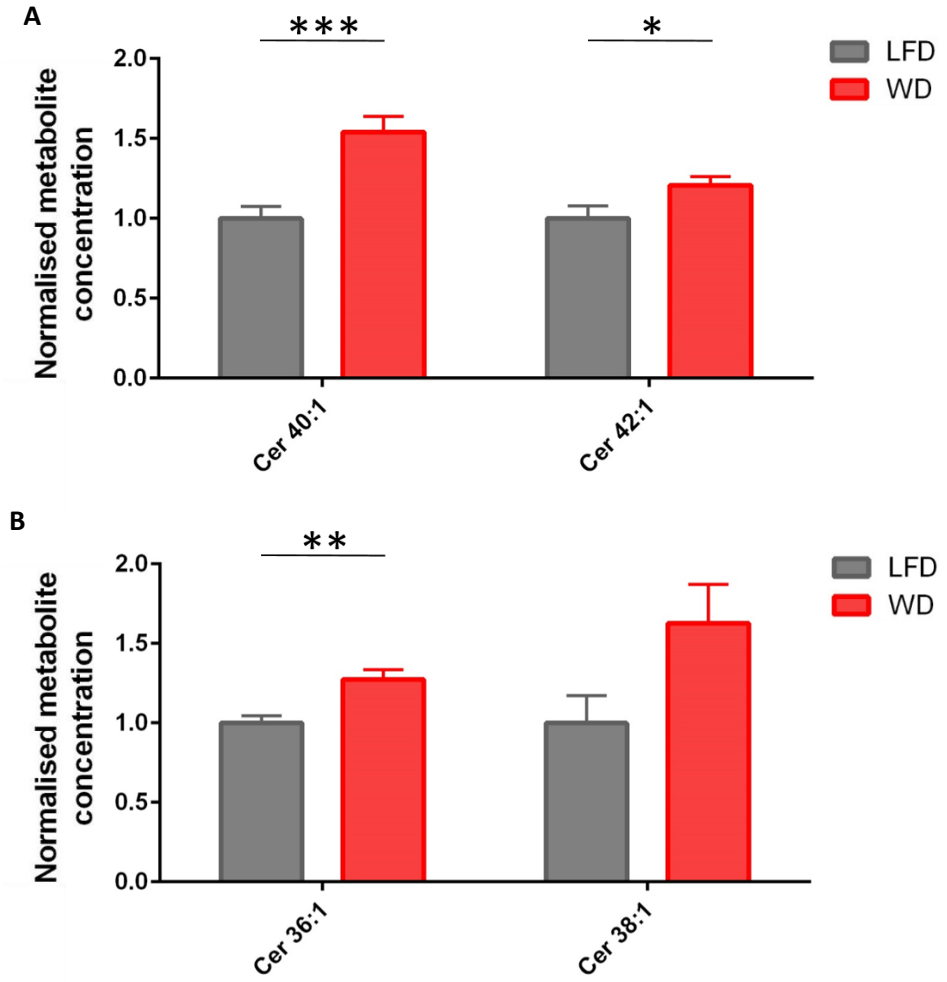

Figure 5.15: Long chain ceramides are increased in the skeletal muscle of mice fed a western diet

Mice were fed either a western diet (WD) for 14 weeks. (A) and (B) Liquid chromatography-mass spectrometry analysis of ceramides extracted from gastrocnemius tissue. Species were analysed using a Student's t-test. * $P \leq 0.05$, ** $P < 0.01$, *** $P < 0.001$, **** $P < 0.0001$. Data are expressed as mean ± SEM (n = 8).

5.4.8 Long chain ceramides are increased in skeletal muscle biopsies from diabetic patients

With ceramides increased in C2C12 myotubes and primary HSkMCs following palmitate treatment, as well as the gastrocnemius of WD and high fat diet-fed mice, the relevance of these results to human disease was assessed through the analysis of human skeletal muscle biopsies. Previous literature has shown that ceramides increase in obese, insulin resistant patients [352]. Biopsies of the *pectoralis major* muscle were taken from patients undergoing routine pacemaker surgery. Patients spanned a wide-range of BMIs and were a mix of non-

diabetic and type 2 diabetic patients. Metabolites were extracted from approximately 20 mg of tissue and the organic phase was analysed using LC-MS. Peaks were annotated using accurate mass and normalised to both a relevant internal standard and dry protein pellet weight.

Correlation between concentrations of ceramides 40:1 and 42:1 and BMI were assessed using linear regression analysis. Gradients of each regression line were not significantly non-zero, whilst R^2 values were low, indicating that ceramide concentrations did not explain the variation in the model (**Figure 5.16A**). Ceramide 40:1 and 42:1 were not significantly changed between diabetic and non-diabetic patients, when considered separately. However, when analysed across groups using two-way ANOVA, long-chain ceramides were found to be increased in the skeletal muscle of diabetic patients, suggesting long-chain ceramides are associated with insulin resistance (**Figure 5.16B**).

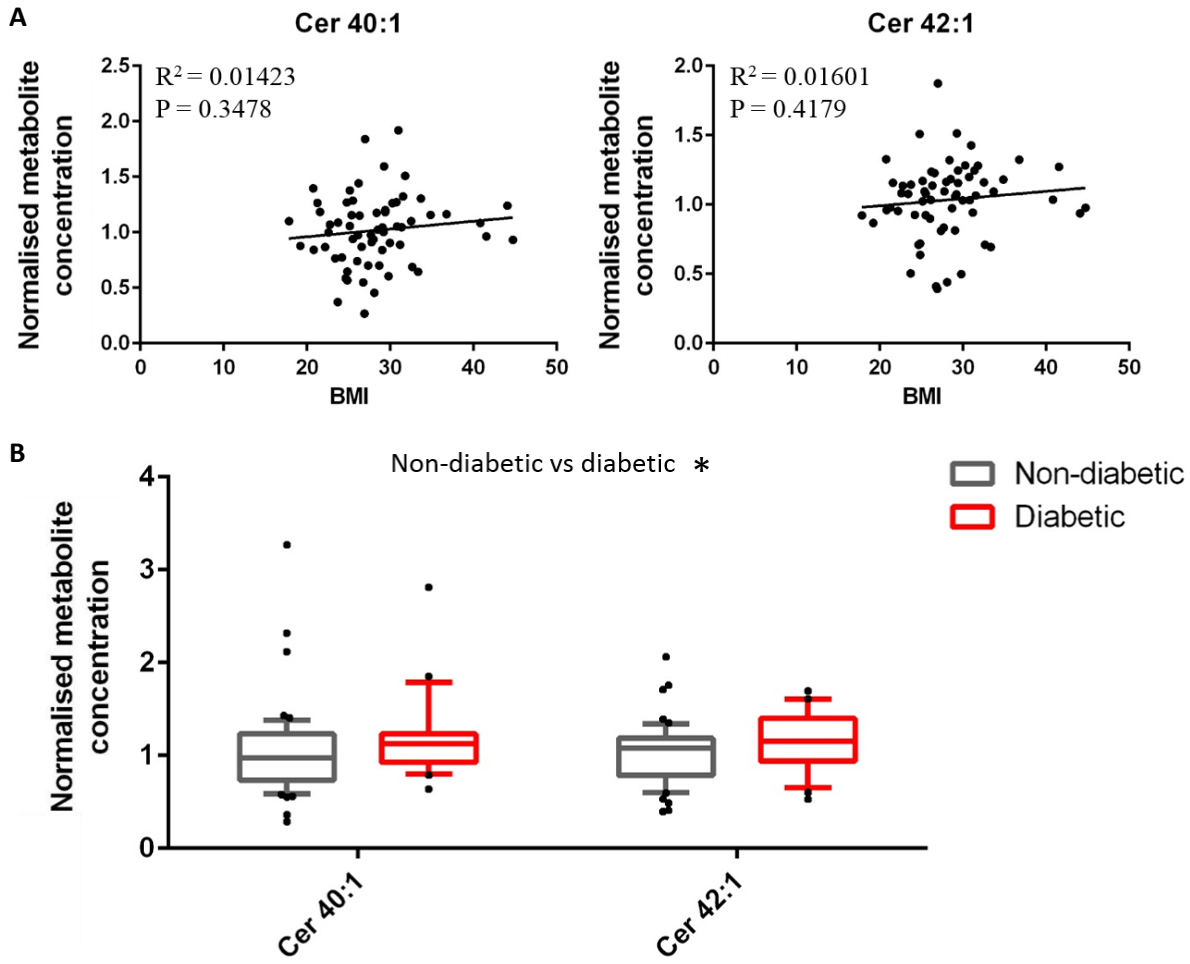

Figure 5.16: Long chain ceramides are increased in skeletal muscle biopsies of diabetic patients

Liquid chromatography-mass spectrometry analysis of skeletal muscle biopsies collected from patients during pacemaker fitting. (A) Linear regression analysis of long-chain ceramide concentrations against patient BMI. (B) Concentration of long-chain ceramides in non-diabetic controls and patients with type 2 diabetes. Species were analysed using a two-way ANOVA test with Sidak's multiple comparison test. * $P \leq 0.05$, ** $P < 0.01$, *** $P < 0.001$, **** $P < 0.0001$. Data are expressed as mean (10-90th percentile) (non-diabetic: n = 53, diabetic: n = 22).

5.5 Discussion

This chapter sought to define the mechanisms linking palmitate exposure with the induction of ER stress in skeletal muscle. Previous work had suggested that the induction of ER stress may be coordinated between tissues, with constitutive activation of Xbp1 in *pomc* neurons activating the UPR in the liver [150]. Here, we have identified long chain ceramides as cell non-autonomous mediators that propagate ER stress signalling from palmitate-treated myotubes to untreated myotubes – the first isolation of a signal of this nature.

The results are in keeping with evidence implicating ceramides in the induction of ER stress and being associated with lipotoxicity in general. Inhibition of ceramide synthesis in pancreatic β-cells reduced palmitate-induced ER stress [338]. Both pharmacological inhibition of ceramide synthase, using fumonisin B1, and siRNA-mediated knockdown of ceramide synthases 5 and 6 highlighted the importance of C14 ceramide in myristate-induced ER stress in intestinal epithelial cells [339]. Furthermore, exogenous treatment with short chain ceramide analogues, which are rapidly converted to longer chain, physiological ceramides, increased ER stress in the hypothalamus and human adenoid cystic carcinoma cells [344,345]. Infusion of a short-chain ceramide analogue in the hypothalamus of rats increased ceramides and induced hypothalamic ER stress, while the thermogenic capacity of brown adipose tissue was reduced. This highlighted how dysregulated sphingolipid metabolism and ER stress in one tissue can impact on the function of a distal tissue [353].

Palmitate treatment also increased intracellular ceramide concentrations, suggesting that increased secretion of ceramides resulted from elevated ceramide synthesis. Similar results have been observed in acute models of palmitate treatment [354]. Ceramides are synthesised via two pathways – the *de novo* and salvage pathways. Since the *de novo* pathway condenses serine with palmitoyl-CoA, it is likely that palmitate stimulates ceramide synthesis in this manner via an increase in substrate. Indeed, myotubes treated acutely with palmitate synthesise ceramides analogously [354]. However, further work is required to confirm the importance of the *de novo* pathway in chronic culture models.

Synthesis of ceramides via the *de novo* pathway is supported by the narrow spectrum of ceramide species detected. Primarily, the ceramides that were synthesised and secreted from myotubes comprised long-chain acyl chains, typically 20 carbons or longer. This specificity likely arises due to expression differences in ceramide synthase isoforms. There are six isoforms – termed ceramide synthase 1-6 – and each has a preference for different acyl chains

[355]. The synthesis of long-chain ceramides is favoured by ceramide synthase 2, which has a particularly high activity for fatty acids containing 22 and 24 carbons [356]. Ceramide synthase 2 is well-expressed in skeletal muscle, although the expression levels of ceramide synthase 1, which favours the formation of C18 ceramide, and ceramide synthase 4, which produces C20 ceramide, are higher [356]. This suggests that there is an alteration in the regulation of ceramide synthase 2 that leads to the preferential formation of long-chain ceramides following palmitate treatment. Previous studies have shown that acute palmitate treatment stimulates the expression of ceramide synthase 2 in both C2C12 myotubes and cardiomyocytes, suggesting one possible regulatory step that explains the results of this chapter [357,358].

Analysis of skeletal muscle from mice fed a western diet showed an increase in long chain ceramides. Furthermore, these ceramides were also increased in skeletal muscle biopsies taken from type 2 diabetic patients. This confirms that results from cultured myotubes translate to *in vivo* models; increased ceramides are a feature of dyslipidaemia. This corresponds well with previous studies demonstrating an increase in ceramide content in skeletal muscle biopsies taken from obese insulin-resistant individuals [352]. Similarly, obese insulin-resistant humans who took part in an 8-week endurance fitness program had reduced ceramide concentrations in skeletal muscle, concomitant with improvements in glucose tolerance [359].

One difference between the *in vitro* and *in vivo* ceramide profiles was the detection of C16 ceramide (ceramide 34:1). While concentrations of C16 ceramide were high in cultured myotubes following palmitate treatment, the species was not detected in skeletal muscle from *in vivo* studies. Previous studies have detected C16 in both murine and human skeletal muscle, so the reason underpinning its absence in the *in vivo* experiments in this thesis is unclear [69,360,361]. However, these studies also place greater importance on long-chain, rather than C16, ceramides in skeletal muscle metabolic disease, in keeping with the results of this chapter.

Murine dietary models of obesity also exhibited elevated plasma ceramides, a result in keeping with previous research. Haus and colleagues correlated plasma ceramides with insulin resistance and plasma TNFα concentration, implicating ceramides in both inflammation and dysregulated insulin signalling [72]. Raised plasma ceramide concentrations highlight the potential for ceramides to act as signalling molecules, transported to distal tissues separate from their site of synthesis. The capacity for plasma ceramides to act as

bioactive signalling mediators was highlighted in a study in which ceramides contained in low-density lipoprotein (LDL) were infused into lean mice, impairing glucose uptake and increasing markers of insulin resistance in skeletal muscle [86].

To demonstrate the capacity for exogenous ceramides to induce ER stress, an ethanol:dodecane vehicle was required, due the poor aqueous solubility of ceramides. However, the vehicle for intercellular trafficking of ceramides is unclear. Ceramides secreted from hepatocytes were packaged into LDL, but myotubes do not synthesise LDL [86]. A similar mechanism of transport, using a vehicle comprising a lipid membrane remains likely. Exosomes are membrane-bound vesicles that have an increasingly important role in cell signalling [362]. Ceramides are enriched in the membrane of exosomes, and so future work should look to the potential of exosomes as a vehicle for ceramide signalling between myotubes [363].

Conclusion

Experiments in this chapter have identified long chain ceramides as cell non-autonomous signals, which propagate palmitate-induced ER stress between myotubes. This is the first identification of a signal of this nature. Furthermore, LC-MS analysis showed increased ceramide concentrations were also a feature of murine *in vivo* models of obesity and type 2 diabetic patients.

Chapter 6

Ceramides are synthesised in a Perk-dependent manner via the *de novo* pathway and enriched in secreted exosomes

6.1 Introduction

Cell non-autonomous signalling has recently emerged as a mechanism controlling the induction of ER stress in distal tissues, but the nature of these signals has remained elusive [146]. In Chapter 5, long-chain ceramides were identified as cell non-autonomous signals that propagate myotube UPR activation following chronic palmitate treatment. However, the pathways regulating this process are unclear.

Increases in intracellular ceramide concentrations suggested that the stimulation of ceramide secretion resulted from elevated synthesis. Ceramides are synthesised via two principal pathways – the *de novo* and salvage pathways (**Figure 6.1**). The *de novo* pathway takes place at the ER. The initial step involves serine palmitoyl transferase (SPT), which condenses serine and palmitoyl-CoA, forming 3-keto-sphinganine [364]. This is then reduced to sphinganine by 3-ketosphinganine reductase. Ceramide synthase adds a fatty acid chain to sphinganine, forming a dihydroceramide that is then reduced to a ceramide by dihydroceramide desaturase. The salvage pathway, on the other hand, takes place in late endosomes and lysosomes, and involves the breakdown of complex sphingolipids, such as sphingomyelin and glucosylceramides, to form ceramides [365]. Previous literature has shown that acute palmitate treatment increases ceramide synthesis via the *de novo* pathway, with the increase in substrate availability elevating flux through SPT [354].

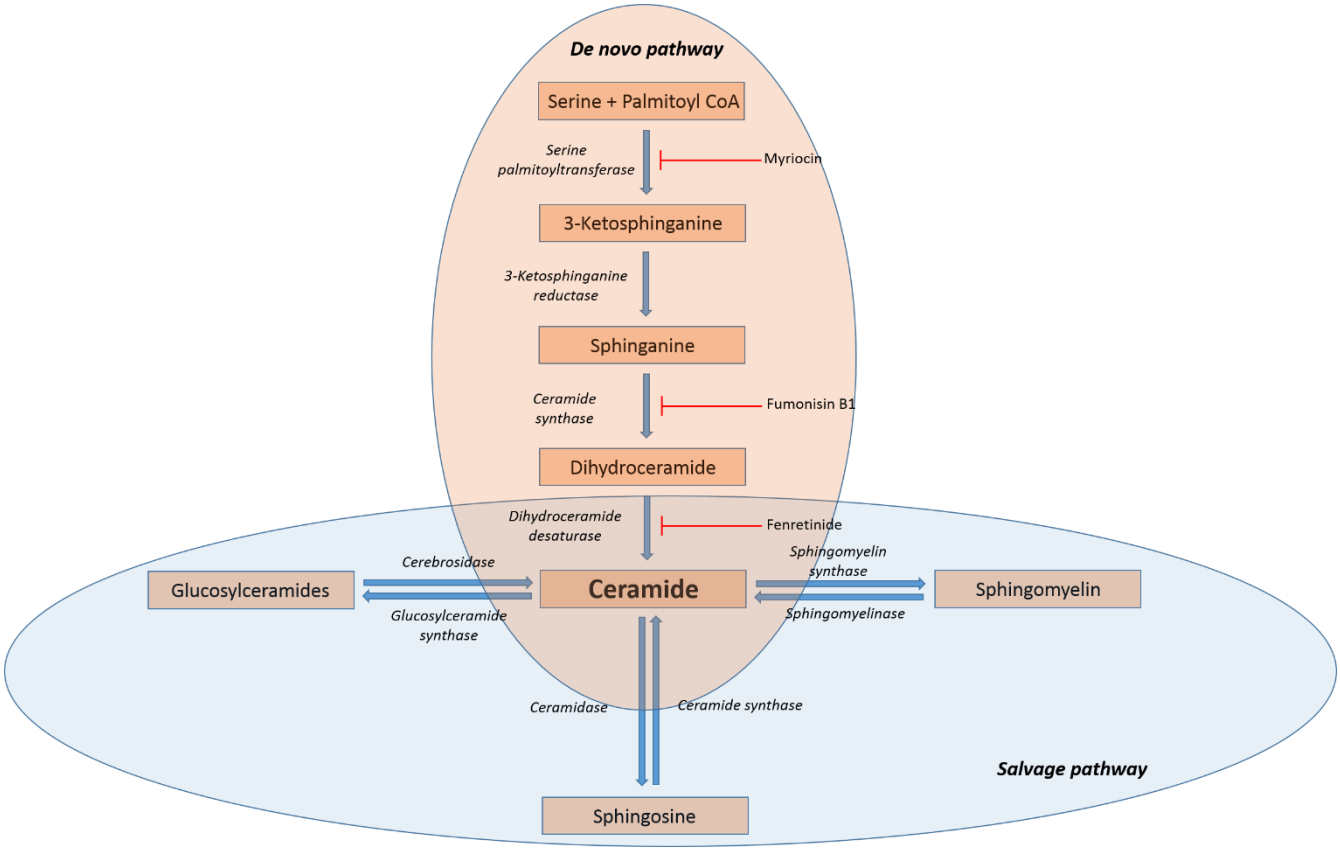

Figure 6.1 Ceramide synthesis pathways

Diagram depicting the two main pathways in the synthesis of ceramides – the *de novo* and salvage pathways. Also shown are the actions of three *de novo* pathway inhibitors: myriocin, which inhibits serine palmitoyltransferase, fumonisin B1, which inhibits ceramide synthase, and Fenretinide, which inhibits dihydroceramide desaturase.

Following synthesis, experiments in Chapter 5 showed that ceramides were secreted from myotubes into the culture media. The poor aqueous solubility of ceramides in these experiments suggests the need for a suitable vehicle. In *C. elegans*, a constitutively active Xbp1 in neurons induced ER stress in distal tissues, and was found to be dependent on the release of small clear vesicles [149]. Furthermore, hepatocytes treated with palmitate release ceramide-enriched extracellular vesicles via Ire1 [363]. Extracellular vesicles, such as exosomes and microvesicles, are membrane-bound particles that can transfer proteins, RNA and small molecules, including lipids, between cells in both a paracrine and endocrine manner [366]. Indeed, increases in ceramides can trigger membrane budding and exosome secretion, while inhibition of neutral sphingomyelinase 2, an enzyme important in the generation of ceramide via the salvage pathway, prevented exosome release [367].

6.2 Aims and Objectives

The aim of this chapter was to investigate the mechanisms underpinning the propagation of ER stress between myotubes. The following set of objectives were designed to achieve this:

1) Use pharmacological inhibition to understand the pathways of importance in ceramide synthesis following palmitate treatment of myotubes.
2) Identify the mode of intercellular signal transport.
3) Combine mass spectrometry and pharmacological inhibition to investigate the mechanisms of ceramide-induced ER stress.

6.3 Materials and Methods

6.3.1 C2C12 culture

C2C12 cells were cultured as described in **Chapter 2 Materials and Methods** (Section 2.1.1 *C2C12 myoblast culture and differentiation*)**.** Pharmacological inhibitors (detailed in section 6.3.7 *Pharmacological inhibitors*) were used for the final 24 hours of experiments. Cells were differentiated and treated in collagen I-coated 12-well plates.

6.3.2 Primary human skeletal muscle cell culture

Primary human skeletal muscle cells (HSkMCs) were cultured as described in **Chapter 2 Materials and Methods** (Section 2.1.2 *Primary human skeletal muscle cell culture and differentiation*)**.** Pharmacological inhibitors (detailed in section 6.3.7 *Pharmacological inhibitors*) were used for the final 24 hours of experiments. Cells were treated in collagen I-coated 12-well plates.

6.3.3 AML-12 cell culture

Alpha mouse liver 12 (AML-12) cells were cultured in 1:1 Dulbecco's modified Eagle's medium and Ham's F12 medium, supplemented with 10% FBS, 1% penicillin/streptomycin, 1% Insulin-Transferrin-Selenium (ITS; 10 mg/L, 5.5 mg/L and 6.7 µg/L respectively) and dexamethasone (100 µM). Cells were grown to confluence in collagen-I coated 12-well plates (Corning). Conditioned media from C2C12 myotubes was transferred on to confluent AML-12 hepatocytes for 10 hours.

6.3.4 Production of conditioned media and conditioned media transfer experimentation

Myocytes were treated with 200 µM palmitate or the BSA vehicle during 6 days of differentiation. At the end of this period culture media was switched to serum-free media, free from any agonists, for 24 hours, allowing for the accumulation of secreted factors from the myocytes. This conditioned media was then transferred on to untreated myocytes for 10 hours.

6.3.5 Exosome purification

Exosomes were purified using Total Exosome Isolation Reagent (from cell culture media) (Thermo Fisher), following the manufacturer's protocol. Briefly, conditioned media was harvested from myocytes and centrifuged (2,000 x *g*, 30 minutes) to remove cell debris. The supernatant was transferred to a fresh tube, and 0.5 volumes of the Total Exosome Isolation Reagent was added. Samples were vortexed well and incubated overnight at 5 ºC. Samples were subsequently centrifuged (10,000 x *g*, 60 minutes, 5 ºC) and the supernatant discarded. The pelleted exosomes were resuspended in serum-free media for conditioned media transfer to untreated myocytes, or extracted using a modified Bligh and Dyer extraction protocol detailed in **Chapter 2 Materials and Methods** (Section 2.5.1 *Cell metabolite extraction for mass spectrometry*) for LC-MS analysis.

6.3.6 Conjugation of palmitate to BSA

Palmitate was bound to BSA following the protocol summarised in **Chapter 2 Materials and Methods** (2.1.3 *Conjugation of palmitate to BSA*)**.**

6.3.7 Pharmacological inhibitors

Fumonisin B1, Fenretinide, AMG PERK 44 and 4μ8c were purchased from Tocris Bioscience, and dissolved in DMSO to a concentration of 20 mM. The inhibitors were diluted into culture media to a final concentration of 10 μM, or 5μM in the case of Fenretinide. Myriocin was purchased from Sigma Aldrich, and dissolved in DMSO, forming a stock solution of 10 mM, and diluted into culture media to a final concentration of 10 μM.

6.3.8 Cell harvesting

Cells were harvested and pelleted as described in **Chapter 2 Materials and Methods** (section 2.1.4 *Cell harvesting*). Cell counts were performed using a Scepter automated cell counter (Millipore).

6.3.9 RNA isolation and purification

RNA was extracted and purified from cells using an RNeasy mini kit (Qiagen), as outlined in **Chapter 2 Materials and Methods** (Section 2.4.1 *RNA isolation and purification*)**.**

6.3.10 cDNA synthesis

RNA concentrations were standardised and cDNA then synthesised using a RT^2 first strand kit (Qiagen), following the manufacturer's instructions as set out in **Chapter 2 Materials and Methods** (Section 2.4.2 *cDNA synthesis*)**.**

6.3.11 Reverse transcription polymerase chain reaction

Transcript levels were analysed using the StepOnePlus Real-Time PCR system, as described in **Chapter 2 Materials and Methods** (Section 2.4.3 *Reverse transcription quantitative polymerase chain reaction*)**.**

6.3.12 Metabolite extraction from cells

Metabolites were extracted from cells using a modified Bligh and Dyer method, described in **Chapter 2 Materials and Methods** (Section 2.5.1 *Cell metabolite and lipid extraction for mass spectrometry*)**.**

6.3.13 Metabolite extraction from media

1 mL of serum-free cell culture media was collected. 800 µL of methanol/chloroform (1:1) was added to each sample and mixed well by vortexing. Samples were centrifuged (16,100*g*, 20 minutes), and the organic layer subsequently separated and dried down under nitrogen gas. Dried samples were stored at -80 ºC.

6.3.14 Liquid chromatography-mass spectrometry analysis of lipids

The dried-down organic fraction was dissolved in 50 µl methanol/chloroform (1:1), and diluted into 190 µl IPA/ACN/H_2O (2:1:1). Samples were then analysed using an Orbitrap Elite mass spectrometer, using a method with two scan events as described in **Chapter 2 Materials and Methods** (Section 2.6 *Liquid chromatography-mass spectrometry open profiling of lipids*)**.** Chromatogram files were converted using MSConvert (Proteowizard), and processed using XCMS within an R script. Peaks were normalised to a relevant internal standard and then either cell number, for *in vitro* experiments, or dry protein pellet weight, for the analysis of skeletal muscle tissue.

6.3.15 Statistics

Statistical significance was assessed using either a one-way ANOVA with Tukey's multiple comparisons test, two-way ANOVA with Sidak's multiple comparisons test or Student's t-test, as detailed in each figure. In each case, $n \geq 3$ and the significance level was set to $P \leq 0.05$. All univariate analysis was conducted using GraphPad (version 6) software.

6.4 Results

6.4.1 Chronic palmitate increases synthesis of ceramides via the *de novo* pathway

Ceramides are synthesised via two principal pathways – the *de novo* and salvage pathways – with previous literature implicating the former in ceramide synthesis following acute exposure to palmitate [354]. To investigate whether chronic palmitate-induced increases in ceramide synthesis are also dependent on *de novo* synthesis, the initial formation of 3-ketosphinganine was prevented using myriocin, an inhibitor of SPT [368]. C2C12 myotubes were grown to confluence, and differentiated for 6 days. During this period, cells were treated with either 200 µM palmitate or the BSA vehicle control. Cells were also co-treated with either 10 µM myriocin or the vehicle control for the final 24 hours. Cells were harvested, and metabolites extracted using a modified Bligh and Dyer extraction. The organic phase was analysed by LC-MS. Peaks were annotated using accurate mass, and peak intensity was normalised to a relevant internal standard and cell number. Palmitate treatment increased the concentrations of ceramides 34:1, 40:1 and 42:1, compared to cells treated with the vehicle control. However, myriocin treatment greatly reduced concentrations of ceramides in all cells regardless of palmitate exposure (**Figure 6.2A**). This highlights that palmitate-induced increases in ceramides are dependent on flux through SPT.

To confirm the dependency on the *de novo* pathway, ceramide synthase was inhibited using fumonisin B1 [369]. C2C12 myotubes were treated with 200 µM palmitate or the BSA vehicle control during a 6-day differentiation period, as well as 10 µM fumonisin B1 (FB1) or the DMSO vehicle control for the final 24 hours. Cells were harvested and extracted using a modified Bligh and Dyer extraction. The organic phase was analysed by LC-MS, with peaks normalised to a relevant internal standard and cell number. As with myriocin treatment, inhibition of ceramide synthase with FB1 ablated concentrations of ceramides 34:1, 40:1 and 42:1 in both palmitate- and BSA-treated cells (**Figure 6.2B**). These results highlight the importance of the *de novo* pathway in chronic palmitate-induced ceramide synthesis.

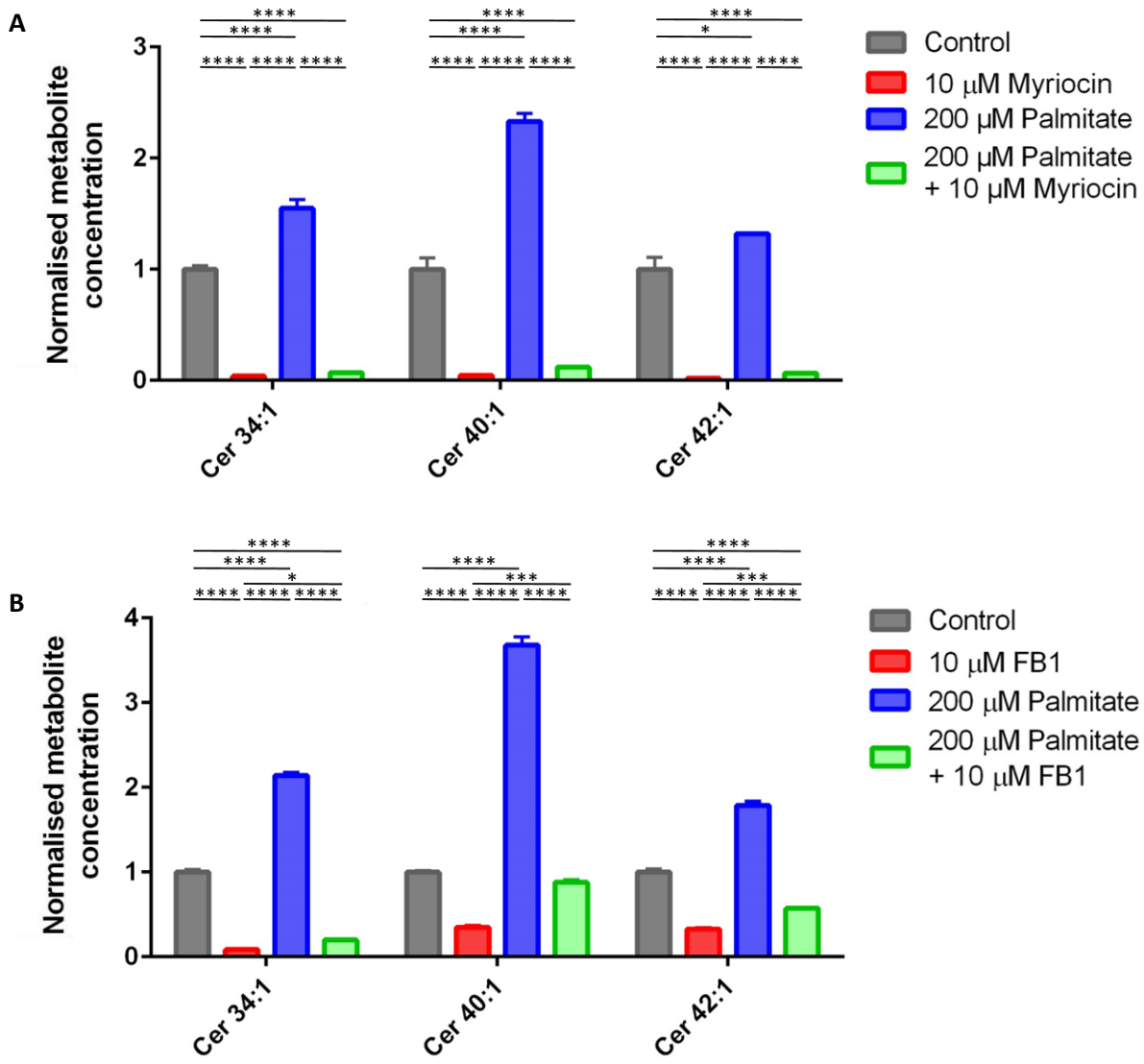

Figure 6.2: Chronic palmitate stimulates ceramide synthesis via the *de novo* pathway

C2C12 myotubes were treated with either 200 μM palmitate, or the vehicle control, during a 6-day differentiation period. Cells were also co-cultured with (A) 10 μM myriocin, (B) 10 μM fumonisin B1 (FB1), or the vehicle control for the final 24 hours. Metabolites were extracted from cells and ceramides were analysed by liquid chromatography-mass spectrometry (LC-MS). Species were analysed using a one-way ANOVA with Tukey's multiple comparison test. * $P \leq 0.05$, ** $P < 0.01$, *** $P < 0.001$, **** $P < 0.0001$. Data are expressed as mean ± SEM (n = 3).

6.4.2 Chronic palmitate treatment increases ceramide synthase 2 expression in skeletal myocytes

There are six identified isoforms of ceramide synthase, termed ceramide synthase 1-6. The enzymes vary in their acyl chain specificity, and, therefore, produce a different subset of (dihydro)ceramides [355]. Ceramide synthase 2 (Cers2) preferentially synthesises longer chain ceramides, including ceramides 40:1 (C22) and 42:1 (C24). Since inhibition of ceramide synthase reduced ceramide concentrations, the effect of chronic palmitate treatment on the expression of *Cers2* was investigated. C2C12 myotubes were treated with either 100 or 200 µM palmitate, or the BSA vehicle control, throughout a 6-day differentiation period. RNA was harvested, and the expression of *Cers2* measured using RT-qPCR. The results showed that chronic 200 µM palmitate increased the expression of *Cers2* 1.5-fold, suggesting that palmitate-induced increases in longer chain ceramides is partially as a result of increased ceramide synthase 2 (**Figure 6.3A**).

This mechanism was also investigated in primary HSkMCs, which were treated with 50 or 100 µM palmitate for 6 days during differentiation. RNA was harvested and expression of *CERS2* analysed by RT-qPCR. Treatment of primary HSkMCs with 100 µM palmitate increased the expression of *CERS2* 1.4-fold, demonstrating that palmitate-induced increases in ceramide synthesis in human myocytes is also partially dependent on elevated concentrations of ceramide synthase 2, rather than simply increased substrate availability (**Figure 6.3B**).

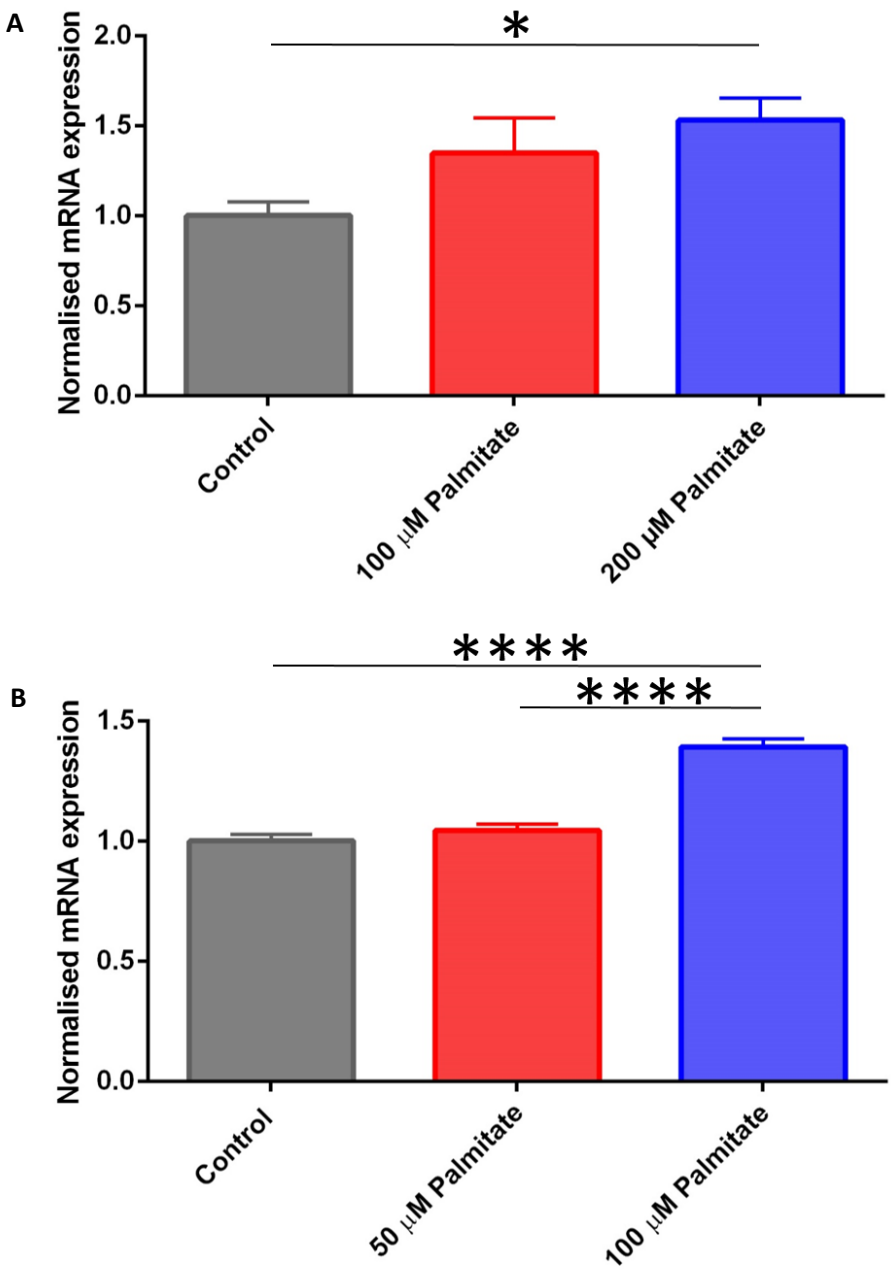

Figure 6.3: Chronic palmitate increases the expression of ceramide synthase 2 in mouse and human skeletal myocytes

(A) C2C12 myotubes were treated with either 100 or 200 µM palmitate, or the vehicle control, during a 6-day differentiation period. RNA was harvested and expression of *Cers2* was analysed by RT-qPCR. (B) Primary human skeletal muscle cells were treated with 50 or 100 µM palmitate, or the vehicle control, for 6 days during differentiation. RNA was harvested and expression of *CERS2* was analysed by RT-qPCR. Species were analysed using a one-way ANOVA test with Tukey's multiple comparison test. * $P \leq 0.05$, ** $P < 0.01$, *** $P < 0.001$, **** $P < 0.0001$. Data are expressed as mean ± SEM (n = 4).

6.4.3 Pharmacological inhibition of Perk reduces palmitate-induced long chain ceramide synthesis

As shown in Chapter 3, chronic palmitate treatment increases not only the concentration of ceramides, but also the expression of UPR target genes. Therefore, the dependence of ceramide synthesis on specific arms of the UPR was investigated using pharmacological inhibition of Ire1 and Perk. C2C12 myotubes were grown to confluence and differentiated for 6 days. During this period, cells were treated with 200 µM palmitate or the BSA vehicle control. For the final 24 hours, cells were also cultured with either 10 µM 4µ8c, an inhibitor of Ire1, 10 µM AMG PERK 44, which inhibits Perk, or the DMSO vehicle control. Cells were harvested and metabolites extracted using a modified Bligh and Dyer method. The organic phase was analysed using LC-MS, with peaks normalised to a relevant internal standard and cell number.

Inhibition of Ire1 had no effect on the concentrations of ceramides 34:1, 40:1 and 42:1, regardless of palmitate treatment (**Figure 6.4A**). However, treatment with AMG PERK 44 attenuated palmitate-induced increases in ceramides 40:1 and 42:1, suggesting a role for Perk in the stimulation of ceramide synthesis (**Figure 6.4B**). Ceramide 34:1concentrations, however, were unaffected by inhibition of Perk, suggesting the effect is limited to longer chain ceramides. BSA-treated cells were also unaffected by Perk inhibition. This suggests little regulation of ceramide concentrations by Perk under resting conditions, but a specific involvement of Perk in the elevation of long chain ceramide concentrations induced by palmitate. These results highlight an important role for the Perk arm of the UPR in mediating palmitate-induced increases in ceramide synthesis, which is a previously unknown link between the induction of ER stress and the generation of lipotoxic intermediates.

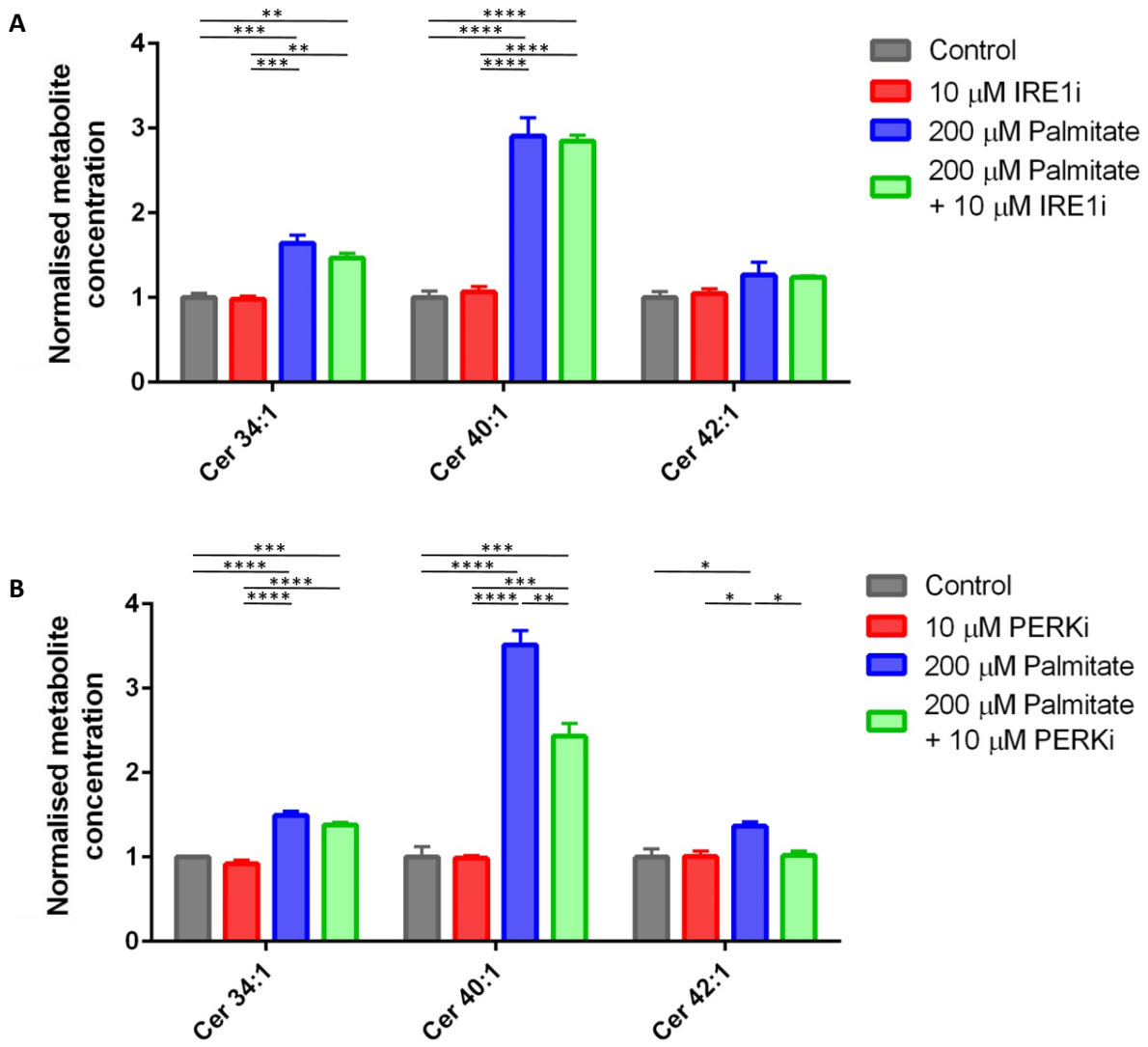

Figure 6.4: Pharmacological inhibition of Perk reduces concentrations of long-chain ceramides

C2C12 myotubes were treated with either 200 μM palmitate, or the vehicle control, during a 6-day differentiation period. Cells were also co-cultured with (A) 10 μM 4μ8c (IRE1i), (B) 10 μM AMG PERK 44 (Perki), or the vehicle control for the final 24 hours. Metabolites were extracted from cells and ceramides were analysed by liquid chromatography-mass spectrometry. Species were analysed using a one-way ANOVA with Tukey's multiple comparison test. * $P \leq 0.05$, ** $P < 0.01$, *** $P < 0.001$, **** $P < 0.0001$. Data are expressed as mean ± SEM (n = 3).

6.4.4 Ceramides are increased in isolated exosomes from media

Results so far have unveiled a mechanism by which palmitate stimulates synthesis of ceramides via the *de* novo pathway, and is dependent on the activation of the Perk arm of the UPR. Ceramides can then be secreted by activated myotubes, propagating ER stress signalling in a cell non-autonomous manner. However, a mechanism of release and trafficking between cells is not yet understood. Extracellular vesicles, such as exosomes, are important mediators of intercellular signalling [362]. A number of studies have shown the importance of ceramide species in the biogenesis of exosomes [363,367]. To investigate a role for exosomes in ceramide trafficking and ER stress activation, C2C12 myotubes were treated with 200 µM palmitate, or the BSA vehicle control, for 6 days during differentiation. Following this, culture media was switched to serum-free media, free of palmitate or BSA, for 24 hours. The conditioned media was then harvested and exosomes purified for analysis. Metabolites were extracted from exosomes using a modified Bligh and Dyer method, and the organic phase was analysed by LC-MS. Peaks were normalised to a relevant internal standard. Ceramides 34:1, 40:1 and 42:1 were all detected within exosomes purified from C2C12 conditioned media (**Figure 6.5A**). Furthermore, these species were all increased following chronic palmitate treatment, suggesting that exosomes are the vehicle for ceramide transport between cells.

The ability for ceramide-enriched exosomes to induce ER stress was also tested. Purified exosomes were reconstituted in serum-free media and transferred on to untreated C2C12 myotubes for 10 hours. The induction of ER stress was assessed using RT-qPCR of target UPR genes (*Atf3*, *Atf4*, *Hspa5* and *Edem1*). Purified exosomes from palmitate-treated myotubes were unable to induce expression of ER stress genes when considered individually. However, when analysed as a group using two-way ANOVA, these exosomes were able to increase the expression of the UPR gene panel (**Figure 6.5B**), suggesting that ceramide-enriched exosomes are capable of propagating ER stress to untreated myotubes.

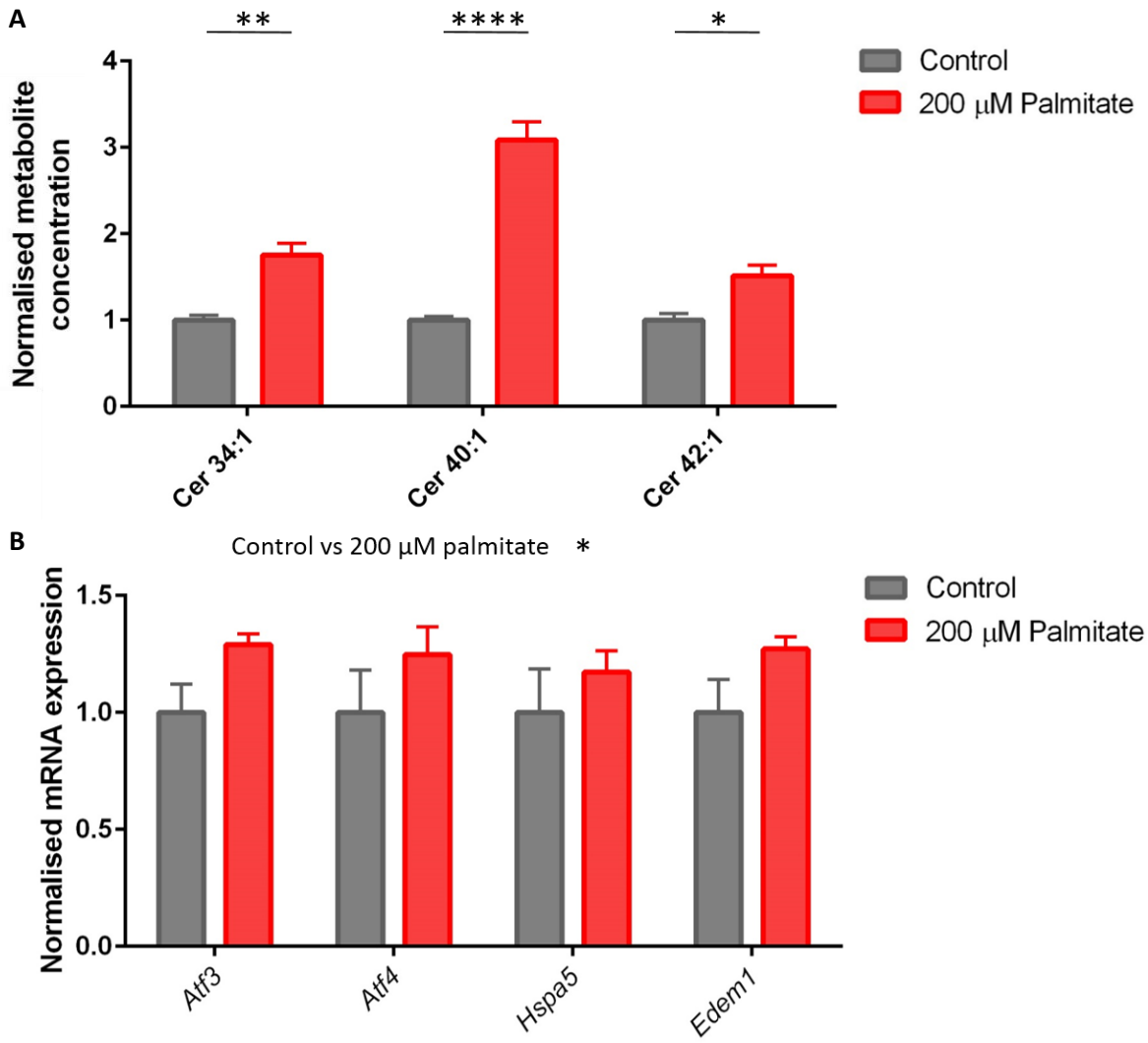

Figure 6.5: Exosomes purified from conditioned media of C2C12 myotubes treated with palmitate are enriched in long chain ceramides

C2C12 myotubes were treated with 200 μM palmitate or the vehicle control for 6 days during differentiation. Conditioned media was collected following a switch to serum-free media for 24 hours and exosomes were subsequently purified from the media. (A) Ceramides were analysed using liquid chromatography-mass spectrometry. (B) Exosomes were reconstituted in serum-free media and transferred to untreated myotubes for 10 hours. The induction of ER stress was assessed using RT-qPCR of a target panel of UPR genes (*Atf3*, *Atf4*, *Hspa5* and *Edem1*). Species were analysed using a two-way ANOVA with Sidak's multiple comparison test. * $P \leq 0.05$, ** $P < 0.01$, *** $P < 0.001$, **** $P < 0.0001$. Data are expressed as mean ± SEM (n = 4).

Experiments were also repeated in primary HSkMCs to confirm that the results were not an artefact of immortalised cells. HSkMCs were grown to confluence and treated with 100 µM palmitate or the BSA vehicle throughout a 6-day differentiation period. Culture media was then switched to basal media, free of any agonists, for 24 hours. Exosomes were then purified from conditioned media for downstream applications. Since primary HSkMCs are cultured at a much lower cell number, purification of exosomes could not provide a detectable level of ceramides as analysed by LC-MS. However, purified exosomes were also reconstituted in basal media and transferred on to untreated, differentiated HSkMCs for 10 hours. RNA was harvested and the induction of ER stress was assessed using RT-qPCR. Exosomes purified from HSkMCs treated with palmitate increased the expression of *ATF3* and *ATF4* 1.2-fold, while *HSPA5* narrowly missed out on significance ($p=0.07$), relative to exosomes purified from BSA-treated myocytes (**Figure 6.6**). *EDEM1* expression, however, was unaffected by palmitate treatment. These results show that exosomes purified from palmitate-treated HSkMCs are capable of increasing transcription of some UPR target genes in untreated myocytes, and suggest that ceramides may propagate ER stress signalling via exosome-mediated transport. However, expression of ER stress genes was weaker in both C2C12 myotubes and primary HSkMCs than observed in previous conditioned media experiments, possibly as a result of a low yield of exosomes during their isolation.

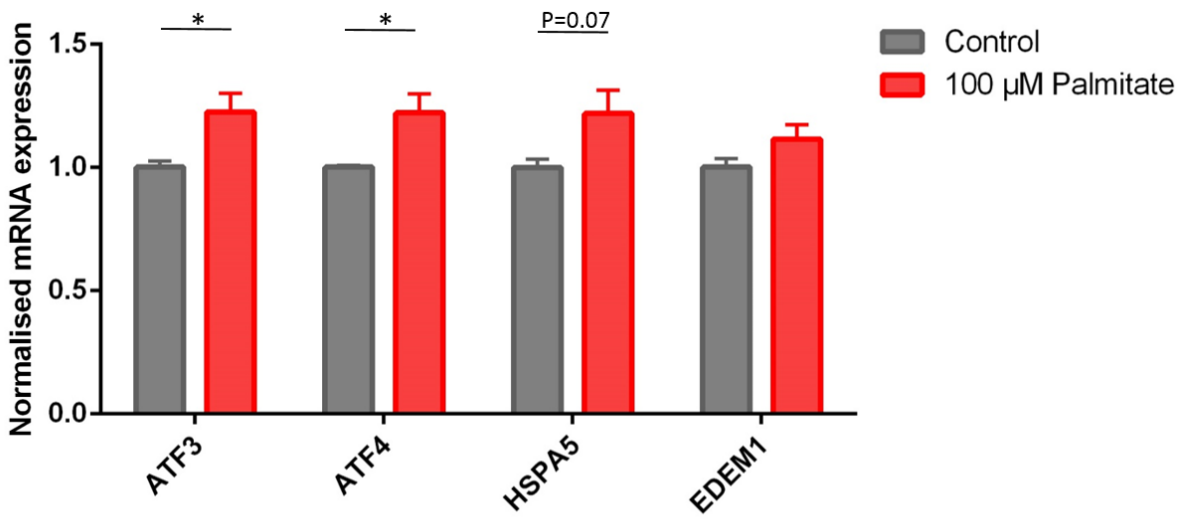

Figure 6.6: Exosomes purified from palmitate-treated myocytes increase ER stress in untreated myocytes

Primary human skeletal muscle cells were treated with 100 µM palmitate or the vehicle control for 6 days during differentiation. Exosomes purified from conditioned media were reconstituted in fresh basal media, prior to transfer to untreated myocytes for 10 hours. Induction of endoplasmic stress was assessed using RT-qPCR of a panel of UPR genes (*ATF3, ATF4, HSPA5* and *EDEM1*). Species were analysed using a one-way ANOVA with Tukey's multiple comparison test. * $P \leq 0.05$, ** $P < 0.01$, *** $P < 0.001$, **** $P < 0.0001$. Data are expressed as mean ± SEM (n=4).

6.4.5 Treatment with Fenretinide increases concentrations of dihydroceramides and the induction of ER stress

Following the identification of mechanisms underpinning palmitate-induced ceramide synthesis and secretion, culminating in the propagation of ER stress signalling, the final set of experiments sought to understand the manner by which ceramides can activate UPR signalling. Initially, LC-MS was used to profile the effects of exogenous ceramide treatment on the lipidome. C2C12 cells were grown to confluence and differentiated for 6 days. For the final 10 hours, cells were treated with either 10 µM C22 ceramide (40:1), 10 µM C24 ceramide (42:1), a combination of the both, or the ethanol/dodecane (98:2) vehicle. Cells were then harvested and metabolites extracted using a modified Bligh and Dyer method. The organic phase was analysed by LC-MS, with peaks normalised to a relevant internal standard and cell number.

Treatment of C2C12 myotubes with each ceramide increased the concentrations of that ceramide intracellularly, suggesting that the ceramides are taken up from the culture media

(**Figure 6.7A**). Furthermore, increases in ceramide 34:1 suggest that the C22 and C24 ceramides are recycled to increase concentrations of other ceramides. Combined treatment with C22 and C24 ceramides increased concentrations of ceramide 34:1, 40:1 and 42:1 in line with the individual treatments.

Consistent with the concept of recycling, concentrations of dihydroceramides (DHCers) were also increased with ceramide treatment. Treatment with C22 ceramide increased the cognate dihydroceramide 40:0, while C24 ceramide raised concentrations of dihydroceramide 42:0 (**Figure 6.7B**). Similarly, both ceramide treatments also raised dihydroceramide 34:0.

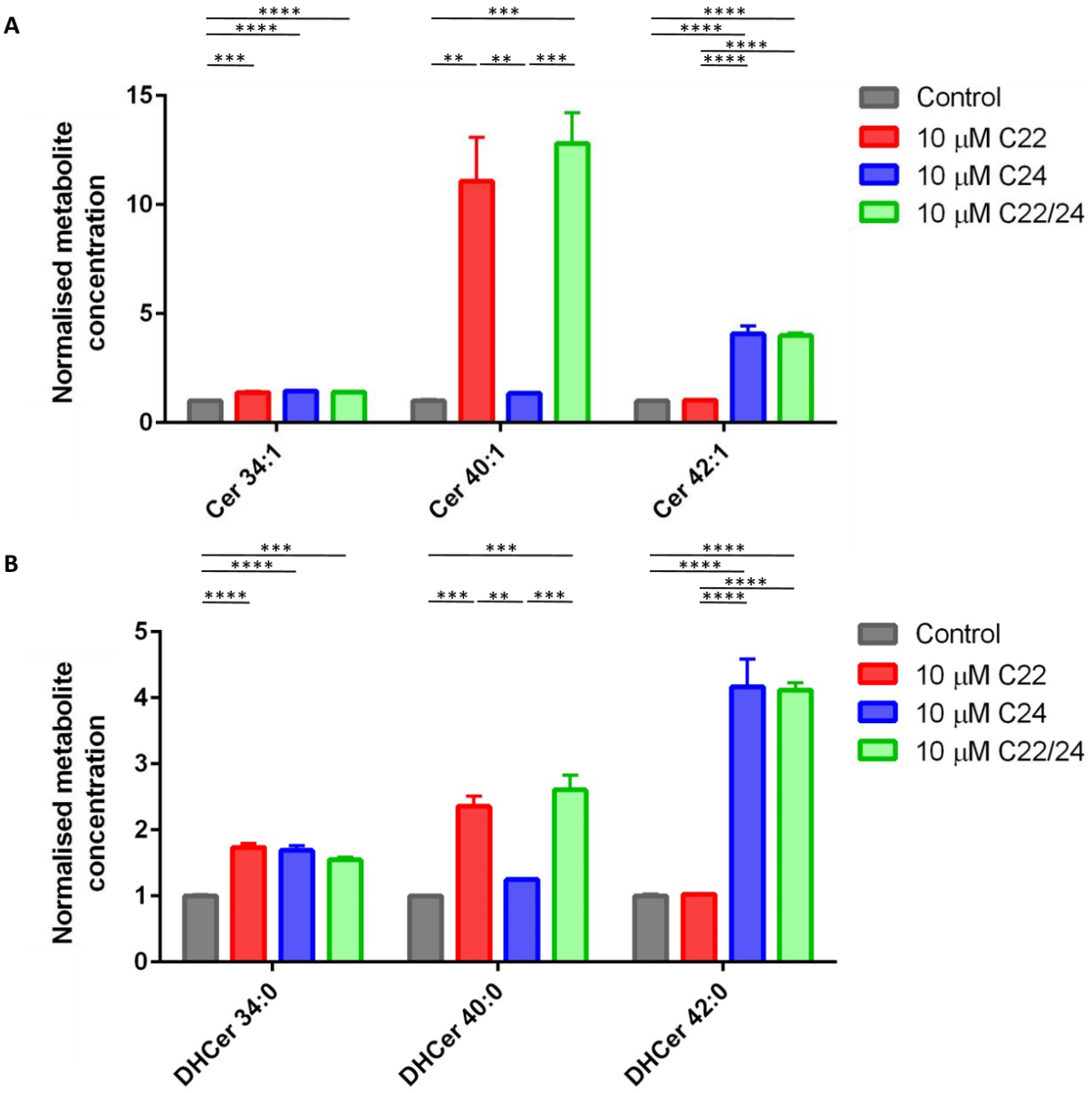

Figure 6.7: Long chain ceramides increase intracellular concentrations of ceramides and dihydroceramides in C2C12 myotubes

C2C12 myoblasts were differentiated for 6 days. During the final 10 hours, myotubes were treated with either 10 μM C22:0 ceramide, 10 μM C24:0 ceramide, a combination of both, or the vehicle control. (A) Ceramides and (B) dihydroceramides were analysed by liquid chromatography-mass spectrometry. Species were analysed using a one-way ANOVA with Tukey's multiple comparison test. * $P \leq 0.05$, ** $P < 0.01$, *** $P < 0.001$, **** $P < 0.0001$. Data are expressed as mean ± SEM (n = 3).

Experiments were repeated in primary HSkMCs to confirm results are consistent between models. HSkMCs were treated with either 10 µM C22 ceramide (40:1), 10 µM C24 ceramide (42:1), a combination of the both, or the ethanol/dodecane (98:2) vehicle for the final 10 hours of a 6-day differentiation period. Metabolites were extracted using a modified Bligh and Dyer method, and the organic phase was analysed using LC-MS. Peaks were normalised to a relevant internal standard and cell number. As observed in C2C12 myotubes, treatment with either C22 or C24 ceramide increased the concentrations of ceramide 40:1 and 42:1, respectively, while combined treatment increased both the ceramides (**Figure 6.8A**). However, ceramide 34:1 was largely unaffected, and C24 ceramide in fact decreased concentrations of ceramide 34:1.

Changes in dihydroceramide 40:0 were also analogous to results observed in C2C12 myotubes (**Figure 6.8B**). However, dihydroceramide 34:0 was unaffected by ceramide treatment, while dihydroceramide 42:0 was only increased by combined C22 and C24 ceramide treatment. These results show that ceramide treatment of both murine and primary human myocytes increase not only ceramide but also concentrations of dihydroceramides, a set of sphingolipids that are normally considered as ceramide precursors in *de novo* synthesis.

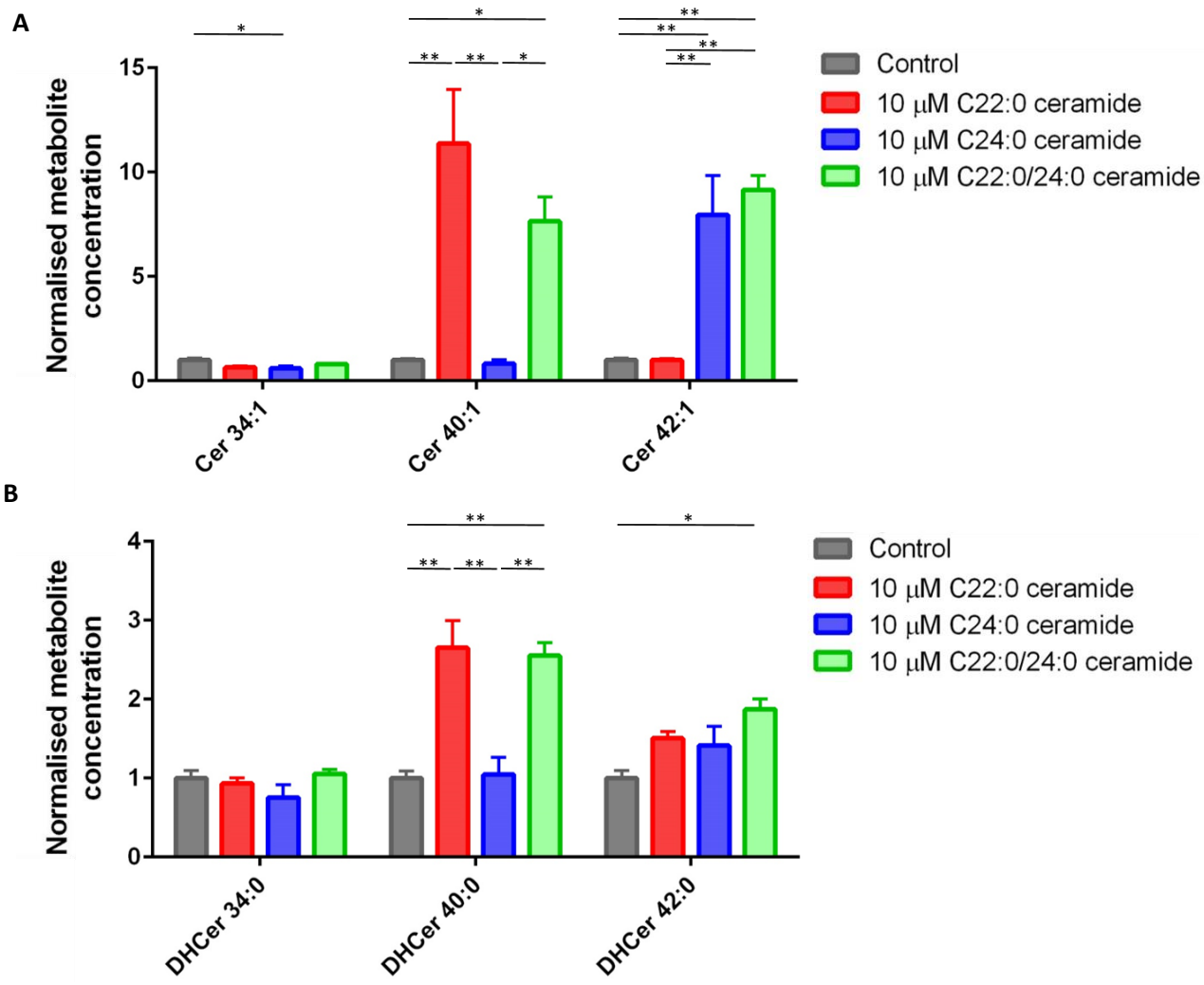

Figure 6.8: Long chain ceramides increase intracellular concentrations of ceramides and dihydroceramides in primary human skeletal myocytes

Primary human skeletal muscle cells were differentiated for 6 days. During the final 10 hours, myotubes were treated with either 10 μM C22:0 ceramide, 10 μM C24:0 ceramide, a combination of both, or the vehicle control. (A) Ceramides and (B) dihydroceramides were analysed by liquid chromatography-mass spectrometry. Species were analysed using a one-way ANOVA with Tukey's multiple comparison test. * $P \leq 0.05$, ** $P < 0.01$, *** $P < 0.001$, **** $P < 0.0001$. Data are expressed as mean ± SEM (n = 3).

Recent work has demonstrated a role for dihydroceramide accumulation in the induction of ER stress. Inhibition of dihydroceramide desaturase in a gastric carcinoma cell line led to the accumulation of dihydroceramides, concomitant with cell cycle arrest and the induction of ER stress [370]. Furthermore, an increase in the dihydroceramide:ceramide ratio increases ER stress and apoptosis in glioma cells [371]. To investigate if dihydroceramides may mediate lipid-induced ER stress, C2C12 cells were grown to confluence and differentiated for 6 days,

during which they were treated with either 200 µM palmitate or the vehicle control. For the final 24 hours, cells were co-cultured with either 5 µM Fenretinide, an inhibitor of dihydroceramide desaturase, or the DMSO vehicle control. Cells were harvested and metabolites were extracted using a modified Bligh and Dyer method. Peaks were normalised to a relevant internal standard and cell number. RNA was also collected, and the induction of ER stress assessed using RT-qPCR.

LC-MS analysis demonstrated that Fenretinide treatment slightly reduced palmitate-induced increases of ceramide 34:1 and 42:1, while ceramide 40:1 was unchanged (**Figure 6.9A**). Concentrations of dihydroceramide 34:0, 40:0 42:0, however, were greatly increased, highlighting effective inhibition of dihydroceramide desaturase (**Figure 6.9B**). This inhibition also increased palmitate-induced levels of *Atf3* (10-fold compared to palmitate-treated cells), *Atf4* (1.7-fold compared to palmitate-treated cells) and *Hspa5* (3.1-fold compared to palmitate-treated cells), although *Edem1* expression was unaffected (**Figure 6.9C**). These results implicate dihydroceramides in mediating palmitate-induced ER stress, and suggest that increases in dihydroceramides following exogenous ceramide treatment may have mechanistic importance.

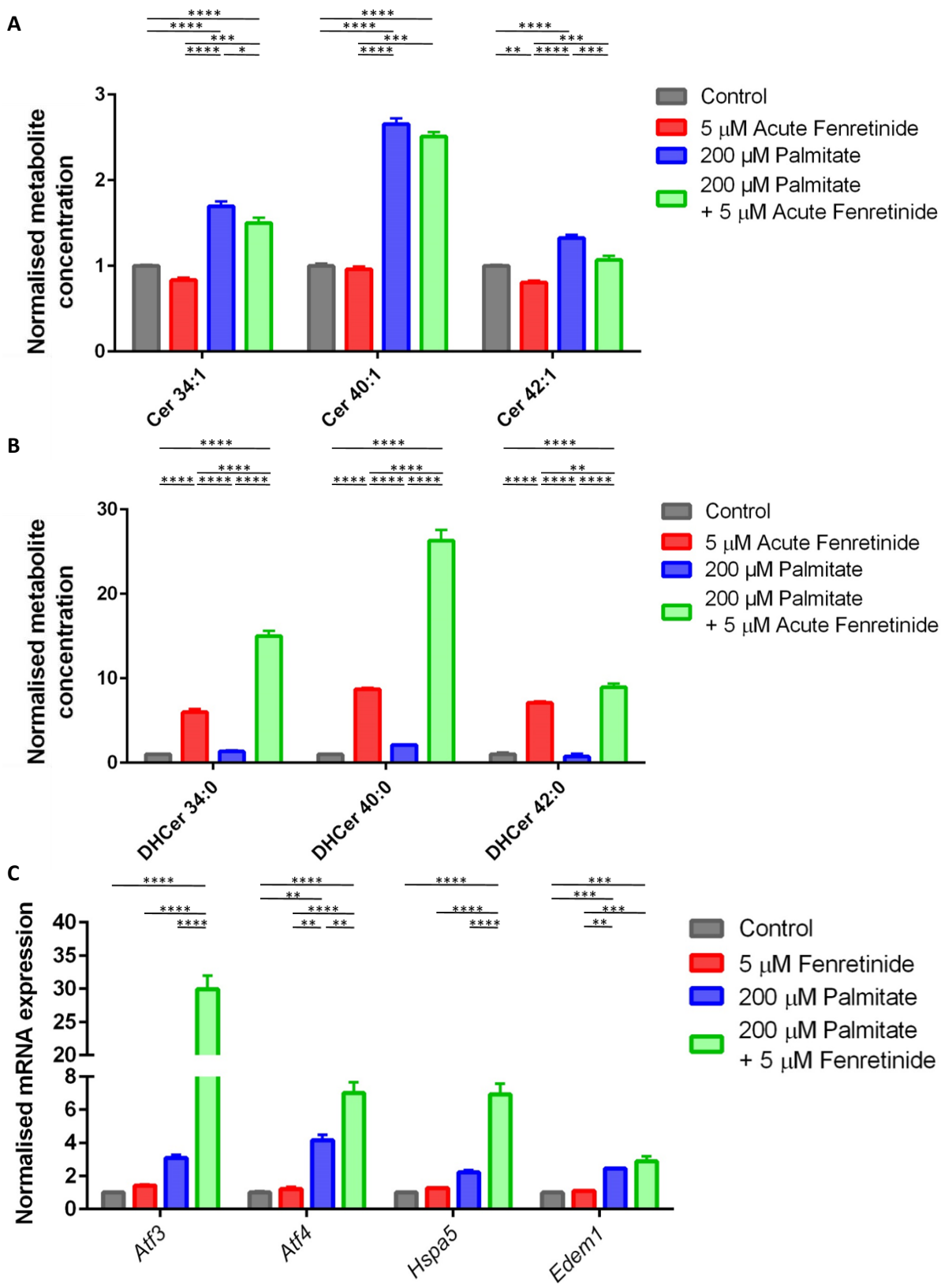

Figure 6.9: Inhibition of dihydroceramide desaturase increases concentrations of dihydroceramides and exacerbates palmitate-induced ER stress

C2C12 myoblasts were treated with 200 μM palmitate or the vehicle control during a 6-day differentiation period. During the final 24 hours, myotubes were treated with either 5 μM Fenretinide, or the vehicle control. (A) Ceramides and (B) dihydroceramides were analysed by liquid chromatography-mass spectrometry. (C) Induction of ER stress was analysed by RT-qPCR of a UPR gene panel (*Atf3*, *Atf4*, *Hspa5* and *Edem1*). Species were analysed using a one-way ANOVA with Tukey's multiple comparison test. * $P \leq 0.05$, ** $P < 0.01$, *** $P < 0.001$, **** $P < 0.0001$. Data are expressed as mean ± SEM (n = 3).

6.4.6 Conditioned media from palmitate-treated myocytes activates ER stress in AML-12 hepatocytes

This chapter has focused on the identification of ceramides, packaged in exosomes, as cell non-autonomous signals that propagate ER stress activation. However, all experiments have considered ceramides as paracrine mediators, increasing UPR signalling in neighbouring skeletal myocytes. Yet, ceramides 40:1 and 42:2, were both increased in the plasma of mice fed a high-fat diet, suggesting that ceramides may be endocrine signalling compounds. Therefore, we hypothesised that conditioned media derived from skeletal myocytes could activate ER stress in other tissue types. To investigate this, conditioned media was collected from C2C12 myotubes treated chronically with either 200 µM palmitate or the BSA vehicle control, as previously described. This conditioned media was then transferred on to untreated AML-12 hepatocytes, and the induction of ER stress assessed using RT-qPCR. Conditioned media from myotubes treated with palmitate increased expression of *Atf3* (2.7-fold), *Atf4* (4-fold), *Hspa5* (1.9-fold), and *Edem1* (1.2-fold), indicating the induction of ER stress (**Figure 6.10**). These results show that secreted factors from stressed myotubes can induce ER stress in cell types of distal tissues. While the nature of this signal is not clear, it is feasible that long chain ceramides may also induce ER stress in hepatocytes and, therefore, have the capacity to act as endocrine signals.

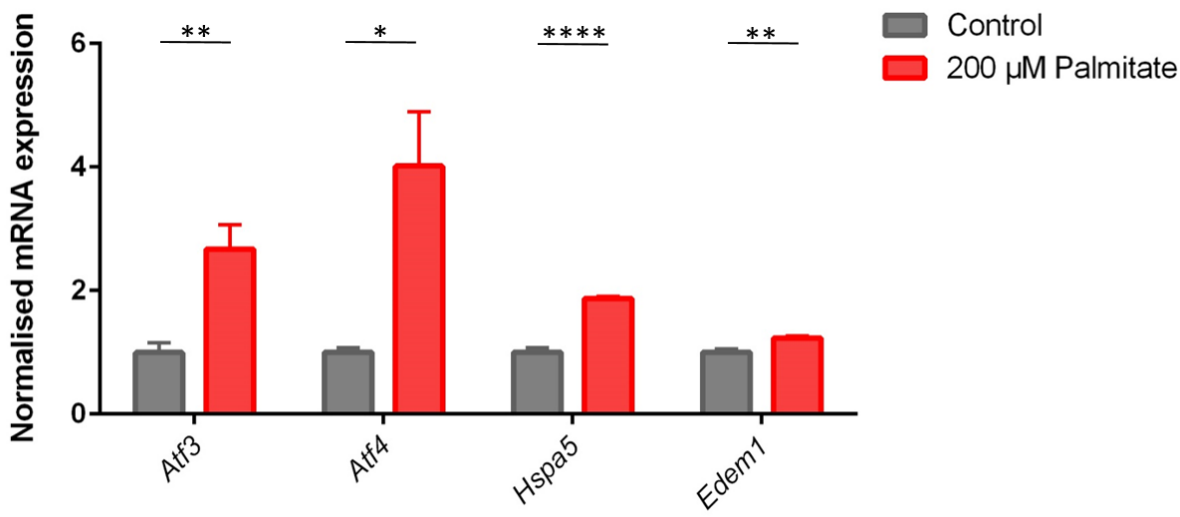

Figure 6.10: Conditioned media from palmitate-treated C2C12 myotubes induces ER stress in untreated AML-12 hepatocytes

C2C12 cells were treated with 200 µM palmitate or the BSA vehicle control during a 6-day differentiation period. Subsequently, media was switched to serum-free media for 24 hours. This conditioned media was then transferred to untreated AML-12 hepatocytes for 10 hours and RT-qPCR was used to analyse the expression of key unfolded protein response genes (*Atf3*, *Atf4*, *Hspa5* and *Edem1*). Each gene was analysed using a one-way ANOVA with Tukey's multiple comparison test. * $P \leq 0.05$, ** $P < 0.01$, *** $P < 0.001$, **** $P < 0.0001$. Data are expressed as mean ± SEM (n = 4).

6.5 Discussion

This chapter aimed to improve mechanistic understanding of ceramide-mediated intercellular propagation of ER stress signalling. Co-treating myotubes with palmitate and inhibitors of ceramide synthase or SPT reduced ceramide concentrations, indicating that chronic palmitate-stimulated synthesis of ceramides is via the *de novo* pathway. This is in line with previous work using acute models of palmitate exposure, which resulted in an increase in flux through SPT [354]. Here, however, palmitate treatment increased expression of *Cers2*, a ceramide synthase isoform that preferentially incorporates long-chain acyl chains, providing an additional level of regulation in the *de novo* pathway. Previous work has highlighted that acute palmitate also stimulates the transcription of *Cers2* in myotubes [358]. The importance of Cers2 in the development of insulin resistance has been questioned, with one study showing that haploinsufficiency for Cers2 increased susceptibility to diet-induced insulin resistance in mice as a result of compensatory increases in C16 ceramide [372]. While this study suggested that Cers6-generated C16 ceramide is important in the dysregulation of insulin signalling, overexpression of *Cers6* in myotubes improved insulin sensitivity in another study [373]. These contradictory results show the difficulty in studying ceramide synthase isoforms, namely due to compensatory changes following genetic ablation. The effects of altering ceramide concentrations are likely to be context-dependent, and more nuanced models, such as tissue-specific and inducible genetic knockout mice, may be required to understand the importance of specific ceramide synthase isoforms in dyslipidaemia and the development of insulin resistance.

The poor solubility of ceramides in water suggested the need for effective packaging of the sphingolipids for extracellular transport a paracrine signal. Exosomes purified from conditioned media were enriched in ceramides, providing a mechanism of transport between cells. Our understanding of the importance of exosomes in cell-cell signalling has increased greatly in recent years, with their role in transporting cargo including proteins, lipids and nucleic acids well-documented [362,374,375]. Inhibition of neutral sphingomyelinase in Oli-neu cells reduced exosome secretion, demonstrating an important role for ceramides in exosome release [367]. Furthermore, exosomes enriched in C16 and C24 ceramide were shown to mediate Tnfα-induced cell death in human oligodendroglioma cells [376]. The results in this chapter, in combination with previous work, highlight the importance of ceramides in both exosome biogenesis and signalling.

Ceramide-enriched exosomes were also secreted from hepatocytes treated with palmitate, capable of increasing macrophage chemotaxis [363]. Both exosome secretion and ceramide concentrations were reduced in hepatocytes derived from IRE1-null mice, showing an interaction between exosome signalling and ER stress. However, this study showed that exosomes were enriched in C16 ceramide, rather than longer chain species, suggesting tissue-differences in the regulation of ceramide synthesis. The importance of C16 ceramide is well-documented in development of insulin resistance in the liver and adipose tissue [377]. However, a role for C16 ceramide is less convincing in skeletal muscle, supported by results in this thesis. Future work should focus on understanding if longer chain ceramides in skeletal muscle function in an analogous manner to C16 ceramide in other insulin-sensitive tissues, or if ceramide signalling is chain length specific.

With previous work showing the importance of ceramide-enriched exosomes in the liver microenvironment, the potential for myocyte-derived exosomes isolated in this chapter to function in an endocrine manner should be pursued in further research. Indeed, results from this chapter showed that conditioned media from palmitate-treated myotubes could induce ER stress in AML-12 hepatocytes, showing that a myotube-derived signal could act on different cell types. Although the nature of this signal is unclear, possible candidates include the long chain ceramides enriched in exosomes. Previous studies have suggested a role for ceramides in saturated fatty acid-induced ER stress in the liver, strengthening this hypothesis [378].

The importance of ER stress in skeletal muscle lipid-induced insulin resistance has been debated [258,259,379]. However, in this chapter, inhibition of Perk activity decreased concentrations of long-chain ceramides. With strong evidence supporting a role for ceramides in the development of insulin resistance, this data suggests a novel mechanistic link between increased ER stress and insulin sensitivity [58,380]. These results should be followed up using siRNA-mediated knockdown of Perk to confirm that decreases in ceramides are not an off-target effect of the inhibitor. Experiments should also probe the mechanism between Perk and ceramide synthesis. Ceramide 34:1 concentrations were unaffected by inhibition of Perk, suggesting a mechanism focusing on ceramide synthase 2, which specifically incorporates longer chain acyl-CoA moieties into ceramides [355].

Preliminary work to isolate the mechanism underpinning ceramide-induced ER stress focused on the role of dihydroceramides, which increased following exogenous ceramide treatment.

Inhibition of dihydroceramide desaturase 1 (Des1) increased the dihydroceramide:ceramide ratio, and activated ER stress. A role for dihydroceramide accumulation in ER stress has also been reported in gastric carcinoma cells [370]. However, conversion of ceramide to dihydroceramide has previously not been reported, and experiments should focus on understanding whether the increases in dihydroceramides result from increases in sphingosine via the salvage pathway or reverse activity of Des1. Mitigating these results is the evidence supporting inhibition of Des1 as a therapeutic intervention in metabolic disease, in which Fenretinide improved ameliorated lipid-induced insulin resistance in cultured myotubes and mice fed a high-fat diet [381,382]. Much work is required to delineate the importance of dihydroceramides in ER stress induction, including siRNA knockdown of Des1 to rule out potential drug-induced ER stress.

Conclusion

Experiments in this chapter have shown that palmitate-stimulated synthesis of ceramides is via the *de novo* pathway, in part due to an increase in expression of *Cers2*. This synthesis was reduced following inhibition of the Perk arm of the UPR, implicating ER stress in the regulation of lipotoxic mediators. Exosomes purified from the conditioned media of palmitate-treated myotubes were enriched with long chain ceramides, providing a mechanism for ceramide secretion. Conditioned media transfer on to hepatocytes indicates the presence of potential endocrine mediators of UPR activation.

Chapter 7

Summary and Discussion

7.1 General Discussion

The increase in the number of individuals with T2DM places a strain on global healthcare systems. To develop improved therapeutic approaches for this growing epidemic, we need to better understand the mechanisms underpinning the aetiology of metabolic dysfunction in T2DM. Obesity is the leading independent risk factor. Recently circulating FFA-induced endoplasmic reticulum stress has emerged as a mechanism linking obesity-mediated dyslipidaemia with the development of insulin resistance [40,57]. This thesis sought to use lipidomic tools to profile metabolic perturbations linking palmitate-induced lipotoxicity to ER stress in skeletal muscle [276].

This thesis compared acute models of palmitate-induced ER stress, typically favoured in the literature [54,103,257–260], with a chronic palmitate exposure model developed in C2C12 myotubes. The chronic model demonstrated greater metabolic disruption in a background of UPR activation more reflective of *in vivo* scenario [275]. In particular, chronic palmitate stimulated catabolism of PUFA-containing PCs in a cPLA2-dependent manner, a metabolic signature that translated to *in vivo* models of obesity and the clinic. While similar correlations between PUFA-containing PCs and insulin resistance had previously been documented in human studies [292], this work suggests palmitate as a driver of this process.

Little previous research has focused on the functional consequences of palmitate-induced phospholipid remodelling within skeletal muscle. The enhanced catabolism of PCs following palmitate exposure is likely to have a profound effect on membrane properties such as fluidity, but this thesis hypothesised that phospholipid remodelling would also provide an increase in free PUFAs as a substrate for bioactive eicosanoid synthesis and inflammatory signalling [294]. The importance of myocyte-derived eicosanoids in metabolic disease is under-investigated. Here, a targeted LC-MS/MS method was employed to profile an array of eicosanoids. The results suggested that myocytes predominantly synthesise and secrete

lipoxygenase-derived eicosanoids, and their release was increased in response to both acute and chronic palmitate exposure. Pharmacological inhibition of 15-LOX in both C2C12 myotubes and primary HSkMCs amplified expression of key inflammatory cytokines *Ccl2* and *Il6*, which suggests a role for 15-LOX-derived eicosanoids in the control of inflammatory cytokine synthesis. Previous studies have also shown a role for eicosanoids in the promotion of inflammation and insulin resistance. Treatment of myotubes with LTB4 increased inflammatory signalling and reduced insulin-stimulated glucose uptake, while inhibition of the LTB4 receptor protected mice from insulin resistance [311]. 12-LOX-KO mice were protected from high-fat diet-induced increases in inflammatory cytokine concentrations in adipose tissue, while markers of insulin sensitivity were increased in skeletal muscle [296]. Similarly, treating adipocytes with LOX-derived 12-HETE increased expression of inflammatory cytokines [383]. However, results from this thesis suggest 15-LOX-derived eicosanoids restrict the synthesis of inflammatory cytokines, acting to fine-tune the inflammatory response stimulated by palmitate. This is the first demonstration that skeletal muscle-derived eicosanoids may be beneficial to metabolic-associated inflammation. With previous studies emphasising 5- and 12-LOX derived eicosanoids in the development of inflammation and insulin resistance, results here suggest an alternative subset of metabolically-beneficial eicosanoids. Therefore, increasing the activity of 15-LOX, or treatment with 15-LOX products, may reduce palmitate-induced inflammation in skeletal muscle, a mechanism well described for the development of insulin resistance [299].

Chronic low-grade inflammation, typified by enhanced tissue macrophage infiltration, is a hallmark of the metabolic syndrome [91,254]. This thesis further investigated the interaction between palmitate-exposed myotubes and macrophages in the setting of enhanced eicosanoid signalling. Previously, conditioned media transfer experiments had suggested that palmitate-treated myocytes secrete signals capable of increasing macrophage activation [321]. This thesis sought to better understand bi-directional signalling by employing a co-culture system. Myotubes chronically treated with palmitate signalled to increase macrophage activation. The use of serum-free media ensured that these effects were independent of palmitate itself, and instead were a result of secreted factors from the myotubes. However, pharmacological inhibition of either cPLA2, 12-LOX or 15-LOX did not dampen the expression of these markers, suggesting that the effects on macrophage activation are likely to be independent of eicosanoids.

Instead, myocyte-derived eicosanoids appear important in the transmission of ER stress from myotubes to macrophages. Co-culture of palmitate-treated myotubes with macrophages increased macrophage expression of UPR target genes, and this response was attenuated with inhibition of cPLA2. While a role for eicosanoids in the regulation of ER stress has been shown previously [297], as far as the author is aware, this thesis is the first to suggest they function in propagating the activation of the UPR between different cell types. Here, inhibition of 12- and 15-LOX did not impact on the propagation of ER stress, suggesting that an alternative subset of eicosanoids, or a separate cPLA2-dependent product such as lysophosphatidylcholines, are involved in this signalling. The consequences of this activation of the UPR are unclear, but literature suggests ER stress can impact on both the polarisation and function of macrophages [384].

Using the co-culture system, the reciprocal assessment of bi-directional crosstalk between myotubes and macrophages was explored. RT-qPCR profiling of C2C12 myotubes subsequent to co-culture showed no difference in UPR target gene expression in response to palmitate. This suggests that macrophage-derived factors may facilitate the suppression of ER stress in skeletal muscle. While the results are preliminary, this could have interesting implications for our understanding of the role the immune system plays in the metabolic syndrome. The importance of macrophage activation in this process also warrants further investigation.

This thesis also highlighted eicosanoid lipids as regulators of UPR signalling in myotube monocultures. Inhibition of 12-LOX exacerbated palmitate-induced ER stress in myotubes, suggesting a role for this subset of eicosanoids in the control of skeletal muscle UPR activation. This is in apparent disagreement with previous literature showing that inhibition of 12-LOX ameliorates chemical-induced ER stress in adipocytes [326]. However, the study by Cole and colleagues utilised both different tissue types and different inducers of ER stress, making comparisons difficult. Furthermore, they also show an increase in the expression of *Hspa5* and *Atf4* in 12-LOX-KO mice, in line with the results of this thesis. A possible role for eicosanoids in the regulation of ER stress has been suggested in other papers as well, namely with the demonstration that pharmacological inhibition of 5-LOX reduces lipid-induced ER stress in C2C12 myotubes [297]. However, this is the first demonstration that a subset of eicosanoid species may function to ameliorate UPR activation. By increasing the activity of 12-LOX or by isolating specific 12-LOX-derived species, it may be possible to reduce the induction of ER stress. These results provided functional validation for not only alterations in

eicosanoid secretion but also remodelling of phospholipids observed within *in vitro* and *in vivo* models of metabolic disease. In addition to a pivotal role in inflammatory signalling, these investigations show myocyte-derived eicosanoids are important in the control of ER stress, providing a novel insight into the regulation of UPR activation by lipid mediators.

Furthermore, this thesis identified the first cell non-autonomous signal functioning in cell-cell activation of the UPR (**Figure 7.1**) [146]. Conditioned media from palmitate-treated myotubes induced ER stress in untreated myotubes, indicating the presence of a signal-molecule. This induction was unaffected by boiling of the media, suggesting the signal was likely to be non-protein. LC-MS lipidomic profiling of the media identified candidate signals, and long-chain ceramides were observed to be paracrine/autocrine mediators of ER stress. These results also translated to primary HSkMCs, suggesting a conserved mechanism in human cells. These results build on previous studies that suggested the presence of cell non-autonomous signals in UPR regulation [150]. A recent study demonstrated retromer-dependent Wnt signalling in the cell non-autonomous regulation of the mitochondrial unfolded protein response in *C. elegans*, a pathway activated in response to an accumulation of unfolded proteins in the mitochondria [385,386]. However, this thesis is the first to show the importance of lipid, rather than protein, signalling in the cell non-autonomous regulation of ER stress activation. Previous studies have emphasised the correlation between plasma ceramide concentrations, insulin resistance and metabolic disease [72,387,388]. Furthermore, ceramides contained within LDL have been shown to target skeletal muscle and promote insulin resistance, showing the capacity for circulating ceramides to elicit signalling changes within myocytes [389]. The results in this thesis, providing the first identification of a cell non-autonomous signal, are crucial for our understanding of protein homeostasis and suggest that a cell autonomous viewpoint of ER stress is insufficient. Furthermore, these results place ceramides at the centre of lipotoxicity and the control of ER stress in metabolic disease.

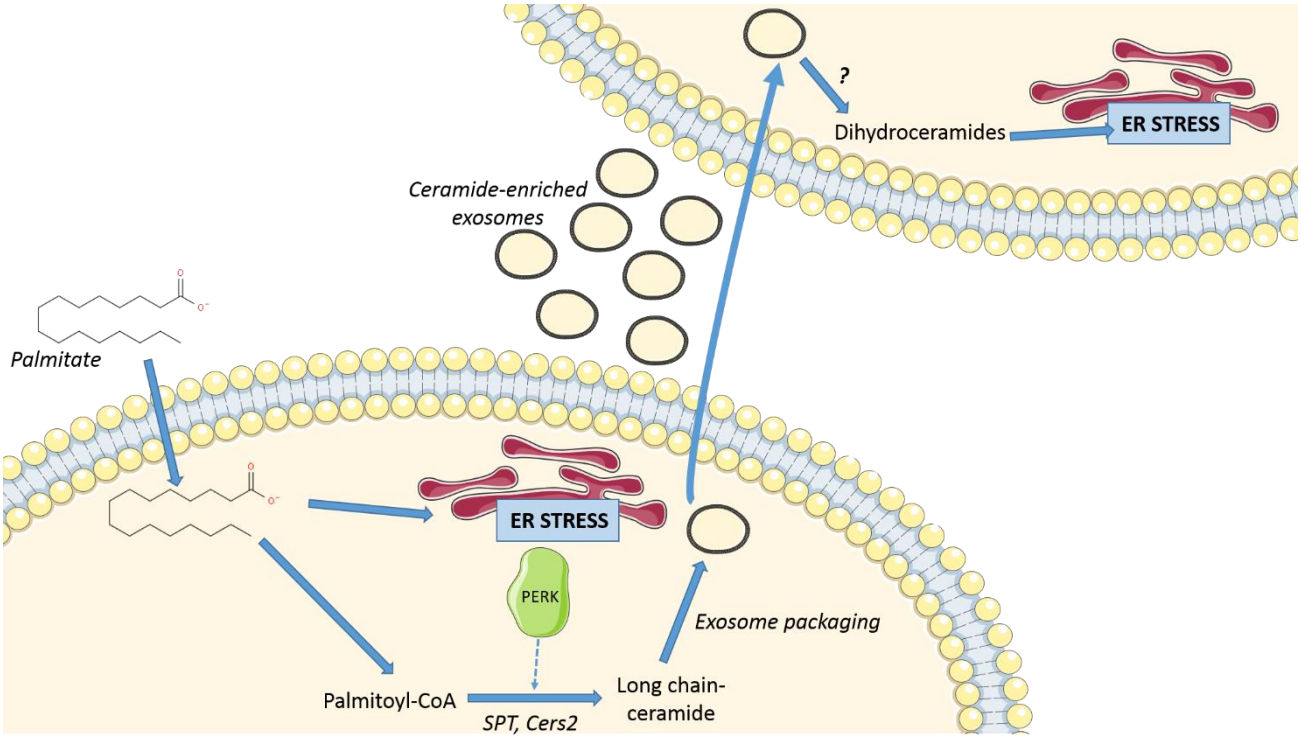

Figure 7.1 Long chain ceramides are cell non-autonomous signals that propagate endoplasmic reticulum stress between myocytes

Exogenous palmitate induces endoplasmic reticulum (ER) stress in myocytes. This includes the activation of the PERK arm of the unfolded protein response, which enhances *de novo* synthesis of long-chain ceramides from palmitoyl-CoA. Ceramides are then packaged into exosomes and secreted from the cell of synthesis. Uptake of ceramide-enriched exosomes stimulates the synthesis of dihydroceramides and the induction of ER stress [405].

Long chain ceramides were also increased in the skeletal muscle of *in vivo* models of obesity and T2DM analysed in this thesis. In particular, a western diet-fed mouse model best reflected the effects of palmitate in culture, while the high-fat diet mouse studies proved inconsistent. Phospholipid remodelling was similarly inconsistent in mice fed a high fat diet, but western diet-fed mice exhibited the PC catabolism observed *in* vitro. The reasons underpinning this observation are unclear but are likely to reflect differences in the diet and whole-body physiology. The western diet is high in sucrose, as well as fat, and mice fed this diet have increased *de novo* lipogenesis (DNL) [291]. With palmitate the major product of DNL, western diet-fed mice may be exposed to more palmitate than mice fed a high fat diet. Furthermore, previous work has shown that palmitate deriving from DNL is more hepatotoxic than dietary palmitate [390]. This toxicity difference may also be important in skeletal muscle metabolism, explaining differences observed between the western diet and

high-fat diet murine studies. These results raise questions with regards to *in vivo* dietary models of obesity. Results not only differed between the studies using a western diet and those using a high fat diet, but also between the two high fat diets. There were profound differences between the two high fat diets, including proportions of protein and carbohydrate. Furthermore, the source of fat in diet F3282 was lard, while fat content in D12492 derived from both lard and soybean oil. This is likely to lead to differences in the fatty acid profile of each diet, clearly impacting on the mouse lipidome. A standardised high fat diet, and associated protocols such as duration of feeding, would help comparisons between different studies both within the same research group and across separate groups [391]. Furthermore, as our mechanistic knowledge of diet, obesity and insulin resistance improves, we can tailor the composition of the high fat diet to optimise the induction of metabolic pathologies. Previous studies have highlighted the benefits of using a western diet compared to a high-fat diet for mouse models of insulin resistance, lipid metabolic dysfunction and contractile dysfunction, suggesting that future studies could focus on this dietary intervention [278,392].

With the identification of ceramides as secreted signals, questions remained about the mechanism of cell-cell transport. The poor aqueous solubility of ceramides suggested a requirement for a vehicle. Exosomes have emerged as important mediators of paracrine and endocrine signalling [362]. Here, purified exosomes from the media of palmitate-treated cells were enriched in long chain ceramides. Treating myotubes with these exosomes increased the expression of UPR target genes, suggesting exosomes function as the extracellular vehicle for ceramides. These results are consistent with the demonstration that palmitate treatment of hepatocytes increased the secretion of ceramide-enriched exosomes [363]. However, the ceramide-content of exosomes has canonically been viewed as secretion mechanism, especially since inhibition of neutral sphingomyelinase 2 prevents the release of exosomes in an oligodendroglial cell line [367]. Research has predominantly focused on the protein and RNA content of exosomes, but the results of this thesis highlight the importance of exosome lipid composition in cell-cell communication [366]. Exosomal-dependent lipid signalling may represent an important mechanism underpinning the progression of metabolic disease, requiring the focus of future research.

Lipidomic tools were employed to investigate the mechanism by which exogenous ceramide enhanced ER stress. LC-MS profiling of ceramide-treated cells showed an increase in dihydroceramides, canonically viewed as precursors to ceramides in the *de novo* synthesis pathway [364]. Previous literature has suggested a role for dihydroceramide accumulation in ER

stress [370]. Here, inhibition of dihydroceramide desaturase increased dihydroceramide concentrations concomitant with the exacerbation of palmitate-induced ER stress, suggesting a similar mechanism. The means by which dihydroceramides may activate UPR signalling is unclear, but may relate to alterations in membrane structure [393,394]. Conversely, inhibition of dihydroceramide desaturase also inhibits lipid-induced insulin resistance in murine models of obesity, while knockdown of dihydroceramide desaturase ameliorated palmitate-induced ER stress in C2C12 myotubes [381]. This appears contrary to a role for dihydroceramides in the activation of the UPR, given the mechanistic links between ER stress and the development of insulin resistance [154]. Further work is required to understand the importance of dihydroceramides in palmitate-induced ER stress, and the consequences for insulin sensitivity.

7.2 Future Directions

The results of this thesis may be expanded upon in a number of ways. **Chapter 4** showed lipoxygenase-derived eicosanoids signal in the regulation of skeletal muscle ER stress. Knockdown of lipoxygenase isoforms with siRNA would complement the use of pharmacological inhibitors, and confirm that the exacerbation of palmitate-induced ER stress is not a result of off-target drug effects. Further work should then focus on the identification of important eicosanoid species that drive the signalling events observed. The effects of candidate eicosanoids could be interrogated with the induction of ER stress profiled transcriptionally using a method similar to that in **Chapter 5**. Eicosanoids predominantly stimulate intracellular signalling by binding to G protein-coupled receptors (GPCRs) [395]. Therefore, the effects of individual species could be confirmed by ablating receptor function or using a high throughput GPCR-reporter linked screen [396,397].

Furthermore, the results of macrophage co-culture with myotubes in **Chapter 4** could also be developed. In this thesis, macrophage activation was assessed using transcriptional markers. This analysis, would be complemented by flow cytometry-based cell sorting using protein markers such as CD64, CD80, CD11 and CD209 [398]. Not only would this provide a more detailed assessment of macrophage activation, but the technique would also provide information on single-cell macrophage phenotypes. Co-cultured macrophages exhibited increased expression of both M1 and M2 markers. Flow cytometry would help ascertain if a mixed population of cells were present or if these increases represented an alternative

macrophage activation state. Flow cytometry work should also be combined with metabolic phenotyping of macrophages. For example, M1 macrophages are characterised by elevated glycolysis, while M2 macrophages have increased fatty acid β-oxidation and arginase-driven production of ornithine [399].

Chapter 4 demonstrated that macrophages suppress palmitate-induced ER stress in C2C12 myotubes. Future work should confirm this observation in an experiment using palmitate treatment of myotubes with and without co-cultured macrophages. In such an experiment, myotubes would be treated chronically with palmitate or the BSA vehicle, as described throughout this thesis. For the final 24 hours, media would be switched to serum-free media and half of the replicates in each treatment group co-cultured with macrophages, while the other half would be macrophage-free. Comparisons between the treatment groups would highlight any protective effect of macrophage co-culture on the activation of myotube UPR signalling. Furthermore, it is important that experiments are extended in to human primary tissue cultures to confirm this is not an artefact of immortalised murine cell lines. An improved characterisation of macrophage phenotypes will aid in the identification of mechanisms underpinning the macrophage-mediated suppression of ER stress – namely if macrophage phenotype affects their capacity to ameliorate myotube stress. If macrophage activation does influence this process, experiments could focus on manipulating macrophages *in vivo* using candidate signal-derived treatments and assess the impact on diet-induced ER stress in murine models of obesity. The impact on insulin sensitivity and glucose homeostasis should also be considered. This is a potentially interesting field of research with little or no literature suggesting a role for macrophages in the control of UPR signalling in peripheral tissues.

Chapter 5 identified the first paracrine mediator of ER stress [146]. To conclusively confirm long chain ceramides as a paracrine mediator of ER stress, conditioned media transfer experiments should use media from cells co-treated with palmitate and an inhibitor of ceramide synthesis, such as myriocin, which should show ameliorated induction of ER stress. This pharmacological approach could also be complemented with siRNA knockdown of ceramide synthase 2, allowing for the investigation specifically of long chain ceramides. This method was recently employed in the investigation of long-chain ceramides in cardiomyocyte lipotoxicity [357]. However, previous literature has shown that knockdown of ceramide synthase isoforms is compensated for with upregulation of alternative isoforms [400]. Future experiments should also seek to confirm ceramides as paracrine mediators *in vivo*. This could

be achieved by treating mice with ceramide species, but this is complicated by the solubility of ceramides, preventing their introduction via drinking water or injection without a toxic vector. Instead, a short-chain ceramide analogue has been used in previous studies, which is rapidly converted into more physiological ceramides [344,401].

Experiments in this thesis have predominantly focused on the metabolic consequences of lipotoxicity and ceramide signalling in skeletal muscle. However, previous studies have highlighted the importance of ceramides for the development of insulin resistance and metabolic dysfunction in other tissue types, including adipose and liver. Indeed, overexpression of hepatic acid ceramidase, which catalyses the breakdown of ceramides, prevents hepatic steatosis and improves insulin sensitivity in both the liver and adipose tissue [402]. These results implicate ceramides in the progression of metabolic disease in tissues other than skeletal muscle. Further work should, therefore, seek to understand if ceramides may act as paracrine mediators within adipose and the liver as well. Indeed, hepatocytes treated with palmitate secrete ceramide-enriched extracellular vesicles [363]. However, this study highlighted an enrichment in C16 ceramide only, while synthesis was dependent on Ire1, suggesting alternative mechanisms to those uncovered in skeletal muscle within this thesis.

The identification of exosomes as a vehicle for secreted ceramides is an interesting area for further research. Understanding of the role exosomes play in cell-cell signalling is improving but the mechanisms relating to their release and uptake are poorly described. Previous work has suggested a role for ceramides in exosome budding, but this is via neutral sphingomyelinase, a member of the salvage pathway [367]. This thesis demonstrates that ceramides synthesised via the *de novo* pathway go on to induce ER stress, suggesting an alternative mechanism. Proteomic profiling of both myotubes and purified exosomes may provide an insight into mediators of exosome release, tissue targeting and uptake. Once mechanisms are identified, the role ceramide enriched exosomes play in whole body glucose homeostasis and dyslipidaemia can be investigated via pharmacological inhibition or genetic ablation of key mediators.

Inhibition of Perk reduced concentrations of long chain ceramides following exposure of myotubes to palmitate. This identified a novel link between ER stress and the synthesis of ceramides. These results should first be confirmed using genetic ablation of this arm of the UPR, as well as translation in primary HSkMCs. Perk-dependent regulation of sphingolipid synthesis could also be pursued *in vivo* using a Perk-null mouse model, challenged with a

western diet. Using glucose uptake assays *in vitro*, and insulin tolerance tests and OGTTs *in vivo* could be used to assay the importance of Perk signalling and ceramide accumulation in the development of insulin resistance and T2DM.

Finally, the role ceramide-enriched exosomes play in endocrine signalling could be investigated. Conditioned media from palmitate-treated myotubes induced ER stress in hepatocytes, while ceramides were increased in the plasma of mice fed a high fat diet, suggesting their transport between tissues *in vivo*. Further work could employ conditioned media transfer from myotubes to other cells of interest, including adipocytes and pancreatic β-cells, followed by the profiling of UPR activation. The induction of ER stress in these tissues has important consequences in cellular pathology and dysfunctional insulin signalling. A role for long chain ceramides could then be confirmed by exposing cells to exogenous ceramide or purified exosomes. Similarly, ceramide-enriched exosomes may be important in associated pathologies of the metabolic syndrome such as endothelial dysfunction, for which ER stress represents a potential mechanism [403]. Features of dysfunctional endothelial cells in culture include increased inflammatory signalling, expression of adhesion molecules and elevated rates of apoptosis, which can then be assayed following conditioned media transfer, or treatment with ceramide-enriched exosomes [404]. Isolating and profiling exosomes in plasma collected from murine *in vivo* models of metabolic disease and clinical samples to assess ceramide enrichment would increase translation from culture experiments. Improvements in our understanding of mechanisms of exosome release and uptake could also aid in *in vivo* assessment of the role ceramide-enriched exosomes play in endocrine signalling. Once identified, use of genetic models in which constituents of pathways involved in exosome release are knocked out specifically in skeletal muscle would be important in the investigation of their biological and pathophysiological significance.

7.3 Conclusions

To conclude, this thesis employed lipidomic techniques to gain a deeper understanding of palmitate-induced ER stress and lipotoxicity in skeletal muscle and its contribution to dyslipidaemia. Combining LC-MS and GC-MS analysis with RT-qPCR of key UPR target genes demonstrated the importance of phospholipid remodelling in the production of bioactive lipid signalling molecules. In particular, chronic palmitate stimulated the breakdown of PUFA-containing PCs to generate lipoxygenase-derived eicosanoids, a metabolic phenotype also observed in skeletal muscle tissue of *in vivo* models of obesity and T2DM. The secretion of eicosanoids synthesised by lipoxygenase isoforms were increased following both acute and chronic palmitate treatment and may have important paracrine roles. Inhibition of key lipoxygenase isoforms implicated a subset of eicosanoids in the control of UPR activation in both myotubes and co-cultured macrophages, highlighting previously unknown paracrine mechanisms that may be important in lipotoxicity and the progression of metabolic disease.

Furthermore, this thesis has also identified exosome-packaged long-chain ceramides as cell non-autonomous signals propagating ER stress between myotubes. Chronic palmitate treatment increases the synthesis of ceramides via ceramide synthase 2, and the ceramides are packaged into exosomes and secreted into the culture media. Ceramides were also increased in the skeletal muscle and plasma of *in vivo* models of obesity. The Perk arm of the UPR links ER stress to the synthesis of ceramides, while the accumulation of dihydroceramides may represent a potential mechanism linking exogenous ceramides with the induction of ER stress. This work is the first identification of non-autonomous signals of its kind and has important implications for our understanding of ER stress regulation in metabolic disease.

References

1. Kaur, J. A comprehensive review on metabolic syndrome. *Cardiol. Res. Pract.* **2014,** 943162 (2014).

2. Huang, P. L. A comprehensive definition for metabolic syndrome. *Dis. Model. Mech.* **2,** 231–7 (2009).

3. Alberti, K. G. & Zimmet, P. Z. Definition, diagnosis and classification of diabetes mellitus and its complications. Part 1: diagnosis and classification of diabetes mellitus provisional report of a WHO consultation. *Diabet. Med.* **15,** 539–53 (1998).

4. International Diabetes Federation. IDF Consensus Worldwide Definition of the Metabolic Syndrome. *2006* Available at: https://www.idf.org/e-library/consensus-statements/60-idfconsensus-worldwide-definitionof-the-metabolic-syndrome.

5. Park, Y.-W. *et al.* The metabolic syndrome: prevalence and associated risk factor findings in the US population from the Third National Health and Nutrition Examination Survey, 1988-1994. *Arch. Intern. Med.* **163,** 427–36 (2003).

6. Ford, E. S., Giles, W. H. & Dietz, W. H. Prevalence of the metabolic syndrome among US adults: findings from the third National Health and Nutrition Examination Survey. *JAMA* **287,** 356–9 (2002).

7. Wilson, P. W., Kannel, W. B., Silbershatz, H. & D'Agostino, R. B. Clustering of metabolic factors and coronary heart disease. *Arch. Intern. Med.* **159,** 1104–9 (1999).

8. Patlak, M. New weapons to combat an ancient disease: treating diabetes. *FASEB J.* **16,** 1853 (2002).

9. Olokoba, A. B., Obateru, O. A. & Olokoba, L. B. Type 2 diabetes mellitus: a review of current trends. *Oman Med. J.* **27,** 269–73 (2012).

10. Hu, F. B. *et al.* Diet, Lifestyle, and the Risk of Type 2 Diabetes Mellitus in Women. *N. Engl. J. Med.* **345,** 790–797 (2001).

11. Centers for Disease Control and Prevention (CDC). Prevalence of overweight and obesity among adults with diagnosed diabetes--United States, 1988-1994 and 1999-

2002. *MMWR. Morb. Mortal. Wkly. Rep.* **53,** 1066–8 (2004).

12. Cox, M. E. & Edelman, D. Tests for Screening and Diagnosis of Type 2 Diabetes. *Clin. Diabetes* **27,** 132–138 (2009).

13. Lebovitz, H. Insulin resistance: definition and consequences. *Exp. Clin. Endocrinol. Diabetes* **109,** S135–S148 (2001).

14. Van Obberghen, E. *et al.* Surfing the insulin signaling web. *Eur. J. Clin. Invest.* **31,** 966–77 (2001).

15. Alessi, D. R. *et al.* Characterization of a 3-phosphoinositide-dependent protein kinase which phosphorylates and activates protein kinase Balpha. *Curr. Biol.* **7,** 261–9 (1997).

16. Cross, D. A. *et al.* The inhibition of glycogen synthase kinase-3 by insulin or insulin-like growth factor 1 in the rat skeletal muscle cell line L6 is blocked by wortmannin, but not by rapamycin: evidence that wortmannin blocks activation of the mitogen-activated protein kinase pathway in L6 cells between Ras and Raf. *Biochem. J.* **303 (Pt 1),** 21–6 (1994).

17. Cong, L.-N. *et al.* Physiological Role of Akt in Insulin-Stimulated Translocation of GLUT4 in Transfected Rat Adipose Cells. *Mol. Endocrinol.* **11,** 1881–1890 (1997).

18. Baumann, C. A. *et al.* CAP defines a second signalling pathway required for insulin-stimulated glucose transport. *Nature* **407,** 202–207 (2000).

19. Chiang, S.-H. *et al.* Insulin-stimulated GLUT4 translocation requires the CAP-dependent activation of TC10. *Nature* **410,** 944–948 (2001).

20. Sutherland, C., O'Brien, R. M., Granner, D. K. & Marshall, C. J. New connections in the regulation of PEPCK gene expression by insulin. *Philos. Trans. R. Soc. Lond. B. Biol. Sci.* **351,** 191–9 (1996).

21. Pilkis, S. J. & Granner, D. K. Molecular Physiology of the Regulation of Hepatic Gluconeogenesis and Glycolysis. *Annu. Rev. Physiol.* **54,** 885–909 (1992).

22. Laplante, M. & Sabatini, D. M. An Emerging Role of mTOR in Lipid Biosynthesis. *Curr. Biol.* **19,** R1046–R1052 (2009).

23. Li, S., Brown, M. S. & Goldstein, J. L. Bifurcation of insulin signaling pathway in rat liver: mTORC1 required for stimulation of lipogenesis, but not inhibition of

gluconeogenesis. *Proc. Natl. Acad. Sci.* **107,** 3441–3446 (2010).

24. Porstmann, T. *et al.* SREBP Activity Is Regulated by mTORC1 and Contributes to Akt-Dependent Cell Growth. *Cell Metab.* **8,** 224–236 (2008).

25. Dimitriadis, G., Mitrou, P., Lambadiari, V., Maratou, E. & Raptis, S. A. Insulin effects in muscle and adipose tissue. *Diabetes Res. Clin. Pract.* **93,** S52–S59 (2011).

26. Zechner, R. *et al.* FAT SIGNALS - Lipases and Lipolysis in Lipid Metabolism and Signaling. *Cell Metab.* **15,** 279–291 (2012).

27. Schweiger, M. *et al.* Adipose Triglyceride Lipase and Hormone-sensitive Lipase Are the Major Enzymes in Adipose Tissue Triacylglycerol Catabolism. *J. Biol. Chem.* **281,** 40236–40241 (2006).

28. Kralisch, S. *et al.* Isoproterenol, TNFα, and insulin downregulate adipose triglyceride lipase in 3T3-L1 adipocytes. *Mol. Cell. Endocrinol.* **240,** 43–49 (2005).

29. Kershaw, E. E. *et al.* Adipose triglyceride lipase: function, regulation by insulin, and comparison with adiponutrin. *Diabetes* **55,** 148–57 (2006).

30. Enoksson, S., Degerman, E., Hagström-Toft, E., Large, V. & Arner, P. Various phosphodiesterase subtypes mediate the in vivo antilipolytic effect of insulin on adipose tissue and skeletal muscle in man. *Diabetologia* **41,** 560–568 (1998).

31. DeFronzo, R. A. & Tripathy, D. Skeletal muscle insulin resistance is the primary defect in type 2 diabetes. *Diabetes Care* **32 Suppl 2,** S157-63 (2009).

32. Abdul-Ghani, M. A. & DeFronzo, R. A. Pathogenesis of insulin resistance in skeletal muscle. *J. Biomed. Biotechnol.* **2010,** 476279 (2010).

33. Thiebaud, D. *et al.* The effect of graded doses of insulin on total glucose uptake, glucose oxidation, and glucose storage in man. *Diabetes* **31,** 957–63 (1982).

34. DeFronzo, R. A., Gunnarsson, R., Björkman, O., Olsson, M. & Wahren, J. Effects of insulin on peripheral and splanchnic glucose metabolism in noninsulin-dependent (type II) diabetes mellitus. *J. Clin. Invest.* **76,** 149–155 (1985).

35. Reynisdottir, S. *et al.* Effects of weight reduction on the regulation of lipolysis in adipocytes of women with upper-body obesity. *Clin. Sci. (Lond).* **89,** 421–9 (1995).

36. Duncan, R. E., Ahmadian, M., Jaworski, K., Sarkadi-Nagy, E. & Sul, H. S. Regulation

of lipolysis in adipocytes. *Annu. Rev. Nutr.* **27,** 79–101 (2007).

37. Johnson, J. A., Fried, S. K., Pi-Sunyer, F. X. & Albu, J. B. Impaired insulin action in subcutaneous adipocytes from women with visceral obesity. *Am. J. Physiol. Metab.* **280,** E40–E49 (2001).

38. Albu, J. B. *et al.* Systemic resistance to the antilipolytic effect of insulin in black and white women with visceral obesity. *Am. J. Physiol.* **277,** E551-60 (1999).

39. Bergman, R. N. & Ader, M. Free fatty acids and pathogenesis of type 2 diabetes mellitus. *Trends Endocrinol. Metab.* **11,** 351–6 (2000).

40. Yazıcı, D. & Sezer, H. Insulin resistance, obesity and lipotoxicity. in *Advances in Experimental Medicine and Biology* **960,** 277–304 (Springer, Cham, 2017).

41. Unger, R. H. Lipid overload and overflow: metabolic trauma and the metabolic syndrome. *Trends Endocrinol. Metab.* **14,** 398–403 (2003).

42. Randle, P. J., Garland, P. B., Hales, C. N. & Newsholme, E. A. The glucose fatty-acid cycle. Its role in insulin sensitivity and the metabolic disturbances of diabetes mellitus. *Lancet* **1,** 785–9 (1963).

43. Griffin, M. E. *et al.* Free fatty acid-induced insulin resistance is associated with activation of protein kinase C theta and alterations in the insulin signaling cascade. *Diabetes* **48,** 1270–4 (1999).

44. Dresner, A. *et al.* Effects of free fatty acids on glucose transport and IRS-1-associated phosphatidylinositol 3-kinase activity. *J. Clin. Invest.* **103,** 253–9 (1999).

45. Roden, M. *et al.* Mechanism of free fatty acid-induced insulin resistance in humans. *J. Clin. Invest.* **97,** 2859–2865 (1996).

46. Belfort, R. *et al.* Dose-response effect of elevated plasma free fatty acid on insulin signaling. *Diabetes* **54,** 1640–8 (2005).

47. Santomauro, A. T. *et al.* Overnight lowering of free fatty acids with Acipimox improves insulin resistance and glucose tolerance in obese diabetic and nondiabetic subjects. *Diabetes* **48,** 1836–41 (1999).

48. Pilon, M. Revisiting the membrane-centric view of diabetes. *Lipids Health Dis.* **15,** 167 (2016).

49. Houten, S. M. & Wanders, R. J. A. A general introduction to the biochemistry of mitochondrial fatty acid β-oxidation. *J. Inherit. Metab. Dis.* **33,** 469–77 (2010).

50. Dennis, E. A. & Norris, P. C. Eicosanoid storm in infection and inflammation. *Nat. Rev. Immunol.* **15,** 511–23 (2015).

51. Lovejoy, J. C. Dietary fatty acids and insulin resistance. *Curr. Atheroscler. Rep.* **1,** 215–220 (1999).

52. Chavez, J. A. & Summers, S. A. Characterizing the effects of saturated fatty acids on insulin signaling and ceramide and diacylglycerol accumulation in 3T3-L1 adipocytes and C2C12 myotubes. *Arch. Biochem. Biophys.* **419,** 101–9 (2003).

53. Dimopoulos, N., Watson, M., Sakamoto, K. & Hundal, H. S. Differential effects of palmitate and palmitoleate on insulin action and glucose utilization in rat L6 skeletal muscle cells. *Biochem. J.* **399,** 473–481 (2006).

54. Salvadó, L. *et al.* Oleate prevents saturated-fatty-acid-induced ER stress, inflammation and insulin resistance in skeletal muscle cells through an AMPK-dependent mechanism. *Diabetologia* **56,** 1372–82 (2013).

55. Imamura, F. *et al.* Effects of Saturated Fat, Polyunsaturated Fat, Monounsaturated Fat, and Carbohydrate on Glucose-Insulin Homeostasis: A Systematic Review and Meta-analysis of Randomised Controlled Feeding Trials. *PLOS Med.* **13,** e1002087 (2016).

56. Oliveira, V. *et al.* Diets containing α-linolenic (ω3) or oleic (ω9) fatty acids rescues obese mice from insulin resistance. *Endocrinology* **156,** 4033–4046 (2015).

57. Han, J. & Kaufman, R. J. The role of ER stress in lipid metabolism and lipotoxicity. *J. Lipid Res.* **57,** 1329–1338 (2016).

58. Pickersgill, L., Litherland, G. J., Greenberg, A. S., Walker, M. & Yeaman, S. J. Key Role for Ceramides in Mediating Insulin Resistance in Human Muscle Cells. *J. Biol. Chem.* **282,** 12583–12589 (2007).

59. Nakamura, S. *et al.* Palmitate induces insulin resistance in H4IIEC3 hepatocytes through reactive oxygen species produced by mitochondria. *J. Biol. Chem.* **284,** 14809–18 (2009).

60. Dries, D. R., Gallegos, L. L. & Newton, A. C. A single residue in the C1 domain

sensitizes novel protein kinase C isoforms to cellular diacylglycerol production. *J. Biol. Chem.* **282,** 826–30 (2007).

61. Samuel, V. T., Petersen, K. F. & Shulman, G. I. Lipid-induced insulin resistance: unravelling the mechanism. *Lancet* **375,** 2267–2277 (2010).

62. Samuel, V. T. *et al.* Inhibition of protein kinase Cepsilon prevents hepatic insulin resistance in nonalcoholic fatty liver disease. *J. Clin. Invest.* **117,** 739–45 (2007).

63. Turban, S. & Hajduch, E. Protein kinase C isoforms: Mediators of reactive lipid metabolites in the development of insulin resistance. *FEBS Lett.* **585,** 269–274 (2011).

64. Yu, C. *et al.* Mechanism by Which Fatty Acids Inhibit Insulin Activation of Insulin Receptor Substrate-1 (IRS-1)-associated Phosphatidylinositol 3-Kinase Activity in Muscle. *J. Biol. Chem.* **277,** 50230–50236 (2002).

65. Li, Y. *et al.* Protein Kinase C θ Inhibits Insulin Signaling by Phosphorylating IRS1 at Ser ^{1101}. *J. Biol. Chem.* **279,** 45304–45307 (2004).

66. Mack, E. *et al.* Prevention of insulin resistance and beta-cell loss by abrogating PKCε-induced serine phosphorylation of muscle IRS-1 in *Psammomys obesus*. *Diabetes. Metab. Res. Rev.* **24,** 577–584 (2008).

67. Morino, K. *et al.* Muscle-Specific IRS-1 Ser->Ala Transgenic Mice Are Protected From Fat-Induced Insulin Resistance in Skeletal Muscle. *Diabetes* **57,** 2644–2651 (2008).

68. Anastasiou, C. A. *et al.* Diabetes mellitus is associated with increased intramyocellular triglyceride, but not diglyceride, content in obese humans. *Metabolism* **58,** 1636–1642 (2009).

69. Amati, F. *et al.* Skeletal Muscle Triglycerides, Diacylglycerols, and Ceramides in Insulin Resistance: Another Paradox in Endurance-Trained Athletes? *Diabetes* **60,** 2588–2597 (2011).

70. Coen, P. M. *et al.* Reduced skeletal muscle oxidative capacity and elevated ceramide but not diacylglycerol content in severe obesity. *Obesity (Silver Spring).* **21,** 2362–71 (2013).

71. Turpin-Nolan, S. M. *et al.* CerS1-Derived C18:0 Ceramide in Skeletal Muscle

Promotes Obesity-Induced Insulin Resistance. *Cell Rep.* **26,** 1–10.e7 (2019).

72. Haus, J. M. *et al.* Plasma ceramides are elevated in obese subjects with type 2 diabetes and correlate with the severity of insulin resistance. *Diabetes* **58,** 337–43 (2009).

73. Kurek, K. *et al.* Inhibition of Ceramide *De Novo* Synthesis Ameliorates Diet Induced Skeletal Muscles Insulin Resistance. *J. Diabetes Res.* **2015,** 1–9 (2015).

74. Powell, D. J., Turban, S., Gray, A., Hajduch, E. & Hundal, H. S. Intracellular ceramide synthesis and protein kinase Cζ activation play an essential role in palmitate-induced insulin resistance in rat L6 skeletal muscle cells. *Biochem. J.* **382,** 619–629 (2004).

75. Powell, D. J., Hajduch, E., Kular, G. & Hundal, H. S. Ceramide disables 3-phosphoinositide binding to the pleckstrin homology domain of protein kinase B (PKB)/Akt by a PKCzeta-dependent mechanism. *Mol. Cell. Biol.* **23,** 7794–808 (2003).

76. Mahfouz, R. *et al.* Characterising the Inhibitory Actions of Ceramide upon Insulin Signaling in Different Skeletal Muscle Cell Models: A Mechanistic Insight. *PLoS One* **9,** e101865 (2014).

77. Yang, X., Nath, A., Opperman, M. J. & Chan, C. The double-stranded RNA-dependent protein kinase differentially regulates insulin receptor substrates 1 and 2 in HepG2 cells. *Mol. Biol. Cell* **21,** 3449–58 (2010).

78. Ertunc, M. E. & Hotamisligil, G. S. Lipid signaling and lipotoxicity in metaflammation: indications for metabolic disease pathogenesis and treatment. *J. Lipid Res.* **57,** 2099–2114 (2016).

79. Boden, G. Fatty acid—induced inflammation and insulin resistance in skeletal muscle and liver. *Curr. Diab. Rep.* **6,** 177–181 (2006).

80. Itani, S. I., Ruderman, N. B., Schmieder, F. & Boden, G. Lipid-induced insulin resistance in human muscle is associated with changes in diacylglycerol, protein kinase C, and IkappaB-alpha. *Diabetes* **51,** 2005–11 (2002).

81. Boden, G. *et al.* Free fatty acids produce insulin resistance and activate the proinflammatory nuclear factor-kappaB pathway in rat liver. *Diabetes* **54,** 3458–65 (2005).

82. Ajuwon, K. M. & Spurlock, M. E. Palmitate Activates the NF-κB Transcription Factor and Induces IL-6 and TNFα Expression in 3T3-L1 Adipocytes. *J. Nutr.* **135,** 1841–1846 (2005).

83. Jové, M. *et al.* Palmitate Induces Tumor Necrosis Factor-α Expression in C2C12 Skeletal Muscle Cells by a Mechanism Involving Protein Kinase C and Nuclear Factor-κB Activation. *Endocrinology* **147,** 552–561 (2006).

84. Haghani, K., Pashaei, S., Vakili, S., Taheripak, G. & Bakhtiyari, S. TNF-α knockdown alleviates palmitate-induced insulin resistance in C2C12 skeletal muscle cells. *Biochem. Biophys. Res. Commun.* **460,** 977–982 (2015).

85. Holland, W. L. *et al.* Lipid-induced insulin resistance mediated by the proinflammatory receptor TLR4 requires saturated fatty acid-induced ceramide biosynthesis in mice. *J. Clin. Invest.* **121,** 1858–70 (2011).

86. Boon, J. *et al.* Ceramides contained in LDL are elevated in type 2 diabetes and promote inflammation and skeletal muscle insulin resistance. *Diabetes* **62,** 401–10 (2013).

87. Cai, D. *et al.* Local and systemic insulin resistance resulting from hepatic activation of IKK-beta and NF-kappaB. *Nat. Med.* **11,** 183–90 (2005).

88. Apovian, C. M. *et al.* Adipose Macrophage Infiltration Is Associated With Insulin Resistance and Vascular Endothelial Dysfunction in Obese Subjects. *Arterioscler. Thromb. Vasc. Biol.* **28,** 1654–1659 (2008).

89. Patsouris, D. *et al.* Insulin Resistance is Associated with MCP1-Mediated Macrophage Accumulation in Skeletal Muscle in Mice and Humans. *PLoS One* **9,** e110653 (2014).

90. Wu, H. & Ballantyne, C. M. Skeletal muscle inflammation and insulin resistance in obesity. *J. Clin. Invest.* **127,** 43–54 (2017).

91. Fink, L. N. *et al.* Pro-Inflammatory macrophages increase in skeletal muscle of high fat-Fed mice and correlate with metabolic risk markers in humans. *Obesity* **22,** 747–757 (2014).

92. Odegaard, J. I. & Chawla, A. Mechanisms of macrophage activation in obesity-induced insulin resistance. *Nat. Clin. Pract. Endocrinol. Metab.* **4,** 619–626 (2008).

93. Murray, P. J. *et al.* Macrophage Activation and Polarization: Nomenclature and Experimental Guidelines. *Immunity* **41,** 14–20 (2014).

94. Goerdt, S. *et al.* Alternative versus Classical Activation of Macrophages. *Pathobiology* **67,** 222–226 (1999).

95. Martinez, F. O. & Gordon, S. The M1 and M2 paradigm of macrophage activation: time for reassessment. *F1000Prime Rep.* **6,** 13 (2014).

96. Kanda, H. *et al.* MCP-1 contributes to macrophage infiltration into adipose tissue, insulin resistance, and hepatic steatosis in obesity. *J. Clin. Invest.* **116,** 1494–505 (2006).

97. Gao, D. *et al.* Interleukin-1β mediates macrophage-induced impairment of insulin signaling in human primary adipocytes. *Am. J. Physiol. Metab.* **307,** E289–E304 (2014).

98. Kang, K. *et al.* Adipocyte-Derived Th2 Cytokines and Myeloid PPARδ Regulate Macrophage Polarization and Insulin Sensitivity. *Cell Metab.* **7,** 485–495 (2008).

99. Riera-Borrull, M. *et al.* Palmitate Conditions Macrophages for Enhanced Responses toward Inflammatory Stimuli via JNK Activation. *J. Immunol.* **199,** 3858–3869 (2017).

100. Kewalramani, G., Fink, L. N., Asadi, F. & Klip, A. Palmitate-Activated Macrophages Confer Insulin Resistance to Muscle Cells by a Mechanism Involving Protein Kinase C θ and ε. *PLoS One* **6,** e26947 (2011).

101. Pararasa, C., Bailey, C. & Griffiths, H. Macrophage polarisation by fatty acids is PPARgamma-dependent. *Free Radic. Biol. Med.* **75,** S31–S32 (2014).

102. Samokhvalov, V., Bilan, P. J., Schertzer, J. D., Antonescu, C. N. & Klip, A. Palmitate- and lipopolysaccharide-activated macrophages evoke contrasting insulin responses in muscle cells. *Am. J. Physiol. Metab.* **296,** E37–E46 (2009).

103. Ozcan, U. *et al.* Endoplasmic reticulum stress links obesity, insulin action, and type 2 diabetes. *Science* **306,** 457–61 (2004).

104. Hotamisligil, G. S. Endoplasmic reticulum stress and the inflammatory basis of metabolic disease. *Cell* **140,** 900–17 (2010).

105. Braakman, I. & Bulleid, N. J. Protein folding and modification in the mammalian

endoplasmic reticulum. *Annu. Rev. Biochem.* **80,** 71–99 (2011).

106. Matsuura, S., Masuda, R., Sakai, O. & Tashiro, Y. Immunoelectron microscopy of the outer membrane of rat hepatocyte nuclear envelopes in relation to the rough endoplasmic reticulum. *Cell Struct. Funct.* **8,** 1–9 (1983).

107. Schwarz, D. S. & Blower, M. D. The endoplasmic reticulum: structure, function and response to cellular signaling. *Cell. Mol. Life Sci.* **73,** 79–94 (2016).

108. Reid, D. W. & Nicchitta, C. V. Diversity and selectivity in mRNA translation on the endoplasmic reticulum. *Nat. Rev. Mol. Cell Biol.* **16,** 221–31 (2015).

109. Blobel, G. Intracellular protein topogenesis. *Proc. Natl. Acad. Sci. U. S. A.* **77,** 1496–500 (1980).

110. Braakman, I. & Hebert, D. N. Protein Folding in the Endoplasmic Reticulum. *Cold Spring Harb. Perspect. Biol.* **5,** a013201–a013201 (2013).

111. Reid, D. W. & Nicchitta, C. V. Primary Role for Endoplasmic Reticulum-bound Ribosomes in Cellular Translation Identified by Ribosome Profiling. *J. Biol. Chem.* **287,** 5518–5527 (2012).

112. Jagannathan, S., Reid, D. W., Cox, A. H. & Nicchitta, C. V. De novo translation initiation on membrane-bound ribosomes as a mechanism for localization of cytosolic protein mRNAs to the endoplasmic reticulum. *RNA* **20,** 1489–1498 (2014).

113. Fagone, P. & Jackowski, S. Membrane phospholipid synthesis and endoplasmic reticulum function. *J. Lipid Res.* **50,** S311–S316 (2009).

114. Cerqueira, N. M. F. S. A. *et al.* Cholesterol Biosynthesis: A Mechanistic Overview. *Biochemistry* **55,** 5483–5506 (2016).

115. Jo, Y. & DeBose-Boyd, R. A. Control of cholesterol synthesis through regulated ER-associated degradation of HMG CoA reductase. *Crit. Rev. Biochem. Mol. Biol.* **45,** 185–198 (2010).

116. Holthuis, J. C. M. & Levine, T. P. Lipid traffic: floppy drives and a superhighway. *Nat. Rev. Mol. Cell Biol.* **6,** 209–220 (2005).

117. Hanada, K., Kumagai, K., Tomishige, N. & Kawano, M. CERT and intracellular trafficking of ceramide. *Biochim. Biophys. Acta - Mol. Cell Biol. Lipids* **1771,** 644–653

(2007).

118. Jaffe, L. F. Sources of calcium in egg activation: a review and hypothesis. *Dev. Biol.* **99,** 265–76 (1983).

119. He, H., Lam, M., McCormick, T. S. & Distelhorst, C. W. Maintenance of calcium homeostasis in the endoplasmic reticulum by Bcl-2. *J. Cell Biol.* **138,** 1219–28 (1997).

120. Samtleben, S. *et al.* Direct Imaging of ER Calcium with Targeted-Esterase Induced Dye Loading (TED). *J. Vis. Exp.* e50317 (2013). doi:10.3791/50317

121. Carreras-Sureda, A., Pihán, P. & Hetz, C. Calcium signaling at the endoplasmic reticulum: fine-tuning stress responses. *Cell Calcium* **70,** 24–31 (2018).

122. Gidalevitz, T., Stevens, F. & Argon, Y. Orchestration of secretory protein folding by ER chaperones. *Biochim. Biophys. Acta - Mol. Cell Res.* **1833,** 2410–2424 (2013).

123. Clapham, D. E. Calcium Signaling. *Cell* **131,** 1047–1058 (2007).

124. Hampton, R. Y. ER stress response: Getting the UPR hand on misfolded proteins. *Curr. Biol.* **10,** R518–R521 (2000).

125. Khan, S. & Wang, C. H. ER stress in adipocytes and insulin resistance: mechanisms and significance (Review). *Mol. Med. Rep.* **10,** 2234–40 (2014).

126. Ron, D. & Walter, P. Signal integration in the endoplasmic reticulum unfolded protein response. *Nat. Rev. Mol. Cell Biol.* **8,** 519–29 (2007).

127. Harding, H. P., Zhang, Y. & Ron, D. Protein translation and folding are coupled by an endoplasmic-reticulum-resident kinase. *Nature* **397,** 271–274 (1999).

128. Walter, P. & Ron, D. The Unfolded Protein Response: From Stress Pathway to Homeostatic Regulation. *Science (80-.).* **334,** 1081–1086 (2011).

129. Ma, Y. & Hendershot, L. M. Delineation of a Negative Feedback Regulatory Loop That Controls Protein Translation during Endoplasmic Reticulum Stress. *J. Biol. Chem.* **278,** 34864–34873 (2003).

130. Ma, Y., Brewer, J. W., Diehl, J. A. & Hendershot, L. M. Two distinct stress signaling pathways converge upon the CHOP promoter during the mammalian unfolded protein response. *J. Mol. Biol.* **318,** 1351–65 (2002).

131. Zinszner, H. *et al.* CHOP is implicated in programmed cell death in response to impaired function of the endoplasmic reticulum. *Genes Dev.* **12,** 982–95 (1998).

132. Harding, H. P. *et al.* Stress-Induced Gene Expression in Mammalian Cells. *Mol. Cell* **6,** 1099–1108 (2000).

133. Harding, H. P. *et al.* An integrated stress response regulates amino acid metabolism and resistance to oxidative stress. *Mol. Cell* **11,** 619–33 (2003).

134. Sidrauski, C. & Walter, P. The Transmembrane Kinase Ire1p Is a Site-Specific Endonuclease That Initiates mRNA Splicing in the Unfolded Protein Response. *Cell* **90,** 1031–1039 (1997).

135. Calfon, M. *et al.* IRE1 couples endoplasmic reticulum load to secretory capacity by processing the XBP-1 mRNA. *Nature* **415,** 92–6 (2002).

136. Smith, M. H., Ploegh, H. L. & Weissman, J. S. Road to ruin: targeting proteins for degradation in the endoplasmic reticulum. *Science* **334,** 1086–90 (2011).

137. Hollien, J. & Weissman, J. S. Decay of endoplasmic reticulum-localized mRNAs during the unfolded protein response. *Science* **313,** 104–7 (2006).

138. Sriburi, R., Jackowski, S., Mori, K. & Brewer, J. W. XBP1: A link between the unfolded protein response, lipid biosynthesis, and biogenesis of the endoplasmic reticulum. *J. Cell Biol.* **167,** 35–41 (2004).

139. Saxton, R. A. & Sabatini, D. M. mTOR Signaling in Growth, Metabolism, and Disease. *Cell* **168,** 960–976 (2017).

140. Pfaffenbach, K. T. *et al.* Rapamycin Inhibits Postprandial-Mediated X-Box-Binding Protein-1 Splicing in Rat Liver. *J. Nutr.* **140,** 879–884 (2010).

141. Ye, J. *et al.* ER stress induces cleavage of membrane-bound ATF6 by the same proteases that process SREBPs. *Mol. Cell* **6,** 1355–64 (2000).

142. Haze, K., Yoshida, H., Yanagi, H., Yura, T. & Mori, K. Mammalian Transcription Factor ATF6 Is Synthesized as a Transmembrane Protein and Activated by Proteolysis in Response to Endoplasmic Reticulum Stress. *Mol. Biol. Cell* **10,** 3787–3799 (1999).

143. Shen, J., Chen, X., Hendershot, L. & Prywes, R. ER Stress Regulation of ATF6 Localization by Dissociation of BiP/GRP78 Binding and Unmasking of Golgi

Localization Signals. *Dev. Cell* **3,** 99–111 (2002).

144. Ferrari, D. M. & Söling, H. D. The protein disulphide-isomerase family: unravelling a string of folds. *Biochem. J.* **339 (Pt 1),** 1–10 (1999).

145. Wu, J. *et al.* ATF6alpha optimizes long-term endoplasmic reticulum function to protect cells from chronic stress. *Dev. Cell* **13,** 351–64 (2007).

146. Schinzel, R. & Dillin, A. Endocrine aspects of organelle stress — cell non-autonomous signaling of mitochondria and the ER. *Curr. Opin. Cell Biol.* **33,** 102–110 (2015).

147. Mahadevan, N. R. *et al.* Transmission of endoplasmic reticulum stress and pro-inflammation from tumor cells to myeloid cells. *Proc. Natl. Acad. Sci.* **108,** 6561–6566 (2011).

148. Cullen, S. J., Fatemie, S. & Ladiges, W. Breast tumor cells primed by endoplasmic reticulum stress remodel macrophage phenotype. *Am. J. Cancer Res.* **3,** 196–210 (2013).

149. Taylor, R. C. & Dillin, A. XBP-1 Is a Cell-Nonautonomous Regulator of Stress Resistance and Longevity. *Cell* **153,** 1435–1447 (2013).

150. Williams, K. W. *et al.* Xbp1s in Pomc Neurons Connects ER Stress with Energy Balance and Glucose Homeostasis. *Cell Metab.* **20,** 471–482 (2014).

151. Basseri, S. & Austin, R. C. Endoplasmic reticulum stress and lipid metabolism: mechanisms and therapeutic potential. *Biochem. Res. Int.* **2012,** 841362 (2012).

152. Cooper, G. M. The Endoplasmic Reticulum. (2000).

153. Virtue, S. & Vidal-Puig, A. Adipose tissue expandability, lipotoxicity and the Metabolic Syndrome--an allostatic perspective. *Biochim. Biophys. Acta* **1801,** 338–49 (2010).

154. Flamment, M., Hajduch, E., Ferré, P. & Foufelle, F. New insights into ER stress-induced insulin resistance. *Trends Endocrinol. Metab.* **23,** 381–90 (2012).

155. Oyadomari, S., Harding, H. P., Zhang, Y., Oyadomari, M. & Ron, D. Dephosphorylation of translation initiation factor 2alpha enhances glucose tolerance and attenuates hepatosteatosis in mice. *Cell Metab.* **7,** 520–32 (2008).

156. Ferre, P. The Biology of Peroxisome Proliferator-Activated Receptors: Relationship

With Lipid Metabolism and Insulin Sensitivity. *Diabetes* **53,** S43–S50 (2004).

157. Wang, C. *et al.* ATF4 regulates lipid metabolism and thermogenesis. *Cell Res.* **20,** 174–84 (2010).

158. Yoshizawa, T. *et al.* The transcription factor ATF4 regulates glucose metabolism in mice through its expression in osteoblasts. *J. Clin. Invest.* **119,** 2807–2817 (2009).

159. Zhang, K. *et al.* The unfolded protein response transducer IRE1α prevents ER stress-induced hepatic steatosis. *EMBO J.* **30,** 1357–75 (2011).

160. Yamamoto, K. *et al.* Induction of Liver Steatosis and Lipid Droplet Formation in ATF6-alpha Knockout Mice Burdened with Pharmacological Endoplasmic Reticulum Stress. *Mol. Biol. Cell* **21,** 2975–2986 (2010).

161. Boden, G. & Merali, S. Measurement of the increase in endoplasmic reticulum stress-related proteins and genes in adipose tissue of obese, insulin-resistant individuals. *Methods Enzymol.* **489,** 67–82 (2011).

162. Sharma, N. K. *et al.* Endoplasmic reticulum stress markers are associated with obesity in nondiabetic subjects. *J. Clin. Endocrinol. Metab.* **93,** 4532–41 (2008).

163. Gregor, M. F. *et al.* Endoplasmic reticulum stress is reduced in tissues of obese subjects after weight loss. *Diabetes* **58,** 693–700 (2009).

164. Xiao, C., Giacca, A. & Lewis, G. F. Sodium phenylbutyrate, a drug with known capacity to reduce endoplasmic reticulum stress, partially alleviates lipid-induced insulin resistance and beta-cell dysfunction in humans. *Diabetes* **60,** 918–24 (2011).

165. Boden, G. Free fatty acids, insulin resistance, and type 2 diabetes mellitus. *Proc. Assoc. Am. Physicians* **111,** 241–8 (1999).

166. Opie, L. H. & Walfish, P. G. Plasma free fatty acid concentrations in obesity. *N. Engl. J. Med.* **268,** 757–60 (1963).

167. Boden, G., Chen, X., Ruiz, J., White, J. V & Rossetti, L. Mechanisms of fatty acid-induced inhibition of glucose uptake. *J. Clin. Invest.* **93,** 2438–46 (1994).

168. Reynoso, R., Salgado, L. M. & Calderón, V. High levels of palmitic acid lead to insulin resistance due to changes in the level of phosphorylation of the insulin receptor and insulin receptor substrate-1. *Mol. Cell. Biochem.* **246,** 155–62 (2003).

169. Hunnicutt, J. W., Hardy, R. W., Williford, J. & McDonald, J. M. Saturated fatty acid-induced insulin resistance in rat adipocytes. *Diabetes* **43,** 540–5 (1994).

170. Liu, P., Peng, G. & Li, L. Endoplasmic Reticulum Stress Mediates Palmitic Acid-induced Insulin Resistance in Skeletal Muscle Cells. *FASEB J* **24,** 690.4- (2010).

171. Guo, W., Wong, S., Xie, W., Lei, T. & Luo, Z. Palmitate modulates intracellular signaling, induces endoplasmic reticulum stress, and causes apoptosis in mouse 3T3-L1 and rat primary preadipocytes. *Am. J. Physiol. Endocrinol. Metab.* **293,** E576-86 (2007).

172. Wei, Y., Wang, D., Topczewski, F. & Pagliassotti, M. J. Saturated fatty acids induce endoplasmic reticulum stress and apoptosis independently of ceramide in liver cells. *Am. J. Physiol. Endocrinol. Metab.* **291,** E275-81 (2006).

173. Gu, X. *et al.* Bip overexpression, but not CHOP inhibition, attenuates fatty-acid-induced endoplasmic reticulum stress and apoptosis in HepG2 liver cells. *Life Sci.* **87,** 724–732 (2010).

174. Cao, J. *et al.* Saturated fatty acid induction of endoplasmic reticulum stress and apoptosis in human liver cells via the PERK/ATF4/CHOP signaling pathway. *Mol. Cell. Biochem.* **364,** 115–129 (2012).

175. Rong, X. *et al.* LXRs regulate ER stress and inflammation through dynamic modulation of membrane phospholipid composition. *Cell Metab.* **18,** 685–97 (2013).

176. Fu, S. *et al.* Aberrant lipid metabolism disrupts calcium homeostasis causing liver endoplasmic reticulum stress in obesity. *Nature* **473,** 528–31 (2011).

177. Jiao, P. *et al.* FFA-Induced Adipocyte Inflammation and Insulin Resistance: Involvement of ER Stress and IKKβ Pathways. *Obesity* **19,** 483–491 (2011).

178. Yin, J. *et al.* Rapamycin Improves Palmitate-Induced ER Stress/NF *κ* B Pathways Associated with Stimulating Autophagy in Adipocytes. *Mediators Inflamm.* **2015,** 1–12 (2015).

179. Peter, A. *et al.* Individual Stearoyl-CoA Desaturase 1 Expression Modulates Endoplasmic Reticulum Stress and Inflammation in Human Myotubes and Is Associated With Skeletal Muscle Lipid Storage and Insulin Sensitivity In Vivo. *Diabetes* **58,** 1757–1765 (2009).

180. Salvadó, L. *et al.* PPARβ/δ prevents endoplasmic reticulum stress-associated inflammation and insulin resistance in skeletal muscle cells through an AMPK-dependent mechanism. *Diabetologia* **57,** 2126–35 (2014).

181. Rieusset, J. *et al.* Reduction of endoplasmic reticulum stress using chemical chaperones or Grp78 overexpression does not protect muscle cells from palmitate-induced insulin resistance. *Biochem. Biophys. Res. Commun.* **417,** 439–45 (2012).

182. Horgan, R. P. & Kenny, L. C. 'Omic' technologies: genomics, transcriptomics, proteomics and metabolomics. *Obstet. Gynaecol.* **13,** 189–195 (2011).

183. Hasin, Y., Seldin, M. & Lusis, A. Multi-omics approaches to disease. *Genome Biol.* **18,** 83 (2017).

184. Abu-Asab, M. S. *et al.* Biomarkers in the age of omics: time for a systems biology approach. *OMICS* **15,** 105–12 (2011).

185. Heather, J. M. & Chain, B. The sequence of sequencers: The history of sequencing DNA. *Genomics* **107,** 1–8 (2016).

186. Kchouk, M., Gibrat, J. F. & Elloumi, M. Generations of Sequencing Technologies: From First to Next Generation. *Biol. Med.* **09,** (2017).

187. Iwamoto, N. & Shimada, T. Recent advances in mass spectrometry-based approaches for proteomics and biologics: Great contribution for developing therapeutic antibodies. *Pharmacol. Ther.* **185,** 147–154 (2018).

188. Ren, J.-L., Zhang, A.-H., Kong, L. & Wang, X.-J. Advances in mass spectrometry-based metabolomics for investigation of metabolites. *RSC Adv.* **8,** 22335–22350 (2018).

189. Buescher, J. M. & Driggers, E. M. Integration of omics: more than the sum of its parts. *Cancer Metab.* **4,** 4 (2016).

190. Baumann, S. *et al.* Requirements and Perspectives for Integrating Metabolomics with other Omics Data. *Curr. Metabolomics* **1,** 15–27 (2012).

191. Kaddurah-Daouk, R., Kristal, B. S. & Weinshilboum, R. M. Metabolomics: a global biochemical approach to drug response and disease. *Annu. Rev. Pharmacol. Toxicol.* **48,** 653–83 (2008).

192. Schmidt, C. Metabolomics Takes Its Place as Latest Up-and-Coming ‘Omic’ Science. *JNCI J. Natl. Cancer Inst.* **96,** 732–734 (2004).

193. Dettmer, K. & Hammock, B. D. Metabolomics--a new exciting field within the ‘omics’ sciences. *Environ. Health Perspect.* **112,** A396-7 (2004).

194. Lei, Z., Huhman, D. V & Sumner, L. W. Mass spectrometry strategies in metabolomics. *J. Biol. Chem.* **286,** 25435–42 (2011).

195. Yang, K. & Han, X. Lipidomics: Techniques, Applications, and Outcomes Related to Biomedical Sciences. *Trends Biochem. Sci.* **41,** 954–969 (2016).

196. Han, X. Lipidomics for studying metabolism. *Nat. Rev. Endocrinol.* **12,** 668–679 (2016).

197. Sneddon, J., Masuram, S. & Richert, J. C. Gas Chromatography-Mass Spectrometry-Basic Principles, Instrumentation and Selected Applications for Detection of Organic Compounds. *Anal. Lett.* **40,** 1003–1012 (2007).

198. Fiehn, O. Metabolomics by Gas Chromatography-Mass Spectrometry: Combined Targeted and Untargeted Profiling. *Curr. Protoc. Mol. Biol.* **114,** 30.4.1-30.4.32 (2016).

199. Gelpi, E., Koenig, W. A., Gibert, J. & Oro, J. Combined Gas Chromatography-Mass Spectrometry of Amino Acid Derivatives. *J. Chromatogr. Sci.* **7,** 604–613 (1969).

200. DeJongh, D. C. *et al.* Analysis of trimethylsilyl derivatives of carbohydrates by gas chromatography and mass spectrometry. *J. Am. Chem. Soc.* **91,** 1728–1740 (1969).

201. Niehaus, W. G. & Ryhage, R. Determination of double bond positions in polyunsaturated fatty acids by combination gas chromatography-mass spectrometry. *Anal. Chem.* **40,** 1840–1847 (1968).

202. James, A. T. & Martin, A. J. Gas-liquid chromatography: the separation and identification of the methyl esters of saturated and unsaturated acids from formic acid to n-octadecanoic acid. *Biochem. J.* **63,** 144–52 (1956).

203. Lopes, A. S., Cruz, E. C. S., Sussulini, A. & Klassen, A. Metabolomic Strategies Involving Mass Spectrometry Combined with Liquid and Gas Chromatography. in 77–98 (Springer, Cham, 2017). doi:10.1007/978-3-319-47656-8_4

204. Quehenberger, O., Armando, A. M. & Dennis, E. A. High sensitivity quantitative lipidomics analysis of fatty acids in biological samples by gas chromatography-mass spectrometry. *Biochim. Biophys. Acta* **1811,** 648–56 (2011).

205. Christie, W. W., Christie, W. W. & Esterification, B. A. Preparation of Ester Derivatives of fatty acids for chromatographic analysis. *Adv. LIPID Methodol. ED. OILY Press LTD* (1993).

206. Morrison, W. R. & Smith, L. M. Preparation of Fatty Acid Methyl Esters and Dimethylacetals From Lipids With Boron Fluoride--Methanol. *J. Lipid Res.* **5,** 600–608 (1964).

207. Kuehnbaum, N. L. & Britz-McKibbin, P. New Advances in Separation Science for Metabolomics: Resolving Chemical Diversity in a Post-Genomic Era. *Chem. Rev.* **113,** 2437–2468 (2013).

208. Engelhardt, H. One century of liquid chromatography: From Tswett's columns to modern high speed and high performance separations. *J. Chromatogr. B* **800,** 3–6 (2004).

209. Cielecka-Piontek, J., Zalewski, P., Jelińska, A. & Garbacki, P. UHPLC: The Greening Face of Liquid Chromatography. *Chromatographia* **76,** 1429–1437 (2013).

210. Schoenmakers, P. J., Bartha, Á. & Billiet, H. A. H. Gradien elution methods for predicting isocratic conditions. *J. Chromatogr. A* **550,** 425–447 (1991).

211. Arsenault, J. C. & McDonald, P. D. *Beginners guide to liquid chromatography*. (Waters Corporation, 2007).

212. El-Aneed, A., Cohen, A. & Banoub, J. Mass Spectrometry, Review of the Basics: Electrospray, MALDI, and Commonly Used Mass Analyzers. *Appl. Spectrosc. Rev.* **44,** 210–230 (2009).

213. March, R. E. Quadrupole ion traps. *Mass Spectrom. Rev.* **28,** 961–989 (2009).

214. Chernushevich, I. V., Loboda, A. V. & Thomson, B. A. An introduction to quadrupole-time-of-flight mass spectrometry. *J. Mass Spectrom.* **36,** 849–865 (2001).

215. Marshall, A. G. & Hendrickson, C. L. High-Resolution Mass Spectrometers. *Annu. Rev. Anal. Chem.* **1,** 579–599 (2008).

216. Konermann, L., Ahadi, E., Rodriguez, A. D. & Vahidi, S. Unraveling the Mechanism of Electrospray Ionization. *Anal. Chem.* **85,** 2–9 (2013).

217. Ho, C. S. *et al.* Electrospray ionisation mass spectrometry: principles and clinical applications. *Clin. Biochem. Rev.* **24,** 3–12 (2003).

218. Banerjee, S. & Mazumdar, S. Electrospray Ionization Mass Spectrometry: A Technique to Access the Information beyond the Molecular Weight of the Analyte. *Int. J. Anal. Chem.* **2012,** 1–40 (2012).

219. Xu, Y.-F., Lu, W. & Rabinowitz, J. D. Avoiding misannotation of in-source fragmentation products as cellular metabolites in liquid chromatography-mass spectrometry-based metabolomics. *Anal. Chem.* **87,** 2273–81 (2015).

220. Abrankó, L., García-Reyes, J. F. & Molina-Díaz, A. In-source fragmentation and accurate mass analysis of multiclass flavonoid conjugates by electrospray ionization time-of-flight mass spectrometry. *J. Mass Spectrom.* **46,** 478–488 (2011).

221. Lee, S. H. & Choi, D. W. Comparison between Source-induced Dissociation and Collision-induced Dissociation of Ampicillin, Chloramphenicol, Ciprofloxacin, and Oxytetracycline via Mass Spectrometry. *Toxicol. Res.* **29,** 107–14 (2013).

222. Douglas, D. J. Applications of Collision Dynamics in Quadrupole Mass Spectrometry. *J. Am. Soc. Mass Spectrom.* **9,** 101–113 (1998).

223. Glish, G. L. & Burinsky, D. J. Hybrid Mass Spectrometers for Tandem Mass Spectrometry. *J. Am. Soc. Mass Spectrom.* **19,** 161–172 (2008).

224. Roberts, L. D., Souza, A. L., Gerszten, R. E. & Clish, C. B. Targeted metabolomics. *Curr. Protoc. Mol. Biol.* **Chapter 30,** Unit 30.2.1-24 (2012).

225. Lee, H.-C. & Yokomizo, T. Applications of mass spectrometry-based targeted and non-targeted lipidomics. *Biochem. Biophys. Res. Commun.* (2018). doi:10.1016/J.BBRC.2018.03.081

226. Derogis, P. B. M. C. *et al.* The Development of a Specific and Sensitive LC-MS-Based Method for the Detection and Quantification of Hydroperoxy- and Hydroxydocosahexaenoic Acids as a Tool for Lipidomic Analysis. *PLoS One* **8,** e77561 (2013).

227. Han, X., Yang, K. & Gross, R. W. Multi-dimensional mass spectrometry-based shotgun lipidomics and novel strategies for lipidomic analyses. *Mass Spectrom. Rev.* **31,** 134–178 (2012).

228. Hu, Q. *et al.* The Orbitrap: a new mass spectrometer. *J. Mass Spectrom.* **40,** 430–443 (2005).

229. Scigelova, M., Hornshaw, M., Giannakopulos, A. & Makarov, A. Fourier transform mass spectrometry. *Mol. Cell. Proteomics* **10,** M111.009431 (2011).

230. Smith, C. A., Want, E. J., O'Maille, G., Abagyan, R. & Siuzdak, G. XCMS: processing mass spectrometry data for metabolite profiling using nonlinear peak alignment, matching, and identification. *Anal. Chem.* **78,** 779–87 (2006).

231. Layre, E. & Moody, D. B. Lipidomic profiling of model organisms and the world's major pathogens. *Biochimie* **95,** 109–15 (2013).

232. Sud, M. *et al.* LMSD: LIPID MAPS structure database. *Nucleic Acids Res.* **35,** D527–D532 (2007).

233. Bustin, S. A. *A-Z of quantitative PCR*. (International University Line, 2004).

234. Ponchel, F. *et al.* Real-time PCR based on SYBR-Green I fluorescence: an alternative to the TaqMan assay for a relative quantification of gene rearrangements, gene amplifications and micro gene deletions. *BMC Biotechnol.* **3,** 18 (2003).

235. Kozera, B. & Rapacz, M. Reference genes in real-time PCR. *J. Appl. Genet.* **54,** 391–406 (2013).

236. Oslowski, C. M. & Urano, F. Measuring ER stress and the unfolded protein response using mammalian tissue culture system. *Methods Enzymol.* **490,** 71–92 (2011).

237. Perry, B. D. *et al.* Palmitate-induced ER stress and inhibition of protein synthesis in cultured myotubes does not require Toll-like receptor 4. *PLoS One* **13,** e0191313 (2018).

238. Achard, C. S. & Laybutt, D. R. Lipid-induced endoplasmic reticulum stress in liver cells results in two distinct outcomes: adaptation with enhanced insulin signaling or insulin resistance. *Endocrinology* **153,** 2164–77 (2012).

239. Laybutt, D. R. *et al.* Endoplasmic reticulum stress contributes to beta cell apoptosis in

type 2 diabetes. *Diabetologia* **50,** 752–763 (2007).

240. Oliveira, A. F. *et al.* In vitro use of free fatty acids bound to albumin: A comparison of protocols. *Biotechniques* **58,** 228–33 (2015).

241. Bligh, E. G. & Dyer, W. J. A rapid method of total lipid extraction and purification. *Can. J. Biochem. Physiol.* **37,** 911–7 (1959).

242. Cajka, T. & Fiehn, O. Increasing lipidomic coverage by selecting optimal mobile-phase modifiers in LC–MS of blood plasma. *Metabolomics* **12,** 34 (2016).

243. Wm. Craig Byrdwell. Resources for lipid analysis in the 21st Century. Available at: http://www.byrdwell.com/PhosphatidylCholine/PCbyName.htm.

244. Boyle, J. P. *et al.* Estimating Prevalence of Type 1 and Type 2 Diabetes in a Population of African Americans with Diabetes Mellitus. *Am. J. Epidemiol.* **149,** 55–63 (1999).

245. Al-Goblan, A. S., Al-Alfi, M. A. & Khan, M. Z. Mechanism linking diabetes mellitus and obesity. *Diabetes. Metab. Syndr. Obes.* **7,** 587–91 (2014).

246. Ogurtsova, K. *et al.* IDF Diabetes Atlas: Global estimates for the prevalence of diabetes for 2015 and 2040. *Diabetes Res. Clin. Pract.* **128,** 40–50 (2017).

247. Boden, G. Obesity and free fatty acids. *Endocrinol. Metab. Clin. North Am.* **37,** 635–46, viii–ix (2008).

248. Sears, B. & Perry, M. The role of fatty acids in insulin resistance. *Lipids Health Dis.* **14,** 121 (2015).

249. Palomer, X., Pizarro-Delgado, J., Barroso, E. & Vázquez-Carrera, M. Palmitic and Oleic Acid: The Yin and Yang of Fatty Acids in Type 2 Diabetes Mellitus. *Trends Endocrinol. Metab.* **29,** 178–190 (2018).

250. Ruiz-Núñez, B., Dijck-Brouwer, D. A. J. & Muskiet, F. A. J. The relation of saturated fatty acids with low-grade inflammation and cardiovascular disease. *J. Nutr. Biochem.* **36,** 1–20 (2016).

251. Unger, R. H., Clark, G. O., Scherer, P. E. & Orci, L. Lipid homeostasis, lipotoxicity and the metabolic syndrome. *Biochim. Biophys. Acta - Mol. Cell Biol. Lipids* **1801,** 209–214 (2010).

252. Lee, J., Cho, H.-K. & Kwon, Y. H. Palmitate induces insulin resistance without significant intracellular triglyceride accumulation in HepG2 cells. *Metabolism* **59,** 927–934 (2010).

253. Jové, M., Planavila, A., Laguna, J. C. & Vázquez-Carrera, M. Palmitate-induced interleukin 6 production is mediated by protein kinase C and nuclear-factor kappaB activation and leads to glucose transporter 4 down-regulation in skeletal muscle cells. *Endocrinology* **146,** 3087–95 (2005).

254. Odegaard, J. I. & Chawla, A. Mechanisms of macrophage activation in obesity-induced insulin resistance. *Nat. Clin. Pract. Endocrinol. Metab.* **4,** 619–626 (2008).

255. Kars, M. *et al.* Tauroursodeoxycholic Acid may improve liver and muscle but not adipose tissue insulin sensitivity in obese men and women. *Diabetes* **59,** 1899–905 (2010).

256. Peng, G. *et al.* Oleate Blocks Palmitate-Induced Abnormal Lipid Distribution, Endoplasmic Reticulum Expansion and Stress, and Insulin Resistance in Skeletal Muscle. *Endocrinology* **152,** 2206–2218 (2011).

257. Panzhinskiy, E., Hua, Y., Culver, B., Ren, J. & Nair, S. Endoplasmic reticulum stress upregulates protein tyrosine phosphatase 1B and impairs glucose uptake in cultured myotubes. *Diabetologia* **56,** 598–607 (2013).

258. Koh, H.-J. *et al.* Tribbles 3 mediates endoplasmic reticulum stress-induced insulin resistance in skeletal muscle. *Nat. Commun.* **4,** 1871 (2013).

259. Hage Hassan, R. *et al.* Endoplasmic reticulum stress does not mediate palmitate-induced insulin resistance in mouse and human muscle cells. *Diabetologia* **55,** 204–14 (2012).

260. Deldicque, L., Bertrand, L., Patton, A., Francaux, M. & Baar, K. ER stress induces anabolic resistance in muscle cells through PKB-induced blockade of mTORC1. *PLoS One* **6,** e20993 (2011).

261. Roberts, L. D. *et al.* Increased hepatic oxidative metabolism distinguishes the action of Peroxisome proliferator-activated receptor delta from Peroxisome proliferator-activated receptor gamma in the ob/ob mouse. *Genome Med.* **1,** 115 (2009).

262. Yaffe, D. & Saxel, O. Serial passaging and differentiation of myogenic cells isolated

from dystrophic mouse muscle. *Nature* **270,** 725–7 (1977).

263. Cox, R. D., Garner, I. & Buckingham, M. E. Transcriptional regulation of actin and myosin genes during differentiation of a mouse muscle cell line. *Differentiation* **43,** 183–191 (1990).

264. McMahon, D. K. *et al.* C2C12 cells: biophysical, biochemical, and immunocytochemical properties. *Am. J. Physiol. Physiol.* **266,** C1795–C1802 (1994).

265. Yang, M. *et al.* Saturated fatty acid palmitate-induced insulin resistance is accompanied with myotube loss and the impaired expression of health benefit myokine genes in C2C12 myotubes. *Lipids Health Dis.* **12,** 104 (2013).

266. ATCC. C2C12 (ATCC CRL-1772) [online]. Available at: https://www.lgcstandards-atcc.org/Products/All/CRL-1772.aspx?geo_country=gb#culturemethod. (Accessed: 3rd August 2018)

267. Glatz, J. F. C., Bonen, A. & Luiken, J. J. F. P. Exercise and insulin increase muscle fatty acid uptake by recruiting putative fatty acid transporters to the sarcolemma. *Curr. Opin. Clin. Nutr. Metab. Care* **5,** 365–70 (2002).

268. Stahl, A., Evans, J. G., Pattel, S., Hirsch, D. & Lodish, H. F. Insulin causes fatty acid transport protein translocation and enhanced fatty acid uptake in adipocytes. *Dev. Cell* **2,** 477–88 (2002).

269. Conejo, R., Valverde, A. M., Benito, M. & Lorenzo, M. Insulin produces myogenesis in C2C12 myoblasts by induction of NF-?B and downregulation of AP-1 activities. *J. Cell. Physiol.* **186,** 82–94 (2001).

270. Psychogios, N. *et al.* The human serum metabolome. *PLoS One* **6,** e16957 (2011).

271. Fusakio, M. E. *et al.* Transcription factor ATF4 directs basal and stress-induced gene expression in the unfolded protein response and cholesterol metabolism in the liver. *Mol. Biol. Cell* **27,** 1536–51 (2016).

272. Sela, D. *et al.* Endoplasmic reticulum stress-responsive transcription factor ATF6α directs recruitment of the Mediator of RNA polymerase II transcription and multiple histone acetyltransferase complexes. *J. Biol. Chem.* **287,** 23035–45 (2012).

273. Luo, S., Baumeister, P., Yang, S., Abcouwer, S. F. & Lee, A. S. Induction of

Grp78/BiP by Translational Block. *J. Biol. Chem.* **278,** 37375–37385 (2003).

274. Olivari, S. & Molinari, M. Glycoprotein folding and the role of EDEM1, EDEM2 and EDEM3 in degradation of folding-defective glycoproteins. *FEBS Lett.* **581,** 3658–3664 (2007).

275. Deldicque, L. *et al.* The unfolded protein response is activated in skeletal muscle by high-fat feeding: potential role in the downregulation of protein synthesis. *Am. J. Physiol. Endocrinol. Metab.* **299,** E695-705 (2010).

276. Boden, G. Obesity, insulin resistance and free fatty acids. *Curr. Opin. Endocrinol. Diabetes. Obes.* **18,** 139–43 (2011).

277. Winzell, M. S. & Ahrén, B. The high-fat diet-fed mouse: a model for studying mechanisms and treatment of impaired glucose tolerance and type 2 diabetes. *Diabetes* **53 Suppl 3,** S215-9 (2004).

278. Bortolin, R. C. *et al.* A new animal diet based on human Western diet is a robust diet-induced obesity model: comparison to high-fat and cafeteria diets in term of metabolic and gut microbiota disruption. *Int. J. Obes.* **42,** 525–534 (2018).

279. Shen, M. *et al.* A novel endoplasmic reticulum stress-induced apoptosis model using tunicamycin in primary cultured neonatal rat cardiomyocytes. *Mol. Med. Rep.* **12,** 5149–5154 (2015).

280. Olou, A. A. *et al.* Mammalian ECD Protein Is a Novel Negative Regulator of the PERK Arm of the Unfolded Protein Response. *Mol. Cell. Biol.* **37,** e00030-17 (2017).

281. Smith, A. L. *et al.* Discovery of 1 *H* -Pyrazol-3(2 *H*)-ones as Potent and Selective Inhibitors of Protein Kinase R-like Endoplasmic Reticulum Kinase (PERK). *J. Med. Chem.* **58,** 1426–1441 (2015).

282. Cross, B. C. S. *et al.* The molecular basis for selective inhibition of unconventional mRNA splicing by an IRE1-binding small molecule. *Proc. Natl. Acad. Sci.* **109,** E869–E878 (2012).

283. Liu, M. *et al.* Activation of the unfolded protein response downregulates cardiac ion channels in human induced pluripotent stem cell-derived cardiomyocytes. *J. Mol. Cell. Cardiol.* **117,** 62–71 (2018).

284. Márquez, S. *et al.* Endoplasmic Reticulum Stress Sensor IRE1α Enhances IL-23 Expression by Human Dendritic Cells. *Front. Immunol.* **8,** 639 (2017).

285. Brøns, C. & Vaag, A. Skeletal muscle lipotoxicity in insulin resistance and type 2 diabetes. *J. Physiol.* **587,** 3977–8 (2009).

286. Hwang, S.-L. *et al.* Inhibitory cross-talk between the AMPK and ERK pathways mediates endoplasmic reticulum stress-induced insulin resistance in skeletal muscle. *Br. J. Pharmacol.* **169,** 69–81 (2013).

287. Macrae, K. *et al.* Defining the role of DAG, mitochondrial function, and lipid deposition in palmitate-induced proinflammatory signaling and its counter-modulation by palmitoleate. *J. Lipid Res.* **54,** 2366–2378 (2013).

288. Green, C. D. & Olson, L. K. Modulation of palmitate-induced endoplasmic reticulum stress and apoptosis in pancreatic β-cells by stearoyl-CoA desaturase and Elovl6. *Am. J. Physiol. Metab.* **300,** E640–E649 (2011).

289. Ariyama, H., Kono, N., Matsuda, S., Inoue, T. & Arai, H. Decrease in membrane phospholipid unsaturation induces unfolded protein response. *J. Biol. Chem.* **285,** 22027–35 (2010).

290. Gregory, M. K., Gibson, R. A., Cook-Johnson, R. J., Cleland, L. G. & James, M. J. Elongase Reactions as Control Points in Long-Chain Polyunsaturated Fatty Acid Synthesis. *PLoS One* **6,** e29662 (2011).

291. Sanders, F. W. B. *et al.* Hepatic steatosis risk is partly driven by increased de novo lipogenesis following carbohydrate consumption. *Genome Biol.* **19,** 79 (2018).

292. Clore, J. N. *et al.* Skeletal muscle phosphatidylcholine fatty acids and insulin sensitivity in normal humans. *Am J Physiol Endocrinol Metab* **275,** E665-670 (1998).

293. Clore, J. N. *et al.* Changes in phosphatidylcholine fatty acid composition are associated with altered skeletal muscle insulin responsiveness in normal man. *Metabolism.* **49,** 232–8 (2000).

294. Dennis, E. A. & Norris, P. C. Eicosanoid storm in infection and inflammation. *Nat. Rev. Immunol.* **advance on,** (2015).

295. Mothe-Satney, I. *et al.* Adipocytes secrete leukotrienes: contribution to obesity-

associated inflammation and insulin resistance in mice. *Diabetes* **61,** 2311–9 (2012).

296. Sears, D. D. *et al.* 12/15-Lipoxygenase Is Required for the Early Onset of High Fat Diet-Induced Adipose Tissue Inflammation and Insulin Resistance in Mice. *PLoS One* **4,** e7250 (2009).

297. Kwak, H. J., Choi, H.-E. & Cheon, H. G. 5-LO inhibition ameliorates palmitic acid-induced ER stress, oxidative stress and insulin resistance via AMPK activation in murine myotubes. *Sci. Rep.* **7,** 5025 (2017).

298. Monteiro, R. & Azevedo, I. Chronic inflammation in obesity and the metabolic syndrome. *Mediators Inflamm.* **2010,** (2010).

299. Hotamisligil, G. S. Inflammation and metabolic disorders. *Nature* **444,** 860–7 (2006).

300. Chen, J. *et al.* Association between inflammation and insulin resistance in U.S. nondiabetic adults: results from the Third National Health and Nutrition Examination Survey. *Diabetes Care* **27,** 2960–5 (2004).

301. Yudkin, J. S., Stehouwer, C. D., Emeis, J. J. & Coppack, S. W. C-reactive protein in healthy subjects: associations with obesity, insulin resistance, and endothelial dysfunction: a potential role for cytokines originating from adipose tissue? *Arterioscler. Thromb. Vasc. Biol.* **19,** 972–8 (1999).

302. Pradhan, A. D., Manson, J. E., Rifai, N., Buring, J. E. & Ridker, P. M. C-reactive protein, interleukin 6, and risk of developing type 2 diabetes mellitus. *JAMA* **286,** 327–34 (2001).

303. Hotamisligil, G., Shargill, N. & Spiegelman, B. Adipose expression of tumor necrosis factor-alpha: direct role in obesity-linked insulin resistance. *Science (80-.).* **259,** 87–91 (1993).

304. Hotamisligil, G. S., Arner, P., Caro, J. F., Atkinson, R. L. & Spiegelman, B. M. Increased adipose tissue expression of tumor necrosis factor-alpha in human obesity and insulin resistance. *J. Clin. Invest.* **95,** 2409–2415 (1995).

305. Gregor, M. F. & Hotamisligil, G. S. Inflammatory Mechanisms in Obesity. *Annu. Rev. Immunol.* **29,** 415–445 (2011).

306. Sartipy, P. & Loskutoff, D. J. Monocyte chemoattractant protein 1 in obesity and

insulin resistance. *Proc. Natl. Acad. Sci. U. S. A.* **100,** 7265–70 (2003).

307. Kern, P. A., Ranganathan, S., Li, C., Wood, L. & Ranganathan, G. Adipose tissue tumor necrosis factor and interleukin-6 expression in human obesity and insulin resistance. *Am. J. Physiol. Metab.* **280,** E745–E751 (2001).

308. Weigert, C. *et al.* Palmitate, but not unsaturated fatty acids, induces the expression of interleukin-6 in human myotubes through proteasome-dependent activation of nuclear factor-kappaB. *J. Biol. Chem.* **279,** 23942–52 (2004).

309. Boyce, J. A. Mast cells and eicosanoid mediators: a system of reciprocal paracrine and autocrine regulation. *Immunol. Rev.* **217,** 168–185 (2007).

310. Harizi, H., Corcuff, J.-B. & Gualde, N. Arachidonic-acid-derived eicosanoids: roles in biology and immunopathology. *Trends Mol. Med.* **14,** 461–9 (2008).

311. Li, P. *et al.* LTB4 promotes insulin resistance in obese mice by acting on macrophages, hepatocytes and myocytes. *Nat. Med.* **advance on,** (2015).

312. Elmasry, K. *et al.* Role of endoplasmic reticulum stress in 12/15-lipoxygenase-induced retinal microvascular dysfunction in a mouse model of diabetic retinopathy. *Diabetologia* 1–13 (2018). doi:10.1007/s00125-018-4560-z

313. Dennis, E. A. Introduction to Thematic Review Series: Phospholipases: Central Role in Lipid Signaling and Disease. *J. Lipid Res.* **56,** 1245–7 (2015).

314. Burke, J. E. & Dennis, E. A. Phospholipase A2 structure/function, mechanism, and signaling. *J. Lipid Res.* **50 Suppl,** S237-42 (2009).

315. Zand, H., Morshedzadeh, N. & Naghashian, F. Signaling pathways linking inflammation to insulin resistance. *Diabetes Metab. Syndr. Clin. Res. Rev.* **11,** S307–S309 (2017).

316. Boittin, F.-X. *et al.* Ca2+-independent phospholipase A2 enhances store-operated Ca2+ entry in dystrophic skeletal muscle fibers. *J. Cell Sci.* **119,** 3733–3742 (2006).

317. Burkholder, T. J. Stretch-induced ERK2 phosphorylation requires PLA2 activity in skeletal myotubes. *Biochem. Biophys. Res. Commun.* **386,** 60–4 (2009).

318. Poulsen, K. A., Pedersen, S. F., Kolko, M. & Lambert, I. H. Induction of group VIA phospholipase A $_2$ activity during in vitro ischemia in C2C12 myotubes is associated

with changes in the level of its splice variants. *Am. J. Physiol. Physiol.* **293,** C1605–C1615 (2007).

319. Sendobry, S. M. *et al.* Attenuation of diet-induced atherosclerosis in rabbits with a highly selective 15-lipoxygenase inhibitor lacking significant antioxidant properties. *Br. J. Pharmacol.* **120,** 1199–1206 (1997).

320. Kenyon, V. *et al.* Discovery of Potent and Selective Inhibitors of Human Platelet-Type 12- Lipoxygenase. *J. Med. Chem.* **54,** 5485–5497 (2011).

321. Pillon, N. J., Arane, K., Bilan, P. J., Chiu, T. T. & Klip, A. Muscle cells challenged with saturated fatty acids mount an autonomous inflammatory response that activates macrophages. *Cell Commun. Signal.* **10,** 30 (2012).

322. Murray, P. J. Macrophage Polarization. *Annu. Rev. Physiol.* **79,** 541–566 (2017).

323. Samaan, M. C. The macrophage at the intersection of immunity and metabolism in obesity. *Diabetol. Metab. Syndr.* **3,** 29 (2011).

324. Wei, Y. *et al.* Skeletal muscle insulin resistance: role of inflammatory cytokines and reactive oxygen species. *Am. J. Physiol. Integr. Comp. Physiol.* **294,** R673–R680 (2008).

325. Mashima, R. & Okuyama, T. The role of lipoxygenases in pathophysiology; new insights and future perspectives. *Redox Biol.* **6,** 297–310 (2015).

326. Cole, B. K. *et al.* 12/15-Lipoxygenase signaling in the endoplasmic reticulum stress response. *Am. J. Physiol. Metab.* **302,** E654–E665 (2012).

327. Freemerman, A. J. *et al.* Metabolic reprogramming of macrophages: glucose transporter 1 (GLUT1)-mediated glucose metabolism drives a proinflammatory phenotype. *J. Biol. Chem.* **289,** 7884–96 (2014).

328. Vats, D. *et al.* Oxidative metabolism and PGC-1beta attenuate macrophage-mediated inflammation. *Cell Metab.* **4,** 13–24 (2006).

329. Zhang, C. *et al.* Interleukin-6/signal transducer and activator of transcription 3 (STAT3) pathway is essential for macrophage infiltration and myoblast proliferation during muscle regeneration. *J. Biol. Chem.* **288,** 1489–99 (2013).

330. Sarvas, J. L., Khaper, N. & Lees, S. J. The IL-6 Paradox: Context Dependent Interplay

of SOCS3 and AMPK. *J. Diabetes Metab.* **Suppl 13,** (2013).

331. Nieto-Vazquez, I., Fernández-Veledo, S., de Alvaro, C. & Lorenzo, M. Dual role of interleukin-6 in regulating insulin sensitivity in murine skeletal muscle. *Diabetes* **57,** 3211–21 (2008).

332. Holloszy, J. O. Exercise-induced increase in muscle insulin sensitivity. *J. Appl. Physiol.* **99,** 338–343 (2005).

333. Steensberg, A. *et al.* Production of interleukin-6 in contracting human skeletal muscles can account for the exercise-induced increase in plasma interleukin-6. *J. Physiol.* **529 Pt 1,** 237–42 (2000).

334. Febbraio, M. A., Hiscock, N., Sacchetti, M., Fischer, C. P. & Pedersen, B. K. Interleukin-6 is a novel factor mediating glucose homeostasis during skeletal muscle contraction. *Diabetes* **53,** 1643–8 (2004).

335. Wensveen, F. M. *et al.* NK cells link obesity-induced adipose stress to inflammation and insulin resistance. *Nat. Immunol.* **16,** 376–385 (2015).

336. Talukdar, S. *et al.* Neutrophils mediate insulin resistance in mice fed a high-fat diet through secreted elastase. *Nat. Med.* **18,** 1407–1412 (2012).

337. Volmer, R., van der Ploeg, K. & Ron, D. Membrane lipid saturation activates endoplasmic reticulum unfolded protein response transducers through their transmembrane domains. *Proc. Natl. Acad. Sci.* **110,** 4628–4633 (2013).

338. Boslem, E. *et al.* A lipidomic screen of palmitate-treated MIN6 β-cells links sphingolipid metabolites with endoplasmic reticulum (ER) stress and impaired protein trafficking. *Biochem. J.* **435,** 267–276 (2011).

339. Choi, S. *et al.* Myristate-induced endoplasmic reticulum stress requires ceramide synthases 5/6 and generation of C14-ceramide in intestinal epithelial cells. *FASEB J.* fj.201800141R (2018). doi:10.1096/fj.201800141R

340. Schmitz-Peiffer, C., Craig, D. L. & Biden, T. J. Ceramide generation is sufficient to account for the inhibition of the insulin-stimulated PKB pathway in C2C12 skeletal muscle cells pretreated with palmitate. *J. Biol. Chem.* **274,** 24202–10 (1999).

341. Mikłosz, A., Łukaszuk, B., Baranowski, M., Górski, J. & Chabowski, A. Effects of

Inhibition of Serine Palmitoyltransferase (SPT) and Sphingosine Kinase 1 (SphK1) on Palmitate Induced Insulin Resistance in L6 Myotubes. *PLoS One* **8,** e85547 (2013).

342. Bhattacharjee, S., Das, N., Mandala, A., Mukhopadhyay, S. & Roy, S. S. Fenofibrate Reverses Palmitate Induced Impairment in Glucose Uptake in Skeletal Muscle Cells by Preventing Cytosolic Ceramide Accumulation. *Cell. Physiol. Biochem.* **37,** 1315–1328 (2015).

343. Blachnio-Zabielska, A. U., Chacinska, M., Vendelbo, M. H. & Zabielski, P. The Crucial Role of C18-Cer in Fat-Induced Skeletal Muscle Insulin Resistance. *Cell. Physiol. Biochem.* **40,** 1207–1220 (2016).

344. Contreras, C. *et al.* Central Ceramide-Induced Hypothalamic Lipotoxicity and ER Stress Regulate Energy Balance. *Cell Rep.* **9,** 366–377 (2014).

345. Liu, Z. *et al.* Induction of ER stress-mediated apoptosis by ceramide via disruption of ER Ca(2+) homeostasis in human adenoid cystic carcinoma cells. *Cell Biosci.* **4,** 71 (2014).

346. Harasim-Symbor, E., Konstantynowicz-Nowicka, K. & Chabowski, A. Additive effects of dexamethasone and palmitate on hepatic lipid accumulation and secretion. *J. Mol. Endocrinol.* **57,** 261–273 (2016).

347. Konstantynowicz-Nowicka, K., Harasim, E., Baranowski, M. & Chabowski, A. New Evidence for the Role of Ceramide in the Development of Hepatic Insulin Resistance. *PLoS One* **10,** e0116858 (2015).

348. Al Fadel, F., Fayyaz, S., Japtok, L. & Kleuser, B. Involvement of Sphingosine 1-Phosphate in Palmitate-Induced Non-Alcoholic Fatty Liver Disease. *Cell. Physiol. Biochem.* **40,** 1637–1645 (2016).

349. Takahashi, H. *et al.* Metabolomics reveal 1-palmitoyl lysophosphatidylcholine production by peroxisome proliferator-activated receptor α. *J. Lipid Res.* **56,** 254–65 (2015).

350. Yea, K. *et al.* Lysophosphatidylcholine activates adipocyte glucose uptake and lowers blood glucose levels in murine models of diabetes. *J. Biol. Chem.* **284,** 33833–40 (2009).

351. Novgorodov, S. A., Gudz, T. I. & Obeid, L. M. Long-chain ceramide is a potent

inhibitor of the mitochondrial permeability transition pore. *J. Biol. Chem.* **283,** 24707–17 (2008).

352. Adams, J. M. *et al.* Ceramide content is increased in skeletal muscle from obese insulin-resistant humans. *Diabetes* **53,** 25–31 (2004).

353. Martínez-Sánchez, N. *et al.* Hypothalamic AMPK-ER Stress-JNK1 Axis Mediates the Central Actions of Thyroid Hormones on Energy Balance. *Cell Metab.* **26,** 212–229.e12 (2017).

354. Hu, W. *et al.* Palmitate increases sphingosine-1-phosphate in C2C12 myotubes via upregulation of sphingosine kinase message and activity. *J. Lipid Res.* **50,** 1852–62 (2009).

355. Levy, M. & Futerman, A. H. Mammalian ceramide synthases. *IUBMB Life* **62,** 347–56 (2010).

356. Laviad, E. L. *et al.* Characterization of Ceramide Synthase 2. *J. Biol. Chem.* **283,** 5677–5684 (2008).

357. Law, B. A. *et al.* Lipotoxic very-long-chain ceramides cause mitochondrial dysfunction, oxidative stress, and cell death in cardiomyocytes. *FASEB J.* **32,** 1403–1416 (2018).

358. Erickson, K. A. *et al.* AICAR inhibits ceramide biosynthesis in skeletal muscle. *Diabetol. Metab. Syndr.* **4,** 45 (2012).

359. Bruce, C. R. *et al.* Endurance training in obese humans improves glucose tolerance and mitochondrial fatty acid oxidation and alters muscle lipid content. *Am. J. Physiol. Metab.* **291,** E99–E107 (2006).

360. Tonks, K. T. *et al.* Skeletal muscle and plasma lipidomic signatures of insulin resistance and overweight/obesity in humans. *Obesity* **24,** 908–916 (2016).

361. Broskey, N. T., Obanda, D. N., Burton, J. H., Cefalu, W. T. & Ravussin, E. Skeletal muscle ceramides and daily fat oxidation in obesity and diabetes. *Metabolism* **82,** 118–123 (2018).

362. Mathivanan, S., Ji, H. & Simpson, R. J. Exosomes: Extracellular organelles important in intercellular communication. *J. Proteomics* **73,** 1907–1920 (2010).

363. Kakazu, E., Mauer, A. S., Yin, M. & Malhi, H. Hepatocytes release ceramide-enriched pro-inflammatory extracellular vesicles in an IRE1α-dependent manner. *J. Lipid Res.* **57,** 233–45 (2016).

364. Merrill, A. H. De novo sphingolipid biosynthesis: a necessary, but dangerous, pathway. *J. Biol. Chem.* **277,** 25843–6 (2002).

365. Kitatani, K., Idkowiak-Baldys, J. & Hannun, Y. A. The sphingolipid salvage pathway in ceramide metabolism and signaling. *Cell. Signal.* **20,** 1010–1018 (2008).

366. Tkach, M. & Théry, C. Communication by Extracellular Vesicles: Where We Are and Where We Need to Go. *Cell* **164,** 1226–1232 (2016).

367. Trajkovic, K. *et al.* Ceramide triggers budding of exosome vesicles into multivesicular endosomes. *Science* **319,** 1244–7 (2008).

368. Wadsworth, J. M. *et al.* The Chemical Basis of Serine Palmitoyltransferase Inhibition by Myriocin. *J. Am. Chem. Soc.* **135,** 14276–14285 (2013).

369. Desai, K. *et al.* Fumonisins and fumonisin analogs as inhibitors of ceramide synthase and inducers of apoptosis. *Biochim. Biophys. Acta* **1585,** 188–92 (2002).

370. Gagliostro, V. *et al.* Dihydroceramide delays cell cycle G1/S transition via activation of ER stress and induction of autophagy. *Int. J. Biochem. Cell Biol.* **44,** 2135–2143 (2012).

371. Hernández-Tiedra, S. *et al.* Dihydroceramide accumulation mediates cytotoxic autophagy of cancer cells via autolysosome destabilization. *Autophagy* **12,** 2213–2229 (2016).

372. Raichur, S. *et al.* CerS2 Haploinsufficiency Inhibits β-Oxidation and Confers Susceptibility to Diet-Induced Steatohepatitis and Insulin Resistance. *Cell Metab.* **20,** 687–695 (2014).

373. Frangioudakis, G. *et al.* Ceramide accumulation in L6 skeletal muscle cells due to increased activity of ceramide synthase isoforms has opposing effects on insulin action to those caused by palmitate treatment. *Diabetologia* **56,** 2697–2701 (2013).

374. van Niel, G., D'Angelo, G. & Raposo, G. Shedding light on the cell biology of extracellular vesicles. *Nat. Rev. Mol. Cell Biol.* **19,** 213–228 (2018).

375. Record, M., Silvente-Poirot, S., Poirot, M. & Wakelam, M. J. O. Extracellular vesicles : lipids as key components of their biogenesis and functions. *J. Lipid Res.* jlr.E086173 (2018). doi:10.1194/jlr.E086173

376. Podbielska, M. *et al.* Cytokine-induced release of ceramide-enriched exosomes as a mediator of cell death signaling in an oligodendroglioma cell line. *J. Lipid Res.* **57,** 2028–2039 (2016).

377. Hla, T. & Kolesnick, R. C16:0-ceramide signals insulin resistance. *Cell Metab.* **20,** 703–705 (2014).

378. Martínez, L. *et al.* Myristic acid potentiates palmitic acid-induced lipotoxicity and steatohepatitis associated with lipodystrophy by sustaning de novo ceramide synthesis. *Oncotarget* **6,** 41479–96 (2015).

379. Bohnert, K. R., McMillan, J. D. & Kumar, A. Emerging roles of ER stress and unfolded protein response pathways in skeletal muscle health and disease. *J. Cell. Physiol.* **233,** 67–78 (2018).

380. Chavez, J. A. & Summers, S. A. A Ceramide-Centric View of Insulin Resistance. *Cell Metab.* **15,** 585–594 (2012).

381. Bikman, B. T. *et al.* Fenretinide Prevents Lipid-induced Insulin Resistance by Blocking Ceramide Biosynthesis. *J. Biol. Chem.* **287,** 17426–17437 (2012).

382. Preitner, F., Mody, N., Graham, T. E., Peroni, O. D. & Kahn, B. B. Long-term Fenretinide treatment prevents high-fat diet-induced obesity, insulin resistance, and hepatic steatosis. *Am. J. Physiol. Endocrinol. Metab.* **297,** E1420-9 (2009).

383. Chakrabarti, S. K., Cole, B. K., Wen, Y., Keller, S. R. & Nadler, J. L. 12/15-lipoxygenase products induce inflammation and impair insulin signaling in 3T3-L1 adipocytes. *Obesity (Silver Spring).* **17,** 1657–63 (2009).

384. Oh, J. *et al.* Endoplasmic Reticulum Stress Controls M2 Macrophage Differentiation and Foam Cell Formation. *J. Biol. Chem.* **287,** 11629–11641 (2012).

385. Zhang, Q. *et al.* The Mitochondrial Unfolded Protein Response Is Mediated Cell-Non-autonomously by Retromer-Dependent Wnt Signaling. *Cell* **174,** 870–883.e17 (2018).

386. Shpilka, T. & Haynes, C. M. The mitochondrial UPR: mechanisms, physiological

functions and implications in ageing. *Nat. Rev. Mol. Cell Biol.* **19,** 109–120 (2017).

387. Summers, S. A. Could Ceramides Become the New Cholesterol? *Cell Metab.* **27,** 276–280 (2018).

388. Lemaitre, R. N. *et al.* Circulating Sphingolipids, Insulin, HOMA-IR, and HOMA-B: The Strong Heart Family Study. *Diabetes* **67,** 1663–1672 (2018).

389. Boon, J. *et al.* Ceramides contained in LDL are elevated in type 2 diabetes and promote inflammation and skeletal muscle insulin resistance. *Diabetes* **62,** 401–10 (2013).

390. Pierce, A. A., Pickens, M. K., Siao, K., Grenert, J. P. & Maher, J. J. Differential hepatotoxicity of dietary and DNL-derived palmitate in the methionine-choline-deficient model of steatohepatitis. *BMC Gastroenterol.* **15,** 72 (2015).

391. Heydemann, A. An Overview of Murine High Fat Diet as a Model for Type 2 Diabetes Mellitus. *J. Diabetes Res.* **2016,** 2902351 (2016).

392. Wilson, C. R., Tran, M. K., Salazar, K. L., Young, M. E. & Taegtmeyer, H. Western diet, but not high fat diet, causes derangements of fatty acid metabolism and contractile dysfunction in the heart of Wistar rats. *Biochem. J.* **406,** 457–67 (2007).

393. Pinto, S. N., Silva, L. C., Futerman, A. H. & Prieto, M. Effect of ceramide structure on membrane biophysical properties: The role of acyl chain length and unsaturation. *Biochim. Biophys. Acta - Biomembr.* **1808,** 2753–2760 (2011).

394. Siddique, M. M., Li, Y., Chaurasia, B., Kaddai, V. A. & Summers, S. A. Dihydroceramides: From Bit Players to Lead Actors. *J. Biol. Chem.* **290,** 15371–9 (2015).

395. van Jaarsveld, M. T. M., Houthuijzen, J. M. & Voest, E. E. Molecular mechanisms of target recognition by lipid GPCRs: relevance for cancer. *Oncogene* **35,** 4021–4035 (2016).

396. Tang, X., Wang, Y., Li, D., Luo, J. & Liu, M. Orphan G protein-coupled receptors (GPCRs): biological functions and potential drug targets. *Acta Pharmacol. Sin.* **33,** 363–71 (2012).

397. Im, D.-S. Intercellular Lipid Mediators and GPCR Drug Discovery. *Biomol. Ther.*

(Seoul). **21,** 411–22 (2013).

398. Tarique, A. A. *et al.* Phenotypic, Functional, and Plasticity Features of Classical and Alternatively Activated Human Macrophages. *Am. J. Respir. Cell Mol. Biol.* **53,** 676–688 (2015).

399. Galván-Peña, S. & O'Neill, L. A. J. Metabolic reprograming in macrophage polarization. *Front. Immunol.* **5,** 420 (2014).

400. Mullen, T. D. *et al.* Selective knockdown of ceramide synthases reveals complex interregulation of sphingolipid metabolism. *J. Lipid Res.* **52,** 68–77 (2011).

401. Campana, M. *et al.* Inhibition of central de novo ceramide synthesis restores insulin signaling in hypothalamus and enhances β-cell function of obese Zucker rats. *Mol. Metab.* **8,** 23–36 (2018).

402. Xia, J. Y. *et al.* Targeted Induction of Ceramide Degradation Leads to Improved Systemic Metabolism and Reduced Hepatic Steatosis. *Cell Metab.* **22,** 266–278 (2015).

403. Cimellaro, A., Perticone, M., Fiorentino, T. V., Sciacqua, A. & Hribal, M. L. Role of endoplasmic reticulum stress in endothelial dysfunction. *Nutr. Metab. Cardiovasc. Dis.* **26,** 863–871 (2016).

404. Onat, D., Brillon, D., Colombo, P. C. & Schmidt, A. M. Human vascular endothelial cells: a model system for studying vascular inflammation in diabetes and atherosclerosis. *Curr. Diab. Rep.* **11,** 193–202 (2011).

405. Servier Medical Art. Available at: https://smart.servier.com/.